Compiled by Library of Korea Polar Research Institute

KOPRI ABSTRACTS contains journal articles written by KOPRI researchers and other researchers funded by KOPRI. The following KOPRI authors can be seen as highlighted in bold text.
The ***KOPRI ABSTRACTS*** are published once a year and distributed world wide by KOPRI since launching in 2014.

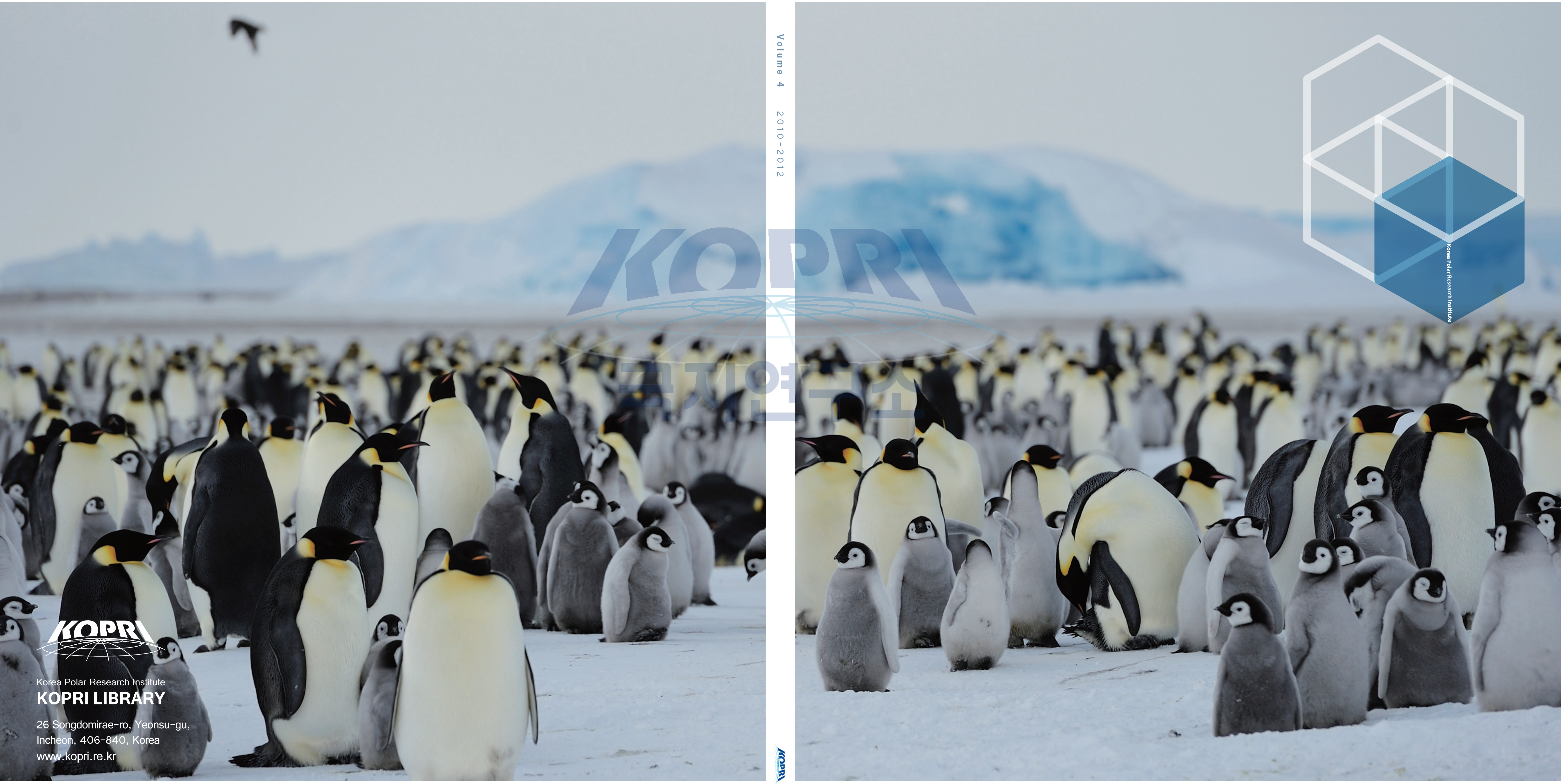

KOPRI
Korea Polar Research Institute
KOPRI LIBRARY
26 Songdomirae-ro, Yeonsu-gu,
Incheon, 406-840, Korea
www.kopri.re.kr

ISSN 2289-0734

KOPRI ABSTRACTS
Volume 4 | 2010-2012
KOPRI 극지연구소

KOPRI ABSTRACTS

Volume 4 (2010-2012)

KOPRI 극지연구소
Korea Polar Research Institute

KOPRI ABSTRACTS

Volume 4 (2010–2012)

CONTENTS

2010

Abstracts

Index

2011

Abstracts

Index

2012

Abstracts

Index

KOPRI ABSTRACTS
Volume 4 (2010-2012)

Published on **30 May 2014**
Published by Korea Polar Research Institute

Editor-in Cheif **Kang, Cheon Yun** cykang@kopri.re.kr
Managing Editor **Park, Hyunyi** hypark@kopri.re.kr
On, Nara onnara@kopri.re.kr

Advisory Editor Choe, Moon Young
Jung, Jinyoung
Lee, Jae Il
Lee, Jun Hyuck
Park, Youngcheol
Yoon, Young Jun

Editorial office KOPRI Library
26 Songdomirae-ro, Yeonsu-gu, Incheon, 406-840, Korea
Tel: +82-32-770-8484 **Fax:** +82-32-770-8488
E-mail: hypark@kopri.re.kr

Cover Photo Chung, Hosung (KOPRI)
Design & Printing Designintro Co.

KOPRI ABSTRACTS 2010


KOPRI
극지연구소

PART 1

Climate Change Sciences

1-1 Bak, Young-Suk, **Jae Il Lee**, **Ho-Il Yoon**, and 2 others. 2010. “Diatom research from the Drake Passage Core Sediment (GC05-DP02), Antarctica”. *Journal of the Geological Society of Korea*, 46(6): 553-560.

Diatom samples have been extracted from core sediment GC05-DP02 in Drake Passage, Antarctica. High number of diatom valves per gram of dry sediment was observed in core, ranging from 0.2 to 2.8 $\times10^6$/g. The open ocean diatoms from the core are dominated by *Fragilariopsis kerguelensis* and *Thalassiosira lentiginosa* which are about 69.8% of the total. We believe that there is little effect by the sea-ice even in the glacial periods, because high abundance of these Southern Ocean endemic taxa indicates sea-ice free waters. Diatom valve abundance and open ocean species are scarce in Unit B, D, F and H, identified as glacial periods (magnetic susceptibility: high). On the contrary, The Unit A, C, E, G and I shows high valve concentration and increasing open ocean species, identified as interglacial periods (magnetic susceptibility: low). The distribution pattern of *Hemidiscus karstenii* (FAO: 0.42 Ma (MIS 11), LAO: 0.19 Ma (MIS 7)) indicates interglacial periods during Marine Isotope Stages 7 and 9 in the Unit E and G, GC05-DP02.

1-2 Bak, Young-Suk, Jong-Deock Lee, **Ho Il Yoon**, **Kyu-Cheul Yoo**, and Seong-Joo Lee. 2010. “Holocene paleoclimate change in the area around Elephant Island, Antarctica: evidence from the diatom record”. *Journal of the Geological Society of Korea*, 46(2): 111-117.

A total of 84 species and varieties belonging to 37 genera are identified from the Core GC03-C1 in the Elephant Island, Antarctic Peninsula. High number of diatom valves per gram of dry sediment was observed in core, ranging from 0.2 ~ 17$\times10^7$/g. The Holocene diatom assemblages from the core are dominated by *Fragilariopsis kerguelensis* and *Eucampia antarctica* which are about 47.7% of the total. The reworked diatoms inculde taxa such as *Actinocyclus ingens*, *Rhizosolenia curvirostris*, *Denticulopsis praedimorpha*, and *D. dimorpha*. Holocene paleoenvironmental history in the Elephant Islands was reconstructed through the diatom assemblage analysis from sediment core GC03-C1. Four diatom zones are identified on the basis of frequency of the critical taxa throughout the section: diatom assemblage zone I from 880 to 312 cm (late Pleistocene including Last Glacial Maximum), diatom assemblage zone II from 312 to 232 cm (transition zone), diatom assemblage zone Ⅲ from 232 to 92 cm (mid-Holocene climatic optimum), and diatom assemblage zone IV from 92 to 0 cm (Neoglacial).

1-3 Chamaillard, Karine, S. GerardJennings, Darius Ceburnis, **Young Jun Yoon**, and Colin O’Dowd. 2010. “Effect of inctrumental particle sizing resolution on the modelling of aerosol radiative parameters”. *Journal of Quantitative Spectroscopy and Radiative Transfer*, 111(5): 753-771.
doi: 10.1016/j.jqsrt.2009.11.005

A more realistic estimation of the scattering and hemispheric backscattering coefficients, σ_{sp} and σ_{bsp}, and their respective optical cross section, C_{sca} and C_{bk}, of aerosol particles is presented on the basis of the exact resolution of the width of the size bins of the particle counter instruments when size distribution measurements are used, and, with the exact optical detector instruments ability. The scattering and hemispheric backscattering cross sections, C_{sca} and C_{bk}, of the particles are averaged over the full size bins of the particle counter instrument, while these quantities are usually estimated only oil the value of the mean geometric diameter of each size bin Six instruments. the APS, ASASP-X, DMPS. FSSP-100, ELPI, and SMPS frequently used in particle size distribution measurements are reviewed. for spherical sea-salt particles at a wavelength λ=0.55 μm. The comparison using the conventional geometric mean diameter versus the use of the full size bin leads to large amount of errors for the optical cross section with non-negligible effects on their respective optical coefficients. The maximal accuracy expected for these optical quantities depend on the particle diameter as well as on the channel width of the instruments. and are also function of the angular detector probe used to measure them.

1-4 Chung, Chull-Hwan, **Hyoun Soo Lim**, and Heon Jong Lee. 2010. “Vegetation and climate history during the late Pleistocene and early Holocene inferred from pollen record in Gwangju area, South Korea”. *Quaternary International*, 227: 61-67.
doi: 10.1016/j.quaint.2010.06.002

A pollen record (ca. 21,700e8100 cal. yr BP) from swamp deposits reveals a detailed history of vegetation and climate changes in Gwangju area, South Korea. The remarkable abundance of *Quercus* (*Lepidobalanus*) and *Ulmus/Zelkova* from ca. 21,700 to 20,700 cal. yr BP indicates deciduous broadleaved forest development under cool and wet conditions. A strong rise in herbs (*Artemisia* and Gramineae) and a remarkable decline in deciduous broadleaved trees between ca. 20,700 and 1,500 cal. yr BP imply vegetation change from closed deciduous broadleaved forest to open woodland with herbaceous understory indicating climate deterioration. After ca. 11,500 cal. yr BP the consistent increase of deciduous broadleaved trees and decrease of xerophytic herbs suggest that the previous open woodland with herbaceous understory was progressively replaced by cool temperate deciduous broadleaved forest with a fern understory in response to climate amelioration during the early Holocene. More humid conditions are also indicated by abundant fern spores and higher pollen concentration.

1-5 Chung, Chull-Hwan, **Hyoun Soo Lim**, and **Ho Il Yoon**. 2010. “Late Pleistocene Paleovegetation and Paleoclimate of the Uiwang Area Based on Pollen Analysis”. *Journal of Korean Earth Science Society,* 31(7): 698-707.
doi: 10.5467/JKESS.2010.31.7.698

The Late Pleistocene pollen record from the Poil-dong, Uiwang, Kyunggi-do, reveals that mixed coniferous and deciduous broadleaved forests were spread along with herb and fern understory. Palynofloral changes reflect climate fluctuations. From ca. 43,100 to 41,900 cal. yr BP, a mixed coniferous and deciduous broadleaved forest combined with open grassland occupied the study area, which indicates cooler condition than today. During the period of ca. 41,900-41,200 cal. yr BP, along with fern understory a decrease in subalpine conifers and an increase in temperate deciduous broadleaved trees suggest a climatic amelioration. A climatic deterioration, as evidenced by an increase in subalpine conifers and a decrease in the density of vegetation cover, occurred from ca. 41,200 to 39,700 cal. yr BP.

1-6 Forwick, Matthias, Tore O. Vorren, Morten Hald, Sergei Korsun, Yul Roh, Christoph Vogt, and **Kyu-Cheul Yoo**. 2010. “Spatial and temporal influence of glaciers and rivers on the sedimentary environment in Sassenfjorden and Tempelfjorden, Spitsbergen”. *Geological Society, London, Special Publications*, 344: 165-195.
doi: 10.1144/SP344.13

Multiproxy analyses including hydrographical, geochemical, foraminferal, lithological and geophysical data reveal variable influences of the glaciers Tunabreen and von Postbreen as well as the river Sassenelva on the sedimentary environment in two Spitsbergen fjords during the Late Weichselian and the Holocene. Grounded ice covered the study area during the last glacial. The glacier fronts retreated stepwise during the latest Weichselian/earliest Holocene, and the glaciers were probably small during the early Holocene. A growth of Tunabreen occurred between 6 and 4 cal ka BP Q2 . Reduced input from Tunabreen from c. 3.7 cal ka BP was probably a result of suppressed iceberg rafting related to the enhanced formation of sea ice and/or reduced meltwater runoff. During the past two millennia, the glacier fronts advanced and retreated several times. The maximum Holocene glacier extent was reached at the end of a surge of von Postbreen in AD 1870. Characteristics of the modern glaciomarine environment include: (1) different colours and bulk-mineral assemblages of the turbid waters emanating from the main sediment sources; (2) variable locations of the turbid-water plumes as a consequence of wind forcing and the Coriolis effect; (3) stratified water masses during summers with interannual variations; (4) increasing productivity with increasing distance from the glacier fronts; (5) foraminifera-faunal assemblages typical for glacierproximal settings; and (6) periodical mass-transport activity.

1-7 **Jee, G., H. -B. Lee**, and 3 others. 2010. “Assessment of GPS global ionosphere maps (GIM) by comparison between CODE GIM and TOPEX/Jason TEC data: Ionospheric perspective”. *Journal of Geophysical Research,* 115: A10319(1-11). doi: 10.1029/2010JA015432

We performed a comprehensive comparison between GPS global ionosphere map (GIM) and TOPEX/Jason (T-J) total electron content (TEC) data for the periods of 1998–2009 in order to assess the performance of GIM over the global ocean where the GPS ground stations are very sparse. Using the GIM model constructed by the Center for Orbit Determination in Europe at the University of Bern, the GIM TEC values were obtained along the T-J satellite orbit at specific locations and times of measurements and then binned into various geophysical conditions for direct comparison with the T-J TEC. On the whole, the GIM model was able to reproduce the spatial and temporal variations of the global ionosphere as well as the seasonal variations. However, the GIM model was not accurate enough to represent the well-known ionospheric structures such as the equatorial anomaly, the Weddell Sea Anomaly, and the longitudinal wave structure. Furthermore, a fundamental limitation of the model seems to be evident in the unexpected negative differences (i.e., GPS < T-J) in the northern high-latitude and the southern middle- and high-latitude regions in comparison with the T-J TECS. The positive relative differences (i.e., GIM > T-J) at night represent the plasmaspheric contribution to GPS TEC, which is maximized, reaching up to 100% of the corresponding T-J TEC values in the early morning sector. In particular, the relative differences decreased with increasing solar activity, and this may indicate that the plasmaspheric contribution to the maintenance of the nighttime ionosphere does not increase with solar activity, which is different from what we normally anticipate.

1-8 Katsuki, Kota, Boo-Keun Khim, Takuya Itaki, Yusuke Okazaki, Ken Ikehara, Yuna Shin, **Ho Il Yoon**, and **Cheon Yun Kang**. 2010. “Sea-ice distribution and atmospheric pressure patterns in southwestern Okhotsk Sea since the Last Glacial Maximum". *Global and Planetary Change,* 72(3): 99-107. doi: 10.1016/j.gloplacha.2009.12.005

Sea-ice diatom taxa (*Fragilariopsis cylindrus* and *Fragilariopsis oceanica*) and their relative abundance in the Okhotsk Sea were used to reconstruct the history of sea-ice distribution and atmospheric pressure patterns since the Last Glacial Maximum (LGM). The temporal state of sea-ice distribution and atmospheric pressure patterns since the LGM can be divided into three modes: northern Aleutian Low mode, southern Aleutian Low mode, and strong Siberian High mode. The Southern Aleutian Low mode was dominant before 15 ka and after 6.5 ka, respectively, showing expanded sea-ice distribution into the central and southern Okhotsk Sea. During the deglaciation period (15 ka to 10 ka), sea-ice retreated from the southern Okhotsk Sea because of the pronounced westerly winds under the strong Siberian High mode. However, sea-ice distribution expanded in the northern Okhotsk Sea, which favors the development of extensive polynyas on the northern continental shelf. Occurrences of northern Aleutian Low mode were frequent between 10 and 6.5 ka, while sea-ice distribution expanded into the eastern Okhotsk Sea. Formation of the Okhotsk Sea Intermediate Water, inferred from radiolarian species *Cycladophora davisiana*, intensified under both northern Aleutian Low mode and strong Siberian High mode.

1-9 Kim, Cheong Bin, Jeong Yul Kim, Kyung Soo Kim, and **Hyoun Soo Lim**. 2010. "New age constraints for hominid footprints found on Jeju Island, South Korea". *Journal of Archaeological Science,* 37(12): 3338-3343. doi: 10.1016/j.jas.2010.08.002

In 2004 numerous hominid footprints, along with diverse animal footprints, were found in the Late Quaternary strata of Jeju Island, South Korea. However, the age of the sediments in which the footprints were found is still controversial. Previous age estimates included radiocarbon ages of ca. 15,000 yr BP (Late Pleistocene) and quartz optically stimulated luminescence ages of ca. 7000 yr BP (mid-Holocene). In this study we report on 11 AMS ^{14}C dating results from a new set of samples collected from the footprintbearing strata and from associated sediments. Despite some variations and age reversal, all samples collected from the footprint-bearing strata yielded ^{14}C ages of late Pleistocene. These ages are comparable with previous radiocarbon dating results. Furthermore, the presence of the proboscidean footprints attributable to woolly mammoths in the footprint-bearing strata supports the radiocarbon dating results. Based on the new radiocarbon dates and the presence of the alleged mammoth footprints, the age of the hominid footprints found at Jeju Island is thought to be late Pleistocene (about 19,000-25,000 cal yr BP). Therefore, this is the second discovery of hominid footprints dated to the Pleistocene age in Asia, and the first to be discovered in Korea.

1-10 Kim, Jeong Woo, Ralph R. B. Von Frese, **Bang Yong Lee**, and 2 others. 2010. "Altimetry-Derived Gravity Predictions of Bathymetry by the Gravity-Geologic Method". *Pure and Applied Geophysics,* 167(8): 1-12. doi: 10.1007/s00024-010-0170-5

The gravity-geologic method (GGM) was implemented for 2' by 2' bathymetric determinations in a 1.6° longitudeby-1.0° latitude region centered on the eastern end of the Shackleton Fracture Zone in the Drake Passage, Antarctica. The GGM used the Bouguer slab approximation to process satellite altimetry-derived marine free-air gravity anomalies and 6,548 local shipborne bathymetric sounding measurements from the Korea Ocean Research and Development

Institute to update the surrounding off-track bathymetry. The limitations of the Bouguer slab for modeling the gravity effects of variable density, rugged bathymetric relief at distances up to several kilometers, were mitigated by establishing ‘tuning’ densities that stabilized the GGM predictions. Tests using two-thirds of the shipborne bathymetric measurements to estimate the remaining third indicated that the tuning densities minimized root-mean-square deviations to about 29 m. The optimum GGM bathymetry model honoring all the ship observations correlated very well with widely available bathymetry models, despite local differences that ranged up to a few kilometers. The great analytical simplicity of GGM facilitates accurately and efficiently updating bathymetry as new gravity and bathymetric sounding data become available. Furthermore, the availability of marine free-air gravity anomaly data ensures that the GGM is more effective than simply extrapolating or interpolating ship bathymetry coverage into unmapped regions.

1-11 **Kim, Jeong-Han**, Yong Ha Kim, Chang-Sup Lee, and **Geonhwa Jee**. 2010. “Seasonal variation of meteor decay times observed at King Sejong Station (62.22°S, 58.78°W), Antarctica”. *Journal of Atmospheric and Solar-Terrestrial Physics,* 72: 883-889.
doi: 10.1016/j.jastp.2010.05.003

We analyzed meteor decay times measured by a VHF radar at King Sejong Station by classifying strong and weak meteors according to their estimated electron line densities. The height profiles of monthly averaged decay times show a peak whose altitude varies with season at altitudes of 80-85 km. The higher peak during summer is consistent with colder temperatures that cause faster chemical reactions of electron removal. By adopting temperature dependent empirical recombination rates from rocket experiments and meteor electron densities of $2\times10^5 - 2\times10^6$ cm^{-3} in a decay time model, we are able to account for decreasing decay times below the peak for all seasons without invoking meteor electron removal by hypothetical icy particles.

1-12 Kim, KiTae, WonYoung Choi, Michael R. Hoffmann, **Ho-Il Yoon**, and **Byong-Kwon Park**. 2010. “Photoreductive Dissolution of Iron Oxides Trapped in Ice and Its Environmental Implications”. *Environmental Science & Technology,* 44(11): 4142-4148.
doi: 10.1021/es9037808

The availability of iron has been thought to be a main limiting factor for the productivity of phytoplankton and related with the uptake of atmospheric CO_2 and algal blooms in fresh and sea waters. In this work, the formation of bioavailable iron ($Fe(II)_{aq}$) from the dissolution of iron oxide particles was investigated in the ice phase under both UV and visible light irradiation. The photoreductive dissolution of iron oxides proceeded slowly in aqueous solution (pH 3.5) but was significantly accelerated in polycrystalline ice, subsequently releasing more bioavailable ferrous iron upon thawing. The enhanced photogeneration of $Fe(II)_{aq}$ in ice was confirmed regardless of the type of iron oxides [hematite, maghemite (γ-Fe_2O_3), goethite (α-FeOOH)] and the kind of electron donors. The iceenhanced dissolution of iron oxides was also observed under visible light irradiation, although the dissolution rate was much slower compared with the case of UV radiation. The iron oxide particles and organic electron donors (if any) in ice are concentrated and aggregated in the liquid-like grain boundary region (*freeze concentration effect*) where protons are also highly concentrated (lower pH). The enhanced photodissolution of iron oxides should occur in this confined boundary region.Wehypothesized that electron hopping through the interconnected grain boundaries of iron oxide particles facilitates the separation of photoinduced charge pairs. The outdoor experiments carried out under ambient solar radiation of Ny-Ålesund (Svalbard, 78°55′N) also showed that the generation of dissolved $Fe(II)_{aq}$ via photoreductive dissolution is enhanced when iron oxides are trapped in ice. Our results imply that the ice(snow)-covered surfaces and ice-cloud particles containing iron-rich mineral dusts in the polar and cold environments provide a source of bioavailable iron when they thaw.

1-13 **Kim, Seong-Joong** and **Eun-Jin Woo**. 2010. “Arctic Climate Change for the last Glacial Maximum Derived from PMIP2 Coupled Model Results”. *The Koeran Society of Climate Change Research,* 1(1): 31-50.

The Arctic climate change for the Last Glacial Maximum(LGM) occurred at 21,000 years ago (21ka) was investigated using simulation results of atmosphere-ocean coupled models from the second phase of the Paleoclimate Modelling Intercomparison Program(PMIP2). In the analysis, we used seven models, the NCAR CCSM of USA, ECHAM3-MPIOM of German Max-Planxk Institute, HadCM3M2 of UK Met Office, IPSL-CM4 of France Laplace Institute, CNRM-CM3 of France Meteorological Institute, MIROC3.2 of Japan CCSR at University of Tokyo, and FGOALS of China Institute of Atmospheric Physics. All the seven models reproduces the Arctic climate features found in the present climate at 0ka(pre-industrial time) in a reasonable degree in comparison to observations. During the LGM, the atmospheric CO_2 concentration and other greenhouse gases were reduced, the ice sheets were expanded over North America and northern Europe, the sea level was lowered by about 120m, and orbital parameters were slightly different. These boundary conditions were implemented to simulated LGM climate. With the implemented LGM conditions, the biggest temperature reduction by more than 24℃ is found over North America and northern Europe owing to ice albedo feedback and the change in lapse rate by high elevation. Besides, the expansion of ice sheets leads to the marked temperature reduction by more then 10℃ over the Arctic Ocean. The temperature reduction in northern winter is larger than in summer around the Arctic and the annual mean temperature is reduced by about 14℃. Compared to low mid-latitudes, the temperature reduction is much larger in high northern altitudes in the LGM. This results mirror the larger warming around the Artic in recent century. We could draw some information for the future under global warming from the knowledge of the LGM.

1-14 **Kim, Seong-Joong**, Jun Mei Lü, Sangheon Yi, **Taejin Choi**, **Baek-Min Kim**, **Bang Yong Lee**, **Sung-Ho Woo**, and **Yoojin Kim**. 2010. “Climate response over Asia/Arctic to change in orbital parameters for the last interglacial maximum”. *Geosciences Journal,* 14(2): 173-190.
doi: 10.1007/s12303-010-0017-1

The climate response over Asia/Arctic to the change in orbital parameters for the last interglacial maximum (LIGM) is investigated using the NCAR CCM3. After implementing LIGM orbital parameters, the insolation decreases in January and increases in July in the northern hemisphere in comparison to present values. The reduced net short-wave radiative heat fluxes in January lead to the surface cooling in low to mid latitudes of Asia, whereas a warming is obtained in northern Asia where the net short-wave radiative heat fluxes change little. The January warming in northern Asia/Arctic in the LIGM, consistent with proxy records, is mainly due to the marked increase in downward long wave heat fluxes associated with the increase in cloud and in part by the increase in the Arctic Oscillation polarity. In July, the increased insolation leads to the surface warming over most Asia, even though a slight cooling is obtained in low latitudes in spite of the increase in insolation, due to the decrease in the short-wave heat fluxes at the surface by the increase in the cloud amount. Precipitation overall increases at south and east Asia in July, due to the stronger southwest and southerly winds. The change in insolation due to the orbital parameters determines the climate change pattern in low- to mid-latitudes over Asia in the LIGM, even though the degree of climate change is much lower than suggested by proxy estimates. The results obtained in this study implies that, under the different climate background such as future global warming, the change greenhouse effect associated with cloud feedback could play an important role in determining the climate change over northern Asia/Arctic.

1-15 **Lee, Jae Il**, Young-Suk Bak, **Kyu-Cheul Yoo**, **Hyoun Soo Lim**, **Ho Il Yoon**, and Suk Hee Yoon. 2010. “Climate changes in the South Orkney Plateau during the last 8600 years”. *The Holocene,* 20(3): 395-404. doi: 10.1177/0959683609353430

Climatic and oceanographic changes in the South Orkney Plateau, western Antarctica, during the last 8600 years are reconstructed from a 525-cm-long gravity core based on sedimentological, geochemical, and diatom analyses. The core sediments are composed mostly of light greyish olive diatomaceous silt and mud with a few diatom ooze laminae in the basal part. The core can be divided at 350 cm into two units (4800 cal yr BP): the lower unit is characterized by variable total organic carbon (TOC) content and higher $CaCO_3$ content, and the upper unit is characterized by higher TOC and lower $CaCO_3$. The content of biogenic silica varies similar to TOC content in the lower unit but does not increase in the upper unit despite increased TOC. The variations in the organic matter composition and the amount of carbonate suggest that Scotia Sea water had been dominant in the study area prior to 4800 cal yr BP. A warmer condition during the middle Holocene is also supported by the fewer sea ice diatom taxa and a more sub-polar form of *Eucampia antarctica* in the lower unit. The increased sea ice and decreased influence of Scotia Sea water in the upper unit reflect climate cooling occurred at 4800 cal yr BP.

1-16 Lü, Jun-Mei, **Seong-Joong Kim**, and 3 others. 2010. “Arctic Oscillation during the Mid-Holocene and Last Glacial Maximum from PMIP2 Coupled Model Simulations”. *Journal of Climate,* 23(14): 3792-3813. doi: 10.1175/2010JCLI3331.1

Changes in the Arctic Oscillation (AO) during the mid-Holocene and the last glacial maximum were compared to pre-industrial simulations using four coupled ocean-atmosphere models (i.e. CCSM, HadCM3M2, IPSL, and MIROC3.2) from the second phase of Paleoclimate Modeling Intercomparison Project. Results show that the amplitude of the simulated AO during the mid-Holocene is a little smaller than that of the pre-industrial simulation. While the AO pattern and vertical structures are similar to those in the pre-industrial simulation, the polar westerlies are slightly weakened and displaced downward to the lower stratosphere, accompanied by weakening of the polar vortex and warming of the cold polar cap region. During the last glacial maximum, when the Northern Hemisphere experiences severe cooling, the intensity of the AO decreases substantially compared to the mid-Holocene, with smaller standard deviation of the AO indices in all models. Furthermore, the magnitude of positive and negative centers of the AO spatial pattern decreases, and the strength of the polar vortex and westerlies weakens further with the center of westerlies displaced into the mid-latitude upper troposphere. The polar cap region becomes anomalously warm in the stratosphere, while it remains cold in the troposphere. The AO appears to be sensitive to background climate state. Upward-propagating stationary Rossby waves are found to be stronger during the mid-Holocene and Last Glacial Maximum than in the preindustrial simulation. This increase in planetary wave activity might be responsible for the simulated weakening of the AO during the mid-Holocene and Last Glacial Maximum. Recent studies have shown that there is a significant correlation between Eurasian fall snow cover and the winter AO. The upward propagation of Rossby waves was further proposed to explain the physical process linking the AO with the snow depth. We suggest that a large increase in fall snow depth during the Last Glacial Maximum strengthens the upward-propagating stationary Rossby waves relative to the PI.

1-17 Park, Youngyun, Jin-Yong Lee, Hyun-Mi Choi, and **Hyoun Soo Lim**. 2010. "A review of researches on groundwater in permafrost regions". *Journal of the Geological Society of Korea,* 46(4): 429-437.

1-18 Yi Sangheon and **Seong-Joong Kim**. 2010. "Vegetation changes in western central region of Korean Peninsula during the last glacial (ca. 21.1–26.1 cal kyr BP)". *Geosciences Journal,* 14(1): 1-10.
doi: 10.1007/s12303-010-0001-9

Age-controlled pollen record from wetland sediments of Hanam, western central Korean Peninsula (KP), reveals vegetation dynamics response to climate changes during last glacial, 26.1–20.1 cal kyr BP. The Hanam pollen assemblages are dominated by conifers, *Picea* and *Pinus* and cold tolerant deciduous broadleaved *Betula*, together with common xerophytic herb like *Artemisia* and Gramineae. Principal taxa are similar to those of subalpine forest in modern vegetation of KP. Humidity variation reconstructed by semi aridity index (AI) indicates that, during 26.1–22.7 cal kyr BP, cold and dry conditions were prevailed with an expansion of subalpine coniferous forest and high value of AI. From 22.5 to 20.5 cal kyr BP, cool and wet conditions were reconstructed with low value of AI due to climatic amelioration, enhanced conifers and temperate deciduous broadleaved mixed forests flourished. Between 20.3 and 20.1 cal kyr BP, an abundance of *Picea* and *Betula* associated with high value of AI infers that subalpine conifers forest colonized again in hinterland montane along with open, low grassland under colder and drier conditions owing to climatic deterioration. The principal pollen taxa suggest that prevailing climate conditions were annual mean temperature about 5-6℃ colder and annual mean precipitation 40% drier than today.

1-19 **Yoon, Ho Il**, **Kyu-Cheul Yoo**, Young-Suk Bak, **Hyoun Soo Lim**, **Yeadong Kim**, and **Jae Il Lee**. 2010. "Late Holocene cyclic glaciomarine sedimentation in a subpolar fjord of the South Shetland Islands, Antarctica, and its paleoceanographic significance: Sedimentological, geochemical, and paleontological evidence". *Geological Society of America Bulletin,* 122(7/8): 1298-1307.
doi: 10.1130/B30178.1

The glaciomarine sedimentary record of the fjord head (Collins Harbor) in Maxwell Bay, South Shetland Islands (West Antarctica), a large marine calving embayment, contains repeating couplets of organic-rich massive diamicton and organic-poor stratified diamicton. The massive diamicton is characterized by high total organic carbon

(TOC) content and carbon to nitrogen (C/N) ratios and was deposited in a cold climate regime by iceberg-rafted sedimentation from coastal fast ice in which algal plants, as well as gravels, were entrained. The stratified diamicton is characterized by low TOC content and C/N ratios and was formed in a warmer climate regime when the flux of icebergs was suppressed, but turbid meltwater discharge continued to produce lamination. When the meltwater discharge decreased in cold climatic conditions, and resultant phytoplankton productivity was reduced due to the increased sea-ice coverage, ice rafting from shorefast sea ice might have played a major role in entraining benthic algae, as well as loads of sand and gravel, along the coastal area, resulting in an increased C/N ratio and gravel content in the massive diamicton. Accelerator mass spectrometry (AMS) radiocarbon analyses conducted on well-preserved calcite shells were used to construct a chronology for the past 3000 years. Fluctuations in TOC are recorded (approximately four cycles over this time period), with the average duration of a cooling cycle being ~500 years. These cycles may be correlative with the high-frequency (550 yr) variability in reduced Circumpolar Deep Water (CDW) on the West Antarctic Peninsula shelf, because a decrease in CDW may be related to reduced deep water production in the North Atlantic during colder periods, as demonstrated for glacial intervals throughout the Pleistocene.

PART 2

Earth-System Sciences

2-1 Choi, Sung Hi Choi, Katsuhiko Suzuki, Samuel B. Mukasa, **Jong-Ik Lee**, and Haemyeong Jung. 2010. “Lu–Hf and Re–Os systematics of peridotite xenoliths from Spitsbergen, western Svalbard: Implications for mantle–crust coupling”. *Earth and Planetary Science Letters,* 297: 121-132.
doi: 10.1016/j.epsl.2010.06.013

The timing of sub-continental lithospheric mantle (SCLM) differentiation beneath Spitsbergen, western Svalbard, has been determined with spinel peridotite xenoliths using two complementary isotopic systems: Lu–Hf and Re–Os. The whole-rock Re–Os systematics (Re–Os errorchron, aluminochron, and Re-depletion age) define Paleoproterozoic/Neoarchean ages for isolation of the studied peridotites from the convecting mantle. We note that the age is independently supported by the Lu–Hf errorchron for the peridotite clinopyroxene grains, and average degree of melt depletion recorded in the samples. The obtained ages are indistinguishable from the oldest crustal ages reported in western Spitsbergen, implying that the mantle lithosphere in this area was stabilized at the same time as formation of the overlying crust. Our data suggest that the Spitsbergen lithosphere is unlikely to have undergone bulk lithospheric delamination since the tectonic transition from transpressional to transtensional which commenced in the Paleocene. We thus discount the delaminated and reactivated SCLM as a potential source for the Dupal-like enriched components in the Arctic upper mantle suggested by other studies.

2-2 Chough, Sung Kwun, Hyun Suk Lee, **Jusun Woo**, and 6 others. 2010. “Cambrian stratigraphy of the North China Platform: revisiting principal sections in Shandong Province, China”. *Geosciences Journal,* 14(3): 235-268.
doi: 10.1007/s12303-010-0029-x

The Cambrian succession in the North China Platform comprises a mixed carbonate-siliciclastic sequence, superbly exposed in the southern part of Shandong

Province, China. In order to refine the lithostratigraphy of the Cambrian succession, this paper presents detailed sedimentary logs of outcrop sections in the Jinan, Laiwu, Jining, and Linyi areas. The entire succession consists of six lithologic units: Liguan, Zhushadong, Mantou, Zhangxia, Gushan, and Chaomidian formations in ascending order. The upper boundary of the Zhushadong Formation is refined as the base of the first purple mudstone bed of the Mantou Formation. The Mantou Formation is, in turn, bounded at the top by a thick oolitic grainstone bed of the Zhangxia Formation. The upper boundary of the Gushan Formation is placed at the base of a distinct bioclastic grainstone bed of the Chaomidian Formation. The constituent members of the Zhushadong, Mantou, and Chaomidian formations are also refined. Seventeen trilobite biozones are recognized, representing the Cambrian Series 2 to the Furongian.

2-3 Dziak, Robert P., **Minkyu Park**, **Won Sang Lee**, and 3 others. 2010. “Tectonomagmatic activity and ice dynamics in the Bransfield Strait back-arc basin, Antarctica”. *Journal of Geophysical Research,* 115: B01102(1-14).
doi: 10.1029/2009JB006295

An array of moored hydrophones was used to monitor the spatiotemporal distribution of small- to moderate-sized earthquakes and ice-generated sounds within the Bransfield Strait, Antarctica. During a 2 year period, a total of 3900 earthquakes, 5925 icequakes and numerous ice tremor events were located throughout the region. The seismic activity included eight space-time earthquake clusters, positioned along the central neovolcanic rift zone of the young Bransfield back-arc basin. These sequences of small magnitude earthquakes, or swarms, suggest ongoing magmatic activity that becomes localized along isolated volcanic features and fissure-like ridges in the southwest portion of the basin. A total of 122 earthquakes were located along the South Shetland trench, indicating continued deformation and possibly ongoing subduction along this margin. The large number of icequakes observed show a temporal pattern related to seasonal freeze-thaw cycles and a spatial distribution consistent with channeling of sea ice along submarine canyons from glacier fronts. Several harmonic tremor episodes were sourced from a large (~30 km^2) iceberg that entered northeast portion of the basin. The spectral character of these signals suggests they were produced by either resonance of a small chamber of fluid within the iceberg, or more likely, due to periodicity of discrete stick-slip events caused by contact of the moving iceberg with the seafloor. These pressure waves appear to have been excited by abrasion of the iceberg along the seafloor as it passed Clarence and Elephant Islands.

2-4 Fernandez-Mosquera, Daniel, **Doshik Hahm**, and Kurt Marti. 2010. “Calculated rates of cosmic ray muon-produced Ne in subsurface quartz”. *Geophysical Research Letters,* 37: L15403(1-5).
doi: 10.1029/2010GL044106

Interactions of cosmic ray secondaries with subsurface rocks produce both stable (^{3}He, ^{21}Ne, ^{22}Ne) and radioactive (^{10}Be, ^{26}Al and ^{36}Cl) cosmogenic nuclides. As the production rates by muons of ^{21}Ne and ^{22}Ne in quartz are not known, these can be estimated from published cross sections of analogous reactions, separately for fast and slow muon reactions. Our calculations show that subsurface ^{21}Ne is affected mainly by fast muon interactions ($P_{\mu f}{}^{21}Ne = 0.39 \pm 0.15$ at $g^{-1}a^{-1}$ vs $P^{21}{}_{\mu-}Ne = 0.12 \pm 0.03$ at $g^{-1}a^{-1}$ sea level-high latitude). We also infer that the resulting production rate ratio ($P^{21}Ne/P^{10}Be$) of ^{21}Ne and ^{10}Be changes with depth below the Earth’s surface. This ratio in turn may provide supplemental erosion rate information in geological settings of varying erosion surface covers and for long time scales, when radionuclide data provide incomplete information. In environments with very low erosion rates, our calculations indicate noticeable differences in the production ratios $P^{21}Ne/P^{10}Be$, specifically for long time scales. However, calibrations are needed and may be carried out on a well documented quartz core.

2-5 Hachikubo, Akihiro, Alexey Krylov, Hirotoshi Sakagami, Hirotsugu Minami, Yutaka Nunokawa, Hitoshi Shoji, Tatiana Matveeva, **Young K. Jin**, and Anatoly Obzhirov. 2010. “Isotopic composition of gas hydrates in subsurface sediments from offshore Sakhalin Island, Sea of Okhotsk”. *Geo-Marine Letters,* 30(3-4): 313-319.
doi: 10.1007/s00367-009-0178-y

Hydrate-bearing sediment cores were retrieved from recently discovered seepage sites located offshore Sakhalin Island in the Sea of Okhotsk. We obtained samples of natural gas hydrates and dissolved gas in pore water using a headspace gas method for determining their molecular and isotopic compositions. Molecular composition ratios C_1/C_{2+} from all the seepage sites were in the range of 1,500-50,000, while $\delta^{13}C$ and δD values of methane ranged from −66.0 to −63.2‰ VPDB and −204.6 to −196.7‰ VSMOW, respectively. These results indicate that the methane was produced by microbial reduction of CO_2. $\delta^{13}C$ values of ethane and propane (i.e., −40.8 to −27.4‰ VPDB and −41.3 to −30.6‰ VPDB, respectively) showed that small amounts of thermogenic gas were mixed with microbial methane. We also analyzed the isotopic difference between hydrate-bound and dissolved gases, and discovered that the magnitude by which the δD hydrate gas was smaller than that of dissolved gas was in the range 4.3-16.6‰, while there were no differences in $\delta^{13}C$ values. Based on isotopic fractionation of guest gas during the formation of gas hydrate, we conclude that the current gas in the pore water is the source of the gas hydrate at the VNIIOkeangeologia and Giselle Flare sites, but not the source of the gas hydrate at the Hieroglyph and KOPRI sites.

2-6 Kim, K. Y., **J. Lee**, M. H. Hong, **J. K. Hong**, and H. Shon. 2010. “Helicopter-borne and ground-towed radar surveys of the Fourcade Glacier on King George Island, Antarctica”. *Exploration Geophysics,* 41: 51-60.
doi: 10.1071/EG09052

To determine subglacial topography and internal features of the Fourcade Glacier on King George Island in Antarctica, helicopter-borne and ground-towed ground-penetrating radar (GPR) data were recorded along four profiles in November 2006. Signature deconvolution, *f-k*migration velocity analysis, and finite-difference depth migration applied to the mixed-phase, single-channel, ground-towed data, were effective in increasing vertical resolution, obtaining the velocity function, and yielding clear depth images, respectively. For the helicopter-borne GPR, migration velocities were obtained as root-mean-squared velocities in a two-layer model of air and ice. The radar sections show rugged subglacial topography, englacial sliding surfaces, and localised scattering noise. The maximum depth to the basement is over 79 m in the subglacial valley adjacent to the south-eastern slope of the divide ridge between Fourcade and Moczydlowski Glaciers. In the ground-towed profile, we interpret a complicated conduit above possible basal water and other isolated cavities, which are a few metres wide. Near the terminus, the GPR profiles image sliding surfaces, fractures, and faults that will contribute to the tidewater calving mechanism forming icebergs in Potter Cove.

2-7 Kim, Ki Young, **Joohan Lee**, **Myung Ho Hong**, **Jong Kuk Hong**, **Young Keun Jin**, and Howong Shon. 2010. "Seismic and radar investigations of Fourcade Glacier on King George Island, Antarctica". *Polar Research,* 29: 298-310.
doi: 10.1111/j.1751-8369.2010.00174.x

To determine P- and S-wave velocities, elastic properties and subglacial topography of the polythermal Fourcade Glacier, surface seismic and radar surveys were conducted along a 470-m profile in November 2006. P- and S-wave velocity structures were determined by travel-time tomography and inversion of Rayleigh wave dispersion curves, respectively. The average P- and S-wave velocities of ice are 3466 and 1839 m s^{-1}, respectively. Radar velocities were obtained by migration velocity analysis of 112 diffraction events. An estimate of 920 kg m^{-3} for the bulk density of wet ice corresponds to water contents of 5.1 and 3.2%, which were derived from the average P-wave and radar velocities, respectively. Using this density and the average P- and S-wave velocities, we estimate that the corresponding incompressibility and rigidity of the ice are 6.925 and 3.119 GPa, respectively. Synergistic interpretation of the radar profile and P- and S-wave velocities indicates the presence of a fracture zone above a subglacial high. Here, the P- and S-wave velocities are approximately 5 and 3% less than in the ice above a subglacial valley, respectively. The S-wave velocities indicate that warmer and less rigid ice underlies 10–15 m of colder ice near the surface of the glacier. Such layering is characteristic of polythermal glaciers. As a relatively simple non-invasive approach, integration of P-wave tomography, Rayleigh wave inversion and ground-towed radar is effective for various glaciological studies, including the elastic properties of englacial and subglacial materials, cold/warm ice interfaces, topography of a glacier bed and location of fracture zones.

2-8 Kim, Kwang-Hee and **Yongcheol Park**. 2010. "The 20 January 2007 M_L 4.8 Odaesan Earthquake and Its Implications for Regional Tectonics in Korea". *Bulletin of the Seismological Society of America,* 100(3): 1395-1405.
doi: 10.1785/0120090234

A moderate-sized earthquake (M_L 4.8) occurred in the mideast Korea Peninsula on 20 January 2007. It was the largest inland earthquake to occur there since the inception of a modern seismic observation system. Although only four aftershocks were noticed in previous studies, a careful review of continuous data revealed that the main event was accompanied by at least 74 micro foreshocks and aftershocks. A subset of 25 events was selected for further analysis to determine precise earthquake locations, focal mechanism solutions, and the current status of regional tectonic stress, as well as to answer questions raised about the sequence. Earthquake hypocenters were seen to be more clustered after the HypoDD relocation. A source radius of 1 km for the main event was estimated based on the distribution of precisely determined aftershock locations. Focal mechanism solutions of larger events in the sequence suggest either a left-lateral strike-slip fault trending west-northwest–east-southeast or a right-lateral strike-slip fault trending north-northeast–south-southwest as the responsible structure. Although the Woljeongsa fault striking north-northeast–southsouthwest in the local geological map matches one of the proposed trends, precise earthquake relocation results gave a contradictory result, showing that a previously unknown west-northwest–east-southeast striking fault was responsible for the earthquake sequence. We also observed an unusual lack of large-magnitude aftershocks, a relatively large stress drop during the main event, and no previous earthquake record in the region.

Observations made in the study consistently indicate the sequence nucleated along a less-developed fault. Focal mechanism solutions suggest the current status of tectonic stress governing earthquake generation in Korea is east-northeast–west-southwest compression and north-northwest–south-southeast extension.

2-9 Kim, Young-Gyun, Sang-Mook Lee, and Osamu Matsubayashi. 2010. “New heat flow measurements in the Ulleung Basin, East Sea (Sea of Japan): relationship to local BSR depth, and implications for regional heat flow distribution”. *Geo-Marine Letters,* 30: 595-603.
doi: 10.1007/s00367-010-0207-x

In July 2007, new marine heat flow data were collected at ten sites (HF01–10) in the central and southwestern sectors of the Ulleung Basin (East Sea or Sea of Japan) as part of regional gas hydrate research. In addition, cores were collected at five of these sites for laboratory analysis. The results show that the geothermal gradient ranged from 103-137 mK/m, and the in-situ thermal conductivity from 0.82-0.95 W/m·K. Laboratory measurements of thermal conductivity were found to deviate by as much as 40% from the in-situ measurements, despite the precautions taken to preserve the cores. Based on the in-situ conductivity, the heat flow was found to increase with water depth toward the center of the basin, ranging from 84-130 mW/m^2. Using a simple model, we estimated the heat flow from the depths of the BSR, and compared this with the observed heat flow. In our study area, the two sets of values were quite consistent, the observed heat flows being slightly higher than the BSR-derived ones. The evaluation of regional pre-1994 data revealed that the heat flow varied widely from 51-157 mW/m^2 in and around the basin. Due to a large scatter in these older data, a clear relationship between heat flow and water depth was not evident, in contrast to what would be expected for a rifted sedimentary basin. This raises the question as to whether the pre-1994 data represent the true background heat flow from the underlying basin crust since the basin opening, and/or whether they contain large measurement errors. In fact, evidence in support of the latter explanation exists. BSRs are generally found in the deep parts of the basin, and vary by only ±15 m in depth below the seafloor. From the average BSR depth, we inferred the background heat flow using a simple model, which in the case of the Ulleung Basin is approximately 120 and 80 mW/m^2 for 2.5 and 1 km below sea level, respectively.

2-10 Lee, Jin-Yong and **Hyoun Soo Lim**. 2010. “Identification and characterization of the encrusting materials in a coastal liquefied petroleum gas storage cavern”. *Environmental Earth Sciences,* 61(6): 1165-1177.
doi: 10.1007/s12665-009-0439-0

An examination was carried out of the encrusting materials on the seepage removal pumps in a bottom sump of an undersea liquefied petroleum gas (LPG) cavern. The studied cavern, constructed at 8 km off the western coast of Korea, facing the Yellow Sea, is at 130-150 m below the seabed. Since the first filling of the LPG into the cavern, it has suffered from the unexpected problem of a thick encrustation of unknown materials on the seepage removal pumps of the cavern. The XRD and XRF analyses revealed that the encrustation materials were mainly iron (hydro)oxides and carbonate mineral (aragonite). Based on the geological setting below the cavern site, it was inferred that iron oxides found in the Pleistocene sandy sediment and the Precambrian gneiss might be supplying ferrous iron to the cavern waters under an anaerobic condition, evidenced by low dissolved oxygen and negative redox potential in the cavern water. A significant change in the hydraulic condition near the pump intake and mixing the cavern water with oxic waters supplied through re-circulated seawater and terrestrial groundwater discharge, would precipitate the dissolved iron. Precipitation of the carbonate mineral is thought to have occurred due to over-saturation of calcium and bicarbonate, which may have resulted from the dissolution of cement grouting materials used during the undersea cavern construction and submarine groundwater discharge (SGD). This study reports the iron and carbonate precipitation in the man-made undersea cavern, which is affected by the surrounding hydrogeological condition and the SGD.

2-11 **Lee, Joohan**, Ki Young Kim, **Jong Kuk Hong**, and **Young Keun Jin**. 2010. “An englacial image and water pathways of the Fourcade glacier on King George Island, Antarctic Peninsula, inferred from ground-penetrating radar”. Science in China Series *D - Earth Sciences,* 53(6): 892-900.
doi: 10.1007/s11430-010-0078-z

The distribution of small fractures and water content of the Fourcade glacier on King George Island, Antarctica, was investi- gated in November 2006 and December 2007 by two ground-based (470- and 490-m-long profiles) and one helicopter-borne (470-m-long profile) ground-penetrating radar (GPR) surveys using 50-, 100-, and 500-MHz antennas. Radar images in the pre-migrated GPR sections are characterized by a smooth ice surface and irregular bed topography, numerous diffraction hyperbolas in the ice and at the glacier bed, strong scattering noise, and near-surface folded layers. Scattering noise above a mound in the center of the profiles is associated with an area of dense fractures extending down from the ice surface that has relatively low reflection strength. Near the northeast ends of the profiles where few englacial fractures occur, scattering noise may result from the presence of warmer ice. A water-filled conduit and an air-filled cavity are interpreted as the source of two distinct hyperbolas in sub-glacial valleys based on the polarity of the reflections. Through migration velocity analysis on 106 hyperbolas, radar velocities were obtained for the 100-MHz ground-based profile. Using the velocities and Paren’s mixture formula, we calculated the water content of the ice to have been in the range of 0.00–0.09. High water content occurs near the glacier margin, in sub-glacial valleys, and in zones of scattering noise.

2-12 **Lee, Won Sang**, **Sukyoung Yun**, and Ji-Young Do. 2010. “Scattering and Intrinsic Attenuation of Short-Period S Waves in the Gyeongsang Basin, South Korea, Revealed from S-Wave Seismogram Envelopes Based on the Radiative Transfer Theory”. *Bulletin of the Seismological Society of America,* 100(2): 833-840.
doi: 10.1785/0120090149

Examining seismic envelopes for local earthquakes that occurred in the Gyeongsang Basin, South Korea, we estimated coda *Q* values in the crust and measured the total scattering coefficients for frequency bands 1-2, 2-4, 4-8, and 8-16 Hz using the Monte Carlo simulation method based on radiative transfer theory. In the seismic envelope synthesis, we assumed acoustic multiple isotropic scattering and adopted a depth-dependent S-wave velocity model that is slightly modified from a receiver function result in the middle of the study region. The estimated total scattering coefficients range from 3.8×10^{-3} to 4.8×10^{-3} km^{-1} at 1-16 Hz, which agrees well with the average values in the crust. These values are corresponding to less than 0.5 of seismic albedo. This result represents that intrinsic absorption is a dominant contributor to the attenuation process for all frequency bands in the Gyeongsang Basin.

2-13 Lee, Yong Il, **Hyoun Soo Lim**, and 2 others. 2010. "Detrital zircon U-Pb ages of the late Paleozoic Sadong Formation in the Pyeongchang coalfield, Gangweon-do Province, Korea: implications for depositional age and provenance". *Journal of the Geological Society of Korea,* 46(1): 73-81.

2-14 Lee, Yong Il, TaeJin Choi, **Hyoun Soo Lim**, and YuJi Orihashi. 2010. "Detrital zircon geochronology of the Cretaceous Sindong Group, Southeast Korea: Implications for depositional age and Early Cretaceous igneous activity". *Island Arc,* 19(4): 647-658. doi: 10.1111/j.1440-1738.2010.00717.x

The Sindong Group forms the lowermost basin-fill of the Gyeongsang Basin, the largest Cretaceous nonmarine basin located in southeastern Korea, and comprises the Nakdong, Hasandong, and Jinju Formations with decreasing age. The depositional age of the Sindong Group has not yet been determined well and the reported age ranges from the Valanginian to Albian. Detrital zircons from the Sindong Group have been subjected to U-Pb dating using laser ablation inductively coupled plasma mass spectrometry. The Sindong Group contains noticeable amounts of detrital magmatic zircons of Cretaceous age (138-106 Ma), indicative of continuous magmatic activity prior to and during deposition of the Sindong Group. The youngest detrital zircon age of three formations becomes progressively younger stratigraphically: 118 Ma for the Nakdong Formation, 109 Ma for the Hasandong Formation, and 106 Ma for the Jinju Formation. Accordingly, the depositional age of the Sindong Group ranges from the late Aptian to late Albian, which is much younger than previously thought. Lower Cretaceous magmatic activity, which supplied detrital zircons to the Sindong Group, changed its location spatially through time; it occurred in the middle and northern source areas during the early stage, and then switched to the middle to southern source areas during the middle to late stages. This study reports first the Lower Cretaceous magmatic activity from the East Asian continental margin, which results in a narrower magmatic gap (*ca* 20 m.y.) than previously known.

2-15 Oh, Youngbok, Jaeryeon Park, Dongbok Shin, and **Mi-Jung Lee**. 2010. "Petrography of Hongcheon carbonatite-phoscorite complex". *Journal of the Geological Society of Korea,* 46(4): 367-380.

Petrographic study on the intrusive rocks comprising the Hongcheon Fe-REE deposits shows that the rocks correspond to carbonatite-phoscorite complex. They show unmixed textures that are either banded or intermingled pattern, and the replacement texture between the rock types is indicative of multi-stage precipitation. These textural features along with microscopic observation reveal that carbonatite and phoscorite in the study area were precipitated over three times, respectively, and those of the same stage show similar mineral assemblages. But, in general, carbonatite is more abundant carbonate minerals and REE minerals such as monazite, whereas phoscorite contains more abundant magnetite and apatite. Electron microprobe analyses for carbonate minerals in both rock types show noticeable Fe-enrichment trends in their chemical compositions from early to late stage, producing dolomite to Fe-dolomite phases in early stage and more Fe-enriched carbonates such as ankerite in late stage. Late stage carbonatite and phoscorite contain large amounts of quartz in addition to Fe-carbonate minerals, which is characteristic feature of final stage of carbonatite magma differentiation. Considering the outcrop features and mineralogical variations of the Hongcheon carbonatite-phoscorite complex, it seems like that these rocks were precipitated over successive fluid immiscibility process accompanied by fractional crystallization of ferrocarbonatite magma.

2-16 **Park, Sung-Hyun**, and 4 others. 2010. "Tracing the origin of subduction components beneath the South East rift in the Manus Basin, Papua New Guinea". *Chemical Geology,* 269(3-4): 339-349.
doi: 10.1016/j.chemgeo.2009.10.008

The Manus Basin to the northeast of Papua New Guinea is an actively spreading/rifting back-arc basin in the Bismarck Sea located between the inactive Manus-Kilinailau trench on the Pacific-plate side and the active New Britain trench on the Solomon-plate side. Spreading/rifting in the Manus Basin takes place in the last 0.78Myr or so. We present major and trace elements, and Sr–Nd–Pb isotope compositions of rock samples taken from the South East Rift (SER) at the eastern end of the Manus Basin. The strong enrichment of Pb and LILE (large ion lithophile elements) relative to HFSE (high field strength elements) and REE (rare earth elements) in the SER lava is also quite similar to other island arc lavas, suggesting that substantial amount of subduction componentswere present in its sourcemantle. To investigate the origin of the subduction components in SER lavas,wecompare the geochemical data of SER lavas to published data fromNew Britain Arc (NBA) and Tabar–Lihir–Tanga–Feni (TLTF) island chain. The volcanisminNBA is related to presently active subduction of the Solomon slab,whereas the TLTF volcanism is located in the forearc area of New Ireland arc which was formed during a former subduction of the Pacific slab. In otherwords, the NBA and TLTF lavas were influenced by subduction components fromthe present and former subduction, respectively. Weargue that the subduction components in SER lava were incorporated in the mantle lithosphere during the active arc volcanism on New Ireland because the amount of the subduction component in SER decreases with increasing in distance from New Ireland. On the other hand, no relationships are found with respect to New Britain. The Sr–Nd–Pb isotopes indicate that SER lavas contain little sediment component and less amount of fluid component derived from altered oceanic crust compared to the TLTF lavas. This is probably due to the fact that SER is located in backarc settings in contrast to TLTFwhich is located in forearc setting with respect to the Pacific slab. Thus it is likely that the sedimentwas removed fromthe slab in the forearc and/or arc areas, and therefore little or none was introduced in the backarcmantle, which is the source region for SER magmas at present. Fluid derived fromaltered oceanic crust also may have made its way into the sub-forearc region more effectively than backare region by shallow dehydration process.

2-17 Park, Tae-Yoon, **Ju-Sun Woo**, and Deok-Keun Choi. 2010. "A TRILOBITE FAUNA FROM THE BRECCIAS OF THE DAEGI FORMATION AT THE DONGJEOM SECTION, TAEBAEK, KOREA AND ITS GEOLOGICAL IMPLICATION". *Journal of Paleontology Society of Korea,* 26(2): 173-181.

The middle Cambrian Daegi Formation is predominantly composed of white to light gray massive to thin-bedded limestone, and oolitic and dolomitic limestone. The formation is generally known to have deposited in a shallow-marine setting. However, some studies suggested that the Daegi formation was deposited in a front-reef or back-reef slope environment, based on the presence of the breccias in the upper part of the formation near the Dongjeom area. Digesting the breccias with hydrochloric acid, five trilobite species were recovered: i.e., Pseudagnostus sp., Jiulongshania regularis, Bergeronites sp., dameseliid gen. et sp. indet. 1, and dameseliid gen. et sp. indet. 2. The faunal assemblage shows a close affinity to the fauna from the Stephanocare Zone of the Sesong Formation, while it is markedly different from the recently reported fauna of the upper part of the Daegi Formation. This result is inconsistent with the interpretation that the Daegi Formation was deposited in a front-reef or back-reef slope environment, and indicates that the breccias within the Daegi Formation were derived from the overlying Sesong Formation by the fault movements in the area.

2-18 **Park, Yongcheol**, Sun-Cheon Park, Kwang-Hee Kim, **Minkyu Park**, and **Joohan Lee**. 2010. “Magnitude scaling relationships from the first 3 s of P-wave arrivals in South Korea”. *Journal of Seismology,* 14(4): 761-768. doi: 10.1007/s10950-010-9198-3

Two empirical magnitude scaling relationships, predominant period (τ_p^{max}) and peak ground displacement (*Pd*) magnitudes, were investigated for the first 3 s after P-wave arrivals using 1,412 vertical waveforms recorded by the Korea National Seismic Network (KNSN) between 2001 and 2007. To evaluate the accuracy of the derived magnitude relationships, we simulated off-line ElarmS tests using 65 events occurring inside the KNSN. While the average magnitude error was ~0.70 magnitude units when using only the closest station to the epicentre, the error dropped to ~0.62 and ~0.42 magnitude units when using the closest two and closest four stations, respectively. For events $M_L \geq 3.0$, the average magnitude error was ~0.33 and showed stable values when the closest four stations were available. Our magnitude scaling relationships may be useful for initial work in developing an earthquake early warning system in South Korea.

2-19 **Seo, Ki-Weon**, Dongryeol Ryu, **Baek-Min Kim**, and 3 others. 2010. “GRACE and AMSR-E-based estimates of winter season solid precipitation accumulation in the Arctic drainage region”. *Journal of Geophysical Research,* 115: D20117(1-18). doi: 10.1029/2009JD013504

Solid precipitation plays a major role in controlling the winter hydrological cycle and spring discharge in the Arctic region. However, it has not been well documented due to sharply decreasing numbers of precipitation gauges, gauge measurement biases, as well as limitations of conventional satellite methods in high latitudes. In this study, we document the winter season solid precipitation accumulation in the Arctic region using the latest new satellite measurements from the Gravity Recovery and Climate Experiment (GRACE) and the Advanced Microwave Scanning Radiometer-Earth Observing System (AMSR-E). GRACE measures the winter total water (mainly from snow water equivalent (SWE)) storage change through gravity changes while AMSR-E measures the winter SWE through passive microwave measurements. The GRACE and AMSR-E measurements are combined with in situ and numerical model estimates of discharge and evapotranspiration to estimate the winter season solid precipitation accumulation in the Arctic region using the water budget equation. These two satellite-based estimates are then compared to the conventional estimates from two global precipitation products, such as the Global Precipitation Climatology Project (GPCP) and Climate Prediction Center’s Merged Analysis of Precipitation (CMAP), and three reanalyses, the National Centers for Environmental

Prediction/National Center for Atmospheric Research (NCEP/NCAR) reanalysis, the European Centre for Medium-Range Weather Forecasts' ERA-Interim, and the Japan Meteorological Agency's Climate Data Assimilation System (JCDAS) reanalysis. The GRACE-based estimate is very close to the GPCP and ERA-Interim estimates. The AMSR-E-based estimate is the most different from the other estimates. This GRACE-based measurement of winter season solid precipitation accumulation can provide a new valuable benchmark to understand the hydrological cycle, to validate and evaluate the model simulation, and to improve data assimilation in the Arctic region.

2-20 **Woo, J.** and S.K. Chough. 2010. "Growth patterns of the Cambrian microbialite: Phototropism and speciation of *Epiphyton*". *Sedimentary Geology,* 229(1-2): 1-8. doi: 10.1016/j.sedgeo.2010.05.006

Microbes started constructing shallow marine stromatolitic bioherms in the Archean, but they transferred their role as a major buildup maker to metazoans in Phanerozoic. Microbial buildups often recovered their predominance in the carbonate platform when reefal metazoan communities collapsed. *Epiphyton*, an extinct taxon of calcified microbe that possessed branching filamentous trichomes, was an important reef builder in the shallow marine carbonate platform during Middle Cambrian, aftermath of an extinction of archaeocyath sponges which were major reef-building sessile organisms in the Early Cambrian. Here we present direct evidence of phototropism of *Epiphyton*, found from fossilized behavior in micro- and macro-structures of meter-scale microbial bioherms of the Zhangxia Formation (Middle Cambrian), North China Platform, Shandong Province, China. The bioherms consist of stacked growth layers with the inner and outer divisions divided by distinct boundary. The inner division of growth layers of the *Epiphyton* bioherm is dominated by dense uniform bush-shaped *Epiphyton* thalli, whereas the curved outer division has layered texture normal to the surface, comprised of elongated and chambered thalli. It suggests that photosynthetic *Epiphyton* reacted actively to the spatial changes in intensity of sunlight, controlled by angle of illumination on the curved growth surface of the bioherm. The inner and the outer divisions comprise different morpho-types of *Epiphyton*. The spatial distributions of different morpho-types in variously illuminated divisions of *Epiphyton* might have caused further speciation of *Epiphyton*.

2-21 Yu, Chanho, Kwang-Hee Kim, Mancheol Suh, Bongchool Suk, Paul Rydelek, Suyoung Kang, **Yongcheol Park**, and Jin-Song Liu. 2010. "Crust and upper mantle structure beneath the Yellow Sea region using receiver function analysis". *Chinese Journal of Geophysics,* 53(6): 1336-1343. doi: 10.3969/j.issn.0001-5733.2010.06.012

Teleseismic events are used to obtain shear-wave velocity models beneath the stations of the Yellow Sea Broadband Seismic Network (YSBSN). Some stations are located on top of either a thick sedimentary basin or highly porous volcanic rocks and receiver functions at these stations exhibit prominent high-amplitude and long-period reverberations which obscure the subtle phases associated with deeper structures. Due to the shallow subsurface effects in receiver functions, shear-wave velocity models beneath only 8 broadband seismic stations are successfully inverted. Depth to the crust-mantle transition (the Moho) varies from 30 to 38 km beneath YSBSN stations. The thickest crust is observed beneath the station JNN in China, which is attributed to the ancient collision boundary between the North

China block and the South China block. Although general increase of the crustal thickness from north to south in Korea is observed with high confidence, it is not possible to delineate the location of potential collision boundary in the southern Korea peninsula, which would require wider coverage by broadband seismic instruments to resolve.

PART 3

Ocean Environment Sciences

3-1 Cai, Wei-Jun, Liqi Chen, Baoshan Chen, Zhongyong Gao, **Sang H. Lee**, and 12 others. 2010. “Decrease in the CO_2 Uptake Capacity in an Ice-Free Arctic Ocean Basin”. *Science,* 329(5991): 556-559. doi: 10.1126/science.1189338

It has been predicted that the Arctic Ocean will sequester much greater amounts of carbon dioxide (CO_2) from the atmosphere as a result of sea ice melt and increasing primary productivity. However, this prediction was made on the basis of observations from either highly productive ocean margins or ice-covered basins before the recent major ice retreat. We report here a high-resolution survey of sea-surface CO_2 concentration across the Canada Basin, showing a great increase relative to earlier observations. Rapid CO_2 invasion from the atmosphere and low biological CO_2 drawdown are the main causes for the higher CO_2, which also acts as a barrier to further CO_2 invasion. Contrary to the current view, we predict that the Arctic Ocean basin will not become a large atmospheric CO_2 sink under ice-free conditions.

3-2 Füri, Evelyn, D.R. Hilton, S.A. Halldórsson, P.H. Barry, **D. Hahm**, and 2 others. 2010. “Apparent decoupling of the He and Ne isotope systematics of the Icelandic mantle: The role of He depletion, melt mixing, degassing fractionation and air interaction”. *Geochimica et Cosmochimica Acta,* 74: 3307-3332. doi: 10.1016/j.gca.2010.03.023

Wepresent new He–Ne data for geothermal fluids and He–Ne–Ar data for basalts from throughout the Icelandic neovolcanic zones and older parts of the Icelandic crust. Geothermal fluids, subglacial glasses, and mafic phenocrysts are characterized by a wide range in helium isotope ratios ($^3He/^4He$) encompassing typical MORB-like ratios through values as high as 36.8R_A (where R_A = air $^3He/^4He$). Although neon in geothermal fluids is dominated by an atmospheric component, samples from the northwest peninsula show a small excess of nucleogenic ^{21}Ne, likely produced in-situ and released to circulating fluids. In contrast, geothermal fluids from the neovolcanic zones show evidence of a contribution of mantle-derived neon, as indicated by ^{20}Ne enrichments up to 3% compared to air. The neon isotope composition of subglacial glasses reveals that mantle neon is derived from both depleted MORB-mantle and a primordial, ‘solar’ mantle component. However, binary mixing between these two endmembers can account for the He–Ne isotope characteristics of the basalts only if the $^3He/^{22}Ne$ ratio of the primordial mantle endmember is lower than in the MORB component. Indeed, the helium to neon elemental ratios ($^4He/^{21}Ne^*$ and $^3He/^{22}Ne_s$ where $^{21}Ne^*$ = nucleogenic ^{21}Ne and $^{22}Ne_s$ = ‘solar’-derived ^{22}Ne) of the majority of Icelandic subglacial glasses are lower than theoretical values for Earth’s mantle, as observed previously for other OIB samples. Helium may be depleted relative to neon in high-$^3He/^4He$ ratio parental melts due to either more compatible behavior during low-degree partial melting or more extensive diffusive loss relative to the heavier noble gases. However, Icelandic glasses show higher ^{4}He/^{40}Ar* (^{40}Ar* = radiogenic Ar) values for a given ^{4}He/^{21}Ne* value compared to the majority of other OIB samples: this observation is consistent with extensive open-system equilibrium degassing, likely promoted by lower confining pressures during subglacial eruptions of Icelandic lavas. Taken together, the He–Ne–Ar systematics of Icelandic subglacial glasses are imprinted with the overlapping effects of helium depletion in the high-^{3}He/^{4}He ratio parental melt, binary mixing of two distinct mantle components, degassing fractionation and interaction with atmospheric noble gases. However, it is still possible to discern differences in the noble gas characteristics of the Icelandic mantle source beneath the neovolcanic zones, with MORB-like He–Ne isotope features prevalent in the Northern Rift Zone and a sharp transition to more primitive ‘solar-like’ characteristics in central and southern Iceland.

3-3 **Ha, Ho Kyung** and Jerome P.-Y. Maa. 2010. “Effects of suspended sediment concentration and turbulence on settling velocity of cohesive sediment”. *Geosciences Journal,* 14(2): 163-171.
doi: 10.1007/s12303-010-0016-2

Using a 5-MHz acoustic Doppler velocimeter (ADV), laboratory experiments were carried out to investigate the effects of suspended sediment concentration (SSC) and turbulence on the settling velocity (w_s) of cohesive sediment. The measurement of w_s with the Clay Bank sediment showed that w_s increased non-linearly with SSC in the range of 300–700 mg L^{-1}, and that turbulence can increase ws up to one order higher than w_s for nonturbulent conditions. This turbulence effect can explain why ws derived by ADV is 1 to 3 orders higher than w_s estimated by Owen tube where the ambient turbulence is totally blocked. When the turbulent shear stress was higher than about 0.14 Pa, however, it contributed to tear apart flocs and reduce w_s. This study suggests that ADV is a useful tool to concurrently measure the instantaneous current velocities, SSC and w_s in turbulence -dominant environments without breaking up flocs and disturbing ambient flow.

3-4 **Ha, Ho Kyung**, and 2 others. 2010. “Acoustic density measurements of consolidating cohesive sediment beds by means of a non-intrusive “Micro-Chirp” acoustic system”. *Geo-Marine Letters,* 30: 585-593.
doi: 10.1007/s00367-010-0206-y

A non-intrusive “Micro-Chirp” acoustic system and a signal-processing protocol have been developed to estimate the bulk density of consolidating cohesive sediment beds. Using high-frequency (300–700 kHz) Chirp acoustic waves, laboratory measurements were conducted with clay–water mixtures. Because acoustic echo strength is proportional to variations in acoustic impedance, and the speed of sound in the clay bed hardly changed during consolidation, the bulk density could be successfully estimated without disturbing the sediment bed. Based on acoustic signal analysis, this study demonstrates that the reflection coefficient and bulk density at the water–sediment interface increase with consolidation time, and that a single speed of sound value can be used for practical bulk density estimation in muddy environments.

3-5 Kim, Ja-Myung, Kitack Lee, **Eun Jin Yang**, and 11 others. 2010. “Enhanced Production of Oceanic Dimethylsulfide Resulting from CO_2-Induced Grazing Activity in a High CO_2 World”. *Environmental Science & Technology,* 44(21): 8140-8143.
doi: 10.1021/es102028k

Oceanic dimethylsulfide (DMS) released to the atmosphere affects the Earth's radiation budget through the production and growth of cloud condensation nuclei over the oceans. However, it is not yet known whether this negative climate feedback mechanism will intensify or weaken in oceans characterized by high CO_2 levels and warm temperatures. To investigate the effects of two emerging environmental threats (ocean acidification and warming) on marine DMS production, we performed a perturbation experiment in a coastal environment. Two sets of CO_2 and temperature conditions (a pCO_2 of ~900 ppmv at ambient temperature conditions, and a pCO_2 of ~900 ppmv at a temperature ~3 ℃ warmer than ambient) significantly stimulated the grazing rate and the growth rate of heterotrophic dinoflagellates (ubiquitous marine microzooplankton). The increased grazing rate resulted in considerableDMSproduction. Our results indicate that increased grazing-induced DMS production may occur in high CO_2 oceans in the future.

3-6 **Kim, Sun Young**, **Eun Jin Yang**, and 2 others. 2010. "Redescription of *Favella ehrenbergii* (Claparède and Lachmann, 1858) Jörgensen, 1924 (Ciliophora: Choreotrichia), with Phylogenetic Analyses Based on Small Subunit rRNA Gene Sequences". *The Journal of Eukaryotic Microbiology,* 57(6): 460-467. doi: 10.1111/j.1550-7408.2010.00500.x

The identification of *Favella ehrenbergii*, a marine planktonic ciliate, has largely been based on its lorica features. This approach is potentially problematic given the polymorphic lorica during this organism's life cycle. We isolated a population of *F. ehrenbergii* from the coastal waters of Incheon, Korea, and revealed its infraciliature using the protargol staining method. Phylogenetic analysis based on small subunit rRNA gene sequences was also performed. Results showed that this population possessed 16 collar membranelles (CM) and about 100 somatic kineties. These features are highly conserved, even in later dividers. As such, the number of CM and somatic kineties can be used as key characteristics for identification of *Favella* species.

3-7 **Lee, Sang H.**, and 2 others. 2010. "Comparison of bottom sea-ice algal characteristics from coastal and offshore regions in the Arctic Ocean". *Polar Biology,* 33: 1331-1337. doi: 10.1007/s00300-010-0820-1

Ice-core observations were conducted at three arctic sites in early April 2003: one clean sediment-free site (Chukchi), one sediment-rich site (Beaufort) on landfast sea ice offshore Barrow, and one oceanic Ice Exercise (ICEX) site. Concentrations of inorganic nutrients at coastal sites were similar to but higher than those at the oceanic site. Chlorophyll-*a* (Chl-*a*) concentration was much higher in the Chukchi bottom ice than at the other two sites. However, large size Chl-*a* (>20 μm) dominated (>70%) the bottom-ice algal Chl-*a* at both the Chukchi and Beaufort sites, whereas the oceanic ICEX site was evenly occupied by large (>20 μm), medium (5–20 μm), and small Chl-*a* (0.7–5 μm). These in situ data were incorporated into an ocean-ecosystem model. The model results revealed that: (1) strong light attenuation by trapped sediments controlled ice-algal production at the Beaufort site; (2) the peak in ice algae occurred later at the oceanic site than at the Chukchi site because of thicker ice and the consequently reduced amount of light reaching the ice algae at the ice bottom; and (3) maximum production at the oceanic site reached only 10% the level at the Chukchi site because of nutrient limitation.

3-8 **Lee, Sang H.**, and 2 others. 2010. "Uptake rates of dissolved inorganic carbon and nitrogen by under-ice phytoplankton in the Canada Basin in summer 2005". *Polar Biology,* 33: 1027-1036.
doi: 10.1007/s00300-010-0781-4

The Ocean Exploration cruise in June–July 2005 allowed detailed description of the in situ under-ice primary productivity of phytoplankton in the Canada Basin. On the basis of a ^{13}C–^{15}N dual isotope tracer technique, the estimated daily carbon production rate of under-ice phytoplankton ranged from 20.4 to 178.3 mg C m^{-2} day^{-1}, whereas the daily nitrogen production rate ranged from 5.5 to 50.9 mg N m^{-2} day^{-1}. These ranges are much higher than those recorded in previous studies, probably due to high seasonal and regional differences in the basin. Reduced nitrogen limitation for phytoplankton and the relative light attenuation through different sea-ice conditions may also be factors influencing the higher carbon and nitrogen uptake rates in 2005. Based on this study, new carbon production by phytoplankton growing beneath sea ice is estimated to range from 0.66 to 6.75 g C m^{-2} year^{-1}, indicating that 25.2–66.4% of total annual primary production might potentially be exported from the euphotic zone in the deep Canada Basin.

3-9 Lee, Yong-Woo, Hyun Je Park, **Eun Jung Choy**, and 2 others. 2010. "Temporal Variation of Phytoplankton Community Related to Water Column Structure in the Korea Strait". *Ocean and Polar Research,* 32(3): 321-329.
doi: 10.4217/OPR.2010.32.3.321

Photosynthetic pigments, nutrients, and hydrographic variables were examined in order to elucidate the spatio-temporal variation of water column structure and its effect on phytoplankton community structure in the western channel of the Korea Strait in fall 2006 and spring 2007. High phytoplankton biomass in the spring was associated with high salinity, implying that nutrients were not supplied by coastal waters or the Yangtze-River Diluted water (YRDW) with low salinity. Expansion of the Korea Strait Bottom Cold Water (KSBCW) and a cold eddy observed during the spring season might enhance the nutrient supply from the subsurface layer to the euphotic zone. Chemotaxonomic examination showed that diatoms accounted for 60-70% of total biomass, followed by dinoflagellates. Nutrient supply by physical phenomena such as the expansion of the KSBCW and the occurrence of a cold eddy appears to be the controlling factors of phytoplankton community composition in the Korea Strait. Further study is needed to elucidate the mechanisms by which the KSBCW is expanded, and its role in phytoplankton dynamics.

3-10 Notholt, J., G. C. Toon, S. Fueglistaler, P. O. Wennberg, F. W. Irion, M. McCarthy, M. Scharringhausen, **T. Siek Rhee**, and 2 others. 2010. "Trend in ice moistening the stratosphere – constraints from isotope data of water and methane". *Atmospheric Chemistry and Physics,* 10: 201-207.
doi: 10.5194/acp-10-201-2010

Water plays a major role in the chemistry and radiative budget of the stratosphere. Air enters the stratosphere predominantly in the tropics, where the very low temperatures around the tropopause constrain water vapour mixing ratios to a few parts per million. Observations of stratospheric water vapour show a large positive long-term trend, which can not be explained by change in tropopause temperatures. Trends in the partitioning between vapour and ice of water entering the stratosphere have been suggested to resolve this conundrum. We present measurements of stratospheric H$_2$O,

HDO, CH_4 and CH_3D in the period 1991–2007 to evaluate this hypothesis. Because of fractionation processes during phase changes, the hydrogen isotopic composition of H_2O is a sensitive indicator of changes in the partitioning of vapour and ice. We find that the seasonal variations of H_2O are mirrored in the variation of the ratio of HDO to H_2O with a slope of the correlation consistent with water entering the stratosphere mainly as vapour. The variability in the fractionation over the entire observation period is well explained by variations in H_2O. The isotopic data allow concluding that the trend in ice arising from particulate water is no more than (0.01±0.13) ppmv/decade in the observation period. Our observations suggest that between 1991 and 2007 the contribution from changes in particulate water transported through the tropopause plays only a minor role in altering in the amount of water entering the stratosphere.

3-11 Park, Jisoo, Im-Sang Oh, **Hyun-Cheol Kim**, and Sinjae Yoo. 2010. "Variability ofSeaWiFschlorophyll-*a* in the southwest Atlantic sector of the Southern Ocean: Strong topographic effects and weak seasonality". *Deep-Sea Research Ⅰ*, 57: 604-620. doi: 10.1016/j.dsr.2010.01.004

This study examined 11-year (1997–2008) weekly and monthly time series of satellite-observed ocean color to underst and the dominant temporal and spatial patterns of chlorophyll-*a* in the southwest Atlantic sector of the Southern Ocean. Using empirical orthogonal function analysis and *k*-means classification, we classified the study area into eight regions, which were in good accordance with the oceanographic and topographic features. Examination of the chlorophyll-*a* time series in each region revealed that contrary to our expectation, regular seasonal phytoplankton blooms were observed only in a limited area. Of the eight regions, only two showed typical seasonal blooms, and one showed weak seasonality, whereas other regions exhibited irregular seasonal blooms of variable duration. We attribute the absence of regularity in seasonal blooms to relatively shallow winter mixing, which would prevent entrainment of limiting micronutrients such as iron and silicate. In the southwest Atlantic sector of the Southern Ocean, topographic effects and sea ice maybe the most important factors controlling primary productivity. In the South Georgia region, chlorophyll-*a* showed a significant correlation with geostrophic current velocity, indicating that topographic effects depend on the interaction of current strength and topographic structure. Interannual variability of the surface chlorophyll in some regions also revealed longer periodicity(~6 years). The periodicity seemed to be related to El Niño–Southern Oscillation and to sea-ice dynamics influenced by the Antarctic Circumpolar Current.

3-12 Park, O. B. and **S. -I. Nam**. 2010. "Late Quaternary high-resolution stratigraphic reconstruction of the East Sea sediment cores based on high resolution images and color parameters". *Journal of the Geological Society of Korea,* 46(5): 439-452.

Using the 3-CCD (charge-coupled device) line scan camera equipped within the Avaatech XRF-Core Scanner, high resolution images and color parameters were estimated from the 3 sediment cores (05GCRP-13, 14, 15), which were taken from the western margin of the East Sea. Based on the high resolution images and color parameters, a precise stratigraphy can be established for the 3 sediment cores. For the establishment of a precise stratigraphy, lightness values (L*), AMS ^{14}C dating and 5 tephra layers deposited in the sediment core 05GCRP-15 are used to correlate with those data recorded in the core MD01-2407 which was retrieved from the Oki Ridge of the southeastern East Sea. According to the precise age model, the 3 investigated sediment cores are likely to represent the paleoceanographic record during the last about 94 ka BP (since the MIS 5.2). In particular, color parameters such L*, a* and b* can be used for the correlation between sediment cores recovered from the East Sea. Moreover, these color parameters are closely related with any chemical composition such as organic carbon and/or carbonate contents. Furthermore, the East Sea sediments that are characterized by alternations of dark and light layers seemed to well reflect the paleoceanographic changes during the late Quaternary glacial-interglacial cycles. These dark and light cycles on millennial scales are well matched the D-O (Dansgaard-Oeschger) cycles recorded in the NGRIP (North Greenland Ice Sheet Project) ice core $\delta^{18}O$ data. As a result, the high resolution images together with color parameters can be used as a reliable proxy for establishing a precise stratigraphy as well as the paleoceanographic reconstruction in the East Sea during the late Quaternary.

3-13 **Yang, Eun Jin**, and 2 others. 2010. “Feeding activity of the copepod *Acartia hongi* on phytoplanktonand micro-zooplankton in Gyeonggi Bay,Yellow Sea”. *Estuarine, Coastal and Shelf Science,* 88(2): 292-301. doi: 10.1016/j.ecss.2010.04.005

To improve our understanding of the trophic link between micro-zooplankton and copepods in Gyeonggi Bay, Yellow Sea, the diet composition, ingestion rates, and prey selectivity of *Acartia hongi*, known as the most abundant and widespread copepod species, was estimated byconducting *in situ* bottle incubation throughout the different seasons. The results showed that *A.hongi* preferentially grazed on ciliate and heterotrophic dinoflagellate of a size ranging from 20 to 100 μm rather than phytoplankton. Although micro-zooplankton comprised only an average 13.7% of the total carbon available in the natural prey pool, micro-zooplankton accounted for >70% ofthe total carbon ration ingested by *A.hongi* throughout the year, except for winter diatom blooming periods when *A.hongi* obtained about 60% of its carbon ration from phytoplankton. Our results demonstrated that *A.hongi* modified their diet composition and feeding rates in response to change in composition and size of prey available to them, and that *A.hongi* preferentially ingested micro-zooplankton over phytoplankton. Feeding activity of *A.hongi* could therefore affect the species composition and size structure of natural plankton communities in this study area, particularly the micro-zooplankton. Strongly selective feeding and high grazing pressure by *A.hongi* on micro-zooplankton shows the role of trophic coupling between copepods and the microbial food web in the pelagic ecosystem of Gyeonggi Bay.

PART 4

Life Sciences

4-1 Cho, Hyo Je Cho, Kyungsun Kim, Seo Yean Sohn, Ha Yeon Cho, Kyung Jin Kim, Myung Hee Kim, **Dockyu Kim**, and 2 others. 2010. “Substrate Binding Mechanism of a Type I Extradiol Dioxygenase”. *The Journal of Biological Chemistry,* 285(45): 34643-34652. doi: 10.1074/jbc.M110.130310

A *meta*-cleavage pathway for the aerobic degradation of aromatic hydrocarbons is catalyzed by extradiol dioxygenases via a two-step mechanism: catechol substrate binding and dioxygen incorporation. The binding of substrate triggers the release of water, thereby opening a coordination site for molecular oxygen. The crystal structures of AkbC, a type I extradiol dioxygenase, and the enzyme substrate (3-methylcatechol) complex revealed the substrate binding process of extradiol dioxygenase. AkbC is composed of an N-domain and an active C-domain, which contains iron coordinated by a 2-His-1-carboxylate facial triad motif. The C-domain includes a β-hairpin structure and a C-terminal tail. In substrate-bound AkbC, 3-methylcatechol interacts with the iron via a single hydroxyl group, which represents an intermediate stage in the substrate binding process. Structure-based mutagenesis revealed that the C-terminal tail and β-hairpin form part of the substrate binding pocket that is responsible for substrate specificity by blocking substrate entry. Once a substrate enters the active site, these structural elements also play a role in the correct positioning of the substrate. Based on the results presented here, a putative substrate binding mechanism is proposed.

4-2 Elvebakk, Arve, Eli Helene Robertsen, **Chae Haeng Park**, and **Soon Gyu Hong**. 2010. "*Psorophorus* and *Xanthopsoroma*, two new genera for yellow-green, corticolous and squamulose lichen species, previously in *Psoroma*". *The Lichenologist,* 42(5): 563-585. doi: 10.1017/S0024282910000083

Psoroma microlepideum is reduced to a synonym of *P. fuegiense*. The species differs in several characters from *P. pholidotum*, and it overlaps geographically with the latter, which is neotypified here. These two species are now placed in the new southern South American genus *Psorophorus*, differing from *Psoroma* s. str. in being corticolous, having adpressed squamules on a distinct, dark prothallus, lacking melanins, having a thin cortical layer and a simpler IKI+ apical ascus structure. Two other widespread, panaustral species are the only ones in *Pannariacae* containing usnic acid. The primarily fertile species has been known as *Psoroma pholidotoides*, but the type contains pannarin rather than usnic acid, and the correct name for the primarily fertile taxon with usnic acid is *Psoroma contextum* Stirt. This is together with *P. soccatum* R. Br. ex Crombie is now placed in the new genus *Xanthopsoroma*. In addition to usnic acid, both species have a series of distinct terpenoids, some in major quantities. Like *Psorophorus*, they are corticolous, but have long, more or less nodulose, apical perispore extensions, and an IKI+ apical ascus tube structure which is longer and thinner, including a diffuse tholus reaction, and often an external apical sheet. Phylogenetically, these two genera are shown to be monophyletic and different from *Psoroma* s. str. based on an analysis of ITS and nrLSU rDNA. This analysis also shows that among the ten species focused on in this study, nine species (two in *Xanthopsoroma*, two in *Psorophorus* and five in *Psoroma* s. str.) are monophyletic, based on two to six sequences of each species. *Psoroma hypnorum* remains polyphyletic. All names now belonging in *Psorophorus* and *Xanthopsoroma* are typified.

4-3 Gwak, In Gyu Gwak, Woong sic Jung, **Hak Jun Kim**, **Sung-Ho Kang**, and EonSeon Jin. 2010. "Antifreeze Protein in Antarctic Marine Diatom, *Chaetoceros neogracile*". *Marine Biotechnology,* 12(6): 630-639. doi: 10.1007/s10126-009-9250-x

The antifreeze protein gene (Cn-AFP) from the Antarctic marine diatom, *Chaetoceros neogracile* was cloned and characterized. The full-length Cn-AFP cDNA contained an open reading frame of 849 bp and the deduced 282 amino acid peptide chain encodes a 29.2 kDa protein, which includes a signal peptide of 30 amino acids at the N terminus. Both the *Cn-AFP* coding region with and without the signal sequence were cloned and expressed in *Escherichia coli*. Recombinant Cn-AFPs were shown to display antifreeze activities based on measuring the thermal hysteresis and modified morphology of single ice crystals.

Recombinant mature Cn-AFP showed 16-fold higher thermal hysteresis activity than that of pre-mature Cn-AFP at the same concentration. The ice crystal shape changed to an elongated hexagonal shape in the presence of the recombinant mature Cn-AFP, while single ice crystal showed a circular disk shape in absence of Cn-AFP. Northern analysis demonstrated a dramatic accumulation of *Cn-AFP* transcripts when the cells were subjected to freezing stress. This rapid response to freeze stress, and the antifreeze activity of recombinant Cn-AFPs, indicates that Cn-AFP plays an important role in low temperature adaptation.

4-4 Hong, Ji Won, **Han-Gu Choi, Sung-Ho Kang**, and Ho-Sung Yoon. 2010. "Axenic purification and cultivation of an Arctic cyanobacterium, *Nodularia spumigena* KNUA005, with cold tolerance potential for sustainable producetion of algae-based biofuel". *Algae,* 25(2): 99-104.
doi: 10.4490/algae.2010.25.2.099

A psychrotolerant cyanobacterium, *Nodularia spumigena* KNUA005, was isolated from a cyanobacterial bloom sample collected near Dasan Station in Ny-Ålesund, Svalbard Islands during the Arctic summer season. To generate an axenic culture, the isolate was subjected to three purification step: centrifugation, antibiotic treatment and streaking. The broad antibacterial spectrum of imipenem killed a wide range of heterotrophic bacteria, while the cyanobacterium was capable of enduring both antibiotics, the remaining contaminants that survived after treatment with imipenem were eliminated by the application of an aminoglycoside antibiotic, kanamycin. Physical separation by centrifugation and streaking techniques also aided axenic culture production. According to the cold-tolerance test, this mat-forming cyanobacterium was able to proliferate at low temperatures ranging between 15 and 20 ℃ which indicates the presence of cold-tolerance related genes in *N. spumigena* KNUA005. This suggests the possibility of incorporating cold-resistance gene into indigenous cyanobacterial strains for the consistent production of algae-based biofuel during the low-temperature seasons. Therefore, it is needed to determine the cold-tolerance mechanisms in the Arctic cyanobacterium in the next research stage.

4-5 Hwang, Dae-Sik, Jin-Seon Lee, Jae-Sung Rhee, Jeonghoon Han, Young-Mi Lee, **Il-Chan Kim**, and 3 others. 2010. "Modulation of *p*53 gene expression in the intertidal copepod *Tigriopus japonicus* exposed to alkylphenols". *Marine Environmental Research,* 69: S77-S80.
doi: 10.1016/j.marenvres.2009.12.002

The copepod, *Tigriopus japonicus* has been recognized as an excellent marine model species for ecotoxicological studies. The present study cloned and characterized the *p*53 gene of this copepod and studied its expression pattern. We discovered that *p*53 expression patterns varied among different developmental stages of the copepod, having the highest expression in the adult. Such variation was possibly associated with the molting cycle. By using real-time RT-PCR, we further investigated the modulatory pattern of the *p*53 gene in the copepod after exposure to three alkylphenols (i.e. nonylphenol, octylphenol, and bisphenol A) which are known as endocrine disruption chemicals (EDCs). The results showed that the three alkylphenols significantly induced p53 gene expression in the copepod, indicating the involvement of *p*53 in such stress-responses. Thus, the copepod *p*53 gene provides one of the stress-response biomarkers for exposure to EDC-like compounds.

4-6 Hyun, Seunghun, **Hyun Park**, and 3 others. 2010. "Fluxes of PAHs from coal tar-impacted river sediment under variable seepage rates". *Chemosphere,* 80: 1261-1267.
doi: 10.1016/j.chemosphere.2010.06.064

The flux of several polycyclic aromatic hydrocarbons (PAHs) from coal tar-impacted river sediment was measured under various seepage rates in a laboratory scale. The batch PAH equilibrium data between aqueous phase (C_{eq}) and sediment phase was well-explained using a Raoult's law approach. In the flux measurement from column study, the steady-state PAH concentrations (C^{∞}) in the effluent solution were affected by a time-dependent nonequilibrium process; the seepage velocity was inversely proportional to the C^{∞} of PAH in the effluents. With a high seepage velocity of 4.06 cm d^{-1}, a large initial concentration was observed, possibly due to the greater disparity between C^{∞} and C_{eq}. This initial-flush export leveled off after a few pore volumes had been displaced. The chemical flux pattern of PAH was conceptually depicted by superimposing two analytical solutions, such as a slug lease followed by rate-limited solute lease. Under quiescent conditions, the sediment pore-water reached dissolution equilibrium with the solid phase. However, under dynamic groundwater seepage conditions, the seepage water flowing through sediment pores did not reach dissolution equilibrium, which was evidence of nonequilibrium dissolution. In conclusion, the mass flux of PAHs from coal tar-impacted sediment is determined by concurrent effect of the groundwater seepage rate and rate-limited PAH concentration in seepage water.

4-7 Jung, Ha Yun, Kyung Ha Kim, Ji Hye Hyoung, Mi Ra Han, Hyun Kyoung Kim, Ki Jeung Lee, Yangmee Kim, **Hak Jun Kim**, and Yong-Seok Heo. 2010. "Preliminary X-ray crystallographic analysis of the breakage–reunion domain of the GyrA subunit of DNA gyrase from *Colwellia psychrerythraea* strain 34H". *Acta Crystallographica Section F,* 66: 439-441.
doi: 10.1107/S1744309110005567

DNA gyrase is a type Ⅱ topoisomerase that is essential for chromosome segregation and cell division owing to its ability to modify the topological forms of bacterial DNA. In this study, the N-terminal breakage–reunion domain of the GyrA subunit of DNA gyrase from *Colwellia psychrerythraea* 34H was overexpressed in *Escherichia coli*, purified and crystallized. Diffraction data were collected to 2.60 Å resolution using a synchrotron radiation source. The crystal belonged to space group $P2_12_12_1$, with unit-cell parameters a = 98.98, b = 101.56, c = 141.83 Å. The asymmetric unit contained two molecules, with a corresponding V_M of 3.18 $Å^3$ Da^{-1} and a solvent content of 59.9%.

4-8 **Jung, Min Gui**, Key Pyoung Lee, **Han-Gu Choi**, **Sung-Ho Kang**, and 3 others. 2010. "Characterization of carbohydrate combining sites of Bryohealin, an algal lectin from *Bryopsis plumosa*". *Journal of Applied Phycology,* 22(6): 793-802.
doi: 10.1007/s10811-010-9521-y

Bryohealin is a lectin involved in the wound-healing process of the marine green alga *Bryopsis plumosa*. In the previous purification study, it has been shown that lectin was composed of two identical subunits of 27 kDa, cross-linked by disulfide bond, and showed binding specificity to *N*-acetyl-ᴅ-glucosamine and *N*-acetyl-ᴅ-galactosamine (GlcNAc and GalNAc, respectively). To determine if the lectin recognize the two different sugars at the same binding domain, the carbohydrate binding sites of Bryohealin was analyzed using chromatography and chemical modification methods. Results showed that the same binding site of the lectin was responsible for the recognition of two sugars, GalNAc as well as GlcNAc. Chemical modification studies showed that hemagglutinating activities of Bryohealin were not affected by modification of histidine, tryptophan, aspartic acid, and glutamic acid. When arginine residues were modified with 1,2-cyclohexanedione, the activity of Bryohealin rapidly decreased. The sugar binding sites remained intact when the lectin was treated with inhibitory sugars (0.2 M GalNAc and/or GlcNAc) prior to 1,2-cyclohexanedione treatment. The sugar binding domain of Bryohealin was predicted from the MALDI-TOF analysis and the full cDNA sequence of the lectin gene.

4-9 Jung, Youn Hong, Ji-Yeun Yi, **Hyun Jung Jung**, **Yoo Kyung Lee**, **Hong Kum Lee**, and 5 others. 2010. “Overexpression of Cold Shock Protein A of *Psychromonas arctica* KOPRI 22215 Confers Cold-Resistance”. *The Protein Journal,* 29: 136-142.
doi: 10.1007/s10930-010-9233-9

A polar bacterium was isolated from Arctic sea sediments and identified as *Psychromonas artica*, based on 16S rDNA sequence. *Psychromonas artica* KOPRI 22215 has an optimal growth temperature of 10 ℃ and a maximum growth temperature of 25 ℃, suggesting this bacterium is a psychrophile. Cold shock proteins (Csps) are induced upon temperature downshift by more than 10 ℃. Functional studies have researched mostly Csps of a mesophilic bacterium *Escherichia coli*, but not on those of psychrophilic bacteria. In an effort to understand the molecular mechanisms of psychrophilic bacteria that allow it withstand freezing environments, we cloned a gene encoding a cold shock protein from *P. artica* KOPRI 22215 ($CspA_{Pa}$) using the conserved sequences in *csp* genes. The 204 bp-long ORF encoded a protein of 68 amino acids, sharing 56% homology to previously reported *E. coli* CspA protein. When $CspA_{Pa}$ was overexpressed in *E. coli*, it caused cell growth-retardation and morphological elongation. Interestingly, overexpression of $CspA_{Pa}$ drastically increased the host’s cold-resistance by more than ten times, suggesting the protein aids survival in polar environments.

4-10 Kang, Chang Duk, **Se Jong Han**, and 2 others. 2010. “Fed-batch culture of astaxanthin-rich *Haematococcus pluvialis* by exponential nutrient feeding and stepwise light supplementation”. *Bioprocess and Biosystems Engineering,* 33: 133-139.
doi: 10.1007/s00449-009-0362-5

A fed-batch culture process followed by subsequent photoautotrophic induction was established for the high density culture of astaxanthin-rich *Haematococcus pluvialis* using a CO_2-fed flat type photobioreactor under unsynchronized illumination. Fed-batch culture was performed with an exponential feeding strategy of the growthlimiting nutrients, nitrate and phosphate, concurrently with the stepwise supplementation of light depending on the cell concentration.During the growth phase, a biomass of 1.47 g/L was obtained at a biomass productivity of 0.33 g/L/day. Photoautotrophic induction of the well-grown vegetative cells was performed consecutively by increasing the light intensity to 400 μmol photon/m^2/s, while keeping the other conditions in the CO_2-fed flat type photobioreactor fixed, yielding an astaxanthin production of 190 mg/L at an astaxanthin productivity of 14 mg/L/day. The proposed sequential photoautotrophic process has high potential as simple and productive process for the production of valuable *Haematococcus* astaxanthin.

4-11 Ki, Jang-Seu, Haakon Hop, Se-Joo Kim, **Il-Chan Kim**, and 2 others. 2010. “Complete mitochondrial genome sequence of the Arctic gammarid, *Onisimus nanseni* (Crustacea; Amphipoda): Novel gene structures and unusual control region features”. *Comparative Biochemistry and Physiology, Part D,* 5: 105-115.
doi: 10.1016/j.cbd.2010.02.002

To analyze the mitogenome of the amphipod Onisimus nanseni, we amplified the complete mitogenome of *O. nanseni* using long-PCR and genome walking techniques. The mitogenome of *O. nanseni* is circular and contains all the typical mt genes (2 rRNAs, 22 tRNAs, and 13 protein-coding genes). It has two peculiar noncoding regions of 148 bp and 194 bp. The latter can be involved in replication and termination processes. The total length of the pooled protein-coding, rRNA, and tRNA genes is shorter than those of other crustaceans. In addition, the intergenic spacers of the *O. nanseni* mitogenome are considerably shorter in length than those of other crustaceans. Fourteen adjacent genes overlap, resulting in a compact mitogenomic structure. In the *O. nanseni* mitogenome, the AT composition is elevated, particularly in the control regions (78.9% AT), as has been demonstrated for two other amphipods. The tRNA order is highly rearranged compared to other arthropod mitogenomes, but the order of protein-coding genes and rRNAs is largely conserved. The gene cluster between the *CO1* and *CO3* genes is completely conserved among all amphipods compared. This provides insights into the evolution and gene structures of crustacean mitochondrial genomes, particularly in amphipods.

4-12 **Kim, Dockyu**, and 5 others. 2010. “Aromatic Hydroxylation of Indan by *o*-Xylene-Degrading *Rhodococcus* sp. Strain DK17”. Applied and Environmental Microbiology*,* 76(1): 375-377.
doi: 10.1128/AEM.01745-09

The metabolically versatile *Rhodococcus* sp. strain DK17 utilizes indan as a growth substrate via the *o*-xylene pathway. Metabolite and reverse transcription-PCR analyses indicate that *o*-xylene dioxygenase hydroxylates indan at the 4,5 position of the aromatic moiety to form *cis*-indan-4,5-dihydrodiol, which is dehydrogenated to 4,5-indandiol by a dehydrogenase. 4,5-Indandiol undergoes ring cleavage by a *meta*-cleavage dioxygenase.

4-13 **Kim, Dockyu**, and 7 others. 2010. “Benzylic and aryl hydroxylations of *m*-xylene by *o*-xylene dioxygenase from *Rhodococcus* sp. strain DK17”. *Applied Microbiology and Biotechnology,* 86(6): 1841-1847.
doi: 10.1007/s00253-009-2418-5

Escherichia coli cells expressing *Rhodococcus* DK17 *o*-xylene dioxygenase genes were used for bioconversion of *m*-xylene. Gas chromatography-mass spectrometry analysis of the oxidation products detected 3 methylbenzylalcohol and 2,4-dimethylphenol in the ratio 9:1. Molecular modeling suggests that *o*-xylene dioxygenase can hold xylene isomers at a kink region between α6 and α7 helices of the active site and α9 helix covers the substrates. *m*-Xylene is unlikely to locate at the active site with a methyl group facing the kink region because this configuration would not fit within the substrate-binding pocket. The *m*-xylene molecule can flip horizontally to expose the *meta*-position methyl group to the catalytic motif. In this configuration, 3 methylbenzylalcohol could be formed, presumably due to the *meta* effect. Alternatively, the *m*-xylene molecule can rotate counterclockwise, allowing the catalytic motif to hydroxylate at C-4 yielding 2,4-dimethylphenol. Site-directed mutagenesis combined with structural and functional analyses suggests that the alanine-218 and the aspartic acid-262 in the α7 and the α9 helices play an important role in positioning *m*-xylene, respectively.

4-14 **Kim, Dockyu**, **Ha Ju Park**, **Yung Mi Lee**, **Soon Gyu Hong**, **Hong Kum Lee**, and **Joung Han Yim**. 2010. “Screening for Cold-Active Protease-Producing Bacteria from the Culture Collection of Polar Microorganisms and Characterization of Proteolytic Activities”. *The Korean Journal of Microbiology,* 46(1): 73-79.

The Korea Polar Research Institute (KOPRI) has assembled a culture collection of cold-adapted bacterial strains from both the Arctic and Antarctic. To identify excellent protease-producers among the proteolytic bacterial collection (874 strains), 78 strains were selected in advance according to their relative activities and were subsequently re-examined for their extracellular protease activity on 0.1×ZoBell plates supplemented with 1% skim milk at various temperatures. This rapid and direct screening method permitted the selection of a small group of 15 cold-adapted bacterial strains, belonging to either the genus *Pseudoalteromonas* (13 strains) or *Flavobacterium* (2 strains), that showed proteolytic activities at temperatures ranging between 5–15℃. The cold-active proteases from these strains were classified into four categories (serine protease, aspartic protease, cysteine protease, and metalloprotease) according to the extent of enzymatic inhibition by a class-specific protease inhibitor. Since highly active and/or cold-adapted proteases have the potential for industrial or commercial enzyme development, the protease-producing bacteria selected in this work will be studied as a valuable natural source of new proteases. Our results also highlight the relevance of the Antarctic for the isolation of protease-producing bacteria active at low temperatures.

4-15 **Kim, Eun Hye**, **Kyeung Hee Cho**, **Yung Mi Lee**, **Joung Han Yim**, **Hong Kum Lee**, Jang-Cheon Cho, and **Soon Gyu Hong**. 2010. “Diversity of Cold-Active Protease-Producing Bacteria from Arctic Terrestrial and Marine Environments Revealed by Enrichment Culture”. *The Journal of Microbiology,* 48(4): 426-432.
doi: 10.1007/s12275-010-0015-z

A new approach for enrichment culture was applied to obtain cold-active protease-producing bacteria for marine and terrestrial samples from Svalbard, Norway. The method was developed for the enrichment of bacteria by long-term incubation at low temperatures in semi-solid agar medium containing meat pieces as the main source of carbon and energy. ZoBell and 0.1x nutrient broth were added for marine and terrestrial microorganisms, respectively, to supply basal elements for growth. One to three types of colonies were observed from each enrichment culture, indicating that specific bacterial species were enriched during the experimental conditions. Among 89 bacterial isolates, protease activity was observed from 48 isolates in the screening media containing skim milk. Good growth was observed at 4℃ and 10℃ while none of the isolates could grow at 37℃. At low temperatures, enzyme activity was equal to or higher than activity at higher temperatures. Bacterial isolates were included in the genera *Pseudoalteromonas* (33 isolates), *Arthrobacter* (24 isolates), *Pseudomonas* (16 isolates), *Psychrobacter* (6 isolates), *Sphingobacterium* (6 isolates), *Flavobacterium* (2 isolates), *Sporosarcina* (1 isolate), and *Stenotrophomonas* (1 isolate). Protease activity was observed from *Pseudoalteromonas* (33 isolates), *Pseudomonas* (10 isolates), *Arthrobacter* (4 isolates), and *Flavobacterium* (1 isolate).

4-16 Kim, Ho Bang, **Hyoungseok Lee**, and 9 others. 2010. “Postembryonic Seedling Lethality in the Sterol-Deficient Arabidopsis *cyp*51A2 Mutant Is Partially Mediated by the Composite Action of Ethylene and Reactive Oxygen Species”. *Plant Physiology,* 152: 192-205.
doi: 10.1104/pp.109.149088

Seedling-lethal phenotypes of Arabidopsis (*Arabidopsis thaliana*) mutants that are defective in early steps in the sterol biosynthetic pathway are not rescued by the exogenous application of brassinosteroids. The detailed molecular and physiological mechanisms of seedling lethality have yet to be understood. Thus, to elucidate the underlying mechanism of lethality, we analyzed transcriptome and proteome profiles of the *cyp51A2* mutant that is defective in sterol 14*a*-demethylation. Results revealed that the expression levels of genes involved in ethylene biosynthesis/signaling and detoxification of reactive oxygen species (ROS) increased in the mutant compared with the wild type and, thereby, that the endogenous ethylene level also increased in the mutant. Consistently, the seedling-lethal phenotype of the *cyp51A2* mutant was partly attenuated by the inhibition of ethylene biosynthesis or signaling. However, photosynthesis-related genes including Rubisco large subunit, chlorophyll *a/b*-binding protein, and components of photosystems were transcriptionally and/or translationally downregulated in the mutant, accompanied by the transformation of chloroplasts into gerontoplasts and a reduction in both chlorophyll contents and photosynthetic activity. These characteristics observed in the *cyp51A2* mutant resemble those of leaf senescence. Nitroblue tetrazolium staining data revealed that the mutant was under oxidative stress due to the accumulation of ROS, a key factor controlling both programmed cell death and ethylene production. Our results suggest that changes in membrane sterol contents and composition in the *cyp51A2* mutant trigger the generation of ROS and ethylene and eventually induce premature seedling senescence.

4-17 **Kim, Jeong-Hoon**, **Hyoun Soo Lim**, **In-Young Ahn**, Sang-Hwan Lee, MinKyun Kim, and **Hyun Park**. 2010. “Polychlorinated biphenyl congeners in Antarctic biota from the Barton Peninsula, King George Island”. *Antarctic Science,* 22(3): 283-284.
doi: 10.1017/S0954102010000052

Although Antarctica is largely pristine, relatively volatile persistent organic pollutants (POPs) can be carried there by long-range atmospheric transport (Risebrough *et al.* 1976). Their highly lipophilic and persistent nature allows ready accumulation in organisms and subsequent biomagnification through the food web. Here, we describe the distribution and concentration profiles of dioxin-like PCB congeners, and estimate transference rates through the food web in various Antarctic organisms.

4-18 **Kim, Jeong-Hoon**, **Hyun Park**, **Eun Jung Choy**, **In-Young Ahn**, and Jeong-Chil Yoo. 2010. “Incubation capacity limits clutch size in south polar skuas”. *Antarctic Science,* 22(1): 19-24.
doi: 10.1017/S0954102009990393

The incubation-limitation hypothesis suggests that clutch size in some birds is limited by incubation capacity. However, this remains disputed amongst ornithologists. This study aimed to test whether incubation capacity limits the maximum clutch size to two eggs in south polar skuas (*Catharacta maccormicki* Saunders) by comparing the egg and nest temperatures as well as hatchability between two-egg and three-egg clutches.

Although the vast majority of clutches contained one or two eggs, four naturally occurring three-egg clutches were found at Barton Peninsula, King George Island over three breeding seasons (2004–2005, 2005–2006 and 2006–2007). Regardless of clutch size, all incubating parents exhibited two discernible brood patches. The mean egg and nest temperatures of the three-egg clutches were significantly lower than were those of the two-egg clutches. The accumulated time that egg temperature decreased below 30℃ in three-egg clutches was approximately eight times longer than that in two-egg clutches. The hatchability of natural one-egg (89.5%) and two-egg clutches (95.4%) were significantly higher than that of the three-egg clutches, which was zero. Our results suggest that the maximum clutch size in south polar skuas is probably restricted by incubation capacity.

4-19 Kim, Jun Pyo, Kyoung-Rok Kim, Seung Phill Choi, **Se Jong Han**, and 2 others. 2010. “Repeated production of hydrogen by sulfate re-addition in sulfur deprived culture of *Chlamydomonas reinhardtii*”. *International Journal of Hydrogen Energy,* 35(24): 13387-13391. doi: 10.1016/j.ijhydene.2009.11.113

Biological hydrogen production by the green alga, *Chlamydomonas reinhardtii* can be induced in conditions of sulfur deprivation. In this study, we investigated the repeated and enhanced hydrogen production afforded by the re-addition of sulfate with monitoring of pH and concentration of chlorophyll and sulfate. Without adjustment of the pH, the optimal concentration of re-added sulfate was 30 μM for the hydrogen production. By the re-addition of 30 μM of sulfate and the adjustment of the pH during 4 cycles of repeated production, we obtained the maximum amount of 789 ml $H_2\,l^{-1}$ culture, which is 3.4 times higher than that of one batch production without adjustment of pH, 236 ml $H_2\,l^{-1}$ culture. This means that the enhancement of the hydrogen production can be achieved by the careful control of the sulfate re-addition and pH adjustment in the sulfur deprived culture.

4-20 Klochkova, Tatyana A., Gwang Hoon Kim, Kyung Min Lee, **Han-Gu Choi**, and 2 others. 2010. “Brown algae (Phaeophyceae) from Russian Far Eastern seas: re-evaluation of *Laminaria multiplicata* Petrov et Suchovejeva”. *Algae,* 25(2): 77-87. doi: 10.4490/algae.2010.25.2.077

Eight unusual individuals of a laminariaceaen species were collected from the Sea of Okhotsk in 1974 and described as a new species, *Laminaria multiplicata* Petrov et Suchovejeva in 1976. Since that time no new information, including pictures and numerical data, has been provided, although the species was cited in floristic lists of the Sea of Okhotsk based on the first record in 1976. We investigated a type and 3 paratypes of *L. multiplicata* and strongly believe that they were wrongfully identified abnormal plants of *L. gurjanovae* A. Zinova. Therefore, the species *L. multiplicata* needs to be closed.

4-21 Koehler, Julia, Endah S. Sulistijo, Masayoshi Sakakura, **Hak Jun Kim**, and 2 others. 2010. “Lysophospholipid Micelles Sustain the Stability and Catalytic Activity of Diacylglycerol Kinase in the Absence of Lipids”. *Biochemistry,* 49(33): 7089-7099. doi: 10.1021/bi100575s

There has been a renewal of interest in interactions of membrane proteins with detergents and lipids, sparked both by recent results that illuminate the structural details of these interactions and also by the realization that some experimental membrane protein structures are distorted by detergent-protein interactions. The integral membrane enzyme diacyglycerol kinase (DAGK) has long been thought to require the presence of lipid as an obligate “cofactor” in order to be catalytically viable in micelles. Here, we report that near-optimal catalytic properties are observed for DAGK in micelles composed of lyso-myristoylphosphatidylcholine (LMPC), with significant activity also being observed in micelles composed of lysomyristoylphosphatidylglycerol and tetradecylphosphocholine. All three of these detergents were also sustained high stability of the enzyme. NMR measurements revealed significant differences in DAGK-detergent interactions involving LMPC micelles versus micelles composed of dodecylphosphocholine. These results highlight the fact that some integral membrane proteins can maintain native-like properties in lipid-free detergent micelles and also suggest that C_{14}-based detergents may be worthy of more widespread use in studies of membrane proteins.

4-22 Kwon, Se Chang, Gwan Sun Lee, Jae Yong Han, Michael Lee, **Young-Mi Lee**, and 2 others. 2010. “Genotoxicity studies on HM10760A, recombinant human erythropoietin conjugated to globin fragment”. *Drug and Chemical Toxicology,* 33(2): 152-159. doi: 10.3109/01480540903196824

HM10760A is a recombinant human erythropoietin chemically conjugated to the N-terminus of human immunoglobulin Fc fragment through a polyethylene glycol linker. HM10760A was shown to have a relatively long half-life, compared with unconjugated recombinant erythropoietin. In this study, the genotoxicity of HM10760A was investigated by using a test battery of three different methods. In the Ames assay, five strains (TA100, TA1535, TA98, TA1537, and *Escherichia coli* WP2 *uvrA*) were tested at six concentrations of 3.13, 6.25, 12.5, 25, 50, and 100 μg/plate. HM10760A did not increase the number of revertant colonies in any tester strains with and without metabolic activation by rat-liver S9 mix. Subsequently, *in vitro* chromosomal aberration test, using Chinese hamster lung cells, were conducted at the concentrations of 25, 50, and 100 μg/mL. HM10760A did not induce chromosomal aberrations either in the short-period (6 hours) test with or without rat-liver S9 mix or in the continuous-treatment (24 hours) test. In the *in vivo* bone marrow micronucleus assay using the male ICR (imprinting control region) mouse, HM10760A was subcutaneously administered twice at 24-hour intervals at doses of 0, 150, 300, and 600 μg/kg. HM10760A produced a slight, but statistically significant, increase in the frequency of micronucleated polychromatic erythrocytes at 600 μg/kg. However, no biological significance was assumed, because this value was within the historical control range. From these findings obtained from the genotoxicity assays performed in this study, it appears unlikely that HM10760A acts as a genotoxic agent *in vitro* and *in vivo*.

4-23 **Lee, Hyoung Seok**, **Ji Hyun Kim**, **MiRa Park**, **Il-Chan Kim**, **Joung Han Yim**, and **Hong Kum Lee**. 2010. “Reference gene validation for qPCR normalization in *Deschampsia antarctica* during abiotic stresses”. *Antarctic Science,* 22(5): 477-484. doi: 10.1017/S0954102010000428

Quantitative real time PCR is the most sensitive and widely used method for the analysis of gene expression. The choice of one or several reference genes is very important for a normalization process, which should not fluctuate under stress conditions, to reduce error rate and bias during experimental procedure. In the present study, the expression stability of nine reference genes (two actins, two tubulins, two elongation factor 1a, two ubiquitins, and cyclophilin) during abiotic stresses such as cold, salt, and PEG treatments, was evaluated on *Deschampsia antarctica* plants using geNorm software. Results from various experimental conditions indicated that cyclophilin and elongation factor 1*a* were the most stable genes in the leaf and the root, respectively. The expression of the other reference genes varied under stress. The relative quantification of the TACR7 gene varied according to the kind and the number of reference genes used, suggesting the importance of considering the implications of a combination of reference genes under different stress conditions and in different tissues.

4-24 Lee, Jae-Seong, Jae-Sung Rhee, Ryeo-Ok Kim, Dae-Sik Hwang, Jeonghoon Han, Beom-Soon Choi, Gyung Soo Park, **Il-Chan Kim**, and 2 others. 2010. "The copepod *Tigriopus japonicus* genomic DNA information (574 Mb) and molecular anatomy". *Marine Environmental Research,* 69: S21-S23.
doi: 10.1016/j.marenvres.2009.12.003

The intertidal copepod, *Tigriopus japonicus*, has been recognized as a promising model species for marine environmental genomics. To obtain extensive genomic DNA sequences from this species, we sequenced genomic DNA from adult copepods using genomic sequencers GS-FLX and GS-FLX-Titanium and attained 1,914,995 reads (average read length 299.8 bp) including 574.2 Mb of genomic DNA information. After subjecting them to assembly, we acquired 193,642 contigs (total contigs length 129.7 Mb), and finally were able to obtain 10,894 unigenes (*E*-value > 0.1; length > 200 bp) containing 33,081,455 bp after a nonredundant (NR) blast search. In this paper, we summarize the genomic DNA sequences of *T. japonicus* and discuss its potential use in environmental genomics and ecotoxicological studies for uncovering mechanisms of environmental stresses and chemical toxicities to marine crustaceans.

4-25 **Lee, Jong Kyu**, **Kyoung Sun Park**, **Seungil Park**, **Hyun Park**, Young Hwan Song, **Sung-Ho Kang**, and **Hak Jun Kim**. 2010. "An extracellular ice-binding glycoprotein from an Arctic psychrophilic yeast". *Cryobiology,* 60: 222-228.
doi: 10.1016/j.cryobiol.2010.01.002

A psychrophilic yeast was isolated from an Arctic pond and its culture supernatant showed ice-binding activity. This isolate, identified as *Leucosporidium* sp. based on an analysis of the D1/D2 and ITS regions of its ribosomal DNA, produced a secretory ice-binding protein (IBP). Yeast IBP was purified from the culture medium to near homogeneity by the ice affinity method and appeared to be glycosylated with a molecular mass of ~26 kDa. In addition, the yeast IBP was shown to have thermal hysteresis (TH) and recrystallization inhibition (RI) activities. The full-length cDNA for yeast IBP was determined and was found to encode a 261 amino acid protein with molecular weight of 26.8 kDa that includes an N-terminal signal peptide and one potential N-glycosylation site. The deduced protein showed high sequence identity with other IBPs and hypothetical IBPs from fungi, diatoms, and bacteria, clustering with a class of iceactive proteins.

4-26 Lee, Soo Young, Ha Yun Jung, Tae-O Kim, Dong-Won Im, Ki-Young You, Jang-Mi Back, Yangmee Kim, **Hak Jun Kim**, and 2 others. 2010. "Cloning, purification, crystallization and preliminary X-ray crystallographic analysis of the N-terminal domain of DEAD-box RNA helicase from *Staphylococcus aureus* strain Mu50". *Acta Crystallographica Section F,* 66: 1674-1676.
doi: 10.1107/S1744309110043149

DEAD-box helicases are enzymes with an ATP-dependent RNA-unwinding function that are involved in a variety of cellular processes including RNA splicing, ribosome biogenesis and RNA degradation. In this study, the N-terminal domain of DEAD-box RNA helicase from *Staphylococcus aureus* strain Mu50 was overexpressed in *Escherichia coli,* purified and crystallized. Diffraction data were collected to 2.60 Å resolution using a synchrotronradiation source. The crystal belonged to space group P1, with unit-cell parameters a = 70.81, b = 80.23, c = 86.25 Å, α = 69.54, β = 66.54, γ = 87.32°. The unit cell contained six molecules, with a corresponding V_M of 2.91 Å^3 Da^{-1} and a solvent content of 56.1%.

4-27 **Lee, Sung Gu**, **Hye Yeon Koh**, Hyuncheol Oh, **Se Jong Han**, **Il-Chan Kim**, **Hong Kum Lee**, and **Joung Han Yim**. 2010. “Human dermal fibroblast proliferation activity of usimine-C from Antarctic lichen *Ramalina terebrata*”. *Biotechnology Letters,* 32(4): 471-475. doi: 10.1007/s10529-009-0191-2

Type I collagen is the major structural protein in dermis and its presence is used to monitor skin cell proliferation and aging. Recently, novel usimine compounds have been found in the Antarctic lichen *Ramalina terebrata*. In the present study, usimine-C induced cell proliferation of human dermal fibroblast, CCD-986SK, up to 1.6-fold after treating with 90 lg/ml for 48 h. Type I procollagen synthesis was significantly increased 1.3-fold, 3-fold, and 5-fold after treating with 0.14, 0.72, and 3.6 μg usimine-C/ml for 24 h, respectively, whereas no significant increase in type I procollagen was observed after treating with usimine-A or -B. Usimines are usnic acid derivatives. Considering that the difference among the derivatives is a side chain, the proliferation activity may be related to this side chain, triggering an internal signal for type I procollagen expression. Further studies still remain to clarify the signaling pathways for the type I procollagen induction, which is activated by usimine-C.

4-28 **Lee, Sung Gu**, **Hye Yeon Koh**, **Se Jong Han**, **Heeyong Park**, **Deuk Chae Na**, **Il-Chan Kim**, **Hong Kum Lee**, and **Joung Han Yim**. 2010. “Expression of recombinant endochitinase from the Antarctic bacterium, *Sanguibacter antarcticus* KOPRI 21702 in *Pichia pastoris* by codon optimization”. *Protein Expression and Purification,* 71: 108-114. doi: 10.1016/j.pep.2010.01.017

An endochitinase was previously purified and the gene was cloned from the psychrophilic Antarctic bacterium, *Sanguibacter antarcticus* (KCTC 13143). In the present study, recombinant endochitinase, rChi21702, was expressed using a yeast expression system (*Pichia pastoris*) and codon optimization. The expressed rChi21702 was purified by Phenyl-Sepharose column chromatography. Optimal expression yielded 1-mg purified enzyme from 1-L bioreactor culture. When p-NP-(GlcNAc)$_2$ was used as a substrate, the specific activity of the enzyme was determined to be 20 U/mg. In vitro assays and thin-layer chromatography demonstrated that the recombinant enzyme has endochitinase activity that produces diacetyl-chitobiose as a dominant end product when chitooligomers, colloidal chitin, and the chromogenic p-NP-(GlcNAc)$_2$ are used as substrates. Optimal activity for rChi21702 was observed at 37 ℃ and a pH of 7.6. Interestingly, rChi21702 exhibited 63% of optimal activity at 10 ℃ and 44% activity at 0 ℃. Taken together, the results indicate that rChi21702 has psychrotolerant endochitinase activity even after recombinant expression in yeast cells.

4-29 Liu, Shenghao, **Hyoungseok Lee**, Pil-Sung Kang, Xiaohang Huang, **Joung Han Yim**, **Hong Kum Lee**, and **Il-Chan Kim**. 2010. "Complementary DNA library construction and expressed sequence tag analysis of an Arctic moss, *Aulacomnium turgidum*". *Polar Biology,* 33(5): 617-626.
doi: 10.1007/s00300-009-0737-8

Unique physiological and metabolic properties of Arctic mosses are responsible for their acclimation to the inclement polar environment. To perform transcriptome analysis of an Arctic moss species adapted to polar conditions, we constructed a complementary DNA (cDNA) library using total high-quality RNA extracted from the moss species *Aulacomnium turgidum*. The library consisted of 1.81 × 10^6 of independent clones with 97.41% of recombinants. A total of 509 cDNA clones were sequenced. After eliminating poor quality sequences, vector trimming and clustering, 360 unigenes consisting of 33 contigs and 327 singletons were identified. Basic Local Alignment Search Tool X searches generated 245 significant hits (E value $<10^{-5}$). For further Gene Ontology analysis, 158 unigenes were annotated and classified with terms for molecular function, biological process and cellular component. Among the expressed sequence tags, seven genes were selected based on their putative roles in stress response, and they showed enhanced transcripts level under various abiotic stresses such as low temperature, heat and high-salinity. Also, two rare-cold-inducible genes showed different expression patterns under low temperature and UV-B treatment, indicating their distinct roles in adaptation to Arctic environment. Although experiments have been conducted on a limited scale, this study provides useful information for better understanding the mechanism of stress acclimation of polar mosses and material basis for potential genomic modification for higher plants to increase stress tolerance.

4-30 Nan, Yong Hai, Sung Haeng Lee, **Hak Jun Kim**, and Song Yub Shina. 2010. "Mammalian cell toxicity and candidacidal mechanism of Arg- or Lys-containing Trp-rich model antimicrobial peptides and their D-enantiomeric peptides". *Peptides,* 31: 1826-1831.
doi: 10.1016/j.peptides.2010.07.003

In this study, we investigated the mammalian cell toxicity and candidacidal mechanism of Arg- or Lys-containing Trp-rich model antimicrobial peptides ($K_6L_2W_3$ and $R_6L_2W_3$) and their d-enantiomeric peptides ($K_6L_2W_{3\text{-D}}$ and $R_6L_2W_{3\text{-D}}$). Arg-containing peptides were more toxic to human erythrocytes and mammalian cells as compared to Lys-containing peptides. Arg-containing peptides is slightly more hydrophobic than Lys-containing counterparts, as judged from their reverse phase-high performance liquid chromatography (RP-HPLC) retention time. These results suggested that a little difference in hydrophobicity of these peptides affect their hemolytic activity and mammalian cell toxicity. Interestingly, $K_6L_2W_3$ and $K_6L_2W_{3\text{-D}}$ almost similar mammalian cell cytotoxicity, whereas $R_6L_2W_{3\text{-D}}$ showed much higher cytotoxicity as compared to $R_6L_2W_3$. A low ability to facilitate fluorescent marker escape from *Candida albicans* membrane-mimicking vesicles suggested that the major target site of Lys-containing peptides may be not the cell membrane but the cytoplasm of *C. albicans*. Confocal laserscanning microscopy revealed that FITC-labeled Lys-containing peptides penetrated the cell wall and cell membrane and accumulated inside the cells, whereas FITC-labeled Arg-containing peptides did not penetrate but associated with the membranes. Collectively, our results suggested that the ultimate target site of action of Arg-containing peptides and Lys-containing peptides may be the membrane and the cytoplasm of *C. albicans*, respectively.

4-31 Nguyen, Tam-Anh D., Kyoung-Rok Kim, **Se Jong Han**, and 5 others. 2010. “Pretreatment of rice straw with ammonia and ionic liquid for lignocellulose conversion to fermentable sugars”. *Bioresource Technology,* 101(19): 7432-7438.
doi: 10.1016/j.biortech.2010.04.053

Pretreatment technology is a prerequisite to facilitate the release of sugars from a lignocellulosic biomass prior to fermentation. Recently, some pretreatment methods have been tried with ionic liquids, but they were still expensive and unpractical. In this study, an efficient pretreatment method using ammonia and ionic liquid was developed for the recovery of bio-digestible cellulose from a lignocellulosic byproduct, rice straw, and the increase of ionic liquid utilization. The combined use of ammonia and ionic liquid ([Emim]Ac) treatment exhibited a synergy effect for rice straw with 82% of the cellulose recovery and 97% of the enzymatic glucose conversion. This cooperative effect showed over 90% of the glucose conversion even with a reduced enzyme usage and incubation time. The ionic liquid was successfully recycled more than 20 times. The 20th-recycled ([Emim]Ac) showed 74% of the cellulose recovery and 78% of the glucose conversion to rice straw. Compared with the conventional pretreatment, our combined method for lignocellulosic biomass pretreatment was an economical and eco-friendly.

4-32 **Park, Hyun**, Sang-Hwan Lee, MinKyun Kim, **Jeong-Hoon Kim**, and **Hyoun Soo Lim**. 2010. “Polychlorinated biphenyl congeners in soils and lichens from King George Island, South Shetland Islands, Antarctica”. *Antarctic Science,* 22(1): 31-38.
doi: 10.1017/S0954102009990472

The levels and distribution of polychlorinated biphenyl (PCB) congeners were analysed in fourteen soil and eight lichen (*Usnea aurantiaco-atra*) samples from King George Island, West Antarctica. A total of 32 PCB congeners were found in five soil samples collected in 2006, and the mean concentration of total PCBs was 20.4 pg g^{-1} dry weight (range, 8.0233.8 pg g^{-1} dry weight). The most abundant PCB isomers in soil samples were di-, tri-, and penta-CBs, which accounted for more than 75% of the total residues. Twelve dioxin-like PCBs were also detected in nine soil and eight lichen samples, and the levels of dioxin-like PCBs were 5-fold higher in lichens than in soil. PCBs were detected at very low levels in most soil and lichen samples. The highest congener concentrations were found for PCB 118 (6.63 and 21.93 pg g^{-1} in soil and lichen, respectively) among dioxin-like PCBs. PCB levels in air samples were highly correlated with those in soil and lichen samples, as were PCB levels in soil and lichen samples collected at the same site. Long-range atmospheric transport is thought to be the main source of PCBs on King George Island. However, PCB levels in soil and lichen samples were also apparently influenced by local sources of PCBs.

4-33 **Park, Kyoung Sun**, **Woong Sic Jung**, **Hak Jun Kim**, and Song Yub Shin. 2010. “Determination of the Minimal Sequence Required for Antifreeze Activity of Type I Antifreeze Protein (AFP 37)”. *Bulletin of the Korean Chemical Society,* 31(12): 3791-3793.
doi: 10.5012/bkcs.2010.31.12.3791

In order to elucidate the minimal sequence required for antifreeze activity of AFP 37, we synthesized a series of N- and C-terminal truncated peptides of AFP 37 with the central two Thr residues (Thr-13 and Thr-24) (Table 1). These truncated peptides (AFP 34, AFP 32, AFP 30, AFP 28, AFP 26, AFP 24, AFP 22 and AFP 20) were synthesized by a stepwise deletion of one residue or two residues from N- and C-terminus of AFP 37. Table 2 summarizes the thermal hysteresis values obtained with a series of truncated peptides of AFP 37. AFP 37, AFP 34, AFP 32, AFP 30 and AFP 28 show a linear dependence of the antifreeze activity on the concentrations of the peptides. AFP 34, AFP 32, AFP 30 and AFP 28 preserved 99.1%, 62.6%, 56.16% and 15.9%thermal hysteresis activity of the wild type AFP (AFP 37) at a peptide concentration of 40 mg/mL, respectively. However, a significant hysteresis was not observed with any of the AFP 26, AFP24, AFP22 and AFP 20 at 40 mg/mL (data not shown). These results suggested that the minimalsequence required for antifreeze activity is from residue 5 toresidue 32 of AFP 37 (AFP 28).

4-34 **Paudel, Babita**, **Hari Datta Bhattarai**, **Hong Kum Lee**, Hyuncheol Oh, Hyun Woung Shin, and **Joung Han Yim**. 2010. "Antibacterial Activities of Ramalin, Usnic Acid and its Three Derivatives Isolated from the Antarctic Lichen *Ramalina terebrata*". *Zeitschrift für Naturforschung,* 65c: 34-38.

The development of new antibacterial compounds is an urgent issue to meet the evolution of resistivity of pathogenic bacteria against the available drugs. The objective of this study was to investigate the antibacterial compounds from the Antarctic lichen species *Ramalina terebrata.* A total of five compounds, usnic acid, usimine A, usimine B, usimine C, and ramalin, were isolated by bioactivity guided-fractionation of the methanol extract of *R. terebrata* after several chromatographic procedures. The qualitative antibacterial activities of the crude extract and isolated compounds were determined by the disk diffusion method while the minimum inhibitory concentration (MIC) determination assay gave the quantitative strength of the test samples. All the test samples showed antibacterial activity against *Bacillus subtilis*. The crude extract and usnic acid showed antibacterial activity against *Staphylococcus aureus*. The MIC values of the isolated compounds against *B. subtilis* were in the range of 1 to 26 μg/mL. These observed experimental data showed the strong antibacterial potential of these compounds against *B. subtilis*.

4-35 Uh, Ji-hyun, Youn Hong Jung, **Yoo Kyung Lee**, **Hong Kum Lee**, and Hana Im. 2010. "Rescue of a Cold-Sensitive Mutant at Low Temperatures by Cold Shock Proteins from *Polaribacter irgensii* KOPRI 22228". *The Journal of Microbiology,* 48(6): 798-802.
doi: 10.1007/s12275-010-0402-5

Exposure to low temperatures induces the biosynthesis of specific sets of proteins, including cold shock proteins (Csps). Since many of the specific functions of pychrophilic Csps are unknown, the roles of Csps from an Arctic bacterium, *Polaribacter irgensii* KOPRI 22228, were examined. The genes encoding CspA and CspC of *P. irgensii* were cloned in this study. Sequence analysis showed that these proteins have cold shock domains containing two RNA-binding motifs, RNP1 and RNP2. Both proteins bound oligo(dT)-cellulose resins, suggesting single-stranded nucleic acid-binding activity. When the *P. irgensii* Csps were overexpressed in *Escherichia coli*, the cold-resistance of the host was increased by more than five-fold. The *P. irgensii* Csps also rescued a cold-sensitive *E. coli csp*-quadruple deletion strain, BX04, at low temperatures. These results suggest that Csps from *P. irgensii* play a role in survival in polar environments.

PART 5

Policy

5-1 **Jin, Dongmin**, **Hyunkyo Seo**, and **Seonung Choi**. 2010. "Arctic Governance and International Organization : A Focus on the

Arctic Council". *Ocean and Polar Research,*
31(1): 85-95.
doi: 10.4217/OPR.2010.32.1.85

There is increasing consensus that global warming is seriously affecting the Arctic region. Sea Ice decreases and sea level rise have led to environmental change in Arctic Ecosystems, while also making the Arctic sea route more accessible to humans. There are complicated international governance dynamics in play, in addition to commercial and scientific interests in the Arctic region. This provides a unique opportunity for Korea to lead the future direction of Arctic policy in response to the global issues such as climate change and economic or scientific interests. Korea acquired Ad-hoc Observer status of the Arctic Council(AC) in 2008, which is the only pan-Arctic intergovernmental organization. It consists of six working groups: ACAP, AMAP, CAFF, PAME, EPPR, SDWG that implement research, survey, and monitoring. AC's Observer country has the opportunity to participate in a diverse range of activities such technical and expertise support, research and monitoring, financial support and conference organization. In order for Korea to expand its activities in the Arctic region, we suggest the following approach: First, Korea should become more actively engaged with the Arctic Council and its activities; Second, Korea should construct organized collaborative networks of national experts to respond to Arctic issues; Third, Korea should develop collaborations with Arctic states; Finally, Korea should intensify its research on international relations and international laws related to the Arctic region.

KOPRI ABSTRACTS 2011


KOPRI
극지연구소

PART 1

Climate Change Sciences

1-1 An, Soon-Il, Ji-Won Kim, Seul-Hee Im, **Beak-Min Kim**, and Jae-Heung Park. 2011. "Recent and future sea surface temperature trends in tropical pacific warm pool and cold tongue regions". *Climate Dynamics,* 39(6): 1373-1383.
doi: 10.1007/s00382-011-1129-7

Using coral data, sea surface temperature (SST) reanalysis data, and Climate Model Intercomparison Project III (CMIP3) data, we analyze 20th-century and future warm pool and cold tongue SST trends. For the last 100 years, a broad La Nina-like SST trend, in which the warming trend of the warm pool SST is greater than that of the cold tongue SST, has appeared in reanalysis SST data sets, 20C scenario experiments of the CMIP3 data and less significantly in coral records. However, most Coupled General Circulation Models subjected to scenarios of future high greenhouse gas concentrations produce larger SST warming trends in cold tongues than in warm pools, resembling El Nino-like SST patterns. In other words, warmer tropical climate conditions correspond to stronger El Nino-like response. Heat budget analyses further verify that warmer tropical climates diminish the role of the ocean's dynamic thermostat, which currently regulates cold tongue temperatures. Therefore, the thermodynamic thermostat, whose efficiency depends on the mean temperature, becomes the main regulator (particularly via evaporative cooling) of both warm pool and cold tongue temperatures in future warm climate conditions. Thus, the warming tendency of the cold tongue SST may lead that of the warm pool SST in near future.

1-2 Bak, Young-Suk, **Kyu-Cheul Yoo**, Jong-Deock Lee, **Ho Il Yoon**, **Jae Il Lee**, and 2 others. 2011. "Deglacial environments in the northeastern of South Shetland Island, Antarctica: evidence from the high resolution diatom record". *Journal of the Geological Society of Korea,* 47(4): 363-369.

A total of 70 species and varieties belonging to 31 genera are identified from 300~350 cm horizons of the Core GC03-C1 in the South Shetland Islands, Antarctic Peninsula. High number of diatom valves per gram of dry sediment was observed in core, ranging from 0.7~6.1×10^7/g. The Holocene diatom assemblages from the core are dominated by *Fragilariopsis kerguelensis* and *Eucampia antarctica* which are about 45.7% of the total. Three diatom subzones are identified on the basis of frequency of the index species throughout the section: diatom assemblage subzone I-a from 350 to 331 cm (late Last Glacial Maximum), diatom assemblage subzone I-b from 330 to 313 cm (deglaciation) and diatom assemblage subzone II-a from 312 to 300 cm (early Holocene). The paleoenvironmental conditions from the late LGM to early Holocene can be subdivided into three intervals based on diatom assemblages: 1) diatom assemblage subzon I-a condition with persistent seasonal sea-ice cover and summer upwelling of Antarctic Circumpolar Deep Water, 2) diatom assemblage subzone I-b condition with collapse of land glaciers and influx of meltwater with increasing warming, and 3) diatom assemblage subzone II-a open ocean conditions more affected by Antarctic Circumpolar Current.

1-3 Burns, A. G., S. C. Solomon, W. Wang, **G. Jee**, and 3 others. 2011. "The summer evening anomaly and conjugate effects". *Journal of Geophysical Research,* 116: A01311(1-9).
doi: 10.1029/2010JA015648

The Constellation Observing System for Meteorology, Ionosphere, and Climate (COSMIC) GPS occultation data have been analyzed in this study to provide a better understanding of the Weddell Sea Anomaly (WSA) and to place it in the wider context of a general phenomenon that occurs near dusk in summer, which we are calling the summer evening anomaly to better capture its global nature. The terminator and the magnetically conjugate points for the terminator in the other hemisphere have been plotted on top of global maps of COSMIC NmF_2 and hmF_2 for 2 months either side of the December and June solstices for 2006–2008. These plots show that there are distinct enhancements of NmF_2 and increases in hmF_2 as soon as the conjugate footprint of the field line on the winter terminator is seen at middle latitudes in the summer hemisphere. This effect is most pronounced where the WSA is formed, but it also occurs across the South Pacific Ocean in the southern summer and across much of the North Atlantic Ocean, Siberia, and Kamchatka during the northern summer. An hmF_2 increase occurs between the two terminators even at locations where there is no increase in NmF_2. A similar, but reversed, effect occurs in hmF_2 near dawn. This behavior appears to be most consistent with upward and poleward ion drifts in the evening, but neutral wind and downward precipitation may make important contributions to this effect.

1-4 Feng, Song, Chang-Hoi Ho, Qi Hu, Robert J. Oglesby, Su-Jong Jeong, and **Baek-Min Kim**. 2011. “Evaluating observed and projected future climate changes for the Arctic using the Köppen-Trewartha climate classification”. *Climate Dynamics,* 38(7-8): 1359-1373. doi: 10.1007/s00382-011-1020-6

The ecosystems in the Arctic region are known to be very sensitive to climate changes. The accelerated warming for the past several decades has profoundly influenced the lives of the native populations and ecosystems in the Arctic. Given that the Köppen-Trewartha (K-T) climate classification is based on reliable variations of land-surface types (especially vegetation), this study used the K-T scheme to evaluate climate changes and their impact on vegetation for the Arctic (north of 50°N) by analyzing observations as well as model simulations for the period 1900–2099. The models include 16 fully coupled global climate models from the Intergovernmental Panel on Climate Change Fourth Assessment. By the end of this century, the annual-mean surface temperature averaged over Arctic land regions is projected to increase by 3.1, 4.6 and 5.3°C under the Special Report on Emissions Scenario (SRES) B1, A1b, and A2 emission scenarios, respectively. Increasing temperature favors a northward expansion of temperate climate (i.e., *Dc* and *Do* in the K-T classification) and boreal oceanic climate (i.e., *Eo*) types into areas previously covered by boreal continental climate (i.e., *Ec*) and tundra; and tundra into areas occupied by permanent ice. The tundra region is projected to shrink by -1.86×10^6 km^2 (−33.0%) in B1, -2.4×10^6 km^2 (−42.6%) in A1b, and -2.5×10^6 km^2 (−44.2%) in A2 scenarios by the end of this century. The *Ec* climate type retreats at least 5° poleward of its present location, resulting in −18.9, −30.2, and −37.1% declines in areal coverage under the B1, A1b and A2 scenarios, respectively. The temperate climate types (*Dc* and *Do*) advance and take over the area previously covered by *Ec*. The area covered by *Dc* climate expands by 4.61×10^6 km^2 (84.6%) in B1, 6.88×10^6 km^2 (126.4%) in A1b, and 8.16×10^6 km^2 (149.6%) in A2 scenarios. The projected redistributions of K-T climate types also differ regionally. In northern Europe and Alaska, the warming may cause more rapid expansion of temperate climate types. Overall, the climate types in 25, 39.1, and 45% of the entire Arctic region are projected to change by the end of this century under the B1, A1b, and A2 scenar ios, respectively. Because the K-T climate classification was constructed on the basis of vegetation types, and each K-T climate type is closely associated with certain prevalent vegetation species, the projected large shift in climate types suggests extensive broad-scale redistribution of prevalent ecoregions in the Arctic.

1-5 Gong, Dao-Yi, Jing Yang, **Seong-Joong Kim**, and 4 others. 2011. “Spring Arctic Oscillation-East Asian summer monsoon connection through circulation changes over the western North Pacific”. *Climate Dynamics,* 37: 2199-2216. doi: 10.1007/s00382-011-1041-1

In the present study the links between spring Arctic Oscillation (AO) and East Asian summer monsoon (EASM) was investigated with focus on the importance of the North Pacific atmospheric circulation and sea surface temperature (SST). To reduce the statistical uncertainty, we analyzed high-pass filtered data with the inter-annual time scales, and excluded the El Niño/Southern Oscillation signals in the climate fields using a linear fitting method. The significant relationship between spring AO and EASM are supported by the changes of multi-monsoon components, including monsoon indices, precipitation, and threedimensional atmospheric circulations. Following a stronger positive spring AO, an anomalous cyclonic circulation at 850 hPa appears in southeastern Asia and the western North Pacific in summer, with the easterly anomalies spanning from the Pacific to Asian continent along 25°N–30°N and the westerly anomalies south of 15°N. At the same time, the summer western North Pacific subtropical high becomes weaker. Consistently, the positive precipitation anomalies are developed over a broad region south of 30°N stretching from southern China to the western Pacific and the negative precipitation anomalies appear in the lower valley of the Yangtze River and southern Japan. The anomalous cyclone in the western North Pacific persisting from spring to summer plays a key role in modulating EASM and monsoon precipitation by a positive air-sea feedback mechanism. During spring the AO-associated atmospheric circulation change produces warmer SSTs between 150° E–180° near the equator. The anomalous sensible and latent heating, in turn, intensifies the cyclone through a Gill-type response of the atmosphere. Through this positive feedback, the tropical atmosphere and SST patterns sustain their strength from spring to summer, that consequently modifies the monsoon trough and the western North Pacific subtropical high and eventually the EASM precipitation. Moreover, the SST response to AO-circulation is supported by the numerical simulations of an ocean model, and the anomalous atmospheric circulation over the western North Pacific is also reproduced by the dedicated numerical simulations using the coupled atmosphere–ocean model. The observation evidence and numerical simulations suggest the spring AO can impact the EASM via triggering tropical air-sea feedback over the western North Pacific.

1-6 Hsiao, Yu-Shen, Jeong Woo Kim, Kwang Bae Kim, **Bang Yong Lee**, and Cheinway Hwang. 2011. “Bathymetry Estimation Using the Gravity-Geologic Method: An Investigation of Density Contrast Predicted by the Downward Continuation Method”. *Terrestrial Atmospheric and Oceanic Sciences,* 22(3): 347-358. doi: 10.3319/TAO.2010.10.13.01(Oc)

The downward continuation (DWC) method was used to determine the density contrast between the seawater and the ocean bottom topographic mass to estimate accurate bathymetry using the gravity-geologic method (GGM) in two study areas, which are located south of Greenland (Test Area #1: 40 - 50°W and 50 - 60°N) and south of Alaska (Test

Area #2: 140 - 150°W and 45 - 55°N). The data used in this study include altimetry-derived gravity anomalies, shipborne depths and gravity anomalies. Density contrasts of 1.47 and 1.30 g cm^{-3} were estimated by DWC for the two test areas. The considerations of predicted density contrasts can enhance the accuracy of 3 ~ 4 m for GGM.
The GGM model provided results closer to the NGDC (National Geophysical Data Center) model than the ETOPO1 (Earth topographical database 1) model. The differences along the shipborne tracks between the GGM and NGDC models for Test Areas #1 and #2 were 35.8 and 50.4 m in standard deviation, respectively. Furthermore, these differences were more strongly correlated with gravity anomalies than bathymetry in the test areas. It is shown that an accuracy of under 40 m can be obtained with comparisons to shipborne depths only in Test Area #1.

1-7 Jeong, Jee-Hoon, Jong-Seong Kug, **Baek-Min Kim**, and 6 others. 2011. “Greening in the circumpolar high-latitude may amplify warming in the growing season”. *Climate Dynamics,* 38(7-8): 1421-1431.
doi: 10.1007/s00382-011-1142-x

We present a study that suggests greening in the circumpolar high-latitude regions amplifies surface warming in the growing season (May–September) under enhanced greenhouse conditions. The investigation used a series of climate simulations with the Community Atmospheric Model version 3—which incorporates a coupled, dynamic global vegetation model—with and without vegetation feedback, under both present and doubled CO_2 concentrations. Results indicate that climate warming and associated changes promote circumpolar greening with northward expansion and enhanced greenness of both the Arctic tundra and boreal forest regions. This leads to additional surface warming in the high-latitudes in the growing season, primarily through more absorption of incoming solar radiation. The resulting surface and tropospheric warming in the high-latitude and Arctic regions weakens prevailing tropospheric westerlies over 45–70N, leading to the formation of anticyclonic pressure anomalies in the Arctic regions. These pressure anomalies resemble the anomalous circulation pattern during the negative phase of winter Arctic Oscillation. It is suggested that these circulation anomalies reinforce the high-latitude and Arctic warming in the growing season.

1-8 Jeong, Jee-Hoon, Tinghai Ou, Hans W. Linderholm, **Baek-Min Kim**, **Seong-Joong Kim**, and 2 others. 2011. “Recent recovery of the Siberian High intensity”. *Journal of Geophysical Research,* 116: D23102(1-9).
doi: 10.1029/2011JD015904

This study highlights the fast recovery of the wintertime Siberian High intensity (SHI) over the last two decades. The SHI showed a marked weakening trend from the 1970s to 1980s, leading to unprecedented low SHI in the early 1990s according to most observational data sets. This salient declining SHI trend, however, was sharply replaced by a fast recovery over the last two decades. Since the declining SHI trend has been considered as one of the plausible consequences of climate warming, the recent SHI recovery seemingly contradicts the continuous progression of climate warming in the Northern Hemisphere. We suggest that alleviated surface warming and decreased atmospheric stability in the central Siberia region, associated with an increase in Eurasian snow cover, in the recent two decades contributed to this rather unexpected SHI recovery. The prominent SHI change, however, is not reproduced by general circulation model (GCM) simulations used in the IPCC AR4. The GCMs indicate the steady weakening of the SHI for the entire 21st century, which is found to be associated with a decreasing Eurasian snow cover in the simulations. An improvement in predicting the future climate change in regional scale is desirable.

1-9 **Jo, Kyoung-nam**, Kyung Sik Woo, **Hyoun Soo Lim**, Hai Cheng, R. Lawrence Edwards, Yongjin Wang, Xiuyang Jiang, Ryeon Kim, **Jae Il Lee**, **Ho Il Yoon**, and **Kyu-Cheul Yoo**. 2011. "Holocene and Eemian climatic optima in the Korean Peninsula based on textural and carbon isotopic records from the stalagmite of the Daeya Cave, South Korea". *Quaternary Science Reviews,* 30(9-10): 1218-1231.
doi: 10.1016/j.quascirev.2011.02.012

Textural and stable isotopic records from the absolute-dated stalagmite of the Daeya Cave (DY-1) provide new insights into the climatic evolution of the Korean Peninsula during the Holocene and Eemian climatic optima. The stalagmite yielded ages of 8572 ± 227 to 5907 ± 158 and 1,23,456 ± 535 to 1,19,837 ± 1089 years, which coincide with the Holocene and Eemian climatic optima, respectively. The stalagmite's δ^{13}C record closely resembles previously reported Chinese speleothem δ^{18}O data. Thus it can be suggested that textural and geochemical results of the DY-1 reflect East Asian monsoon intensity, which is forced by summer insolation patterns in the northern hemisphere. Lighter carbon isotopic compositions, well-developed fibrous calcite crystals, and their relatively faster growth rate in the stalagmite sample are interpreted to reflect the warmest and wettest climate conditions of the Holocene and Eemian interglacials. Both climatic optima took place when insolation was decreasing from its maximum level, temperature in Greenland was highest, and sea level approached its maximum level. These climatic optima also coincide with decreasing Antarctic temperatures. Compared the DY-1 data to other proxies, it is suggested that the Holocene and Eemian climatic optima developed through a balance among boreal insolation, monsoon intensity, and sea level (also continental ice volume), which are the main climatic forcing factors in the northern hemisphere. These trends also follow the bi-polar seesaw mechanism as previously described.

1-10 **Kim, Baek-Min** and Soon-Il An. 2011. "Understanding ENSO Regime Behavior upon an Increase in the Warm-Pool Temperature Using a Simple ENSO Model". *Journal of Climate,* 24(5): 1438-1450.
doi :10.1175/2010JCLI3635.1

The regime behavior of the low-order El Niño–Southern Oscillation (ENSO) model, according to an increase in the radiative–convective equilibrium sea surface temperature (SST; *Tr*), is studied to provide a possible explanation for the observed increase in ENSO irregularity characterized by decadal modulation. During recent decades, a clear increasing trend of the warm-pool SST has been observed. In this study, the increase in the warm-pool maximum SST is interpreted as an increase in T_r following previous studies. A bifurcation analysis with T_r as a control parameter is conducted to reveal that the degree of ENSO irregularity in the model is effectively controlled by the equilibrium states of the model. At a critical value of T_r, bifurcation analysis reveals that period-doubling bifurcation occurs and an amplitude-modulated ENSO emerges. At this point, a subcycle appears within the preexisting ENSO cycle, which initiates decadal modulation of ENSO. As T_r increases further, nested oscillations are successively generated, illustrating clear decadal modulation of ENSO. The qualitative regime changes revealed in this study are supported by the observation of regime shifts in the 1970s. With increasing T_r, the mean zonal SST gradient increases, and the model adjusts toward a ‘‘La Niña–like’’ mean state. Further constraint with shoaling of the mean thermocline depth and increasing stratification causes ENSO to exhibit stronger amplitude modulation. Furthermore, the timing of the period-doubling bifurcation advances with these two effects.

1-11 Kim, Eojin, Jong-Kyun Chung, Yong Ha Kim, **Geonhwa Jee**, Sun-hak Hong, and **Jeong-ho Choe**. 2011. “A climatology study on ionospheric *F2* peak over Anyang, Korea”. *Earth Planets Space,* 63: 335-349. doi: 10.5047/eps.2011.03.011

We analyzed peak electron densities (N_mF_2) and peak heights (h_mF_2) of F_2 layer, measured by a digisonde at Anyang (37.4°N, 127.0°E, Geomag = 27.7°N, 196.9°E) during the period of April 1998 through April 2008. The Anyang N_mF_2 and h_mF_2 values averaged over each month show generally good linear relationship with increasing solar activities for all local time and for various geomagnetic activities. The change of the noon N_mF_2 with increasing solar flux indices ($F_{10.7}$) is much slower in summer than in other seasons, and the N_mF_2 difference between noon and midnight is minimized in summer. The h_mF_2 varies with $F_{10.7}$ from 200 km to 350 km at noon and from 300 to 450 km at midnight, but the h_mF_2 variations do not show seasonal difference significantly for all local time. The semi-annual variations of N_mF_2 and h_mF_2 are apparent and the winter anomaly of N_mF_2 is also clearly seen for most cases of geomagnetic and solar activities. The Anyang N_mF_2 values are in good agreement with the IRI 2007 model except for high solar and geomagnetic activity cases. However, the Anyang h_mF_2 values at midnight are significantly higher than the IRI model, being higher by up to ~100 km for high solar activities.

1-12 Kim, Kwang Bae, Yu-Shen Hsiao, Jeong Woo Kim, **Bang Yong Lee**, and 2 others. 2011. “Bathymetry enhancement by altimetry-derived gravity anomalies in the East Sea (Sea of Japan)”. *Marine Geophysical Research,* 31(4): 285-298. doi: 10.1007/s11001-010-9110-0

The gravity-geologic method (GGM) was used to enhance the bathymetry of the East Sea (Sea of Japan) with satellite altimetry-derived free-air gravity anomalies and shipborne depth measurements. By comparison with the bathymetry model of Smith and Sandwell’s (SAS) approach (1994), GGM was found to have an advantage with short wavelength (≤ 12 km) components, while SAS better predicts longer wavelength (≥ 25 km) components, despite its dependency on density contrast. To mitigate this limitation, a tuning density contrast of 10.25 g/cm^3 between seawater and the seafloor was primarily estimated by the downward continuation method and then validated by the check points method with GGM. Similarly, SAS is limited by the ‘‘*A*’’ value in low-pass part of the Wiener filter, which defines the effective range of the wavelength components on bathymetry. As a final result, we present an enhanced GGM bathymetry model by integrating all available data.

1-13 **Kim, Seong-Joong**, **Eun-Jin Woo**, and **Baek-Min Kim**. 2011. “Antarctic surface temperature change for the Last Glacial Maximum (LGM) reproduced in the second phase of the Paleoclimate Modelling Intercomparison Program (PMIP2)”. *Journal of the Geological Society of Korea,* 47(5): 443-457.

The Antarctic surface temperature change for the Last Glacial Maximum (LGM) was investigated using the results of atmosphere-ocean-ice coupled models from the second phase of the Paleoclimate Modelling Intercomparison Program (PMIP2). In the analysis, we used seven models; the NCAR CCSM of USA, ECHAM3-MPIOM of German Max-Plank Institute, HadCM3M2 of UK Met Office, IPSL-CM4 of France Laplace Institute, CNRM-CM3 of France Meteorological Institute, MIROC3.2 of Japan CCSR at University of Tokyo, and FGOALS of China Institute of Atmospheric Physics. All seven models tend to underestimate the present Antarctic temperatures in comparison to the observed. In the LGM simulations, the atmospheric CO_2 concentration and other greenhouse gases were reduced to the LGM level, the 5-G ice sheet reconstruction data were implemented, and orbital parameters of 21,000 years BP were used. With the implemented LGM conditions, the temperature over Antarctica has simulated about 8-12℃ below compared to the present in austral winter, while in summer it is 6-9℃ below. Overall, the annual mean surface temperature is about 7℃ below the present climate which is slightly lower than the temperature change obtained in the proxy evidence (about 10℃). The surface temperature reduction tends to bigger toward the high latitudes and biggest temperature reduction is found around the south pole. In austral winter, the surface temperature reduction is bigger around 65°S than in 70°S. This seems to be due to the increase in sea ice extent in the LGM in those latitudes.

1-14 **Kim, Seong-Joong**, **Sung-Ho Woo**, **Baek-Min Kim**, and **Soon-Do Hur**. 2011. “Trends in Sea Surface Temperature (SST) Change Near the Korean Peninsula for the Past 130 Years”. *Ocean and Polar Research,* 33(3): 281-290. doi: 10.4217/OPR.2011.33.3.281

This study examined the change in sea surface temperature (SST) around the Korean peninsula since industrialization at year 1880, and its possible causes using observation based data from the Hadley Center, the Goddard Institute of Space Studies, and National Climate Data Center. Since year 1880, There have been multi-decadal fluctuations with a gradual reduction from 1880 to around 1940, and from 1950-1980. There has then been a marked increase from 1940-1950, and from 1980 to the present. The ocean surface warming is larger during the boreal winter than summer, and greater in the south. The multi-decadal SST fluctuations around the Korean Peninsula are largely consistent with the negative phase of the Pacific Decadal Oscillation (PDO), which fluctuates with periods of about 20-50 years. Secondly, the El Niño-Southern Oscillation (ENSO), whose long period component moves along with the PDO, appears to influence the SST near the Korean Peninsula, especially in recent decades. Overall, the SST around the Korean Peninsula has warmed since year 1880 by about 1℃, which is about twice the global-mean ocean surface warming. This long-term warming is aligned with an increase in greenhouse gas concentration, as well as local factors such as the PDO.

1-15 **Lee, Min Kyung**, Yong Il Lee, **Hyoun Soo Lim**, **Jae Il Lee**, Jeong Heon Choi, and **Ho Il Yoon**. 2011. “Comparison of radiocarbon and OSL dating methods for a Late Quaternary sediment core from Lake Ulaan, Mongolia”. *Journal of Paleolimnology,* 45(2): 127-135. doi: 10.1007/s10933-010-9484-7

Both radiocarbon and optically stimulated luminescence (OSL) dating methods were applied to test their suitability for establishing a chronology of arid-zone lacustrine sediments using a 5.88-m-long core drilled from Lake Ulaan, southern Mongolia. Although the radiocarbon and OSL ages agree in some samples, the radiocarbon ages are older than the corresponding OSL ages at the 550-cm depth horizon (late Pleistocene) and in the 100–300-cm interval (early to late Holocene). In the early to late Holocene, radiocarbon ages are consistently older than

OSL ages by 4,100–5,800 years, and in the late Pleistocene by 2,700–3,000 years. Grain-size analysis of early to late Holocene sediments and one late Pleistocene sediment sample (550-cm depth) indicates that eolian processes were the dominant sediment-transport mechanism. Also, two late Pleistocene sediments samples (from 400- to 500-cm depths) are interpreted to have been deposited by both eolian and glaciofluvial processes. Accordingly, the radiocarbon ages that were older than the corresponding OSL ages during the Holocene seem to have been a consequence of the influx of ^{14}C-deficient carbon delivered from adjacent soils and Paleozoic carbonate rocks by the westerly winds, a process that is also active today. In addition to the input of old reworked carbon by eolian processes, the late Pleistocene sediments were also influenced by old carbon delivered by deglacial meltwater. The results of this study suggest that when eolian sediment transport is suspected, especially in lakes of arid environments, the OSL dating method is superior to the radiocarbon dating method, as it eliminates a common 'old-carbon' error problem.

1-16 Maskey, Shila, Hong Geng, Young-Chul Song, **HeeJin Hwang**, **Young-Jun Yoon**, and 2 others. 2011. "Single-Particle Characterization of Summertime Antarctic Aerosols Collected at King George Island Using Quantitative Energy-Dispersive Electron Probe X-ray Microanalysis and Attenuated Total Reflection Fourier Transform-Infrared Imaging Techniques". *Environmental Science & Technology,* 45: 6275-6282. doi: 10.1021/es200936m

Single-particle characterization of Antarctic aerosols was performed to investigate the impact of marine biogenic sulfur species on the chemical compositions of sea-salt aerosols in the polar atmosphere. Quantitative energy-dispersive electron probe X-ray microanalysis was used to characterize 2900 individual particles in 10 sets of aerosol samples collected between March 12 and 16, 2009 at King Sejong Station, a Korean scientific research station located at King George Island in the Antarctic. Two size modes of particles, i.e., $PM_{2.5-10}$ and $PM_{1.0-2.5}$, were analyzed, and four types of particles were identified, with sulfur-containing sea-salt particles being the most abundant, followed by genuine seasalt particles without sulfur species, iron-containing particles, and other species including $CaCO_3/CaMg(CO_3)_2$, organic carbon, and aluminosilicates. When a sulfur-containing sea-salt particle showed an atomic concentration ratio of sulfur to sodium of >0.083 (seawater ratio), it is regarded as containing nonsea-salt sulfate (nss-SO_4^{2-}) and/or methanesulfonate ($CH_3SO_3^-$), which was supported by attenuated total reflection Fourier transform-infrared imaging measurements. These internal mixture particles of sea-salt/$CH_3SO_3^-/SO_4^{2-}$ were very frequently encountered. As nitratecontaining particles were not encountered, and the air-masses for all of the samples originated from the Pacific Ocean (based on 5-day backward trajectories), the oxidation of dimethylsulfide (DMS) emitted from phytoplanktons in the ocean is most likely to be responsible for the formation of the mixed sea-salt/$CH_3SO_3^-/SO_4^{2-}$ particles.

1-17 Park, Soo-Je, Byoung-Joon Park, Man-Young Jung, So-Jeong Kim, Jong-Chan Chae, Yul Roh, Matthias Forwick, **Ho-Il Yoon**, and Sung-Keun Rhee. 2011. "Influence of Deglaciation on Microbial Communities in Marine Sediments Off the Coast of Svalbard, Arctic Circle". *Environmental Microbiology,* 62(3): 537-548. doi: 10.1007/s00248-011-9860-5

Increases in global temperatures have been shown to enhance glacier melting in the Arctic region. Here, we have evaluated the effects of meltwater runoff on the microbial communities of coastal marine sediment located along a transect of Temelfjorden, in Svalbard. As close to the glacier front, the sediment properties were clearly influenced by deglaciation. Denaturing gradient gel electrophoresis profiles showed that the sediment microbial communities of the stations of glacier front (stations 188–178) were distinguishable from that of outer fjord region (station 176). Canonical correspondence analysis indicated that total carbon and calcium carbonate in sediment and chlorophyll a in bottom water were key factors driving the change of microbial communities. Analysis of 16S rRNA gene clone libraries suggested that microbial diversity was higher within the glacier–proximal zone (station 188) directly affected by the runoffs than in the outer fjord region.While the crenarchaeotal group I.1a dominated at station 176 (62%), Marine Benthic Group-B and other Crenarchaeota groups were proportionally abundant. With regard to the bacterial community, alpha-*Proteobacteria* and *Flavobacteria* lineages prevailed (60%) at station 188, whereas delta-*Proteobacteria* (largely sulfatereducers) predominated (32%) at station 176. Considering no clone sequences related to sulfate-reducers, station 188 may be more oxic compared to station 176. The distance-wise compositional variation in the microbial communities is attributable to their adaptations to the sediment environments which are differentially affected by melting glaciers.

1-18 Song, Hyo-Jong, Gyu-Ho Lim, and **Baek-Min Kim**. 2011. "A comparison between a Monte Carlo implementation of retrospective optimal interpolation and an ensemble Kalman filter in nonlinear dynamics". *Computational Geosciences,* 16(1): 177-192. doi: 10.1007/s10596-011-9261-3

To more correctly estimate the error covariance of an evolved state of a nonlinear dynamical system, the second and higher-order moments of the prior error need to be known. Retrospective optimal interpolation (ROI) may require relatively less information on the higher-order moments of the prior errors than an ensemble Kalman filter (EnKF) because it uses the initial conditions as the background states instead of forecasts. Analogous to the extension of a Kalman filter into an EnKF, an ensemble retrospective optimal interpolation (EnROI) technique was derived using the Monte Carlo method from ROI. In contrast to the deterministic version of ROI, the background error covariance is represented by a background ensemble in EnROI. By sequentially applying EnROI to a moving limited analysis window and exploiting the forecast from the average of the background ensemble of EnROI as a guess field, the computation costs for EnROI can be reduced. In the numerical experiment using a Lorenz-96 model and a Model-III of Lorenz with a perfect-model assumption, the cost-effectiveness of the suboptimal version of EnROI is demonstrated to be superior to that of EnKF using perturbed observations.

1-19 Unterman, M. B., T. J. Crowley, K. I. Hodges, **S. J. Kim**, and D. J. Erickson. 2011. "Paleometeorology: High resolution Northern Hemisphere wintertime mid-latitude dynamics during the Last Glacial Maximum". *Geophysical Research Letters,* 38: L23702(1-6). doi: 10.1029/2011GL049599

Hourly winter weather of the Last Glacial Maximum (LGM) is simulated using the Community Climate Model version 3 (CCM3) on a globally resolved T170 (75 km) grid. Results are compared to a longer LGM climatological run with the same boundary conditions and monthly saves. Hourly-scale animations are used to enhance interpretations. The purpose of the study is to explore whether additional insights into ice age conditions can be gleaned by going beyond the standard employment of monthly average model statistics to infer ice age weather and climate. Results for both LGM runs indicate a decrease in North Atlantic and increase in North Pacific cyclogenesis. Storm trajectories react to the mechanical forcing of the Laurentide Ice Sheet, with Pacific storms tracking over middle Alaska and northern Canada, terminating in the Labrador Sea. This result is coincident with other model results in also showing a significant reduction in Greenland wintertime precipitation – a response supported by ice core evidence. Higher-temporal resolution puts in sharper focus the close tracking of Pacific storms along the west coast of North America. This response is consistent with increased poleward heat transport in the LGM climatological run and could help explain "early" glacial warming inferred in this region from proxy climate records. Additional analyses shows a large increase in central Asian surface gustiness that support observational inferences that upper-level winds associated with Asian-Pacific storms transported Asian dust to Greenland during the LGM.

1-20 Vollmer, Martin K., Benjamin R. Miller, Matthew Rigby, Stefan Reimann, Jens Mühle, Paul B. Krummel, Simon O'Doherty, Jooil Kim, **Tae Siek Rhee**, and 19 others. 2011. "Atmospheric histories and global emissions of the anthropogenic hydrofluorocarbons HFC-365mfc, HFC-245fa, HFC-227ea, and HFC-236fa". *Journal of Geophysical Research,* 116: D08304(1-16). doi: 10.1029/2010JD015309

We report on ground-based atmospheric measurements and emission estimates of the four anthropogenic hydrofluorocarbons (HFCs) HFC-365mfc ($CH_3CF_2CH_2CF_3$, 1,1,1,3,3-pentafluorobutane), HFC-245fa ($CHF_2CH_2CF_3$, 1,1,1,3,3-pentafluoropropane), HFC-227ea (CF_3CHFCF_3, 1,1,1,2,3,3,3-heptafluoropropane), and HFC-236fa ($CF_3CH_2CF_3$, 1,1,1,3,3,3-hexafluoropropane). In situ measurements are from the global monitoring sites of the Advanced Global Atmospheric Gases Experiment (AGAGE), the System for Observations of Halogenated Greenhouse Gases in Europe (SOGE), and Gosan (South Korea). We include the first halocarbon flask sample measurements from the Antarctic research stations King Sejong and Troll. We also present measurements of archived air samples from both hemispheres back to the 1970s. We use a two-dimensional atmospheric transport model to simulate global atmospheric abundances and to estimate global emissions. HFC-365mfc and HFC-245fa first appeared in the atmosphere only ~1 decade ago; they have grown rapidly to globally averaged dry air mole fractions of 0.53 ppt (in parts per trillion, 10^{-12}) and 1.1 ppt, respectively, by the end of 2010. In contrast, HFC-227ea first appeared in the global atmosphere in the 1980s and has since grown to ~0.58 ppt. We report the first measurements of HFC-236fa in the atmosphere. This long-lived compound was present in the atmosphere at only 0.074 ppt in 2010. All four substances exhibit yearly growth rates of > 8% yr^{-1} at the end of 2010. We find rapidly increasing emissions for the foam-blowing compounds HFC-365mfc and HFC-245fa starting in ~2002. After peaking in 2006 (HFC-365mfc: 3.2 kt yr^{-1}, HFC-245fa: 6.5 kt yr^{-1}), emissions began to decline. Our results for these two compounds suggest that recent estimates from long-term projections (to the late 21st century) have strongly overestimated emissions for the early years of the projections (~2005–2010). Global HFC-227ea and HFC-236fa emissions have grown to average values of 2.4 kt yr^{-1} and 0.18 kt yr^{-1} over the 2008–2010 period, respectively.

PART 2

Earth-System Sciences

2-1 Han, Yeongcheol, Youngsook Huh, Sungmin Hong, **Soon Do Hur**, and 4 others. 2011. “Quantification of Total Mercury in Antarctic Surface Snow using ICP-SF-MS: Spatial Variation from the Coast to Dome Fuji”. *Bulletin of the Korean Chemical Society,* 32(12): 4258-4264.
doi: 10.5012/bkcs.2011.32.12.4258

The total mercury concentration (Hg_T) of surface snow samples collected along a ~1500 km transect in east Queen Maud Land was determined using inductively coupled plasma sector field mass spectrometry to address the behavior of Hg on the Antarctic Plateau. Due to the volatile nature of mercury, measures were taken against Hg loss from standard solutions by choosing appropriate container material and stabilizing agents. Glass bottles with Teflon-lined caps were superior to Teflon and polyethylene containers in protecting against Hg loss, but addition of gold chloride ($AuCl_3$) or bromine chloride (BrCl) was necessary to ensure preservation of Hg. As Hg loss was also observed in snowmelt samples, our analysis may underestimate the actual amount of HgT in the snow. Even so, the measured HgT was still very low (< 0.4-10.8 pg g^{-1}, $n = 44$) without a signal of depositional enhancement accompanying photo-oxidation of atmospheric elemental mercury in austral midsummer. Moreover, the dynamic variation along the traverse implies spatial and temporal heterogeneity in its source processes.

2-2 **Hong, Sang-Bum**, and 5 others. 2011. “Ionic composition comparison of atmospheric aerosols at coastal and mountainous sites of jeju island”. *Analytical Science & Technology,* 24(1): 24-37.

The ionic compositions of atmospheric aerosols were investigated and characterized in coastal and mountainous sites of Jeju Island, which were Gosan and Mt. Halla-1100 sites respectively. It was found that the concentrations of nss-SO_4^{2-} (non-sea salt sulfate) and NH_4^+ at two measurement sites were almost similar and they showed high concentrations in June at the same time. The concentration of soil-originated nss-Ca^{2+} (non-sea salt calcium) was generally associated with that of anthropogenic NO_3^- and its concentration was increased during spring season. From the comparison of time-series variation and regression analysis of ionic species between two measurement sites, TSP (total suspended particulate) in Gosan site was directly influenced by sea salt particles and the concentration levels of nss-SO_4^{2-}, NH_4^+, nss-Ca2+, K+, and NO_3^- were mainly related with long-range transported air pollutants rather than local pollution sources.

2-3 **Hong, Sang-Bum**, and 5 others. 2011. “Characteristics of formate and acetate concentrations in precipitation at Jeju Island, Korea”. *Atmospheric Research,* 101(1-2): 427-437.
doi: 10.1016/j.atmosres.2011.04.001

$HCOO^-$ and CH_3COO^- concentrations were analyzed in precipitation samples collected at two sites on Jeju Island during 1997–2003: one at Mt. Halla and the other within Jeju City. The volume-weighted mean concentrations of $HCOO^-$ and CH_3COO^- were 1.28 and 0.89 μmol/L at Mt. Halla, and 2.06 and 1.15 μmol/L in Jeju City, respectively. Those ionic components showed low concentrations in summer compared to other seasons. In order to investigate major factors to affect the concentration variations of the organic acids in precipitation, the concentrations of the organic acids between growing and non-growing seasons of plants, the regression analyses and the ratios of $HCOO^-/CH_3COO^-$ were xamined. As a result, it is considered that the concentrations of $HCOO^-$ and CH_3COO^- in precipitation might be influenced mainly by photochemical conversion of precursors emitted from terrestrial vegetation during active plant growing seasons, but by direct emission from the anthropogenic sources such as vehicles during non-growing seasons. The high concentrations of $HCOO^-$ and CH_3COO^- were mostly associated with northwesterly winds from the continental area, on the other hand, the low concentrations with the winds coming from the North Pacific. The contributions to precipitation acidity by HCOOH and CH_3COOH tended to increase during the plant growing seasons, remaining at a low 10% throughout most of the events, while increasing to 30–40% during occasional precipitation events.

2-4 Howell, Jason, **Jusun Woo**, and Sung Kwun Chough. 2011. "Dendroid morphology and growth patterns: 3-D computed tomographic reconstruction". *Palaeogeography, Palaeoclimatology, Palaeoecology,* 299(1-2): 335-347.
doi: 10.1016/j.palaeo.2010.11.013

This paper analyzes the growth patterns of dendrolite in the Zhangxia Formation (Middle Cambrian), Shandong Province, China, using the technique of 3-D computed tomographic reconstruction. Dendroids are classified into V-dendroids, columnar dendroids, and arborescent dendroids, based on morphological characteristics. The means of interconnection between dendroids are classified into trunks, nodules, shoots, and fingers. Stacking and tiering control the gross morphology and structural framework of dendrolite. Stacking is a process of vertical growth, in which V-dendroids create a staircase-like structure. Tiering occurs when a layer of dendroids is covered by sediment, and then partially eroded, allowing a new layer of dendroids to form. A comprehensive blueprint of the structural divisions of dendrolite is presented, according to scale, being divided into micro-, meso-, macro-, and megastructures. The mesostructure, which includes individual dendroids and their combined structures, is subsequently divided into primary (V-dendroid), secondary (columnar and arborescent dendroid), and tertiary (stair and tier) structures and a basic growth model is provided for V-dendroids. The stages of V-dendroid growth are: 1) trunk extension and base expansion, 2) divergence, 3) expansion and convergence, followed by repetition of stages 2 and 3, until 4) growth completion, followed by the subsequent emergence of a new dendroid by either stacking or tiering. This development of systematically ordered structures is suggestive of the reaction of microbial colonies to external environmental conditions.

2-5 Hwang, Jeong, Zheng Xiangshen, Edward M Ripley, **Jong-Ik Lee**, Dongbok Shin. 2011. "Isotope Geochemistry of Volcanic Rocks from the Barton Peninsula, King George Island, Antarctica". *Journal of Earth Science,* 22(1): 40-51.
doi: 10.1007/s12583-011-0156-y

C, O, H, S and Sr isotopes were investigated to characterize the isotopic composition of the Paleocene–Eocene volcanic rocks in Barton Peninsula, King George Island, Antarctica. The analyzed samples of volcanic rocks cover a range from basalt to andesite. The $\delta^{13}C$ and $\delta^{18}O$ values of calcite in volcanic rocks range from -7.5‰ to -3.2‰ and 0.4‰ to 5.1‰, respectively. The homogenous $\delta^{13}C_{cal}$ and depleted $\delta^{18}O_{cal}$ values relative to primary magmatic values reflect the effect of high temperature alteration of volcanic rocks. The $\delta^{18}O$ of volcanic rocks ranges from -1.1‰ to 7.2‰, and the majority of values are significantly lower than those of primary magmatic values. The low $\delta^{18}O_{WR}$ values are compatible with high temperature alteration. The initial values of $^{87}Sr/^{86}Sr$ of volcanic rocks span a narrow range from 0.703 312 to 0.703 504 which belong to the present mid-oceanic ridge basalt. The values of $^{87}Sr/^{86}Sr$ of volcanics in the Barton Peninsula are similar to those determined in the Fildes Peninsula, King George Island. The δD_{WR} and H_2O contents of volcanic rocks range from -74‰ to -66‰ and 0.67 wt.% to 2.74 wt.%, respectively. The higher δD_{WR} and H_2O wt.% of volcanic rocks relative to fresh basalts also result from high temperature alteration. Sulfur isotope compositions of the volcanic rocks range from -12.5‰ to -7.0‰; these values may represent fractionation accompanying partial oxidation of magmatic S or incorporation of some bacteriogenic sulfide. The low S contents and negative correlation with C and H_2O reflect the formation of calcite and breakdown of sulfide as a result of high temperature water-rock interaction.

2-6 Hyeong, Kiseong, Jonguk Kim, Thomas Pettke, Chan Min Yoo, and **Soon-do Hur**. 2011. “Lead, Nd and Sr isotope records of pelagic dust: Source indication versus the effects of dust extraction procedures and authigenic mineral growth”. *Chemical Geology,* 286(3-4): 240-251.
doi: 10.1016/j.chemgeo.2011.05.009

Eolian silicate dust of the 328 cm long piston core KODOS 02-01-02 from the northeast equatorial Pacific was analyzed for chemical compositions and Nd, Sr, and Pb isotopic ratios to evaluate their use as hemispheric dust source discriminator and to examine the potential influence of authigenic smectite on these source signals. Neodymium and Sr isotope ratios of the core determine a change from southern to northern hemisphere dust deposition at about 7.6 Ma. Samples deposited between 15.5 and 7.6 Ma resemble southeast equatorial Pacific surface and down-core dust values, while younger samples correspond to signatures typical for dust derived from central Asia. The 15.5 to 7.6 Ma lower interval of the core is smecite-rich; however, previously proposed chemical fingerprints for authigenic smectite such as positive Eu anomalies or high Fe/Al ratios are not observed in the KODOS samples. The up to 40% smectite in the KODOS core dust are thus interpreted to represent largely detrital smectite, and no evidence is found for authigenic modification of Nd–Sr isotopic or element ratio source signals of the dust records. Lead isotope results of the core lack prominent down-core variation with changing source regimes as reported above. A compilation of Pacific Pb isotope dust records reveals that Pb isotope ratios vary as a function of silicate dust extraction procedures. The step of removing biogenic silica thereby appears critical. Use of NaOH appears most effective, while minimally attacking eolian silicate material. It is concluded that of the Pb isotopic dust records published so far, only a few are useful for dust source identification. However, once the silicate dust extraction procedure is further optimized for retrieving the pristine silicate dust Pb isotopic composition, specific source signatures should become well resolvable.

2-7 **Jin, Young Keun**, **Young-Gyun Kim**, and 3 others. 2011. “Distribution and expression of gas seeps in a gas hydrate province of the northeastern Sakhalin continental slope, Sea of Okhotsk”. *Marine and Petroleum Geology,* 28(20): 1844-1855.
doi: 10.1016/j.marpetgeo.2011.03.007

Multidisciplinary surveys were conducted to investigate gas seepage and gas hydrate accumulation on the northeastern Sakhalin continental slope (NESS), Sea of Okhotsk, during joint KoreaneRussian eJapanese expeditions conducted from 2003 to 2007 (CHAOS and SSGH projects). One hundred sixtyone gas seeps were detected in a 2000 km^2 area of the NESS (between 53°45'N and 54°45'N). Active gas seeps in a gas hydrate province on the NESS were evident from features in the water column, on the seafloor, and in the subsurface: well-defined hydroacoustic anomalies (gas flares), side-scan sonar structures with high backscatter intensity (seepage structures), bathymetric structures (pockmarks and mounds), gas- and gas-hydrate-related seismic features (bottom-simulating reflectors, gas chimneys, high-amplitude reflectors, and acoustic blanking), high methane concentrations in seawater, and gas hydrates in sediment near the seafloor. These expressions were generally spatially related; a gas flare would be associated with a seepage structure (mound), below which a gas chimney was present. The spatial distribution of gas seeps on the NESS is controlled by four types of geological structures: faults, the shelf break, seafloor canyons, and submarine slides. Gas chimneys that produced enhanced reflection on high-resolution seismic profiles are interpreted as active pathways for upward gas migration to the seafloor. The chimneys and gas flares are good indicators of active seepage.

2-8 **Kang, JH, SD Hur**, and 3 others. 2011. “MONITORING OF HEXACHLOROCYCLOHEXANES IN SNOW FROM THE EAST ANTARCTICA”. *Organohalogen Compounds (OHC),* 73(1): 1091-1093.

2-9 Kim, Dae Seong, **Sang Bum Hong**, and 2 others. 2011. “Evaluation of particle growth systems for sampling and analysis of atmospheric fine particles”. *Particuology,* 9(6): 606-610. doi: 10.1016/j.partic.2011.04.007

Three types of water-based condensational growth systems, which can enable particles to grow in size to facilitate sampling and subsequent chemical analysis, were evaluated. The first one is a mixing type growth system where aerosols are mixed with saturated water vapor, the second one is a thermal diffusive growth system where warm flow enters cold-walled tube, and the third one is a laminar flow type where cold flow enters a warm wet-wall tube. Hygroscopic sodium chloride (NaCl), ammonium sulfate $((NH_4)_2SO_4)$ and ammonium nitrate (NH_4NO_3), and non-hygroscopic polystyrene latex (PSL) particles, in the size range of 50–400 nm, were used to determine their growth factors through the growth systems. Our data showed that the third-type growth system could enable particles to grow most efficiently regardless of their hygroscopic property. Collection efficiency of particles in the size range of 0.05–2.5 m, in a continuous aerosol sampler after they passed through the third-type growth system was about 100%, suggesting that the third-type growth system would be the most useful among the tested growth systems for sampling and subsequent chemical analysis of fine and ultrafine particles.

2-10 **Lee, Choon-Ki**, and 3 others. 2011. “Validation of international reference ionosphere models using in situ measurements from GRACE K-band ranging system and CHAMP planar Langmuir probe”. *Journal of Geodesy,* 85(12): 921-929. doi: 10.1007/s00190-011-0442-6

The in situ measurements of electron contents from GRACE K-band (dual-frequency) ranging system and CHAMP planar Langmuir probe were used to validate the international reference ionosphere (IRI) models. The comparison using measurements from year 2003 to 2007 shows a general agreement between data and themodel outputs. The improvement in the newer IRI model (IRI-2007) is evident with the measurements from the GRACE satellites orbiting at the higher altitude. We present the comparison between the models and data comprehensively for various cases in solar activity, local time, season, and latitude. The IRI models do not well predict the electron density in the years 2006 and later, when the solar activity is extremely low. The IRI models generally overestimate the electron density during local winter while they underestimate during local summer. In the equatorial region, the large difference at local sunrise lasts for all years and all seasons. The IRI models do not perform well in predicting the anomaly in the polar region such as the Weddell Sea Anomaly. These discrepancies are likely due to smoothed (12-month averaged) solar activity indices used in the IRI models and due to insufficient spherical harmonic representation not able to capture small spatial scales. In near future, further improvement on the IRI models is expected by assimilating those in situ satellite data by implementing higher resolution (spatial and temporal) parameterizations.

2-11 **Lee, Jeonghoon** and Kyung-Seok Ko. 2011. “An Energy Budget Algorithm for a Snowpack-Snowmelt Calculation”. *Journal of Soil and Groundwater Environment,* 16(5): 82-89.

Understanding snowmelt movement to the watershed is crucial for both climate change and hydrological studies because the snowmelt is a significant component of groundwater and surface runoff in temperature area. In this work, a new energy balance budget algorithm has been developed for melting snow from a snowpack at the Central Sierra Snow Laboratory (CSSL) in California, US. Using two sets of experiments, artificial rain-on-snow experiments and observations of diel variations, carried out in the winter of 2002 and 2003, we investigate how to calculate the amount of snowmelt from the snowpack using radiation energy and air temperature. To address the effect of air temperature, we calculate the integrated daily solar radiation energy input, and the integrated discharge of snowmelt under the snowpack and the energy required to generate such an amount of meltwater. The difference between the two is the excess (or deficit) energy input and we compare this energy to the average daily temperature. The resulting empirical relationship is used to calculate the instantaneous snowmelt rate in the model used by Lee et al. (2008a; 2010), in addition to the net-short radiation. If for a given 10 minute interval, the energy obtained by the melt calculation is negative, then no melt is generated. The input energy from the sun is considered to be used to increase the temperature of the snowpack. Positive energy is used for melting snow for the 10-minute interval. Using this energy budget algorithm, we optimize the intrinsic permeability of the snowpack for the two sets of experiments using one-dimensional water percolation model, which are 52.5×10^{-10} m^2 and 75×10^{-10} m^2 for the artificial rain-on-snow experiments and observations of diel variation, respectively.

2-12 **Lee, Khanghyun**, **Soon Do Hur**, and 6 others. 2011. “Isotopic signatures for natural versus anthropogenic Pb in high-altitude Mt. Everest ice cores during the past 800 years”. *Science of the Total Environment,* 412-413: 194-202. doi: 10.1016/j.scitotenv.2011.10.002

A long-term record, extending back 800 years (1205 to 2002 AD), of the Pb isotopic composition ($^{206}Pb/^{207}Pb$ and $^{208}Pb/^{207}Pb$) as well as Pb concentrations from high altitude Mt. Everest ice cores has the potential to identify sources and source regions affecting natural and anthropogenic Pb deposition in central Asia. The results show that the regional natural background Pb isotope signature (~1.20 for ^{206}Pb/^{207}Pb and ~2.50 for ^{208}Pb/^{207}Pb) in the central Himalayas was dominated by mineral dust over the last ~750 years from 1205 to 1960s, mostly originating from local sources with occasional contributions of long-range transported dust probably from Sahara desert and northwestern India. Since the 1970s, the Pb isotope ratios are characterized by a continuous decline toward less radiogenic ratioswith the leastmean ratios of 1.178 for ^{206}Pb/^{207}Pb and 2.471 for ^{208}Pb/^{207}Pb in the period 1990–1996. The depression of the ^{206}Pb/^{207}Pb and ^{208}Pb/^{207}Pb values during the corresponding periods ismost likely due to an increasing influence of less radiogenic Pb of anthropogenic originmainly from leaded gasoline used in South Asia (India aswell as possibly Bangladesh and Nepal). From 1997 to 2002, isotopic composition tends to show a shift to slightly more radiogenic signature. This is likely attributed to reducing Pb emissions from leaded gasoline in source regions, coinciding with the nationwide reduction of Pb in gasoline and subsequent phase-out of leaded gasoline in South Asia since 1997. An interesting feature is the relatively high levels of Pb concentrations and enrichment factors (EF) between 1997 and 2002. Although the reason for this feature remains uncertain, it would be probably linked with an increasing influence of anthropogenic Pb emitted from other sources such as fossil fuel combustion and non-ferrous metal production.

2-13 **Lee, Mi Jung**, **Jong Ik Lee**, Sung-Tack Kwon, **Mi Kyung Choo**, and 3 others. 2011. "Sr-Nd-Pb isotopic compositions of submarine alkali basalts recovered from the South Korea Plateau, East Sea". *Geosciences Journal,* 15(2): 149-160.
doi: 10.1007/s12303-011-0017-9

We present geochemical and isotope results (Sr, Nd, Pb) on submarine basalts dredged from the southeastern margin of the South Korea Plateau. The present data are the first geochemical result obtained on submarine basaltic lavas recovered from the Korea Plateau, which is considered to be one of rifted remnants of continent in the East Sea (Sea of Japan) and partially segmented from the Korean Peninsula. The South Korea Plateau basalts (SKPB) show alkali affinities and are characterized by Ocean Island Basalts (OIB)-like trace element compositions relatively enriched in Ba, Nb and Pb. They display relatively flatter [(Ce/Yb)n = 4.49~5.46] and less fractionated HREE [(Dy/Yb)n = 1.11~1.29] patterns compared to average OIB, implying that the SKPB were derived from a relatively shallower mantle depth with a larger degree of partial melting. The Sr, Nd and Pb isotopic compositions of the SKPB display a range of values for ^{87}Sr/^{86}Sr (0.70378 to 0.70409), ^{143}Nd/^{144}Nd (0.512846 to 0.512860) and ^{206}Pb/^{204}Pb (17.88–18.44). They show a considerably high range of ^{207}Pb/^{204}Pb (15.48–15.62) and ^{208}Pb/^{204}Pb (37.86–38.46) values, indicating the involvement of a DUPAL-like MORB source. According to our two-stage magma mixing model, the isotopic compositions of SKPB can be explained by magma source mixing by the addition of an EMII-like mantle component (up to 2%) to the DUPAL-like MORB source embedded with endogenous EMI-like material (about 2%).

2-14 **Lee, Won Sang**. 2011. "Observation of Underwater Earthquakes by Using a Hydroacoustic Monitoring System". *Physics & High Technology,* 20(7): 2-7.
doi: 10.3938/PhiT.20.029

Substantial advances in seismograph technology enable us to precisely and extensively monitor earthquakes occurring everywhere in the world, yet underwater tectonic events have remained insufficiently studied due to a dearth of seismic networks in the oceans. Hydroacoustic monitoring allows the detection and the precise location of small submarine earthquakes and volcanic activity. Furthermore, through hydroacoustic observation, we are able to examine cryogenic signals, which are closely associated with changes in the polar environment, baleen whale calls, and catastrophic tsunamis.

2-15 **Lee, Won Sang**, Dong-Hoon Sheen, **Sukyoung Yun**, and **Ki-Weon Seo**. 2011. “The Origin of Double-Frequency Microseism and Its Seasonal Variability at King Sejong Station, Antarctica”. *Bulletin of the Seismological Society of America,* 101(3): 1446-1451. doi: 10.1785/0120100143

Korea Polar Research Institute has been operating a broadband seismic station (KSJ1) at the King George Island (KGI), Antarctica, since 2001. Examining ambient seismic noise level using power spectral analysis for the period of 2006-2008 at the KSJ1, we observed a seasonal pattern at 4-10 s period. The amplitude of double-frequency (DF) microseism reaches a peak in May. Correlation of the DF energy and its predominant period with significant ocean wave height and peak wave period models from the WAVEWATCH III, and polarization analysis consistently indicate that ocean swell in the Drake Passage is a possible source to excite the DF microseism at the KGI. We also found that the temporal variation of DF amplitude is coincident with the seasonal change of ocean acoustic ambient noise level around the KGI, which implies that incorporating long-term seismic and hydroacoustic noise information might give us an opportunity to figure out the characteristics of local climate variation near the Antarctic Peninsula.

2-16 Liu, Yaping, Shugui Hou, **Sungmin Hong**, **Soon Do Hur**, **Khanghyun Lee**, and Yetang Wang. 2011. “High-resolution trace element records of an ice core from the eastern Tien Shan, central Asia, since 1953 AD”. *Journal of Geophysical Research,* 116: D12307(1-14). doi: 10.1029/2010JD015191

High-resolution records of trace elements (Ba, V, Cr, Mn, Co, Ni, Cu, As, Rb, Sr, Mo, Cd, Sn, Sb, Tl, Pb, Bi, Th, and U) quantified in an ice core recovered from the Miaoergou glacier in the eastern Tien Shan, central Asia, spanning the period 1953–2004 AD, provide the first comprehensive time series on characterizing the relative contributions from natural and anthropogenic sources to the deposition of trace elements in central Asia. It is suggested that rock and soil dust is the most important natural source for most of elements investigated. Slight decreases in concentrations (or fallout fluxes) of crustal elements, such as Ba, Mn, Rb, Th, U, and Sr are observed during recent decades, which may be due to decreases in dust emissions from source regions and a decrease of accumulation rate since 1980s. The increasing trends of median concentrations and crustal enrichment factors (EF_C) of V, Cr, Co, Ni, Cu, and Mo, during the period 1953–2004 AD, are insignificant in comparison to their respective levels prior to 1953 AD. However, slight enhancements of both concentrations and EF_C are observed for Cd, Sb, Pb, Bi, Tl, and Sn since 1950s. Such recent increases are likely to be attributed to enhanced anthropogenic emissions, such as metal smelting, mining, stationary fossil fuel combustion, and combustion of gasoline due to human activities in Eurasia, particularly Xinjiang in northwestern China, Russia, and Kazakhstan. Our study supports evidence that environmental contamination has become a global problem for Pb and Bi and a large-scale phenomenon for Cd, Sb, Tl, and Sn.

2-17 Liu, Yaping, Shugui Hou, **Sungmin Hong**, **Soon-Do Hur**, **Khanghyun Lee**, and Yetang Wang. 2011. “Atmospheric pollution indicated by trace elements in snow from the northern slope of Cho Oyu range, Himalayas". *Environmental Earth Sciences,* 63(2): 311-320. doi: 10.1007/s12665-010-0714-0

Samples collected from a 0.87 m snow pit at a high altitude site in the Cho Oyu range, Himalayas were measured for V, Cr, Mn, Co, Ni, Cu, Zn, As, Rb, Sr, Cd, Sn, Sb, Ba, Tl, Pb, Bi, Th, and U using inductively coupled plasma mass spectrometry. In addition, major ions, oxygen stable isotopes, and microparticles were also measured to assist the interpretation of seasonal variation of trace elements. The trace elements show a distinct seasonality, i.e., higher concentrations during the non-monsoon season than those during the monsoon season. Significant correlation is observed between Ba and the other trace elements. Crustal enrichment factor (EF_C) analysis indicates that V, Mn, Co, Ni, Rb, Sr, and Th originate mainly from crustal dust, while anthropogenic inputs make an important contribution to the other trace elements (i.e., Cu, Zn, As, Cd, Sn, Sb, Ti, Pb, Bi, and U). Evidence from air mass back trajectories suggests that atmospheric trace element pollution reaching the studied area is transported dominantly by Indian summer monsoon during the monsoon season, while it is transported mainly by the westerlies during the non-monsoon season.

2-18 **Seo, Ki-Weon**. 2011. "Data Reductions of Gravity Recovery and Climate Experiment (GRACE) Gravity Solutions and Their Applications". *Journal of Korean Earth Science Society,* 32 (6): 586-594. doi: 10.5467/JKESS.2011.32.6.586

Gravity Recovery and Climate Experiment (GRACE), launched in April, 2002, makes it possible to monitor Earth's mass redistribution with its time-varying gravity observation. GRACE provides monthly gravity solutions as coefficients of spherical harmonics, and thus ones need to convert the gravity spectrum to gravity grids (or mass grids) via the spherical harmonics. GRACE gravity solutions, however, include spatial alias error as well as noise, which requires to suppress in order to enhance signal to noise ratio. In this study, we present the GRACE data processing procedures and introduce some applications of time-varying gravity, which are studies of terrestrial water storage changes, Antarctic and Greenland ice melting, and sea level rise. Satellite missions such as GRACE will continue up to early 2020, and they are expected to be an essential resource to understand the global climate changes.

2-19 **Soyol-Erdene, Tseren-Ochir**, Youngsook Huh, Sungmin Hong, and **Soon Do Hur**. 2011. "A 50-Year Record of Platinum, Iridium, and Rhodium in Antarctic Snow: Volcanic and Anthropogenic Sources". *Environmental Science & Technology,* 45(14): 5929-5935. doi: 10.1021/es2005732

Antarctic snow preserves an atmospheric archive that enables the study of global atmospheric changes and anthropogenic disturbances from the past. We report atmospheric deposition rates of platinum group elements (PGEs) in Antarctica during the last 50 years based on determinations of Pt, Ir, and Rh in snow samples collected from Queen Maud Land, East Antarctica to evaluate changes in the global atmospheric budget of these noble metals. The 50-year average PGE concentrations in Antarctic snow were 17 fg g^{-1} (4.7–76 fg g^{-1}) for Pt, 0.12 fg g^{-1} (<0.05–0.34 fg g^{-1}) for Ir, and 0.71 fg g^{-1} (0.12–8.8 fg g^{-1}) for Rh. The concentration peaks for Pt, Ir, and Rh were observed at depths corresponding to volcanic eruption periods, indicating that PGEs can be used as a good tracer of volcanic activity in the past. A significant increase in concentrations and crustal enrichment factors for Pt and a slight enhancement in enrichment factors for Rh were observed after the 1980s. This suggests that there has been large-scale atmospheric pollution for Pt and probably for Rh since the 1980s, which may be attributed to the increasing emissions of these metals from anthropogenic sources such as automobile catalysts and metal production processes.

2-20 **Soyol-Erdene, Tseren-Ochir**, Youngsook Huh, Sungmin Hong, **Hee Jin Hwang**, and **Soon Do Hur**. 2011. “Quantification of Ultra-Trace Levels of Pt, Ir and Rh in Polar Snow and Ice Using ICP-SFMS Coupled with a Pre-Concentration and Desolvation Nebulization System”. *Bulletin of the Korean Chemical Society,* 32(6): 2105-2108. doi: 10.5012/bkcs.2011.32.6.2105

A revised analytical method is presented for the quantification of ultra trace level (fg mL^{-1}) PGEs (Pt, Ir and Rh) in polar snow and ice samples by focusing on the following issues: (i) evaluation of the efficiency of a non-boiling preconcentration procedure for analyses at the fg mL^{-1} level of PGEs in our laboratory; (ii) establishment of the appropriate instrumental conditions to obtain low detection limits, high accuracy and precision; and (iii) verification of the contributions of possible contamination during the ice core decontamination process using an artificial ice core as a sample.

2-21 Yang, Jin-Yong, **Kyung-Ho Chung**, **Young-Keun Jin**, and Kyung-Hoon Shin. 2011. “Characterizing lipid biomarkers in methanotrophic communities of gas hydrate-bearing sediments in the Sea of Okhotsk”. *Marine and Petroleum Geology,* 28(10): 1884-1898. doi: 10.1016/j.marpetgeo.2011.03.010

We studied specific lipid biomarkers of archaea and bacteria, that are associated with the anaerobic oxidation of methane (AOM) in a cold seep environment as well as the origin of sedimentary organic matter on the continental slope off NE Sakhalin in the Sea of Okhotsk. The organic geochemical parameters demonstrated that most of the sedimentary organic matter containing hydrate layers could be derived from marine phytoplankton and bacteria, except for a station (LV39-29H) which was remarkably affected by terrestrial vascular plant. Specific methanotrophic archaea biomarkers was vertically detected in hydrate-bearing cores (LV39-40H), coinciding with the negative excursion of the $\delta^{13}C_{org}$ at core depths of 90e100 cm below the seafloor. These results suggest that methane provided from gas hydrates are already available substrates for microbes thriving in this sediment depth. In addition, the stable isotope mass balance method revealed that approximately 2.77-3.41% of the total organic carbon (or 0.036-0.044% dry weight sediment) was generated by the activity of the AOM consortium in the corresponding depth of core LV39-40H. On the other hand, the heavier $\delta^{13}C$ values of archaeol in the gas hydrate stability zone may allow ongoing methanogenesis in deeper sediment depth.

2-22 Yoshimura, Kei, Christian Frankenberg, **Jeonghoon Lee**, and 3 others. 2011. “Comparison of an isotopic atmospheric general circulation model with new quasi-global satellite measurements of water vapor isotopologues”. *Journal of Geophysical Research,* 116: D19118(1-15). doi: 10.1029/2011JD016035

We performed an intensive comparison of an isotope-incorporated atmospheric general circulation model with vapor isotopologue ratio observation data by two quasi-global satellite sensors in preparation for data assimilation of water isotope ratios. A global Isotope-incorporated Global Spectral Model simulation nudged toward the reanalysis wind field, atmospheric total column data from Scanning Imaging Absorption Spectrometer for Atmospheric Cartography (SCIAMACHY) on Envisat, and midtropospheric (800 to 500 hPa) data from Tropospheric Emission Spectrometer (TES) on Aura were used. For the mean climatological δD of both the total atmospheric column and the midtroposphere layer, the model reproduced their geographical variabilities quite well. There is, however, some degree of underestimation of the latitudinal gradient (higher δD in the tropics and lower δD in midlatitudes) compared to the SCIAMACHY data, whereas there is generally less disagreement except lower δD over the Maritime Continent compared to the TES data. It was also found that the two satellite products have different relationships between water vapor amount and isotopic composition. Particularly, atmospheric column mean δD, which is dominated by lower-tropospheric vapor, closely follows the fractionation pattern of a typical Rayleigh-type "rain out" process, whereas in the midtroposphere the relationship between isotopic composition and vapor amount is affected by a "mixing" process. This feature is not reproduced by the model, where the relationships between δD and the vapor are similar to each other for the atmospheric column and midtroposphere. Comparing on a shorter time scale, it becomes clear that the data situation for future data assimilation for total column δD is most favorable for tropical and subtropical desert areas (i.e., Sahel, southern Africa, mideastern Asia, Gobi, Australia, and the southwest United States), whereas the available midtropospheric δD observations cover wider regions, particularly over tropical to subtropical oceans.

PART 3

Ocean Environment Sciences

3-1 Brey, Thomas, Matthias Voigt, Kristen Jenkins, and **In-Young Ahn**. 2011. "The bivalve *Laternula elliptica* at King George Island – A biological recorder of climate forcing in the West Antarctic Peninsula region". *Journal of Marine Systems,* 88: 542-552. doi: 10.1016/j.jmarsys.2011.07.004

The West Antarctic Peninsula (WAP) has experienced marked recent climate change. Air temperature increased by ≤3℃ since the 1950s, glaciers are in retreat, and adjacent ocean sea ice cover has decreased. WAP also exhibits considerable inter-annual ocean–atmosphere variability, governed by the Southern Hemisphere Annular Mode (SAM) and by the Antarctic Dipole (ADI), which is itself modulated by ENSO. Both climate trends and oscillations affect WAP ecosystems, but sound evidence for mechanistic coupling of distinct processes to climate change is scarce. We analyzed decadal variability in shell growth over the past 49 years for the bivalve *Laternula elliptica* at Maxwell Bay, King George Island. Distinct changes in shell growth pattern include a near doubling of specific growth rate, a 25% decrease in maximum size, and a shift in individual energy expenditure from production to respiration. ENSO forces shell growth through local air temperature that constitutes the major link between regional climate forcing and the direct marine drivers of *L. elliptica* growth. The close coupling of shell growth to local and regional climate variability renders *L. elliptica* a promising tool for tracking climate forcing of Antarctic coastal systems ingeneral, aswell as for the reconstruction of coastal ecosystem variability from fossil shells.

3-2 Chang, Tae Soo and **Seung-Il Nam**. 2011. "Geochemical logging of shallow-sea tidal bar sediment cores using a XRF core scanner: an application of XRF core-scanning to lithostratigraphic analysis". *Journal of the Geological Society of Korea,* 47(5): 471-484.

In order to evaluate the relationship between lithostratigraphy and geochemistry of core sediments using a XRF core scanner, two drilled-cores collected on a large tidal bar, outer Asan Bay of Korea were examined. Stable isotopes of organic carbon and nitrogen and organic carbon and $CaCO_3$ measured by a CHN analyzer were additionally used for correlation of the investigated cores, complemented by ^{14}C ages of foraminifera. The Asan bay tidal bar deposits can be divided into four major facies assemblages: a) fluvial deposits, b) transgressive gravel lag deposits, c) estuarine tidal flat deposits and d) tidal bar deposits in ascending order. The Holocene stratigraphy reveals an overall trend of upward-coarsening textural composition indicative of transgressive deposition coupled with local sea-level rise, tidal-flat muds being overlain by sand-dominated tidal bar successions. These lithostratigraphic units correlate well with the chemical logging data. Terrigenous elements such as Al, Si, K, Ti and Fe show distinctly the greatest value at the interval of fluvial deposits, and medium value in tidal mud beds. However, these elements are poorer in uppermost tidal bar succession. The opposite pattern is shown in biogenic elements such as Ca, Mn, Br and Sr. Organic matter contents and stable isotopes of organic carbon and nitrogen reveal that terrigenous organic matters were dominated in tidal mud deposits, by contrast, at the upper sand bar interval, organic matters were derived from marine environment. The XRF core scanning data seem to be thus applicable, thereby chemical logging data being paleoenvironmental proxy.

3-3 **Choy, Eun Jung**, **Hyun Park**, **Jeong-Hoon Kim**, **In-Young Ahn**, and Chang-Keun Kang. 2011. "Isotopic shift for defining habitat exploitation by the Antarctic limpet *Nacella concinna* from rocky coastal habitats (Marian Cove, King George Island)". *Estuarine, Coastal and Shelf Science,* 92(3): 339-346. doi: 10.1016/j.ecss.2011.01.009

$\delta^{13}C$ and $\delta^{15}N$ of the Antarctic limpet *Nacella concinna* tissues and their potential food sources were used to determine their dietary origins and their movements between diverse habitats of intertidal and subtidal rocky shores and tide pools of Marian Cove, King George Island, Antarctica in the austral summer. $\delta^{13}C$ and $\delta^{15}N$ of the organic matter sources of epilithic microalgae, macroalgae and suspended particulate organic matter (SPOM) were readily distinguishable to iscern their relative contribution to the limpet diets, with the most depleted values being found in SPOM and the most enriched in macroalgae. The limpets exhibited a spatial trend in distribution due to their seasonal migration, with smaller individuals in the subtidal zone compared with larger ones on the intertidal sites. The limpet isotopes had relatively broad ranges of $\delta^{13}C$ and $\delta^{15}N$ (-26.6 to -12.8‰ and 2.6-7.1‰, respectively), suggesting a dietary shift between habitats as well as size classes. The stable isotope ratios for each habitat seem likely to reflect the differing availabilities of the three potential food sources. Isotope mixing model results indicate a spatial shift in dietary mixture between habitats as well as limpet size classes. Epilithic microalgae and phytoplankton made great contributions to the diet of the subtidal limpets. Together with epilithic microalgae, macroalgae were significant contributors to the intertidal limpets where macroalgae were abundant. A higher contribution of macroalgae to the limpet diets was found in the tide pools. In contrast, while phytoplankton was an important food source for the limpet spat, a great dietary dependence on epilithic microalgae was found in the small-size limpets from the lower intertidal zone. Our results suggest that limpet grazing can determine microalgal and/or macroalgal abundance and coverage on the Antarctic rocky-shore ecosystem, and trophic structure of benthic food web can change along environmental gradients even at spatial scales of tens or hundreds of metres in the Antarctic.

3-4 Dzwonkowski, Brian, Kyeong Park, **Ho Kyung Ha**, and 3 others. 2011. "Hydrographic variability on a coastal shelf directly influenced by estuarine outflow". *Continental Shelf Research,* 31(9): 939-950. doi: 10.1016/j.csr.2011.03.001

Hydrographic variability on the Alabama shelf just outside of Mobile Bay, a major source of river discharge into the Gulf of Mexico, is examined using time series of water column temperature and surface and bottom salinity from a mooring site with a depth of 20 m in conjunction with a series of across-shelf CTD surveys. The time series data show variability in a range of time scales. The density variation is affected by both salinity and temperature, with its relatively strong annual signal mostly determined by temperature and its year to year variability mostly determined by salinity. Seasonal mean structures of temperature, salinity, and density show a transition from estuarine to shelf conditions in which three regions with distinct seasonal characteristics in their horizontal and vertical gradient structures are identified. Correlation analysis with the available forcing functions demonstrates the influence of Mobile Bay on the variability at the mooring site. At low frequencies, river discharge from Mobile Bay has a varying influence on salinity, which is absent during the periods with unusually low discharge. At shorter synoptic time scales, both the estuarine response to the crossshelf wind stress and the shelf response to the along-shelf wind stress are significantly correlated with temperature/salinity variability: the former becoming important for the surface layer during winter whereas the latter for the bottom layer during both winter and summer. These forcing functions are important players in determining the estuarine–shelf exchange, which in turn is found to contribute to the shelf hydrographic structure.

3-5 **Ha, H. K.**, and 3 others. 2011. "Estimation of high-resolution sediment concentration profiles in bottom boundary layer using pulse-coherent acoustic Doppler current profilers". *Marine Geology,* 279(1-4): 199-209. doi: 10.1016/j.margeo.2010.11.002

The capability of two acoustic profilers — SonTek's 1.5-MHz pulse-coherent acoustic Doppler profiler (PC-ADP) and RDI's 600-kHz acoustic Doppler current profiler (ADCP) with pulse-coherent mode — was evaluated for estimating high-resolution suspended sediment concentration (SSC) profiles in bottom boundary layer. In the laboratorymeasurementswith a PC-ADP, two types of sedimentswere tested to study acoustic responses to grain size. A natural sediment sample from Clay Bank, a mixture of clay and very fine sand, showed a good linear relationship between range-corrected volume scattering ($\overline{S_v}$) and backscattered strength (E) until SSC increased up to about 10 g l^{-1}. In contrast, a commercially available kaolinite exhibited earlier signal saturation and nonunified linear regressions between $\overline{S_v}$ and E, most likely because the particle size is much smaller than the transmitted acousticwavelength. Using a pulse-coherent ADCP, the fieldmeasurement results fromMobile Bay, Alabama showed that the acoustically-derived SSC profiles were well matched with the optically-derived outcomes although slight discrepancieswere noted. The overestimation of acoustically-derived SSC near the bed may be related to the side lobe interferencenear the bed and the enhanced acoustic sensitivity by coarser particles and denser aggregates eroded fromthe bed.Mean absolute error of acoustic estimateswas within 4.1–7.3% of the optically-derived SSC range, which is attributable to the different acoustic and optical scattering responses to given sediment size spectra.Despite someerror sources in acoustic inversion, the results fromlaboratory and field experiments suggest that the pulse-coherent acoustic profiler is able to reveal the evolution of in-situ near-bed SSC profiles with high vertical and temporal resolutions.

3-6 **Hong, Sung Soo**, **Soo Young Lee**, **Young Nam Kim**, **Sung-Ho Kang**, and **Hak Jun Kim**. 2011. “A Modified Cryopreservation Method of Psychrophilic Chlorophyta *Pyramimonas* sp. from Antarctica”. *Ocean and Polar Research,* 33(3): 303-308.
doi: 10.4217/OPR.2011.33.3.303

Polar psychrophiles which thrive under extreme conditions such as cold temperature, high salinity, and high dose ultraviolet light, emerge as novel targets for biotechnology. To prevent genetic drift and the possibility of contamination by subculturing, cryopreservation was employed for two psychrophilic microalgae, *Porosira* sp. (KOPRI AnM0008) and *Pyramimonas* sp. (KOPRI AnM0046), which have antifreeze activities. Five cryoprotectants (dimethyl sulphoxide, ethylene glycol, glycerol, methanol and propylene glycol) showed toxicity at 20-30% (v/v). The optimal cryoprotectant concentration and equilibration time were less than 20% and 10 min, respectively. Cryopreservation was carried out in the presence of cryoprotectants either by direct freezing in liquid nitrogen (LN_2) or controlled freezing using a controlled rate freezer followed by storage in the LN_2 tank. As a result, *Pyramimonas* sp. (KOPRI AnM0046), a psychrophilic chlorophyta was revived. Cryopreserved *Porosira* sp. was not revived from either freezing protocols probably due to the silicic cell wall and its relatively large cell size. In the case of *Pyramimonas* sp. (KOPRI AnM0046), the controlled freezing method showed higher revival yield than the direct freezing method.

3-7 **Joo, Hyoung Min**, and 4 others. 2011. “Latitudinal variation of phytoplankton communities in the western Arctic Ocean”. *Deep-Sea Research II,* 81-84(15): 3-17.
doi: 10.1016/j.dsr2.2011.06.004

Recent studies have shown that photosynthetic eukaryotes are an active and often dominant component of Arctic phytoplankton assemblages. In order to explore this notion at a large scale, samples were collected to investigate the community structure and biovolume of phytoplankton along a transect in the western Arctic Ocean. The transect included 37 stations at the surface and subsurface chlorophyll a maximum (SCM) depths in the Bering Sea, Chukchi Sea, and Canadian Basin from July 19 to September 5, 2008. Phytoplankton (>2 μm) were identified and counted. A cluster analysis of abundance and biovolume data revealed different assemblages over the shelf, slope, and basin regions. Phytoplankton communities were composed of 71 taxa representing Dinophyceae, Cryptophyceae, Bacillariophyceae, Chrysophyceae, Dictyochophyceae, Prasinophyceae, and Prymnesiophyceae. The most abundant species were of pico- to nano-size at the surface and SCM depths at most stations. Nano- and pico-sized phytoplankton appeared to be dominant in the Bering Sea, whereas diatoms and nano-sized plankton provided the majority of taxon diversity in the Bering Strait and in the Chukchi Sea. From the western Bering Sea to the Bering Strait, the abundance, biovolume, and species diversity of phytoplankton provided a marked latitudinal gradient towards the central Arctic. Although pico- and nano-sized phytoplankton contributed most to cell abundance, their chlorophyll a contents and biovolumes were less than those of the larger micro-sized taxa. Micro-sized phytoplankton contributed most to the biovolume in the largely ice-free waters of the western Arctic Ocean during summer 2008.

3-8 Kang, Chang-Keun, **Eun Jung Choy**, and 4 others. 2011. “Physiological energetics and gross biochemical composition of the ascidian *Styela clava* cultured in suspension in a temperate bay of Korea”. *Aquaculture,* 319: 168-177.
doi: 10.1016/j.aquaculture.2011.06.016

The ascidian *Styela clava* has recently become a common species for suspended aquaculture in Korea. Because of the ecological and commercial importance of this species, it is important to understand seasonal variations in its physiological energetics and gross biochemical composition. The purpose of this study was to determine fundamental biological traits for the cultivation of *S. clava*. Physiological processes (food consumption, feces production, ammonia excretion and respiration), and gross biochemical composition (protein, lipids, and carbohydrates) of the ascidian were measured monthly from April 2008 to April 2009 under *in situ* environmental conditions in a mariculture region on the temperate coast of Jindong Bay, Korea. Changes in the physiology and somatic growth of *S. clava* were largely influenced by seasonal variation in water temperatures. The reduced importance of food availability in explaining their physiological adjustments seems to be due to low seston concentrations in water column of the bay. Seasonal variations in the ingestion and respiration rates of the ascidians were mismatched, resulting in an energy imbalance (i.e. an increased metabolic energy cost and lowered ingestion rate; and *vice versa*). This mismatched activity resulted in negative scope for growth (SFG) values during spring–summer, followed by rapid exhaustion of energy reserves and flesh weight loss. Weight loss during this period was also related to spring spawning. During autumn–winter, the ascidians had a positive SFG as a result of decreased oxygen consumption and elevated ingestion rates, showing accumulation of nutrient reserves and weight gain. The ascidians showed positive SFG, even in cold conditions below 12 ℃ in the present study. In this respect, an autumn–winter culturing period is recommended to maximize ascidian production in long-line suspended culture under the natural environmental conditions occurring in the study area.

3-9 Kim, Gwang Hoon, Tatyana A. Klochkova, Jong Won Han, **Sung-Ho Kang**, **Han Gu Choi**, and 2 others. 2011. “Freshwater and Terrestrial Algae from Ny-Ålesund and Blomstrandhalvøya Island (Svalbard)”. *Arctic,* 64(1): 25-31.

A field survey of algae and cyanobacteria from terrestrial and freshwater habitats in the vicinity of Ny-Ålesund and on Blomstrandhalvøya Island (Svalbard) was performed in June 2009, and results were compared with data from our fieldwork in June 2006. In total, we identified 30 taxa belonging to 23 genera from the specimens collected near Ny-Ålesund (26 taxa) and on Blomstrandhalvøya Island (24 taxa). Five species previously unrecorded from this locality are depicted, including astaxanthin-containing *Haematococcus* sp. collected from Blomstrandhalvøya Island. This is the first report on a *Haematococcus* species from the High Arctic.

3-10 Kim, Ja-Myung, Kitack Lee, Kyungsoon Shin, **Eun Jin Yang**, and 2 others. 2011. "Shifts in biogenic carbon flow from particulate to dissolved forms under high carbon dioxide and warm ocean conditions". *Geophysical Research Letters,* 38: L08612(1-5). doi: 10.1029/2011GL047346

Photosynthesis by phytoplankton in sunlit surface waters transforms inorganic carbon and nutrients into organic matter, a portion of which is subsequently transported vertically through the water column by the process known as the biological carbon pump (BCP). The BCP sustains the steep vertical gradient in total dissolved carbon, thereby contributing to net carbon sequestration. Any changes in the vertical transportation of the organic matter as a result of future climate variations will directly affect surface ocean carbon dioxide (CO_2) concentrations, and subsequently influence oceanic uptake of atmospheric CO_2 and climate. Here we present results of experiments designed to investigate the potential effects of ocean acidification and warming on the BCP. These perturbation experiments were carried out in enclosures (3,000 L volume) in a controlled mesocosm facility that mimicked future pCO_2 (~900 ppmv) and temperature (3℃ higher than ambient) conditions. The elevated CO_2 and temperature treatments disproportionately enhanced the ratio of dissolved organic carbon (DOC) production to particulate organic carbon (POC) production, whereas the total organic carbon (TOC) production remained relatively constant under all conditions tested. A greater partitioning of organic carbon into the DOC pool indicated a shift in the organic carbon flow from the particulate to dissolved forms, which may affect the major pathways involved in organic carbon export and sequestration under future ocean conditions.

3-11 **Kim, So-Young** and **Seung-Il Nam**. 2011. "A brief review of palynological studies The western Arctic paleoenvironmental changes". *Journal of the Geological Society of Korea,* 47(5): 547-560.

Recently, the Arctic environments have experienced dramatic and rapid changes. The most remarkable feature can be observed in the Arctic sea ice coverage, which shows rapid changes in its extent and thickness according to satellite observation during the last three decades. Recent rapid reduction in the sea ice extent is related to a major shift in the Arctic atmospheric and oceanic circulations, which plays a crucial role in regulating the global earth's climate. Of particular interest is the sea ice changes in the western Arctic, which is considered as a key parameter in past climate changes in Arctic and subarctic regions. They control the intensity and direction of sea ice drifts in the Beaufort Gyre and Transpolar Drift areas, and consequently regulate sea-ice and freshwater exports toward the North Atlantic. However, records of the past sea ice changes in the western Arctic especially on centennial to millennial scales have not been well-computed in climate models due to the rarity of suitable marine sedimentary records. Remnants of microscopic organisms in marine sediments such as spore, pollen and dinoflagellate cysts have been suggested as a useful tool for reconstructing paleoclimate changes in the western Arctic, inferring the past terrestrial environment and sea surface conditions such as sea surface temperature, sea surface salinity and the sea ice extent. In order to provide more complete and spatially extensive records of past sea ice conditions in the western Arctic, the spatial distribution of organic microfossil data sets and the accuracy of the environmental data need to be developed. This will enhance the reliability of the transfer function applied, which has been generally quite limited in the Arctic region.

3-12 Landry, Michael R., Karen E. Selph, and **Eun Jin Yang**. 2011. “Decoupled phytoplankton growth and microzooplankton grazing in the deep euphotic zone of the eastern equatorial Pacific”. *Marine Ecology Progress Series,* 421: 13-24.
doi: 10.3354/meps08792

We conducted dilution depth-profile experiments in the eastern equatorial Pacific (EEP) to define regional characteristics of phytoplankton growth and microzooplankton grazing and to test the hypothesis that the process rates decouple in the deep euphotic zone where growth is negligible. We used an abbreviated 2-treatment dilution protocol to produce daily profiles at 8 depths of phytoplankton growth, microzooplankton grazing and cellular changes in chlorophyll a (chl a) content from surface waters to the 0.1% light depth. Experiments were conducted at 16 stations from 2° N to 4° S at 110°W and from 110° to 140°W along the equator. Results were surprisingly robust and coherent over this broad spatial area and showed a euphotic zone essentially divided into 3 equal depth intervals. Mean (±SD) growth rates (0.83 ± 0.16 d^{-1}) exceeded grazing rates (0.42 ± 0.15 d^{-1}) in the light-saturated upper third of the water column. Growth, and to a lesser extent grazing, declined with light in the middle third. Effective cell growth was negligible (0.02 ± 0.21 d^{-1}) in the lower third (1 to 0.1% of surface irradiance), with grazing (0.18 ± 0.17 d^{-1}) exceeding growth in this layer. The deep euphotic zone accounted for 25.4 ± 8.4% of the total euphotic zone chl *a*, 0.5 ± 7.8% of depth-integrated phytoplankton growth and 12.7 ± 7.2% of depth-integrated microzooplankton grazing on phytoplankton. The decoupling of growth and grazing processes under low light conditions at the base of the euphotic zone substantially affected our estimates of microzooplankton consumption of phytoplankton, which ranged from 51% of daily chlorophyll growth for experiments conducted in the upper euphotic zone to 69% for the depth-integrated euphotic zone. In addition, the excess of grazing over growth processes in the deepest stratum, which is typically overlooked in experimental studies, suggests that protistan grazers may have a much larger role in biogeochemical transformations of export fluxes than previously appreciated.

3-13 Lee, Kitack, Christopher L. Sabine, Toste Tanhua, Tae-Wook Kim, Richard A. Feely, and **Hyun-Cheol Kim**. 2011. “Roles of marginal seas in absorbing and storing fossil fuel CO_2”. *Energy & Environmental Science,* 4: 1133-1146.
doi: 10.1039/c0ee00663g

We review data on the absorption of anthropogenic CO_2 by Northern Hemisphere marginal seas (Arctic Ocean, Mediterranean Sea, Sea of Okhotsk, and East/Japan Sea) and its transport to adjacent major basins, and consider the susceptibility to recent climatic change of key factors that influence CO_2 uptake by these marginal seas. Dynamic overturning circulation is a common feature of these seas, and this effectively absorbs anthropogenic CO_2 and transports it from the surface to the interior of the basins. Amongst these seas only the East/Japan Sea has no outflow of intermediate and deep water (containing anthropogenic CO_2) to an adjacent major basin; the others are known to be significant sources of intermediate and deep water to the open ocean. Consequently, only the East/Japan Sea retains all the anthropogenic CO_2 absorbed during the anthropocene. Investigations of the properties of the water column in these seas have revealed a consistent trend of waning water column ventilation over time, probably because of changes in local atmospheric forcing. This weakening ventilation has resulted in a decrease in transport of anthropogenic CO_2 from the surface to the interior of the basins, and to the adjacent open ocean. Ongoing measurements of anthropogenic CO_2, other gases and hydrographic parameters in these key marginal seas will provide information on changes in global oceanic CO_2 uptake associated with the predicted increasing atmospheric CO_2 and future global climate change.We also review the roles of other marginal seas with no active overturning circulation systems in absorbing and storing anthropogenic CO_2. The absence of overturning circulation enables anthropogenic CO_2 to penetrate only into shallowdepths, resulting in less accumulationof anthropogenic CO_2 in these basins. As a consequence of their proximity to populated continents, these marginal seas are particularly vulnerable to human-induced perturbations. Maintaining observation programs will make it possible to assess the effects of human-induced changes on the capacity of these seas to uptake and store anthropogenic CO_2.

3-14 Lee, Sang H., **Hyoung Min Joo**, **Mi Sun Yun**, Terry E. Whitledge. 2011. “Recent phytoplankton productivity of the northern Bering Sea during early summer in 2007”. *Polar Biology,* 35(1): 83-98.
doi: 10.1007/s00300-011-1035-9

Although the northern Bering Sea is one of the most productive regions in the northern North Pacific Ocean and currently considered a declining productivity region, no recent primary productivity measurements have been collected in this region. Phytoplankton productivity was measured in the northern Bering Sea in 2007 using a dual ^{13}C–^{15}N isotope tracer technique to quantify present rates of primary productivity and to assess changes under recent environmental conditions in this area. We found that large diatoms (mostly *Fragilaria* sp.) dominated the phytoplankton during the initial part of the cruise, whereas unidentified nano + pico phytoplankton largely dominated at the surface about 2 weeks later (at ‘‘revisited stations’’). At the 1% light depth, diatoms and *Phaeocystis* sp. were the dominant species, whereas diatoms and unidentified nano + pico cells were dominant at the revisited sites. Based on nitrate and ammonium uptake rates, the estimated *f*-ratios (the ratio of nitrate uptake rate/nitrate + ammonium uptake rates of phytoplankton) were high (0.65–0.74), indicating that nitrate was an important nitrogen source supporting primary production in the northern Bering Sea during the cruise in 2007. Compared with previous studies performed several decades ago, we found significantly lower chlorophyll-a concentrations and carbon uptake rates of phytoplankton in the northern Bering Sea in 2007. This is consistent with recent studies that have shown lower rates of production in the Chukchi Sea and declines in benthic biomass and sediment oxygen uptake in the northern Bering Sea.

3-15 Lee, Sang H., **Hyoung M. Joo**, and 3 others. 2011. “Phytoplankton productivity in newly opened waters of the Westen Arctic Ocean”. *Deep-Sea Research II,* 81-84(15): 18-27.
doi: 10.1016/j.dsr2.2011.06.005

Phytoplankton carbon and nitrogen production in newly opened waters of the Western Arctic Ocean were measured using a ^{13}C–^{15}N dual isotope tracer technique in summer 2008, when Arctic sea ice was at its second lowest extent since 1979. Daily integrated carbon-uptake rates were highest (675.8 ± 931.3 mg C m^{-2} d^{-1}) in ice-free shelf regions of the Chukchi Sea. In deeper regions, the daily integrated carbon-uptake rates (73.5 ± 45.0 mg C m^{-2} d^{-1}) in newly opened deep waters with adjacent sea ice cover (10–90%) were significantly higher than those (32.0 ± 22.8 mg C m^{-2} d^{-1}) in ice-free deep waters. The average contributions of small cell-size phytoplankton (0.7–5 µm) to total carbon-uptake rates were 19.8%, 62.8%, and 55.5% in shelf regions, ice-free deep waters, and newly opened waters, respectively, although the average biomass contributions of the small phytoplankton was 54.9–96.5% of total algal biomass in the three study areas. Daily total nitrogen-uptake rates were similar between newly opened deep waters and ice-free deep waters, although nitrate assimilation rates were higher in newly opened waters compared to ammonium uptake rates in ice-free waters. Lower carbon- and nitrate-assimilation rates in ice-free waters were due to strong stratification in the euphotic layer caused by melted sea ice, which limited nutrient availability to phytoplankton, although phytoplankton had greater light availability in ice-free waters than in newly opened waters.

3-16 Lee, Sang Heon, C. Peter Mc Roy, **Hyoung Min Joo**, Rolf Gradinger, Xue Hua Cui, **Mi Sun Yun**, **Kyung Ho Chung**, **Sung-Ho Kang**, Chang-Keun Kang, **Eun Jung Choy**, and 3 others. 2011. “Holes in Progressively Thinning Arctic Sea Ice Lead to New Ice Algae Habitat”. *Oceanography,* 24(3): 302-308.

The retreat and thinning of Arctic sea ice associated with climate warming is resulting in ever-changing ecological processes and patterns. One example is our discovery of myriad new "marine aquaria" formed by melt holes in the perennial sea ice. In previous years, these features were closed, freshwater melt ponds on the surface of sea ice. Decreased ice thickness now allows these ponds to melt through to the underlying ocean, thus creating a new marine habitat and concentrating a food source for the ecosystem through accumulation of algae attached to refreezing ice in late summer. This article describes the formation of these late-season algal masses and comments on their overall contribution to Arctic ecosystems and the consequences of a continued decline in sea ice.

3-17 **Nam, Seung-Il**. 2011. “Current Research Issues on Paleoclimate and Paleoceanography in Korea: From Korean Peninsula to Antarctic -Arctic Polar Areas”. *Journal of the Geological Society of Korea,* 47(5): 441-442.

3-18 **Rhee, Tae Siek**. 2011. “Non-CO_2 greenhouse gases survey”. *Berichte zur Polar- und Meeresforschung,* 632: 51-52.

The present climate change is driven by human activities by which a variety of greenhouse gases in the atmosphere accumulate exponentially. While CO_2 is the primary driver, CH_4, N_2O, O_3, and halocarbons altogether are compatible with CO_2 in radiative forcing (Forster et al., 2007). CO and H_2 are not direct greenhouse gases. However, as reacting with OH radical, which destroys CH4 in the atmosphere and being a precursor of O_3 for CO, they contribute to global radiative forcing in an indirect way. The ocean acts as a source of CH_4, N_2O, H_2, and CO (e.g., Bates et al., 1995; Rhee et al., 2009). Microbes produce CH_4 and N_2O in the water column while photochemical degradation of organic matters is a major source of CO and likely for H_2 in the ocean. However, oceanic source strengths of these gases to the atmospheric budget are not well quantified mainly due to insufficient observations in the ocean. In this expedition, we aim to estimate emission rates of these gases in the Southern Ocean, which shall help to narrow the uncertainty of source strength of the ocean.

3-19 **Rhee, Tae Siek**. 2011. “Inorganic carbon system observation”. *Berichte zur Polar- und Meeresforschung,* 632: 47-50.

The Pacific sector of the Southern Ocean plays a crucial role in the global carbon cycle (Daly et al., 2001; Marinov et al., 2006). Atmospheric CO_2 is substantially absorbed at the surface and is transported into greater depths with the formation of the Antarctic Intermediate Water (AAIW) off the west coast of the Chile before spreading northwards in the Pacific. In addition, biological activity south of the polar front plays an important role in absorbing atmospheric CO_2, which is in turn exported to the deep water. In spite of the significant role of the inorganic carbon cycle of this region, insufficient observations on inorganic carbon distribution and biogeochemical cycles in the interior have been carried out, due largely to remoteness of the area. In this study we will investigate the inorganic carbon system of the water column, its connection to the ecosystem, and the anthropogenic impact in order to fill in the gap of our knowledge of the carbon cycle in the Southern Ocean and, in particular its the capacity to absorb anthropogenic CO_2 emitted to the atmosphere since the industrial revolution.

3-20 Selph, Karen E., Michael R. Landry, Andrew G. Taylor, **Eun-Jin Yang**, and 5 others. 2011. “Spatially-resolved taxon-specific phytoplankton production and grazing dynamics in relation to iron distributions in the Equatorial Pacific between 110 and 140°W”. *Deep-Sea Research II,* 58: 358-377. doi: 10.1016/j.dsr2.2010.08.014

Phytoplankton dynamics were investigated in the eastern equatorial Pacific at 32 stations sampled during two cruises (December 2004 and September 2005). Based on standing stock analyses from HPLC pigments, flow cytometry and microscopy, we used amodified 2-treatment approach of the seawater dilution method to estimate taxon-specific phytoplankton growth and mortality rates in 8-depth per station profiles. These data were complemented by contemporaneous measurements of dissolved iron(Fe). The stations encompassed an equatorial zonal gradient (110 to 140°W) of diminishing eastward Fe availability in the euphotic zone from upwelling of the Equatorial Undercurrent (EUC). Latitudinal variation was assessed by meridional transects at 110 and 140°W. Overall, euphotic zone averaged growth rates were 0.53±0.17 d^{-1} (total chlorophyll *a*), 0.34±0.15 d^{-1} (divinyl chlorophyll *a*) and 0.86±0.32 d^{-1} (fucoxanthin). Microzooplankton grazing accounted for 50-60% of daily production of eukaryotic algae, whereas essentially all growth of phototrophic prokaryotes was consumed daily. Fucoxanthin, representing diatoms, was a minor component of the accessory pigments, but diatom growth rates were both significantly higher than other taxonomically defined groups and dropped off more sharply with depth (low light level). Strikingly, no spatial or temporal trends were seen in the 256 growth rate measurements for each measured pigment. However, the diminishing eastward equatorial Fe gradient was associated with deepening subsurface pigment maxima and decreasing surface-layer pigment stocks (down to the 8% light level). Inaddition, integrated standing stocks of total chlorophyll *a* and *Prochlorococcus* (divinyl chlorophyll *a*) were strongly correlated with integrated iron at equatorial upwelling stations, yet no correlation with Fe was seen for any of the eukaryotic groups, including diatoms. This latter result is contrary to expectations from previous Fe addition experiments (*in situ* or in bottles), where diatom biomass increased relative to other phytoplankton. We hypothesize that the natural supply of Fe to the base of the euphotic zone from the EUC is less favorable for diatoms because of light limitation. Rather, new Fe is rapidly incorporated into a small phytoplankton-dominated community in the deep euphotic zone, and tightly coupled grazing control results in a system regulated by return of recycled Fe.

3-21 Son, Young Baek, Joji Ishizaka, Jong-Chul Jeong, **Hyun-Choel Kim**, and Taehee Lee. 2011. "*Cochlodinium polykrikoides* Red Tide Detection in the South Sea of Korea using Spectral Classification of MODIS Data". *Ocean Science Journal,* 46(4): 239-263.
doi: 10.1007/s12601-011-0019-6

To distinguish true red tide water (particularly *Cochlodinium polykrikoides* blooms) from non-red tide water (false satellite high chlorophyll water) in the South Sea of Korea, we developed a systematic classification method using spectral information from MODIS level products and applied it to five different harmful algal bloom events. Red tide and nonred tide waters were classified based on four different criteria. The first step revealed that the radiance peaks of potential red tide water occurred at 555 and 678 nm. The second step separated optically different waters that were influenced by relatively low and high contributions of colored dissolved organic matter (CDOM) (including detritus) to chlorophyll. The third and fourth steps discriminated red tide water from non-red tide water based on the blue-to-green ratio in areas with lower and higher contributions of CDOM to chlorophyll, respectively. After applying the red tide classification (using the four criteria), the spectral response of the red tide water, which is influenced by pigment concentration, showed different slopes for the blue and green bands (lower slope at blue bands and higher slope at green bands). The opposite result was found for non-red tide water, due to decreasing phytoplankton absorption and increasing detritus/CDOM absorption at blue bands. The results were well matched with the discoloration of water (blue to dark red/brown) and delineated the areal coverage of *C. polykrikoides* blooms, revealing the nature of spatial and temporal variations in red tides. This simple spectral classification method led to increase user accuracy for *C. polykrikoides* and non-red tide blooms (> 46% and > 97%) and provided a more reliable and robust identification of red tides over a wide range of oceanic environments than was possible using chlorophyll *a* concentration, chlorophyll anomaly, fluorescence analysis, or proposed red tide detection algorithms.

3-22 Taylor, Andrew G., Michael R. Landry, Karen E. Selph, and **Eun Jin Yang**. 2011. "Biomass, size structure and depth distributions of the microbial community in the eastern equatorial Pacific". *Deep-Sea Research II,* 58: 342-357.
doi: 10.1016/j.dsr2.2010.08.017

We investigated the biomass, size structure and composition of microbial communities over a broad area of the eastern equatorial Pacific (4°N-4°S, 110-140°W) during cruises in December 2004 (EB04) and September 2005 (EB05). Vertical-profile samples were collected at 30 stations at depths extending from the surface to the 0.1% light level, and each sample was analyzed quantitatively by flow cytometry and epifluorescence microscopy. Autotrophic biomass averaged 14.8±4.2 (1 s.d.) μg C L^{-1} for the euphotic zone, with dinoflagellates comprising 39%, *Prochlorococcus* 28%, other flagellates 18%, *Synechococcus* 7.5%, and diatoms 6.3%. Nanoplankton accounted for 46% of autotroph biomass, while pico- and microphytoplankton comprised 39 and 16%, respectively. C:Chl averaged 64±14 for the euphotic zone, with a mean mixed-layer value of 78±20 and a minimum of 36±15 at the 1% light level. Heterotrophic biomass averaged 7.0±1.2 μg C L^{-1} for prokaryotes, 1.6±0.9 μg C L^{-1} for dinoflagellates, 1.5±1.1 μg C L^{-1} for other flagellates, and 2.1±0.4 μg C L^{-1} for ciliates. Euphotic zone integrated biomass varied 2-fold, 1.2 to 2.5 g C m^{-2}, among stations, decreasing west to east with the gradient in euphotic zone concentrations of dissolved iron. Overall, community biomass and the contributions of functional groups displayed remarkable constancy over our study area, but some patterns were evident, such as the enhancement of picophytoplankton in the leading (upwelling) edges of tropical instability waves and larger diatoms in the trailing (downwelling) edges. *Prochlorococcus*, in particular, exhibited more variability than expected, given its generally assumed role as a stable background species in the tropical oceans, and was positively associated with the areas of enhanced autotrophic carbon and Chl *a*. With corrections for different methodological assumptions taken into account, our EB05 estimates of mixed-layer community biomass are 27-35% higher than values for JGOFS studies in 1992.

3-23 Tian, Liyan, Paterno R. Castillo, Peter F. Lonsdale, **Doshik Hahm**, and David R. Hilton. 2011. “Petrology and Sr-Nd-Pb-He isotope geochemistry of postspreading lavas on fossil spreading axes off Baja California Sur, Mexico”. *Geochemistry Geophysics Geosystems,* 12(2): Q0AC10(1-22).
doi: 10.1029/2010GC003319

Postspreading volcanism has built large seamounts and volcanic ridges along the short axes of a highly segmented part of the East Pacific Rise crest that ceased spreading at the end of the middle Miocene, offshore Baja California Sur, Mexico. Lava samples from Rosa Seamount, the largest volcano, are predominantly alkalic basalts, mugearites, and benmoreites. This lavas series was generated through fractional crystallization and is compositionally similar to the moderately alkalic lava series in many oceanic islands. Samples from volcanic ridges at three adjacent failed spreading axes include mildly alkalic, transitional, and tholeiitic basalts and differentiated trachyandesites and andesite. The subtle but distinct petrologic and isotopic differences among the four sites may be due to differences in the degree of partial melting of a common, heterogeneous source. Postspreading lavas from these four abandoned axes off Baja California Sur together with those from other fossil spreading axes and from seamount volcanoes that grew on the East Pacific Rise flanks define a compositional continuum ranging from normal mid-ocean ridge basalt (NMORB)-like to ocean island basalt (OIB)-like. We propose that the compositional spectrum of these intraplate volcanic lavas is due to different degrees of partial melting of the compositionally heterogeneous suboceanic mantle in the eastern Pacific. A large degree of partial melting of this heterogeneous mantle during vigorous mantle upwelling at an active spreading center produces NMORB melts, whereas a lesser degree of partial melting during weak mantle upwelling following cessation of spreading produces OIBlike melts. The latter melts have a low (< 8 R_A) $^3He/^4He$ signature indicating their formation is different from that of OIBs from major “hot spot” volcanoes in the Pacific with high $^3He/^4He$ ratios, such as Hawaii and Galapagos.

3-24 Xu, Kuidong, Joong Ki Choi, Yanli Lei, and **Eun Jin Yang**. 2011. “Marine ciliate community in relation to eutrophication of coastal waters in the Yellow Sea”. *Chinese Journal of Oceanology and Limnology,* 29(1): 118-127.
doi: 10.1007/s00343-011-9106-x

We assessed the potential of marine ciliate community as an indicator to coastal water quality using water samples collected from four stations in the Yellow Sea in the summer 2000. The four stations were characterized by different levels of pollution. The ciliate communities consisted primarily of tintinnids and aloricate ciliates that were < 30 μm. A total of 78 species were classified: 55 species at Station 2, 51 species each at Stations 1 and 4, and 47 species at Station 3. The mean number of species at each site was 29.2±2.0 (Station 1), 28.5±2.9 (Station 2), 27.8±1.7 (Station 3), and 24.5±2.3 (Station 4). The abundance was highly variable: 19 331±11 187 ind./L at Station 1, 7 960±5 639 ind./L at Station 2, 29 015±12 999 ind./L at Station 3, and 8 190±4 658 ind./L at Station 4. Our results suggest that neither the simple chemical analysis (e.g. chemical oxygen demand, dissolved inorganic nitrogen, and phosphate) nor the eutrophication/pollution index adequately described the water quality at the four stations. The same was true of the number of species and their abundance, both of which had no correlation with the chemical indices. In contrast, Margalef's diversity index values (3.12 at Station 2, 2.89 at Station 1, and 2.64 at Stations 3 and 4) generally discriminated the water quality status of the four stations. The difference in water quality among the stations was strongly supported by the pattern of species richness (i.e. the total number of species) of ciliates at each station. Our evaluation was consistent with the results of long-term water quality monitoring at the four stations. With increasing eutrophication, we observed also a compositional and functional shift in the ciliate assemblages from algivorous oligotrich/choreotrich to nonselective-omnivorous gymnostomatids to bacterivorous-detrivorous scuticociliatids. Thus, ciliates may be used to indicate the coastal water quality status of a given site.

3-25 **Yang, Eun Jin**, and 2 others. 2011. "Trophic Role of Heterotrophic Nano- and Microplankton in the Pelagic Microbial Food Web of Drake Passage in the Southern Ocean during Austral Summer". *Ocean and Polar Research,* 33(4): 457-472. doi: 10.4217/OPR.2011.33.4

To elucidate the trophic role of heterotrophic nano- and microplankton (HNMP), we investigated their biomass, community structure, and herbivory in three different water masses, namely, south of Polar Front (SPF), Polar Front Zone (PFZ), the Sub-Antarcitc Front (SAF) in the Drake Passage in the Southern Ocean, during the austral summer in 2002. We observed a spatial difference in the relative importance of the dominant HNMP community in these water masses. Ciliates accounted for 34.7% of the total biomass on an average in the SPF where the concentration of chlorophyll-*a* was low with the dominance of pico- and nanophytoplankton. Moreover, the importance of ciliates declined from the SPF to the SAF. In contrast, heterotrophic dinoflagellates (HDFs) were the most dominant grazers in the PFZ where the concentration of chlorophyll-*a* was high with the dominance of net phytoplankton. HNMP biomass ranged from 321.9 to 751.4 ㎎ Cm^{-2} and was highest in the PFZ and lowest in the SPF. This result implies that the spatial dynamic of HNMP biomass and community was significantly influenced by the composition and concentration of phytoplankton as a food source. On an average, 75.6%, 94.5%, and 78.9% of the phytoplankton production were consumed by HNMP in the SPF, PFZ, and SAF, respectively. The proportion of phytoplankton grazed by HNMP was largely determined by the composition and biomass of HNMP, as well as the composition of phytoplankton. However, the herbivory of HNMP was one of the most important loss processes affecting the biomass and composition of phytoplankton, particularly in the PFZ. Our results suggest that the bulk of the photosynthetically fixed carbon was likely reprocessed by HNMP rather than contributing to the vertical flux in Drake Passage during the austral summer in 2002.

3-26 **Yun, Mi Sun**, **Kyung Ho Chung**, Sarah Zimmermann, Jinping Zhao, **Hyoung Min Joo**, and Sang H. Lee. 2011. “Phytoplankton productivity and its response to higher light levels in the Canada Basin”. *Polar Biology,* 35(2): 257-268.
doi: 10.1007/s00300-011-1070-6

Phytoplankton productivity in the Canada Basin was measured in the late summer season, from mid- September to mid-October 2009, using a ^{13}C–^{15}N dual tracer technique. To understand potential production changes associated with sea ice melting in the Arctic Ocean, we examined the effects of light enhancement and nitrate enrichment on the carbon productivity of phytoplankton from the chlorophyll a maximum layer. The daily carbon productivity in the Canada Basin in 2009 was very low, with a mean of 4.1 mg C m^{-2} (SD = 3.6 mg C m^{-2}), compared with those reported in previous studies in the region. Among several explanations, the most plausible reason for the large difference in carbon productivity between this and the previous studies was strong seasonal variation in biomass and photosynthetic rate of the phytoplankton in the study region. Based on our results from light enhancement and nitrate enrichment experiments, we found that carbon productivity of phytoplankton in the chlorophyll *a* maximum layer could be stimulated by increased light condition rather than nitrate addition. Thus, potentially increasing light availability from current and ongoing decreases in the sea ice cover could increase the carbon production of the phytoplankton in the chlorophyll a maximum layer and produce a well-developed maximum layer at a deeper depth in the Canada Basin.

PART 4

Life Sciences

4-1 Ahn, Dong-Ha, Mi-Hyun Park, Jae-Ho Jung, Mi-Jin Oh, **Sanghee Kim**, and 2 others. 2011. “Isolation and characterization of microsatellite loci in the Korean crayfish, Cambaroides similis and application to natural population analysis”. *Animal Cells and Systems,* 15(1): 37-43.
doi: 10.1080/19768354.2011.555137

The Korean freshwater crayfish, *Cambaroides similis*, has recently suffered from range reduction and habitat degradation caused by environmental changes and water pollution. For the conservation and restoration of this species, it is necessary to understand the current population structures of Korean *C. similis* using estimation of their genetic variation. In this study, eight microsatellite loci were developed and characterized from 49 individuals collected from four locations: one population from Mt. Bukhan (BH) and three populations from Mt. Gwanak (GA) in Seoul, Korea. As a result, the number of alleles per locus ranged from 2 to 12. The observed heterozygosities and expected heterozygosities ranged from 0.000 to 0.833 and from 0.125 to 0.943, respectively, and the former values were significantly lower than the latter ones expected under the Hardy-Weinberg equilibrium. No significant linkage disequilibrium was revealed between any of the locus pairs after Bonferroni correction. From the pairwise *F*st results over all samples, higher differentiation between GA-BH population pairs (mean 0.1789) was observed than between GA population pairs (mean 0.0454). This was also supported by Mantel’s test showing that the genetic distances of these crayfish populations were significantly correlated with geographic distances. This result may show the regional differentiation caused by restricted gene flow between northern (BH) and southern (GA) populations within Seoul. These microsatellite markers have the potential for use in analyses of the genetic diversity and population structure of *C. similis* species, with implications for its conservation and management plans.

4-2 Cho, Eunjeong, Yurry Um, Seung Kwan Yoo, **Hyoungseok Lee**, and 4 others. 2011. "An Expressed Sequence Tag Analysis for the Fast-Growing Shoots of *Bambusa edulis* Murno". *Journal of Plant Biology,* 54(6): 402-408.
doi: 10.1007/s12374-011-9179-2

Bamboo is one of the fastest growing plants in the world and is an economically important crop species in Asia. To identify the genes involved in fast shoot growth, an expressed sequence tag analysis was performed on *Bambusa edulis* Murno fast-growing shoots. Sequencing of the cDNA clones generated 1,402 5′-end high-quality expressed sequence tags (JG296384-JG297785, average length 655 bp), of which 1,101 clusters (143 consensus and 958 singletons) were revealed by sequence comparison to be unique and 597 (54% of total clusters) of them have a putative ATG start codon. These results suggest that this high-quality library could be a good resource for understanding molecular events of bamboo shoot elongation, and the full-length clones could be used for crop improvement studies in the future.
fast-growing shoots. Sequencing of the cDNA clones generated 1,402 5′-end high-quality expressed sequence tags (JG296384 -JG297785, average length 655 bp), of which 1,101 clusters (143 consensus and 958 singletons) were revealed by sequence comparison to be unique and 597 (54% of total clusters) of them have a putative ATG start codon. These results suggest that this high-quality library could be a good resource for understanding molecular events of bamboo shoot elongation, and the full-length clones could be used for crop improvement studies in the future.

4-3 **Han, Se Jong**, **Heeyong Park**, **Sung Gu Lee**, **Hong Kum Lee**, and **Joung Han Yim**. 2011. "Optimization of cold-active chitinase production from the Antarctic bacterium, *Sanguibacter antarcticus* KOPRI 21702". *Applied Microbiology and Biotechnology,* 89: 613-621.
doi: 10.1007/s00253-010-2890-y

In the present study, cultivation conditions and medium components were optimized using statistical design and analysis to enhance the production of Chi21702, a cold-active extracellular chitinase from the Antarctic bacterium *Sanguibacter antarcticus* KOPRI 21702. Identification of significant carbon sources and other key elements was performed using a statistical design technique. Chitin and glycerol were selected as main carbon sources, and the ratio of complex nitrogen sources to carbon sources was determined to be 0.5. Among 15 mineral components included in basal medium, NaCl, Fe ($C_6H_5O_7$), and $MgCl_2$ were found to have the most influence on Chi21702 production. The optimal parameters of temperature, initial pH, and dissolved oxygen level were found to be 25℃, 6.5, and above 30% of air saturation, respectively. The maximum Chi21702 activity obtained under the optimized conditions was 90 U/L. Through statistical optimization methods, a 7.5-fold increase in Chi21702 production was achieved over unoptimized conditions. Chi21702 showed relatively high activity, even at low temperatures close to 0℃. The information obtained in the present study could be applied to the production of cold-active endochitinase on a large scale, suitable for a process at low temperature in industry.

4-4 Jang, Gwang Il, Chung Yeon Hwang, **Han-Gu Choi**, **Sung-Ho Kang**, and Byung Cheol Cho. 2011. “Description of *Spongiibacter borealis* sp. nov., isolated from Arctic seawater, and reclassification of *Melitea salexigens* Urios *et al.* 2008 as a later heterotypic synonym of *Spongiibacter marinus* Graeber *et al.* 2008 with emended descriptions of the genus *Spongiibacter* and *Spongiibacter marinus*”. *International Journal of Systematic and Evolutionary Microbiology,* 61(12): 2895-2900.
doi: 10.1099/ijs.0.028795-0

A Gram-negative, rod-shaped and motile strain, designated CL-AS9^T, was isolated from polar seawater of the Arctic. Analysis of the 16S rRNA gene sequence of the strain showed an affiliation with the genus *Spongiibacter*, sharing 93.9% and 93.7% sequence similarities with the type strains of *Spongiibacter tropicus* CL-CB221^T and *Spongiibacter marinus* HAL40b^T, respectively. Phylogenetic analyses revealed that strain CL-AS9^T formed a separate branch that was distinct from a clade comprising *Spongiibacter marinus* HAL40b^T, *Spongiibacter tropicus* CL-CB221^T and *Melitea salexigens* 5IX/A01/131^T. Cells of the strain grew optimally at 20–25 6C and pH 6.6–8.0 in the presence of 3–4% (w/v) sea salts. The major polar lipids were diphosphatidylglycerol, phosphatidylglycerol and an unidentified aminophospholipid. The major quinone was ubiquinone 8. The major cellular fatty acids were $C_{16:1}\omega7c$ and/or iso-$C_{15:0}$ 2-OH (23.1 %), $C_{17:1}\omega8c$ (22.1 %) and $C_{18:1}\omega7c$ (15.6 %). The genomic DNA G+C content was 53.6 mol%. Based on the phylogenetic, chemotaxonomic and phenotypic data presented, we propose the name *Spongiibacter borealis* sp. nov. with the type strain CL-AS9^T (=KCCM 90094^T =JCM 17304^T) and the reclassification of *Melitea salexigens* as a later heterotypic synonym of *Spongiibacter marinus*. We also provide emended descriptions of the genus *Spongiibacter* and *Spongiibacter marinus*.

4-5 Jung, Jae-Ho, Ye-Seul Baek, **Sanghee Kim**, **Han-Gu Choi**, and Gi-Sik Min. 2011. “A New Marine Ciliate, *Metaurostylopsis antarctica* nov. spec. (Ciliophora, Urostylida) from the Antarctic Ocean”. *ACTA Protozologica,* 50: 289-300.
doi: 10.4467/16890027AP.11.026.0063

In this study, a new marine urostylid ciliate, *Metaurostylopsis antarctica* nov. spec. collected from the Antarctic Ocean was investigated using morphological, morphometrical, and molecular methods. *Metaurostylopsis antarctica* nov. spec. is characterized as follows: slender to ellipsoid form in body shape; two types of cortical granules, ellipsoid large one (type I, yellow -green, 1.5 × 1 µm) in rows along dorsal kineties and cirri, circular small one (type II, colourless, 0.3 µm in diameter) scattered throughout whole body; 19–24 adoral membranelles, 4 frontal cirri, 2–5 frontoterminal cirri, 1 buccal and 2 transverse cirri; 3–5 midventral pairs, 10–15 cirri of midventral row; 1 right and 2 left marginal rows; 3 dorsal kineties; about 43 macronuclear nodules. This new species mainly differs from the congeners by the number of marginal rows (1 vs. 3 or more on right side; 2 vs. 3 or more on left side). In addition, proter’s oral primordium developed on the right side of the oral cavity (vs. in center of oral cavity), and the rightmost anlage splits into two parts, namely, the frontoterminal cirri and a transverse cirrus (vs. only frontoterminal cirri). Inter-specific dissimilarities of the SSU rRNA gene between the congeners range from 3.3 to 4.4%.

4-6 Jung, Jaejoon, Jinki Yeom, Jisun Kim, Jiwon Han, **Hyoun Soo Lim**, **Hyun Park**, and 2 others. 2011. “Change in gene abundance in the

nitrogen biogeochemical cycle with temperature and nitrogen addition in Antarctic soils". *Research in Microbiology,* 162: 1018-1026.
doi: 10.1016/j.resmic.2011.07.007

The microbial community (bacterial, archaeal, and fungi) and eight genes involved in the nitrogen biogeochemical cycle (*nifH*, nitrogen fixation; bacterial and archaeal *amoA*, ammonia oxidation; *narG,* nitrate reduction; *nirS, nirK*, nitrite reduction; *norB,* nitric oxide reduction; and *nosZ*, nitrous oxide reduction) were quantitatively assessed in this study, via real-time PCR with DNA extracted from three Antarctic soils. Interestingly, AOB *amoA* was found to be more abundant than AOA *amoA* in Antarctic soils. The results of microcosm studies revealed that the fungal and archaeal communities were diminished in response to warming temperatures (10 ℃) and that the archaeal community was less sensitive to nitrogen addition, which suggests that those two communities are well-adapted to colder temperatures. AOA *amoA* and *norB* genes were reduced with warming temperatures. The abundance of only the *nif*H and *nir*K genes increased with both warming and the addition of nitrogen. NirS-type denitrifying bacteria outnumbered NirK-type denitrifiers regardless of the treatment used. Interestingly, dramatic increases in both NirS and NirK-types denitrifiers were observed with nitrogen addition. NirK types increase with warming, but NirS-type denitrifiers tend to be less sensitive to warming. Our findings indicated that the Antarctic microbial nitrogen cycle could be dramatically altered by temperature and nitrogen, and that warming may be detrimental to the ammonia-oxidizing archaeal community. To the best of our knowledge, this is the first report to investigate genes associated with each process of the nitrogen biogeochemical cycle in an Antarctic terrestrial soil environment.

4-7 Ki, Jang-Seu, Hans-Uwe Dahms, **Il-Chan Kim**, and 3 others. 2011. "Molecular relationships of gammaridean amphipods from Arctic sea ice". *Polar Biology,* 34: 1559-1569.
doi: 10.1007/s00300-011-1016-z

The information on the biology and ecology of the Arctic sea ice-associated amphipods (*Apherusa glacialis*, *Gammarus wilkitzkii*, *Onisimus glacialis*, and *O. nanseni*) has increased, but their molecular taxonomic information still remains undisclosed. In the present study, we investigated long-range DNA sequences spanning 18S to 28S rDNA of these four sea ice-associated amphipods and analyzed their genetic relationships with other amphipod taxa. Variations of rDNA within the individuals of the same species were not detected. Phylogenetic analyses showed that each ice amphipod was separated, forming clusters with other conspecifics. Pairwise comparisons led to similar phylogenetic results, showing that the molecular taxonomy of the ice amphipods was in accordance with morphological systematics. In addition, these findings suggest that all four amphipods have little genetic variation compared with their morphologically defined conspecifics from temperate regions. Based on DNA taxonomy, *G. wilkitzkii* was supported as a species in good standing, refuting a recent synonymization with *Gammarus duebeni*. Considerably low genetic divergences of *O. glacialis* and *O. nanseni* in 18S, ITS, and 28S rDNA suggest the presence of population distinctions within species.

4-8 **Kim, Dockyu**, Miyoun Yoo, Ki Young Choi, Beom Sik Kang, **Tai Kyoung Kim**, **Soon Gyu Hong**, and 2 others. 2011. "Differential Degradation of Bicyclics with Aromatic and Alicyclic Rings by *Rhodococcus* sp. Strain DK17". *Applied and Environmental Microbiology,* 77(23): 8280-8287.
doi: 10.1128/AEM.06359-11

The metabolically versatile *Rhodococcus* sp. strain DK17 is able to grow on tetralin and indan but cannot use their respective desaturated counterparts, 1,2-dihydronaphthalene and indene, as sole carbon and energy sources. Metabolite analyses by gas chromatography-mass spectrometry and nuclear magnetic resonance spectrometry clearly show that (i) the *meta*-cleavage dioxygenase mutant strain DK180 accumulates 5,6,7,8-tetrahydro-1,2-naphthalene diol, 1,2-indene diol, and 3,4-dihydro-naphthalene-1,2-diol from tetralin, indene, and 1,2-dihydronaphthalene, respectively, and (ii) when expressed in *Escherichia coli*, the DK17 *o*-xylene dioxygenase transforms tetralin, indene, and 1,2-dihydronaphthalene into tetralin *cis*-dihydrodiol, indan-1,2-diol, and *cis*-1,2-dihydroxy-1,2,3,4-tetrahydronaphthalene, respectively. Tetralin, which is activated by aromatic hydroxylation, is degraded successfully via the ring cleavage pathway to support growth of DK17. Indene and 1,2-dihydronaphthalene do not serve as growth substrates because DK17 hydroxylates them on the alicyclic ring and further metabolism results in a dead-end metabolite. This study reveals that aromatic hydroxylation is a prerequisite for proper degradation of bicyclics with aromatic and alicyclic rings by DK17 and confirms the unique ability of the DK17 *o*-xylene dioxygenase to perform distinct regioselective hydroxylations.

4-9 **Kim, Eun Hye**, **Hyun-Jeong Jeong**, **Yoo Kyoung Lee**, Eun Young Moon, Jang-Cheon Cho, **Hong Kum Lee**, and **Soon Gyu Hong**. 2011. “*Actimicrobium antarcticum* gen. nov., sp. nov., of the Family *Oxalobacteraceae*, Isolated from Antarctic Coastal Seawater”. *Current Microbiology,* 63(2): 213-217. doi: 10.1007/s00284-011-9962-9

A Gram-negative, non-motile, catalase- and oxidase- positive, strictly aerobic, and short rod-shaped bacterium that was designated strain KOPRI 25157^T was isolated from coastal seawater sample in Antarctica. The temperature and pH ranges for growth on R2A agar were 10–20℃, and 5.0–10.0, respectively. Phylogenetic analyses of the 16S rRNA gene sequence of strain KOPRI 25157^T showed it to belong to the family *Oxalobacteraceae* of the class *Betaproteobacteria*, and it formed a distinct clade from other recognized members of the family. DNA G+C content was 65.9 mol%. Major ubiquinone was Q-8. Predominant cellular fatty acids were $C_{16:1}$ ω7c/15 iso 2OH (56.4%) and $C_{16:1}$ (30.5%). Major polar lipids were phosphatidylglycerol, phosphatidylethanolamine, and unknown lipid. On the basis of these data, it is proposed that strain KOPRI 25157^T is the representative of a novel genus, for which the name *Actimicrobium* gen. nov. is proposed in the family *Oxalobacteraceae*. The type strain for *Actimicrobium antarcticum* sp. nov. is KOPRI 25157^T (=JCM 16673^T =KCTC 23040^T).

4-10 Kim, Kyungsun, **Dockyu Kim**, and 3 others. 2011. “Heat Shock-Induced Physical Changes of Megaplasmids in *Rhodococcus* sp. Strain DK17”. *The Korean Journal of Microbiology,* 47(1): 92-96.

Rhodococcus sp. strain DK17 possesses three megaplasmids (380 kb pDK1, 330 kb pDK2, and 750 kb pDK3). The alkylbenzene-degrading genes (*akbABCDEF*) are present on pDK2 while the phthalate operons which are duplicated are present on both pDK2 (*ophA’B’C’R’*) and pDK3 (*ophABCR*). DK17 with an optimal temperature of 30℃ showed no growth at 37℃. When transferred to 30℃, however, the 37℃ culture began to grow immediately, indicating that 37℃ is not lethal but stressful for DK17 growth. In addition, when exposed to 37℃ even for a short time, a part of DK17 cells lost the ability to degrade *o*-xylene (a model compound of alkylbenzenes). When two hundred colonies were randomly selected for colony PCR for pDK2-specific *akbC*, *ophC'*, or pDK3-specific *ophC*, a total of 29 colonies were found to have lost at least one of the three genes. PFGE analysis clearly showed that all the mutants have different megaplasmid profiles from that of DK17 wild type, which are divided into five different cases: Type I (10 mutants, pDK2 loss and acquisition of a new ~700 kb plasmid), Type II (9 mutants, pDK2 loss), Type III (8 mutants, pDK3 loss and acquisition of a new ~400 kb plasmid), Type IV (1 mutant, pDK3 loss), and Type V (1 mutant, pDK2 and pDK3 loss and acquisition of the ~400 kb and ~700 kb plasmids). The above results showing that growth temperature changes can induce physical changes in bacterial genomes suggest that environmental changes in habitats including temperature fluctuations affect significantly the evolution of bacteria.

4-11 **Kim, SangHee**, Sang-Hwa Lee, Mi-Hyun Park, **Han-Gu Choi**, and 2 others. 2011. "The complete mitochondrial genome of the American lobster, *Homarus americanus* (Crustacea, Decapoda)". *Mitochondrial DNA,* 22(3): 47-49.
doi: 10.3109/19401736.2011.597389

Although relatively a large number of the complete mitochondrial genome sequences have been determined from various decapod species (29 mtDNA sequences reported so far), the information for the infraorder Astacidea (including lobsters, crayfishes, and their relatives) is very limited and represented by only one complete sequence from the Australian freshwater crayfish species *Cherax destructor*. In this study, we determined the complete mitochondrial DNA sequence of *Homarus americanus*, the first representative of the family Nephropidae to be fully characterized. Comparison of the gene arrangement reveals that *H. americanus* mtDNA is identical to those of other pancrustacean species but differs from the other astacidean species (*C. destructor*). Based on these data, it can be assumed that an idiosyncratic gene order discovered in *C. destructor* mtDNA may be secondarily acquired from the ancestral lineage of the Astacidea.

4-12 **Kim, SangHee**, TaeHo Kim, **Han-Gu Choi**, and 3 others. 2011. "The complete mitochondrial genome of the Japanese mud shrimp *Upogebia major* (Crustacea, Decapoda)". *Mitochondrial DNA,* 22(4): 94-96.
doi: 10.3109/19401736.2011.624609

We determined a full-length sequence of mitochondrial (mt) genome from *Upogebia major.* This is the first complete mt genome report for infraorder Thalassinidea in Decapoda, Crustacea. Our result showed that *U. major* generally followed a typical pancrustacean gene order but some tRNA genes showed a very unique gene arrangement such as duplication or translocation. Since none of the complete mt genome sequences in the infraorder Thalassinidea are available yet, this report will provide additional information in relation to mt genome diversity and evolution of the decapods.

4-13 Kokubun, Nobuo, **Jeong-Hoon Kim**, **Hyoung-Chul Shin**, and 2 others. 2011. "Penguin head movement detected using small accelerometers: a proxy of prey encounter rate". *The Journal of Experimental Biology,* 214(22): 3760-3767.
doi: 10.1242/jeb.058263

Determining temporal and spatial variation in feeding rates is essential for understanding the relationship between habitat features and the foraging behavior of top predators. In this study we examined the utility of head movement as a proxy of prey encounter rates in medium-sized Antarctic penguins, under the presumption that the birds should move their heads actively when they encounter and peck prey. A field study of free-ranging chinstrap and gentoo penguins was conducted at King George Island, Antarctica. Head movement was recorded using small accelerometers attached to the head, with simultaneous monitoring for prey encounter or body angle. The main prey was Antarctic krill (> 99% in wet mass) for both species. Penguin head movement coincided with a slow change in body angle during dives. Active head movements were extracted using a high-pass filter (5 Hz acceleration signals) and the remaining acceleration peaks (higher than a threshold acceleration of 1.0 g) were counted. The timing of head movements coincided well with images of prey taken from the back-mounted cameras: head movement was recorded within ±2.5 s of a prey image on 89.1±16.1% (*N*=7 trips) of images. The number of head movements varied largely among dive bouts, suggesting large temporal variations in prey encounter rates. Our results show that head movement is an effective proxy of prey encounter, and we suggest that the method will be widely applicable for a variety of predators.

4-14 Kong, Min Kyung, **Joung Han Yim**, and Pyung Cheon Lee. 2011. “Separation of Xanthorhodopsin from *Salinibacter ruber* and Its in vitro Reconstruction”. *Clean Technology,* 17(3): 280-282.

Capture and conversion of abundant solar energy using biotechnology will be essential for the development of sustainable and future energy. Photosynthesis is used for the production of biofuels such as biohydrogen. In this study, lightharvesting xanthorhodopsin consisting of retinal and salinixanthin was isolated from a photosynthetic microorganism *Salinibacter ruber* by aqueous two phase extraction. To stabilize the light-harvesting machine, artificial xanthorhodopsin-liposome system was reconstructed to have photoelectron absorption activity.

4-15 **Lee, Jong Kyu**, **Yeon Ju Kim**, **Kyoung Sun Park**, **Seung Chul Shin**, **Hak Jun Kim**, Young Hwan Song, and **Hyun Park**. 2011. “Molecular and comparative analyses of type IV antifreeze proteins (AFPIVs) from two Antarctic fishes, *Pleuragramma antarcticum* and *Notothenia coriiceps”. Comparative Biochemistry and Physiology, Part B,* 159: 197-205. doi: 10.1016/j.cbpb.2011.04.006

Antifreeze protein type IV (AFPIV) cDNAs and genomic DNAs from the Antarctic fishes *Pleuragramma antarcticum* (Pa) and *Notothenia coriiceps* (Nc) were cloned and sequenced, respectively. Each cDNA encoded 128 amino acids, with 94% similarity between the two and 83% similarity with AFPIV of the longhorn sculpin, *Myoxocephalus octodecemspinosus*. The genome structures of both genes consisted of four exons and three introns, and were highly conserved in terms of sequences and positions. In contrast, the third intron of PaAFPIV had additional nucleotides with inverted repeats at each end, which appeared to be a MITE-like transposable element. Comparative analysis revealed that fish AFPIVs were widely distributed across teleost fishes,well conserved in their intron positions, but more variable in intron sequences and sizes. However, the intron sequences of two Antarctic fishes were highly conserved, indicating recent radiation of notothenioids in the evolutionary lineage. The recombinant PaAFPIV and NcAFPIV were expressed in *E. coli*, and examined antifreeze activity. PaAFPIV and NcAFPIV gave ice crystalswith star-shaped morphology, and thermal hysteresis (TH) values were 0.08℃ at the concentration of 0.5 mg/ml.

4-16 **Lee, Jun Hyuck**, HaJeung Park, Soo Jeong Park, **Hak Jun Kim**, and Soo Hyun Eom. 2011. "The structural flexibility of the shank1 PDZ domain is important for its binding to different ligands". *Biochemical and Biophysical Research Communications,* 407: 207-212. doi: 10.1016/j.bbrc.2011.02.141

The PDZ domain of the shank protein interacts with numerous cell membrane receptors and cytosolic proteins via the loosely defined binding motif X-(Ser/Thr)-X-Φ-COOH (Φ represents hydrophobic residues) at the carboxyl terminus of its target protein. This enables shank to serve as a membrane-associated scaffold for the assembly of signaling complexes. As the list of proteins that bind to the shank PDZ domain grows, it is not immediately clear what structural element(s) mediate this domain's target specificity or the plasticity required to bind its different targets. Here, we have determined the crystal structure of the shank1 PDZ in complex with the βPIX C-terminal pentapeptide (642-646, DETNL) at 2.3 Å resolution and modeled shank1 PDZ binding to selected pentapeptide ligands. The resulting structures revealed a large hydrophobic pocket within the PDZ domain that can accommodate a variety of ligand residues at the P(0) position. A H-bond between His735 and Ser/Thr at the P(-2) position is invariant throughout the model structures. In addition, we identified multiple PDZ domain residues that are able to form H-bonds and salt bridges with an incoming target protein. Overall, our study provides a new level of understanding of the specificity and structural plasticity of the shank PDZ domain.

4-17 **Lee, Jun Hyuck**, Jun Yop An, HaJeung Park, **Hak Jun Kim**, and Soo Hyun Eom. 2011. "Crystallization and preliminary X-ray crystallographic analysis of the human kindlin-2 PH domain". *Acta Crystallographica Section F,* 67: 696-699. doi: 10.1107/S1744309111013820

Kindlins contribute the correct assembly of integrin-containing focal adhesion sites through their direct interaction with the cytoplasmic tail of β-integrins. The FERM domain of kindlins has a unique subdomain organization: the F2 subdomain harbors a centrally located pleckstrin homology (PH) domain thought to be involved in the membrane targeting of kindlins. FERM domains are found in a number of cytoskeletal proteins that mediate the interaction between integrins and cytosolic proteins. In the present study, the PH domain of human kindlin-2 was subcloned, solubly expressed in *Escherichia coli* and crystallized using the hanging-drop vapor-diffusion method. A diffraction data set was collected at 2.8 Å resolution using a synchrotron X-ray radiation source at the BL- 4A of the Pohang Accelerator Laboratory (Pohang, Repulbic of Korea).

4-18 **Lee, Jun Hyuck**, **Sung Gu Lee**, and **Hak Jun Kim**. 2011. "Recent Advances in Structural Studies of Antifreeze Proteins". *Ocean and Polar Research,* 33(2): 159-169. doi: 10.4217/OPR.2011.33.2.159

Antifreeze proteins (AFPs) have ice binding affinity, depress freezing temperature and inhibit ice recystallization which protect cellular membranes in polar organisms. Recent structural studies of antifreeze proteins have significantly expanded our understanding of the structure-function relationship and ice crystal growth inhibition. Although AFPs (Type I-IV AFP from fish, insect AFP and Plant AFP) have completely different fold and no sequence homology, they share a common feature of their surface area for ice binding property. The conserved ice-binding sites are relatively flat and hydrophobic. For example, Type I AFP has an amphipathic, single α-helix and has regularly spaced Thr-Ala residues which make direct interaction with oxygen atoms of ice crystals. Unlike Type I AFP, Type II and III AFP are compact globular proteins that contain a flat ice-binding patch on the surface. Type II and Type III AFP show a remarkable structural similarity with the sugar binding lectin protein and C-terminal domain of sialic acid synthase, respectively. Type IV is assumed to form a four-helix bundle which has sequence similarity with apolipoprotein. The results of our modeling suggest an ice-binding induced structural change of Type IV AFP. Insect AFP has β-helical structure with a regular array of Thr-X-Thr motif. Threonine residues of each Thr-X-Thr motif fit well into the ice crystal lattice and provide a good surface-surface complementarity. This review focuses on the structural characteristics and details of the ice-binding mechanism of antifreeze proteins.

4-19 Lee, Sang-Hwan, Eui Young Kim, **Hyun Park**, and 2 others. 2011. “In situ stabilization of arsenic and metal-contaminated agricultural soil using industrial by-products”. *Geoderma,* 161(1): 1-7.
doi: 10.1016/j.geoderma.2010.11.008

The usefulness of limestone, red mud, and furnace slag on the in situ stabilization of arsenic (As) and heavy metals was evaluated relative to different endpoints (microorganisms, plants, and humans). Individually or combined treatment of iron-rich amendments were effectively lowered the availability of trace elements. Compared to control soil, $Ca(NO_3)_2$-eatractable As, Cd, Pb, and Zn was reduced by 58%, 98%, 98%, and 99%, respectively, by combined treatment of limestone and red mud. The decreased availability of trace elements was accompanied by increased microbial activity (respiration, glucose mineralization, and soil enzyme activity) and decreased plant uptake of trace elements. Compared to non amended control soil, only 13%, 28%, 47%, and 12% of the As, Cd, Pb, and Zn, respectively, detected in combined treatment of limestone and red mud. These results suggest that iron-rich industrial by-products could be used for remediation of soils cocontaminated with metals and arsenic.

4-20 Lee, Sang-Hwan, **Hyun Park**, and 3 others. 2011. “Evaluation of the effectiveness of various amendments on trace metals stabilization by chemical and biological methods”. *Journal of Hazardous Materials,* 188: 44-51.
doi: 10.1016/j.jhazmat.2011.01.046

We evaluated the effects of five different kinds of amendments on heavy metals stabilization. The five amendments were: zero valent iron, limestone, acid mine drainage treatment sludge, bone mill, and bottom ash. To determine bioavailability of the heavy metals, different chemical extraction procedures were used such as, extraction with ($Ca(NO_3)_2$, DTPA; toxic characteristic leaching procedure (TCLP), physiologically based extraction test (PBET) that simulates gastric juice, and sequential extraction test. Bioavailability was also determined by measuring uptake of the heavy metals by lettuce (*Lactuca sativa* L.) and earthworms (*Eisenia fetida*). In addition, dehydrogenase activity was measured to determine microbial activity in the soil with the different amendments. The addition of amendments, especially limestone and bottom ash, resulted in a significant reduction in extractable metal contents. Biological assays using lettuce, earthworm, and enzyme activity were found as appropriate indicators of available metal fraction after *in situ* stabilization of heavy metals. In conclusion, TCLP and sequential extraction test appear to be promising surrogate measure of metal bioavailability in soils for several environment endpoints.

4-21 **Lee, Yung Mi**, So-Yeon Kim, Jia Jung, **Eun Hye Kim**, **Kyeung Hee Cho**, Franz Schinner, Rosa Margesin, **Soon Gyu Hong**, and **Hong Kum Lee**. 2011. "Cultured Bacterial Diversity and Human Impact on Alpine Glacier Cryoconite". *Journal of Microbiology,* 49(3): 355-362. doi: 10.1007/s12275-011-0232-0

The anthropogenic effect on the microbial communities in alpine glacier cryoconites was investigated by cultivation and physiological characterization of bacteria from six cryoconite samples taken at sites with different amounts of human impact. Two hundred and forty seven bacterial isolates were included in *Antinobacteria* (9%, particularly *Arthrobacter*), *Bacteroidetes* (14%, particularly *Olleya*), *Firmicutes* (0.8%), *Alphaproteobacteria* (2%), *Betaproteobacteria* (16%, particularly, *Janthinobacterium*), and *Gammaproteobacteria* (59%, particularly *Pseudomonas*). Among them, isolates of *Arthrobacter* were detected only in samples from sites with no human impact, while islates affiliated with *Enterobacteriaceae* were detected only in samples from sites with strong human impact. Bacterial isolates included in *Actinobacteria* and *Bacteroidetes* were frequently isolated from pristine sites and showed low maximum growth temperature and enzyme secretion. Bacterial isolates included in *Gammaproteobacteria* were more frequently isolated from sites with stronger human impact and showed high maximum growth temperature and enzyme secretion. Ecotypci differences were not evident among isolates of *Janthinobacterium lividum*, *Pseudomonas fluorescens*, and *Pseudomonas veronii*, which were frequently isolated from sites with different degrees of anthropogenic effect.

4-22 Na, Hyunsoo, **Ok-Sun Kim**, and 3 others. 2011. "Comparative Approach to Capture Bacterial Diversity of Coastal Waters". *Journal of Microbiolgoy,* 49(5): 729-740. doi: 10.1007/s12275-011-1205-z

Despite the revolutionary advancements in DNA sequencing technology and cultivation techniques, few studies have been done to directly compare these methods. In this study, a 16S rRNA gene-based, integrative approach combining culture-independent techniques with culture-dependent methods was taken to investigate the bacterial community structure of coastal seawater collected from the Yellow Sea, Korea. For culture-independent studies, we used the latest model pyrosequencer, Roche/454 Genome Sequencer FLX Titanium. Pyrosequencing captured a total of 52 phyla including 27 candidate divisions from the water column, whereas the traditional cloning approach captured only 15 phyla including 2 candidate divisions. In addition, of 878 genera retrieved, 92.1% of the sequences were unique to pyrosequencing. For culture-dependent analysis, plate culturing, plate washing, enrichment and high-throughput culturing (HTC) methods were applied. Phylogenetic analysis showed that the plate-washing clones formed a cluster devoid of any previously cultured representatives within the family *Rhodobacteraceae*. One HTC isolate (SF293) fell into the OM182 clade, which was not recovered by other culturing methods described here. By directly comparing the sequences obtained from cultures with those from culture-independent work, we found that only 33% of the culture sequences were identical to those from clone libraries and pyrosequences. This study presents a detailed comparison of common molecular and dultivation techniques availagble in microbial ecology. As different methods yeilded different coverage, we suggest choosing the approach after carefully examining the scientific questions being asked.

4-23 Park, Ae Kyung, **Kyoung Sun Park**, **Hak Jun Kim**, **Hyun Park**, **In Young Ahn**, and 2 others. 2011. “Crystallization and preliminary X-ray crystallographic studies of the ice-binding protein from the Antarctic yeast *Leucosporidium* sp. AY30”. *Acta Crystallographica Section F*, 67: 800-802. doi: 10.1107/S1744309111018446

Freezing is dangerous to cellular organisms because it causes an increase in the concentration of ions and other solutes in the plasma, denatures biomolecules and ruptures cell membranes. Some cold-adapted organisms can survive at subzero temperatures by producing proteins that bind to and inhibit the growth of ice crystals. To better understand the structure and function of these proteins, the ice-binding protein from *Leucosporidium* sp. AY30 (LeIBP) was overexpressed, purified and crystallized. The native crystal belonged to space group $P4_32_12$, with unit-cell parameters $a = b = 98.05$, $c = 106.13$ Å. Since LeIBP lacks any cysteine or methionine residues, two leucine residues (Leu69 and Leu155) were substituted by methionine residues in order to obtain selenomethioninesubstituted LeIBP for use in multiple-wavelength anomalous diffraction (MAD) phasing. The selenomethionine-substituted mutant crystallized in the same space group as the native protein.

4-24 Park, HaJeung, **Jun Hyuck Lee**, and 3 others. 2011. “The *Rickettsia Surface* Cell Antigen 4 Applies Mimicry to Bind to and Activate Vinculin”. *Journal of Biological Chemistry,* 286(40): 35096-35103. doi: 10.1074/jbc.M111.263855

Pathogenic *Rickettsia* species cause high morbidity and mortality, especially *R. prowazekii*, the causative agent of typhus. Like many intracellular pathogens, *Rickettsia* exploit the cytoskeleton to enter and spread within the host cell. Here we report that the cell surface antigen sca4 of *Rickettsia* co-localizes with vinculin in cells at sites of focal adhesions in sca4-transfected cells and that sca4 binds to and activates vinculin through two vinculin binding sites (VBSs) that are conserved across all *Rickettsia*. Remarkably, this occurs through molecular mimicry of the vinculin-talin interaction that is also seen with the IpaA invasin of the intracellular pathogen *Shigella*, where binding of these VBSs to the vinculin seven-helix bundle head domain (Vh1) displaces intramolecular interactions with the vinculin tail domain that normally clamp vinculin in an inactive state. Finally, the vinculin sca4-VBS crystal structures reveal that vinculin adopts a new conformation when bound to the C-terminal VBS of sca4. Collectively, our data define the mechanism by which sca4 activates vinculin and interacts with the actin cytoskeleton, and they suggest important roles for vinculin in *Rickettsia* pathogenesis.

4-25 **Paudel, Babita**, **Hari Datta Bhattaraia**, **Hye Yeon Koh**, **Sung Gu Lee**, **Se Jong Han**, **Hong Kum Lee**, Hyuncheol Oh, Hyun Woung Shin, and **Joung Han Yim**. 2011. “Ramalin, a novel nontoxic antioxidant compound from the Antarctic lichen *Ramalina terebrata*”. *Phytomedicine,* 18(14): 1285-1290. doi: 10.1016/j.phymed.2011.06.007

Ramalin (γ-glutamyl-N'-(2-hydroxyphenyl)hydrazide), a novel compound, was isolated from the methanol–water extract of the Antarctic lichen *Ramalina terebrata* by several chromatographic methods. The molecular structure of ramalin was determined by spectroscopic analysis. The experimental data showed that ramalin was five times more potent than commercial butylated hydroxyanisole (BHA) in scavenging 1-diphenyl-2-picryl-hydazil (DPPH) free radicals, 27 times more potent in scavenging 2,2'-azino-bis (3-ethylbenzthiazoline-6-sulfonic acid free radicals ($ABTS^{\bullet+}$) than the vitamin E analogue, trolox, and 2.5 times more potent than BHT in reducing Fe^{3+} to Fe^{2+} ions. Similarly, ramalin was 1.2 times more potent than ascorbic acid in scavenging superoxide radicals and 1.25 times more potent than commercial kojic acid in inhibiting tyrosinase enzyme activity, which ultimately leads to whitening of skin cells. Ramalin showed no or very little cytotoxicity in human keratinocyte and fibroblast cells at its antioxidant concentration. Furthermore, ramalin was assessed to determine its antioxidant activity *in vivo*. One microgram per milliliter ramalin significantly reduced the released nitric oxide (NO) and 0.125 μg/ml ramalin reduced the produced hydrogen peroxide (H_2O_2) in LPS (lipopolysaccharide)-stimulated murine macrophage Raw264.7 cells. Considering all the data together, ramalin can be a strong therapeutic candidate for controlling oxidative stress in cells.

4-26 Peña, Viviana, Walter H. Adey, Rafael Riosmena-Rodríguez, **Moon-Yung Jung**, Julio Afonso-Carrillo, **Han-Gu Choi**, and Ignacio Bárbara. 2011. *"MESOPHYLLUM SPHAERICUM* SP. NOV. (CORALLINALES, RHODOPHYTA): A NEW MAËRL-FORMING SPECIES FROM THE NORTHEAST ATLANTIC". *Journal of Phycology,* 47(5): 911-927.
doi: 10.1111/j.1529-8817.2011.01015.x

Mesophyllum sphaericum sp. nov. is described based on spherical maërl individuals (up to 10 cm) collected in a shallow subtidal maërl bed in Galicia (NW Spain). The thalli of these specimens are radially organized, composed of arching tiers of compact medullary filaments. Epithallial cells have flattened to rounded outermost walls, and they occur in a single layer. Subepithallial initials are as long as, or longer than the daughter cells that subtend them. Cell fusions are abundant. Multiporate asexual conceptacles are protruding, mound-like with a flattened pore plate, lacking a peripheral raised rim. Filaments lining the pore canal and the conceptacle roof are composed of five to six cells with straight elongate and narrow cells at their base. Carposporangial conceptacles are uniporate, protruding, and conical. Spermatangial conceptacles were not observed. Molecular results placed *M. sphaericum* near to *M. erubescens*, but *M. sphaericum* is anatomically close to *M. canariense*. The examination of the holotype and herbarium specimens of *M. canariense* indicated that both species have pore canal filaments with elongate basal cells, but they differ in number of cells (five to six in *M. sphaericum* vs. four in *M. canariense*). Based on the character of pore canal filaments, *M. canariense* shows similarities with *M. erubescens* (three to five celled). The outermost walls of epithallial cells of *M. canariense* are flared compared to the round to flattened ones of *M. erubescens*, the latter being widely accepted for the genus *Mesophyllum*. The addition of *M. sphaericum* as new maërl-forming species suggests that European mae¨rl beds are more biodiverse than previously understood.

4-27 Rangarajan, Erumbi S., **Jun Hyuck Lee**, and Tina Izard. 2011. "Apo raver1 structure reveals distinct RRM domain orientations". *Protein Science,* 20: 1464-1470.
doi: 10.1002/pro.664

Raver1 is a multifunctional protein that modulates both alternative splicing and focal adhesion assembly by binding to the nucleoplasmic splicing repressor polypyrimidine tract protein (PTB) or to the cytoskeletal proteins vinculin and α-actinin. The amino-terminal region of raver1 has three RNA recognition motif (RRM1, RRM2, and RRM3) domains, and RRM1 interacts with the vinculin tail (Vt) domain and *vinculin* mRNA. We previously determined the crystal structure of the raver1 RRM1–3 domains in complex with Vt at 2.75 Å resolution. Here, we report crystal structure of the unbound raver1 RRM1–3 domains at 2 Å resolution. The apo structure reveals that a bound sulfate ion disrupts an electrostatic interaction between the RRM1 and RRM2 domains, triggering a large relative domain movement of over 30°. Superposition with other RNA-bound RRM structures places the sulfate ion near the superposed RNA phosphate group suggesting that this is the raver1 RNA binding site. While several single and some tandem RRM domain structures have been described, to the best of our knowledge, this is the second report of a three-tandem RRM domain structure.

4-28 Seo, Changon, **Joung Han Yim, Hong Kum Lee**, and Hyuncheol Oh. 2011. "PTP1B inhibitory secondary metabolites from the Antarctic lichen *Lecidella carpathica*". *Mycology,* 2(1): 18-23.
doi: 10.1080/21501203.2011.554906

Protein tyrosine phosphatase 1B (PTP1B) is an attractive therapeutic target for diabetes, playing a major role in negative regulation of the insulin signaling pathway. Bioassay-guided investigations of an MeOH extract of the Antarctic lichen, *Lecidella carpathica*, afforded three PTP1B inhibitory metabolites: hopane-6α,22-diol (1), brialmontin 1 (2), and atraric acid (3), along with two aromatic metabolites (4 and 5) previously isolated from a different Antarctic lichen species. Their structures were determined by analysis of NMR and MS data. Compounds 1–3 inhibited PTP1B activity in a dose-dependent manner with IC_{50} values of 3.7, 14.0 and 51.5 μM, respectively, and kinetic analyses of PTP1B inhibition by compounds 1 and 2 suggested that these compounds inhibit PTP1B activity in a competitive manner. In addition, 6,22-hopanediol (1) displayed some selectivity toward PTP1B over other protein tyrosine phosphatases, such as TCPTP (IC_{50} = 8.4 μM), SHP-2 (IC_{50} > 68 μM), LAR (IC_{50} > 68 μM), and CD45 (IC_{50} > 68 μM).

4-29 Sutherland, Judith E., Sandra C. Lindstrom, Wendy A. Nelson, Juliet Brodie, Michael D. J. Lynch, Mi Sook Hwang, **Han-Gu Choi**, and 8 others. 2011. "A NEW LOOK AT AN ANCIENT ORDER: GENERIC REVISION OF THE BANGIALES (RHODOPHYTA)". *Journal of Phycology,* 47(5): 1131-1151.
doi: 10.1111/j.1529-8817.2011.01052.x

The red algal order Bangiales has been revised as a result of detailed regional studies and the development of expert local knowledge of Bangiales floras, followed by collaborative global analyses based on wide taxon sampling and molecular analyses. Combined analyses of the nuclear SSU rRNA gene and the plastid RUBISCO LSU (*rbc*L) gene for 157 Bangiales taxa have been conducted. Fifteen genera of Bangiales, seven filamentous and eight foliose, are recognized. This classification includes five newly described and two resurrected genera. This revision constitutes a major change in understanding relationships and evolution in this order. The genus *Porphyra* is now restricted to five described species and a number of undescribed species. Other foliose taxa previously placed in *Porphyra* are now recognized to belong to the genera *Boreophyllum* gen. nov., *Clymene* gen. nov., *Fuscifolium* gen. nov., *Lysithea* gen. nov., *Miuraea* gen. nov., *Pyropia*, and *Wildemania*. Four of the seven filamentous genera recognized in our analyses already have generic names (*Bangia*, *Dione*, *Minerva*, and

Pseudobangia), and are all currently monotypic. The unnamed filamentous genera are clearly composed of multiple species, and few of these species have names. Further research is required: the genus to which the marine taxon *Bangia fuscopurpurea* belongs is not known, and there are also a large number of species previously described as *Porphyra* for which nuclear SSU ribosomal RNA (nrSSU) or *rbc*L sequence data should be obtained so that they can be assigned to the appropriate genus.

4-30 Yoo, Miyoun, **Dockyu Kim**, and 3 others. 2011. "Biphenyl hydroxylation enhanced by an engineered *o*-xylene dioxygenase from *Rhodococcus* sp. strain DK17". *Research in Microbiology,* 162: 724-728.
doi: 10.1016/j.resmic.2011.04.013

Hydroxylation of the non-growth substrate biphenyl by recombinant *o*-xylene dioxygenases from *Rhodococcus* sp. strain DK17 was studied through bioconversion experiments. The metabolites from the biphenyl hydroxylation by each enzyme were identified and quantified by gas chromatography-mass spectrometry. The L266F mutant enzyme produced much more 2-hydroxybiphenyl (2.43 vs. 0.1 ㎍/L) and 3-hydroxybiphenyl (1.97 vs. 0.03 ㎍/L) than the wild-type. Site-directed mutagenesis combined with structural and functional analyses indicated that hydrophobic interactions and shielding effects against water are important factors in the hydroxylation of biphenyl by the *o*-xylene dioxygenase. The residue at position 266 plays a key role in coordinating the reaction.


KOPRI
극지연구소

KOPRI ABSTRACTS 2012


KOPRI
극지연구소

PART 1

Climate Change Sciences

1-1 An, Soon-Il, Hyerim Kim, and **Baek-Min Kim**. 2012. “Impact of freshwater discharge from the Greenland ice sheet on North Atlantic climate variability”. *Theoretical and Applied Climatology,* 112: 29–43.
doi: 10.1007/s00704-012-0699-6

Using a coupled ocean–atmosphere general circulation model, we investigated the impact of Greenland ice sheet melting on North Atlantic climate variability. The positive-degree day (PDD) method was incorporated into the model to control continental ice melting (PDD run). Models with and without the PDD method produce a realistic pattern of North Atlantic sea surface temperature (SST) variability that fluctuates from decadal to multidecadal periods. However, the interdecadal variability in PDD run is significantly dominated in the longer time scale compared to that in the run without PDD method. The main oscillatory feature in these experiments likely resembles the densitydriven oscillatory mode. A reduction in the ocean density over the subpolar Atlantic results in suppression of the Atlantic Meridional Overturning Circulation (AMOC), leading to a cold SST due to a weakening of northward heat transport. The decreased surface evaporation associated with the cold SST further reduces the ocean density and thus, simultaneously acts as a positive feedback mechanism. The southward meridional current associated with the suppressed AMOC causes a positive tendency in the ocean density through density advection, which accounts for the phase transition of this oscillatory mode. The Greenland ice melting process reduces the mean meridional current and meridional density gradient because of additional fresh water flux, which suppress the delayed negative feedback due to meridional density advection. As a result, the oscillation period becomes longer and the transition is more delayed.

1-2 An, Soon-Il, Jae-Heung Park, **Baek-Min Kim**, and 2 others. 2012. “Impacts of ocean gateway and basin width on Tertiary tropical climate variability in a prototype model”. *Theoretical and Applied Climatology,* 107: 155–164.
doi: 10.1007/s00704-011-0469-x

Using a simple tropical climate model, we investigated possible impacts of changes in oceanic seaways (Panama and Tethys) and ocean basin sizes (great Pacific and narrow Atlantic) on tropical climate variability during Tertiary. Our model showed that the opening of seaways had little influence on climate variability in the tropical Pacific because the climate variability in the Pacific Ocean’s large basins were internally generated, regardless of the variation in the tropical Atlantic Ocean. Conversely, the climate variability in the tropical Atlantic Ocean was highly dependent on the tropical Pacific Ocean; thus, an opening seaway, particularly the Panama seaway, was crucial in generating the interannual variability in the tropical Atlantic Ocean. We also found that in the Pacific Ocean, basin size strongly modified the period and amplitude of the interannual variability of both the Pacific and Atlantic Oceans due to ocean wave dynamics.

1-3 Cheon, Woo Geun, Young-Gyu Park, Sang-Wook Yeh, and **Baek-Min Kim**. 2012. “Atmospheric impact on the northwestern Pacific under a global warming scenario”. *Geophysical Research Letters,* 39: L16709(1-6).
doi: 10.1029/2012GL052364

Eleven climate models, one high-resolution and ten low-resolution, were analyzed to investigate the response of the northwestern

Pacific under a global warming scenario. Application of scenario A1B of the Special Report on Emission Scenarios (SRES) weakens (intensifies) the southern (northern) part of the interior subtropical gyre both in highresolution and low-resolution model. Such a dipole type change is mainly due to a basin-scale dynamic atmosphereto-ocean process. Namely, under global warming the Hadley circulation is weakened and expanded poleward. The Ferrel circulation is also displaced poleward, leading to weakening of ascending (descending) air motion and a high (low) sea level pressure anomaly in the northwestern (southeastern extratropical) North Pacific. Finally, a negative wind stress curl anomaly developed along the zero wind stress curl line of the present-day climate to enhance the northern part of the gyre. The high-resolution model results show greater changes in the structure of the Kuroshio and Kuroshio Extension, with strong intensification of the Kuroshio Extension front and jet, while in the low-resolution models the changes are small. The Kuroshio between Taiwan and the southern coast of Japan is significantly intensified in the high-resolution model results, but is slightly weakened in the ensemble of the lowresolution models.

1-4 Ho, C. -H., **S. -J. Park**, and 3 others. 2012. “Observational Evidences of Double Cropping Impacts on the Climate in the Northern China Plains”. *Journal of Climate,* 25(13): 4721-4728. doi: 10.1175/JCLI-D-11-00224.1

The impacts of harvested cropland in the double cropping region (DCR) of the northern China plains (NCP) on the regional climate are examined using surface meteorological data and the satellite-derived normalized difference vegetation index (NDVI) and land surface temperature (LST). The NDVI data are used to distinguish the DCR from the single cropping region (SCR) in the NCP. Notable increases in LST in the period May–June are found in the area identified as the DCR on the basis of the NDVI data. The difference between the mean daily maximum temperature averaged over the DCR and SCR stations peaks at 1.27℃ in June. The specific humidity in theDCRis significantly smaller than in the SCR. These results suggest that the enhanced agricultural production by multiple cropping may amplify regional warming and aridity to further modify the regional climate in addition to the global climate change. Results in this study may also be used as a quantitative observed reference state of the crop/vegetation effects for future climate modeling studies.

1-5 Jeong, Su-Jong, Chang-Hoi Ho, **Baek-Min Kim**, and 2 others. 2012. “Non-linear response of vegetation to coherent warming over northern high latitudes”. *Remote Sensing Letters,* 4(2): 123-130. doi: 10.1080/2150704X.2012.703790

This study evaluates the large-scale changes in vegetation greenness at northern high latitudes (>60° N) using satellite-measured normalized difference vegetation index (NDVI) and station-merged temperature, precipitation and soil moisture for the period 1982–2008. During this 27-year period, although coherent warming trends were observed at most of the high latitudes, changes in the NDVI showed apparent spatial and temporal heterogeneity. In particular, changes in the hemi- spheric mean NDVI increased until 1997, but decreased thereafter. Maximum covariance analysis, which is a statistical method to detect large-scale covariability between two variables over time, reveals significant relationships between NDVI and soil moisture (and/or precipitation) in the regions of negative NDVI trends. These results further suggest that local moisture availability also plays a consider- able role in the large-scale changes in vegetation as well as coherent warming over the northern high latitudes. moisture for the period 1982–2008. During this 27-year period, although coherent warming trends were observed at most of the high latitudes, changes in the NDVI showed apparent spatial and temporal heterogeneity. In particular, changes in the hemi- spheric mean NDVI increased until 1997, but decreased thereafter. Maximum covariance analysis, which is a statistical method to detect large-scale covariability between two variables over time, reveals significant relationships between NDVI and soil moisture (and/or precipitation) in the regions of negative NDVI trends. These results further suggest that local moisture availability also plays a consider- able role in the large-scale changes in vegetation as well as coherent warming over the northern high latitudes.

1-6 **Kim, Jeong-Han**, Yong Ha Kim, **Geonhwa Jee**, and Changsup Lee. 2012. “Mesospheric Temperature Estimation from Meteor Decay Times of Weak and Strong Meteor Trails”. *Journal of Atmospheric and Solar-Terrestrial Physics,* 89: 18-26.
doi: 10.1016/j.jastp.2012.07.003

Neutral temperatures near the mesopause region were estimated from the decay times of the meteor echoes observed by a VHF meteor radar during a period covering 2007 to 2009 at King Sejong Station (62.22°S, 58.78°W), Antarctica. While previous studies have used all meteor echoes to determine the slope from a height profile of log inverse decay times for temperature estimation, we divided meteor echoes into weak and strong groups depending on the strength of estimated relative electron line densities within meteor echoes. We found that the slopes from the strong group are inappropriate for temperature estimation because the decay times of strong meteors are considerably scattered, whereas the slopes from the weak group clearly define the variation of decay times with height. We thus utilize the slopes only from the weak group in the altitude region between 86 and 96 km to estimate mesospheric temperatures. The meteor estimated temperatures show a typical seasonal variation near the mesopause region and the monthly mean temperatures are in good agreement with SABER temperatures within a mean difference of 4.8 K throughout the year. The meteor temperatures, representing typically the region around the altitude of 91 km, are lower on average by 2.1 K than simultaneously measured SATI OH(6-2) rotational temperatures during winter (March ~ October).

1-7 Kim, Jongchul, **Jung-Ho Kang**, and 4 others. 2012. “Assessment of polybrominated diphenyl ethers (PBDEs) in serum from the Korean general population”. *Environmental Pollution,* 164: 46-52.
doi: 10.1016/j.envpol.2012.01.016

In 2009 and 2010, 720 serum samples were collected from non-occupationally exposed study participants at four Korean locations and monitored for the presence of 27 polybrominated diphenyl ether (PBDE) congeners. The median concentrations of $\sum_{27}$PBDEs (the sum of 27 congeners) and $\sum_{3\text{-}7}$PBDEs (the sum of tri- to hepta-BDE congeners) were 6.04 and 4.97 ng/g lipid, respectively. The most abundant congener detected in serum samples was BDE-153, followed by BDE-47 and BDE-99. The median value of $\sum_{3\text{-}7}$PBDEs was similar to the median values observed in Asia and Europe, but much lower than that observed in North America. Some significant differences, based on geographic region and sex, were observed. We also observed a positive increase of BDE-153 with regard to age. In addition, we estimated the daily exposure to PBDEs from previously published reports of PBDE concentrations in food and dust, and determined the individual contributions of a variety of sources.

1-8 **Kim, Seong-Joong** and **Baek-Min Kim**. 2012. “Ocean Response to the Pinatubo and 1259 Volcanic Eruptions”. *Ocean and Polar Research,* 34(3): 305-323. doi: 10.4217/OPR.2012.34.3.305

The ocean’s response to the Pinatubo and 1259 volcanic eruptions was investigated using an ocean general circulation model equipped with an energy balance model. Volcanic eruptions release gases into the atmosphere which increases the aerosol optical depth and acts to reduce the incoming short-wave radiation. For example, there was a huge volcanic eruption (Pinatubo) in 1991 which reduced the global mean radiative forcing by about 3 W m^{-2}. Two numerical experiments were simulated. The first experiment features the Pinatubo eruption and the second experiment simulates the much larger volcanic eruption that occurred in 1259 when the radiative forcing was reduced by 7 times compared to the Pinatubo event. With the reduced radiative forcing due to the Pinatubo eruption at about 3 W m^{-2} and 1259 eruption at about 21 W m^{-2}, the global mean sea surface temperature (SST) decreased to its lowest in the second year after each event by about 0.4℃ and 1.6℃, respectively. Sea surface salinity (SSS) increased substantially in the northern North Pacific, northern North Atlantic, and the Southern Ocean. The reduced SST together with SSS increased ocean convection, which yielded an increase in North Atlantic Deep Water, Antarctic Bottom Water, and North Pacific Intermediate Water production and their outflows. The increase in overturning circulation eventually increased the pole-ward ocean heat fluxes. In conclusion, huge volcanic eruptions perturb the ocean substantially and their hallmarks last for more than a decade, confirming the importance of volcanic eruptions in illustrating the decadal-climate variability recorded in the paleoclimate proxy data for the past million years.

1-9 Lampert, Astrid, Johan Ström, Christoph Ritter, Roland Neuber, **Young Jun Yoon**, **Nam Yi Chae**, and Masataka Shiobara. 2012. “Inclined Lidar Observations of Boundary Layer Aerosol Particles above the Kongsfjord, Svalbard”. *Acta Geophysica,* 60(5): 1287-1307. doi: 10.2478/s11600-011-0067-4

An inclined lidar with vertical resolution of 0.4 m was used for detailed boundary layer studies and to link observations at Zeppelin Mountain (474 m) and Ny-Ålesund, Svalbard. We report on the observation of aerosol layers directly above the Kongsfjord. On 29 April 2007, a layer of enhanced backscatter was observed in the lowest 25 m above the open water surface. The low depolarization ratio indicated spherical particles. In the afternoon, this layer disappeared. The ultrafine particle concentration at Zeppelin and Corbel station (close to the Kongsfjord) was low. On 1 May 2007, a drying process in the boundary layer was observed. In the morning, the atmosphere up to Zeppelin Mountain showed enhanced values of the backscatter coefficient. Around noon, the top of the highly reflecting boundary layer decreased from 350 to 250 m. The top of the boundary layer observed by lidar was confirmed by radiosonde data.

1-10 **Lee, Jae Il**, **Ho Il Yoon**, **Kyu-Cheul Yoo**, **Hyoun Soo Lim**, and 4 others. 2012. “Late Quaternary glacial–interglacial variations in sediment supply in the southern Drake Passage”. *Quaternary Research,* 78: 119-129. doi: 10.1016/j.yqres.2012.03.010

Geochemical characteristics of marine sediment from the southern Drake Passage were analyzed to reconstruct variations in sediment provenance and transport paths during the late Quaternary. The 5.95 m gravity core used in this study records paleoenvironmental changes during the last approximately 600 ka. Down-core variations in trace element, rare earth element, and Nd and Sr isotopic compositions reveal that sediment provenance varied according to glacial cycles. During glacial periods, detrital sediments in the southern Drake Passage were mostly derived from the nearby South Shetland Islands and shelf sediments. In contrast, interglacial sediments are composed of mixed sediments, derived from both West Antarctica and East Antarctica. The East Antarctic provenance of the interglacial sediments was inferred to be the Weddell Sea region. Sediment input from the Weddell Sea was reduced during glacial periods by extensive ice sheets and weakened current from the Weddell Sea. Sediment supply from the Weddell Sea increased during interglacial periods, especially those with higher warmth such as MIS 5, 9, and 11. This suggests that the influence of deep water from the Weddell Sea increases during interglacial periods and decreases during glacial periods, with the degree of influence increasing as interglacial intensity increases.

1-11 Oh, Ji-Hyun, **Baek-Min Kim**, and 3 others. 2012. “The impact of the diurnal cycle on the MJO over the Maritime Continent: a modeling study assimilating TRMM rain rate into global analysis”. *Climate Dynamics,* 40: 893-911. doi: 10.1007/s00382-012-1419-8

In the present study, we use modeling experiments to investigate the impact of the diurnal cycle on the Madden-Julian Oscillation (MJO) during the Australian summer. Physical initialization and a nudging technique enable us to assimilate the observed Tropical Rainfall Measuring Mission (TRMM) rain rate and atmospheric variables from the National Centers for Environmental Prediction—National Center for Atmospheric Research Reanalysis 2 (R2) into the Florida State University Global Spectral Model (FSUGSM), resulting in a realistic simulation of the MJO. Model precipitation is also significantly improved by TRMM rain rate observation via the physical initialization. We assess the influence of the diurnal cycle on the MJO by modifying the diurnal component during the model integration. Model variables are nudged toward the daily averaged values from R2. Globally suppressing the diurnal cycle (NO_DIURNAL) exerts a strong impact on the Maritime Continent. The mean state of precipitation increases and intraseasonal variability becomes stronger over the region. It is well known that MJO weakens as it passes over the Maritime Continent. However, the MJO maintains its strength in the NO_DIURNAL experiment, and the diminution of diurnal signals during the integration does not change the propagating speed of the MJO. We suggest that diminishing the diurnal cycle in NO_DIURNAL consumes less moist static energy (MSE), which is required to trigger both diurnal and intraseasonal convection. Thus, the remaining MSE may play a major role along with larger convective instability and stronger lower level moisture convergence in intensifying the MJO over the Maritime Continent in the model simulation.

1-12 Park, Jaeheung, Hermann Lühr, Norbert Jakowski, Tatjana Gerzen, Hyosub Kil, **Geonhwa Jee**, and 3 others. 2012. “A long-lived band of plasma density enhancement at mid-latitudes during the 2003 Halloween magnetic storm”. *Journal of Atmospheric and Solar-Terrestrial Physics,* 80: 100-110. doi: 10.1016/j.jastp.2012.03.009

During the magnetic storm recovery phase between 08 and 13 UT on 30th October 2003 (so-called Halloween Storm), CHAMP, GRACE and TIMED satellites encountered an unusual post-midnight streak of high plasma density. The streak was latitudinally narrow (~0.5° GLAT), zonally elongated (>10° GLON), and vertically extended for several hundred kilometers. Inside the streak, as observed by CHAMP, the deviation of the magnetic field from the background is greater in the zonal component than in the meridional component. This observation is consistent with the zonally extended nature of the streak, as confirmed by TIMED/GUVI optical observations. The field-aligned current (FAC) direction is generally upward (downward) at the equatorward (poleward) edge of the streak. We discuss the time history of observed features. We suggest the following scenario of the streak formation. A storm-enhanced density (SED) was generated before 19 h local time by a sub-auroral polarization stream (SAPS). The SED gradually separated from the poleward-retreating region of strong westward plasma drift and turned into an electron density enhancement fossil (EDEF). This EDEF at mid-latitude (about 40°S MLAT) practically co-rotated with the Earth for more than 10 h through the night till dawn. We suggest that the enhanced plasma pressure was counter-balanced by magnetic pressure gradient and kept stable over many hours.

1-13 Park, S., K. -H. Kim, H. Kil, **G. Jee**, and 2 others. 2012. “The source of the steep plasma density gradient in middle latitudes during the 11–12 April 2001 storm”. *Journal of Geophysical Research,* 117: A05313(1-9). doi: 10.1029/2011JA017349

A steep plasma density gradient has been observed in the middle-latitude *F* region during large geomagnetic storms. This phenomenon can be understood as a special form of the middle-latitude ionization trough (hereafter trough), but its causal linkage has not yet been clarified. We investigate the association of the steep density gradient and the trough by comparing their morphologies and occurrence locations using the satellite and ground observation data during the 11–12 April 2001 storm. Steep density gradients are detected in the dusk sector at the equatorward edges of the aurora by the Defense Meteorological Satellite Program (DMSP) F13 spacecraft. The locations of the steep density gradients coincide with the locations of the ionospheric footprints of the plasmapause identified by the Imager for Magnetopause-to-Aurora Global Exploration satellite. These observations demonstrate that the steep density gradient is created at the typical location of the trough. However, the steep density gradient is not produced by the formation of an intense trough during the storm. The temporal evolution of the total electron content maps shows that the steep density gradient observed at dusk by DMSP is associated with the plasma density enhancement in the dayside and its corotation into the dusk sector. The severe plasma density enhancement in middle latitudes, in combination with the trough and presumably the plasma depletion in high latitudes by the neutral composition change, produces the steep density gradient in the subauroral region during the storm.

1-14 Risi, Camille, David Noone, John Worden, Christian Frankenberg, Gabriele Stiller, Michael Kiefer, Bernd Funke, Kaley Walker, Peter Bernath, Matthias Schneider, Debra Wunch, Vanessa Sherlock, Nicholas Deutscher, David Griffith, Paul O. Wennberg, Kimberly Strong, Dan Smale, Emmanuel Mahieu, Sabine Barthlott, Frank Hase, Omaira García, Justus Notholt, Thorsten Warneke, Geoffrey Toon, David Sayres, Sandrine Bony, **Jeonghoon Lee**, and 3 others. 2012. “Process-evaluation of tropospheric humidity simulated by general circulation models using water vapor isotopologues: 1. Comparison between models and observations”. *Journal of Geophysical Research,* 117: D05303(1-26).

doi: 10.1029/2011JD016621

The goal of this study is to determine how H_2O and HDO measurements in water vapor can be used to detect and diagnose biases in the representation of processes controlling tropospheric humidity in atmospheric general circulation models (GCMs). We analyze a large number of isotopic data sets (four satellite, sixteen ground-based remote-sensing, five surface in situ and three aircraft data sets) that are sensitive to different altitudes throughout the free troposphere. Despite significant differences between data sets, we identify some observed HDO/H_2O characteristics that are robust across data sets and that can be used to evaluate models. We evaluate the isotopic GCM LMDZ, accounting for the effects of spatiotemporal sampling and instrument sensitivity. We find that LMDZ reproduces the spatial patterns in the lower and mid troposphere remarkably well. However, it underestimates the amplitude of seasonal variations in isotopic composition at all levels in the subtropics and in midlatitudes, and this bias is consistent across all data sets. LMDZ also underestimates the observed meridional isotopic gradient and the contrast between dry and convective tropical regions compared to satellite data sets. Comparison with six other isotope-enabled GCMs from the SWING2 project shows that biases exhibited by LMDZ are common to all models. The SWING2 GCMs show a very large spread in isotopic behavior that is not obviously related to that of humidity, suggesting water vapor isotopic measurements could be used to expose model shortcomings. In a companion paper, the isotopic differences between models are interpreted in terms of biases in the representation of processes controlling humidity.

1-15 Risi, Camille, David Noone, John Worden, Christian Frankenberg, Gabriele Stiller, Michael Kiefer, Bernd Funke, Kaley Walker, Peter Bernath, Matthias Schneider, Sandrine Bony, **Jeonghoon Lee**, and 2 others. 2012. “Process-evaluation of tropospheric humidity simulated by general circulation models using water vapor isotopic observations: 2. Using isotopic diagnostics to understand the mid and upper tropospheric moist bias in the tropics and subtropics”. *Journal of Geophysical Research,* 117: D05304(1-25). doi: 10.1029/2011JD016623.

Evaluating the representation of processes controlling tropical and subtropical tropospheric relative humidity (RH) in atmospheric general circulation models (GCMs) is crucial to assess the credibility of predicted climate changes. GCMs have long exhibited a moist bias in the tropical and subtropical mid and upper troposphere, which could be due to the mis-representation of cloud processes or of the large-scale circulation, or to excessive diffusion during water vapor transport. The goal of this study is to use observations of the water vapor isotopic ratio to understand the cause of this bias. We compare the three-dimensional distribution of the water vapor isotopic ratio measured from space and ground to that simulated by several versions of the isotopic GCM LMDZ. We show that the combined evaluation of RH and of the water vapor isotopic composition makes it possible to discriminate the most likely cause of RH biases. Models characterized either by an excessive vertical diffusion, an excessive convective detrainment or an underestimated in situ cloud condensation will all produce a moist bias in the free troposphere. However, only an excessive vertical diffusion can lead to a reversed seasonality of the free tropospheric isotopic composition in the subtropics compared to observations. Comparing seven isotopic GCMs suggests that the moist bias found in many GCMs in the mid and upper troposphere most frequently results from an excessive diffusion during vertical water vapor transport. This study demonstrates the added value of water vapor isotopic measurements for interpreting shortcomings in the simulation of RH by climate models.

1-16 Son, Hye-Young, Wonsun Park, Jee-Hoon Jeong, Sang-Wook Yeh, **Baek-Min Kim**, and 2 others. 2012. "Nonlinear impact of the Arctic Oscillation on extratropical surface air temperature". *Journal of Geophysical Research,* 117: D19102(1-13).
doi: 10.1029/2012JD018090

The Arctic Oscillation (AO) is the leading climate mode of sea level pressure (SLP) anomalies during cold season in the Northern Hemisphere. To a large extent, the atmospheric climate anomalies associated with positive and negative phases of the AO are opposite to each other, indicating linear impact. However, there is also significant nonlinear relationship between the AO and other winter climate variability. We investigate nonlinear impacts of the AO on surface air temperature (SAT) using reanalysis data and a multimillennial long climate simulation. It is found that SAT response to the AO, in terms of both spatial pattern and magnitude, is almost linear when the amplitude of the AO is moderate. However, the response becomes quite nonlinear as the amplitude of the AO becomes stronger. First, the pattern shift in SAT depends on AO phase and magnitude, and second, the SAT magnitude depends on AO phase. In particular, these nonlinearities are distinct over the North America and Eurasian Continent. Based on the analyses of model output, we suggest that the nonlinear zonal advection term is one of the critical components in generating nonlinear SAT response, particularly over the North America.

1-17 Woo, Sung-Ho, **Baek-Min Kim**, Jee-Hoon Jeong, **Seong-Joong Kim**, and Gyu-Ho Lim. 2012. "Decadal changes in surface air temperature variability and cold surge characteristics over northeast Asia and their relation with the Arctic Oscillation for the past three decades (1979–2011)". *Journal of Geophysical Research,* 117: D18117(1-16).
doi: 10.1029/2011JD016929

Decadal changes in surface air temperature (SAT) variability and cold surge characteristics over Northeast Asia during late winter (January–March) are analyzed for the past three decades. Power spectrum analysis of SAT reveals that the low-frequency variabilities with a period longer than 10 days are significantly enhanced, while the high-frequency variabilities with a period shorter than 10 days are weakened in the 1980s and 2000s. Moreover, cold surges were stronger and lasted longer during the 1980s and 2000s compared to those that occurred in the 1990s. Here, we propose that large-scale atmospheric conditions manifested by a different phase of the Arctic Oscillation (AO) provide preconditioning for a cold surge event, which showed a prominent decadal fluctuation. The more (less) frequent strong and long-lasting cold surge occurrences in the 1980s and 2000s (1990s) are preceded by the more dominant negative (positive) phase of the AO. Lag-composite analyses for cold surge events categorized by the AO phases indicate that stronger and longer-lasting cold air advection dominates at the lower-level, when upper-level wave train and coastal trough are developed over East Asia under the strong negative AO phase. These results suggest that the decadal changes in SAT variability and cold surge characteristics are strongly associated with the decadal changes in the phase distribution of the AO.

1-18 **Woo, Sung-Ho**, Jee-Hoon Jeong, **Baek-Min Kim**, and **Seong-Joong Kim**. 2012. “Impact of Snow Depth Initialization on Seasonal Prediction of Surface Air Temperature over East Aisa for Winter Season”. *The Atmosphere,* 22(1): 117-128.

Does snow depth initialization have a quantitative impact on sub-seasonal to seasonal prediction skill? To answer this question, a snow depth initialization technique for seasonal forecast system has been implemented and the impact of the initialization on the seasonal forecast of surface air tempreature during the wintertime is examined. Since the snow depth observation can not be directly used in the model simulation due to the large systematic bias and much smaller model variability, an anomaly resacling method to the snow depth initialization is applied. Snow depth in the model is initialized by adding a rescaled snow depth observation anomaly to the model snow depth climatology. A suite of seasonal forecast is performed for each year in recent 12 years (1999-2010) with and without the snow depth initialization to evaluate the performance of the developed technique. The results show that the seasonal forecast of surface air temperature over East Asian region sensitively depends on the initial snow depth anomaly over the region. However, the sensitivity shows large differences for different timing of the initialization and forecast lead time. Especially, the snow depth anomaly initialized in the late winter (Mar. 1) is the most effective in modulating the surface air temperature anomaly after one month. The real predictability gained by the snow depth initialization is also examined from the comparison with observation. The gain of the real predictability os generally small except for the forecasting experiment in the early winter (Nov. 1), which shows some skillful forecasts. Implications of these results and future directions for further development are discussed.

1-19 Yoojin Kim, Kwang-Yual Kim, and **Baek-Min Kim**. 2012. “Physical mechanisms of European winter snow cover variability and its relationship to the NAO”. *Climate Dynamics,* 40: 1657-1669.
doi: 10.1007/s00382-012-1365-5

Annual snow cover in the Northern Hemisphere has decreased in the past two decades, an effect associated with global warming. The regional scale changes of snow cover during winter, however, vary significantly from one region to another. In the present study, snow cover variability over Europe and its connection to other atmospheric variables was investigated using Cyclostationary Empirical Orthogonal Function (CSEOF) analysis. The evolution of atmospheric variables related to each CSEOF mode of snow cover variability was derived via regression analysis in CSEOF space. CSEOF analysis clearly shows that the North Atlantic Oscillation (NAO) is related to European snow cover, particularly in January and February. A negative NAO phase tends to result in a snow cover increases, whereas a positive NAO phase results in snow cover decreases. The temporal changes in the connection between the NAO and European snow cover are explained by time-dependent NAO-related temperature anomalies. If the NAO phase is negative, the temperature is lower in Europe and snow cover increases; by contrast, when the NAO phase is positive, the temperature is higher and snow cover decreases. Temperature and snow cover variations in Europe are associated with the thermal advection by anomalous wind by NAO. CSEOF analysis also shows an abrupt increase of snow cover in December and January and a decrease in February and March since the year 2000, approximately. This abrupt change is associated with sub-seasonal variations of atmospheric circulation in the study region.

1-20 Zo, Il Sung, Joon Bum Jee, Kyu Tae Lee, **Namy Chae**, and **Young Jun Yoon**. 2012. “Change of Temperature using the Twentieth Century Reanalysis Data (20CR) on Antarctica”. *Ocean and Polar Research,* 34(1): 73-83.
doi: 10.4217/OPR.2012.34.1.073

Antarctica is very sensitive to climate change but the number of stations is not sufficient to accurately analyze climate change in this regoin. Model reanalysis data supplements the lack of observation and can be used as long term data to verify climate change. In this study, the 20CR (Twentieth Century Reanalysis) Project data from NCEP/NCAR and monthly mean data (temperature, solar radiation and longwave radiation) from 1871 to 2008, was used to analyze the temperature trend and change in radiation. The 20CR data was used to validate the observation data from Antarctica since 1950 and the correlation coefficients between these data were determined to be over 0.95 at all stations. The temperature increased by approximately 0.23℃/decade during the study period and over 0.20℃/decade over all of the months. This increasing trend was observed throughout the Antarctica and a slight increase was observed in the Antarctic Peninsula. In addition, solar radiation (surface) and longwave radiation (surface and top of atmosphere) trends correlated with the increase in temperature. As a result, outgoing longwave radiation at the surface is attenuated by atmospheric water vapor or clouds and radiation at the top of the atmosphere was reduced. In addition, the absorbed energy in the atmosphere increases the temperature of the atmosphere and surface, and then the heated surface emits more longwave radiation. Eventually these processes are repeated in a positive feedback loop, which results in a continuous rise in temperature.

PART 2

Earth-System Sciences

2-1 **Ahn, Insu**, **Jong Ik Lee**, and 2 others. 2012. “Oxygen isotope measurements of terrestrial silicates using a CO_2-laser BrF_5 fluorination technique and the slope of terrestrial fractionation line”. *Geosciences Journal,* 16(1): 7-16.
doi: 10.1007/s12303-012-0011-x

Here we report oxygen isotopic compositions (both $\delta^{18}O$ and $\delta^{17}O$) of San Carlos olivine, Juan de Fuca basalt glass, garnet standard at University of Wisconsin (UWG-2 garnet), National Bureau of standard #28 quartz (NBS-28 quartz), a hydrothermal quartz from China (CQ4 quartz), chert flint standard and a serpentine measured with a CO_2-laser BrF_5 fluorination system installed at Korea Polar Research Institute. In addition we measured VSMOW (Vienna standard mean ocean water) and SLAP (standard light Antarctic precipitation) with the same line; a scaling factor of 1.056 was obtained to fit the measured SLAP data to the recommended value of $\delta^{18}O_{SMOW} = -55.5$‰. All the other data were corrected using the VSMOW-SLAP scaling factor. Majority of the samples in this work have been measured by several laboratories; our data in general agree very well with previous data. We report data using the delta prime notation, since linearity of a mass-dependent fractionation line holds in $\delta'^{17}O$ vs. $\delta'^{18}O$ diagram for wide range of oxygen isotopic compositions. Average $\delta'^{18}O$ values and 2σ standard error of means are 5.27 ± 0.04‰ for San Carlos olivine, 5.49 ± 0.02‰ for Juan de Fuca basalt glass, 5.73 ± 0.05‰ for UWG-2 garnet, 9.18 ± 0.08‰ for NBS-28 quartz, 23.14 ± 0.36‰ for CQ4 quartz, 33.97 ± 0.16‰ for chert flint standard and 0.78 ± 0.07‰ for the serpentine. Slope of terrestrial fractionation was obtained using these data, which is 0.5248 ± 0.0003 (R^2 = 0.99992).

2-2 Barry, P. H., D. R. Hilton, S. A. Halldórsson, **D. Hahm**, and K. Marti. 2012. “High precision nitrogen isotope measurements in oceanic basalts using a static triple collection noble gas mass spectrometer”. *Geochemistry Geophysics Geosystems,* 13: Q01019(1-16).
doi: 10.1029/2011GC003878

We describe a new system for the simultaneous static triple-collection of nitrogen isotopes at the <10 μcm^3 STP [N_2] (< $1 \times 10^{-5} cm^3$ STP; < 0.5 nmol) level using a modified VG-5440 noble gas mass spectrometer. The system consists of an internal N_2-STD with a δ^{15}Nvalue of -0.11 ± 0.22‰ (1σ) calibrated against an air-standard (Air-STD). The N_2-STD was measured repeatedly with an average uncertainty on an individual $\delta^{15}N$ measurement being 0.03 ‰ (1σ) versus an average single day reproducibility of 0.38 ‰ (1σ). Additional refinements include (1) monitoring of interfering CO contributions at mass 30, allowing a comprehensive CO correction to be applied to all samples, (2) quantification of procedural N_2 blanks (n = 22) in both size (4.2 ± 0.5 μcm^3 STP) and isotopic composition ($\delta^{15}N$ = 12.64 ± 2.04 ‰), allowing consistent blank corrections to all samples, and (3) independent measurement of N_2/Ar ratios using a quadrupole mass spectrometer (QMS). The new system was tested by measuring nitrogen isotopes ($\delta^{15}N$), concentrations and N_2/Ar ratios on 11 submarine basalt glasses. Results show that the uncertainty on the $\delta^{15}N$ data is improved as a consequence of multiple standards being run per day. Reduced analytical times, afforded by triple collection, also minimize sample depletion and memory effects, thus improving measurement statistics. Additionally, we show that CO corrections can be accomplished using mass 30 to monitor CO interferences, leading to substantial improvements in reproducibility and the overall accuracy of results when the contribution of CO is significant.

2-3 Choi, Duck K., **Jusun Woo**, and **Tae-yoon Park**. 2012. “The Okcheon Supergroup in the Lake Chungju area, Korea: Neoproterozoic volcanic and glaciogenic sedimentary successions in a rift basin”. *Geosciences Journal,* 16(3): 229-252.
doi: 10.1007/s12303-012-0031-6

The Okcheon Belt in southern Korea is an NE-SW trending fold-and-thrust belt consisting of two sedimentary basins of different origins: namely, the Chungcheong Basin and the Taebaeksan Basin. The Chungcheong Basin was a Neoproterozoic rift basin belonging to the South China Craton, while the Taebaeksan Basin was a Paleozoic shallow marine to non-marine sedimentary basin fringing the Sino-Korean Craton. These two basins merged to form the Okcheon Belt in the early Triassic by the collision of Sino-Korean and South China cratons and their boundary is currently demarcated by the South Korean Tectonic Line. The Okcheon Supergroup is herein refined to include the Neoproterozoic volcanic and glaciogenic sedimentary successions deposited in the Chungcheong Basin and is divided into the two groups: the Chungju Group consists of the Gyemyeongsan Formation, Hyangsanni Dolomite, and Daehyangsan Quartzite and the Suanbo Group is proposed to include the Munjuri, Hwanggangni, Myeongori, and Gounni formations in ascending order. The Myeongori Formation is emended to comprise the Geumgang Limestone and the Seochangni members. This lithostratigraphic scheme is correlatable with that of the Nanhua Basin in South China, suggesting that the Chungcheong Basin was an eastward extension of the Nanhua Basin during the Neoproterozoic. The geological structure of the Okcheon Supergroup in the Lake Chungju area is characterized by a number of isoclinal to tight, frequently overturned, anticlines and synclines. No major thrust faults were recognized within the study area, except the constraining bend of the South Korean

Tectonic Line. Three deformational phases are empirically differentiated: D1 deformation most strongly affected the rocks of the Okcheon Supergroup; D2 deformation was produced by the collision between the Sino-Korean and South China cratons; and D3 deformation is represented by normal to strike-slip faults. D1, D2 and D3 deformational phases are referred to the Okcheon (mid-Paleozoic), Songnim (Triassic) and/or Daebo (Jurassic) orogenies, and post-Jurassic events, respectively. The Chungcheong Basin was initiated as a part of an intracratonic rift basin (Nanhua Basin) within the South China Craton in association with early Neoproterozoic break-up event of the supercontinent Rodinia. The bimodal volcanic succession of the Gyemyeongsan Formation corresponds to the initial rift episode of the Chungcheong Basin, and was succeeded by shallow marine Hyangsanni Dolomite and Daehyang an Quartzite. The second phase of rifting at ~750 Ma accumulated a thick bimodal volcanic succession of the Munjuri Formation which is overlain by the diamictites of the Hwanggangni Formation representing the Cryogenian global glacial event, snowball Earth. The immediately-succeeding cap carbonate, Geumgang Limestone Member of the Myeongori Formation, recorded the deglaciation event. The Seochangni Member of the Myeongori Formation is characterized by dark gray slate/phyllite facies indicating a poorly-oxygenated basin during the Ediacaran. No stratigraphic unit overlying the Gounni Formation, the youngest Neoproterozoic formation of the Okcheon Supergroup, occurs in the Lake Chungju area, and thus little is known on the Paleozoic tectonic evolution of the Chungcheong Basin. It is inferred that the medium-pressure type regional metamorphism and the predominance of ductile deformation of the Okcheon Supergroup can be attributed to the mid-Paleozoic Okcheon Orogeny which would have been in line with the Wuyun Orogeny of South China. The South China and Sino-Korean cratons should have been drifted away from the Gondwana sometime during the mid-Paleozoic and collided to form the East Asian continent at ~250 Ma.

2-4 **Choo, Mi Kyung**, **Mi Jung Lee**, **Jong Ik Lee**, and 2 others. 2012. “Geochemistry and Sr-Nd-Pb isotopic constraints on the petrogenesis of Cenozoic lavas from the Pali Aike and Morro Chico area (52°S), southern Patagonia, South America”. *Island Arc,* 21(4): 327-350. doi: 10.1111/iar.12002

Geochemical and isotopic analyses (Sr–Nd–Pb) of late Miocene to Quaternary plateau lavas from the Pali Aike and Morro Chico areas (52°S) were undertaken to constrain the melting processes and mantle sources that contributed to magma generation and the geodynamic evolution of southernmost Patagonia, South America. The Pali Aike and Morro Chico lavas are alkaline (Pali Aike, 45–49 wt.% SiO_2; 4.3–5.9 wt.% Na_2O+K_2O) and subalkaline (Morro Chico, 50.5–50.8 wt.% SiO_2; 4.0–4.4 wt.% Na_2O+K_2O), relatively primitive (Pali Aike, 9.5–13.7 wt.% MgO; Morro Chico, 7.6–8.8 wt.% MgO) mafic volcanic rocks that have typical intraplate ocean island basalt-like signatures. Incompatible trace element ratios and isotopic ratios of the Pali Aike and Morro Chico lavas differ from those of the majority of Neogene southern Patagonian slab window lavas in showing more enriched characteristics and are similar to high-μ (HIMU)-like basalts. The rare earth element (REE) modeling to constrain mantle melting percentages suggests that these lavas were produced by low degrees of partial melting (1.0–2.0% for Pali Aike lavas and about 2.6–2.7% for Morro Chico lavas) of a garnet lherzolite mantle source. The major systematic variations of Sr–Nd–Pb isotopes in southern Patagonian lavas are related to geographic location. The Pali Aike and Morro

Chico lavas from the southernmost part of Patagonia have lower $^{87}Sr/^{86}Sr$ and higher $^{143}Nd/^{144}Nd$ and $^{206}Pb/^{204}Pb$ ratios, relative to most of the southern Patagonian lavas erupted north of 49.5°S, pointing to a HIMU-like signature. An isotopically depleted and HIMU-like asthenospheric domain may have been the main source of magmas in the southernmost part of Patagonia (e.g. Pali Aike, Morro Chico, and Camusu Aike volcanic field), suggesting the presence of a major discontinuity in the isotopic composition of the asthenosphere in southern Patagonia. On the basis of geochemical and isotope data and the available geological and geotectonic reconstructions, a link between the HIMU asthenospheric mantle domain beneath southernmost Patagonia and the HIMU mega-province of the southwestern Pacific Ocean is proposed.

2-5 **Hahm, Doshik**, and 5 others. 2012. "An overview of the volatile systematics of the Lau Basin – Resolving the effects of source variation, magmatic degassing and crustal contamination". *Geochimica et Cosmochimica Acta,* 85: 88-113.
doi: 10.1016/j.gca.2012.02.007

The Lau Basin erupts lavas with a range of geochemical features reflecting a complex history of interaction involving different mantle sources. The Valu Fa Ridge (VFR) and Mangatolu Triple Junction (MTJ) region have lavas with arc-like characteristics, Niuafo'ou Island (NV), Peggy Ridge and Central and Eastern Lau Spreading Centers (PR, CLSC and ELSC) erupt mid-ocean ridge basalt (MORB)-like volcanics, whereas the Rochambeau Bank (RB) has features akin to ocean island basalt (OIB). To characterize the volatile systematics of these various regions, we report a comprehensive study of 39 submarine lavas from these various eruptive centers encompassing analyses of the noble gases (He, Ne, and Ar) and carbon (CO_2) – both isotopes and abundances – together with other major volatile phases (H_2O, S, Cl, and F). Helium isotope ratios of the NV, MTJ, CLSC, and ELSC are MORB-like for the most part except for differentiated lavas that tend to have lower, more radiogenic $^3He/^4He$ values. The RB has considerably higher $^3He/^4He$ ratios (up to 23 R_A in this work) which extend as far south as the PR. The influence of 'plume-like' sources in the RB is also apparent in Ne isotopes: RB samples follow a trend similar to Hawaiian basalts in 3-isotope neon space. However, RB lavas have lower $^{40}Ar/^{36}Ar$ (300–730) and higher [^{36}Ar] than CLSC and ELSC, suggesting greater air contamination. Elemental He/Ne ratios ($^3He/^{22}Ne_S$ and $^4He/^{21}Ne^*$ where S = solar and * = nucleogenic) are high throughout the Lau Basin and identify the Lau mantle as one of only two high $^3He/^4He$ provinces worldwide with such an enrichment of He relative to Ne. Magmatic CO_2 and $\delta^{13}C$ fall in the range 7–350 ppm and –28‰ to –6‰, respectively. RB lavas have less [CO_2] and slightly lower $\delta^{13}C$ than CLSC and ELSC. The lowest values are found among MTJ lavas. These lavas also have the highest [H_2O], [F], [Cl], and [S] whereas the PR, ELSC and CLSC have the lowest. RB has intermediate [H_2O]. We estimate primary [CO_2] in primary melts using [CO_2]–δ13C relationships, and find that RB lavas have higher [CO_2] (~935 ± 168 ppm) than ELSC/CLSC (638 ± 115 ppm). They also possess higher initial $\delta^{13}C$ values, consistent with observations at other hotspotrelated localities. However, there are no discernible differences in primary CO_2/Nb ratios between mantle sources characterized by high 3He/^{4}He and MORB-like ratios. On the other hand, reconstructed values are considerably higher than that envisaged for depleted MORB mantle based on olivine-hosted melt inclusions.

2-6 **Hong, Sang-bum**, **Soon-do Hur**, Sun-Mee Kim, Sungmin Hong, **Ji-woong Chung**, and 2 others. 2012. “Uncertainties of ionic species in snowpit samples determined with ion chromatography system”. *Analytical Science & Technology,* 25(6): 350-363.
doi: 10.5806/AST.2012.25.6.350

To determine ionic species in snowpit samples using ion chromatography system, we described the performance of ion chromatography(IC) system, cleaning method of bottle, and interference by filtering procedure. The limit of detection, reproducibilities, and accuracies determined with BCR®-408 were 0.01-0.26 μg/L, 0.4-17.4%, 4.5-12.0% for cations and 0.02-0.26 μg/L, 0.1-27.6%, 1.3-5.6% for anions, respectively. Lab blank test for sample bottle indicated that $CH_3CO_2^-$, HCO_2^-, and NH_4^+ can be easily contaminated in the lab environment. The positive interferences of NO_3^- were partly attributed to the cleaning method of bottle. The filtering of melted snow sample should be carefully applied because it can positively affect the concentration levels of some ionic species. Finally, this method was applied to measure ionic species in snowpit samples from the upward area near NEEM camp and the uncertainties of measurement data of F^- were also estimated.

2-7 Hong, Sungmin, **Tseren-Ochir Soyol-Erdene**, **Hee Jin Hwang**, **Sang Bum Hong**, **Soon Do Hur**, and Hidaeki Motoyama§. 2012. “Evidence of Global-Scale As, Mo, Sb, and Tl Atmospheric Pollution in the Antarctic Snow”. *Environmental Science and Technology,* 46: 11550-11557.
doi: 10.1021/es303086c

We report the first comprehensive and reliable time series for As, Mo, Sb, and Tl in the snowpack from Dome Fuji in the central East Antarctic Plateau. Our results show significant enrichment of these elements due to either anthropogenic activities or large volcanic eruptions during the past 50 years. With respect to the values reported from 1960 to 1964, we observed the maximum increases in crustal enrichment factors (EFs) for As (a factor of ~15), Mo (~4), Sb (~4), and Tl (~2) during the period between the 1970s and 1990s, reflecting the global dispersion of anthropogenic pollutants of these elements, even to the most remote areas on Earth. Such enrichments are likely related to emissions of trace elements from nonferrous metal smelting and fossil fuel combustion processes in South America, especially in Chile. A drastic decrease in the As concentration and its EF values was observed after the year 2000 in response to the introduction of environmental regulations in the 1990s to reduce As emissions from the copper industry, primarily in Chile. The observed decrease suggests that governmental regulations for pollution control are effective in reducing air pollution at both the regional and global level.

2-8 Jeon, Taehyeon, Ki Young Kim, **Yongcheol Park**, and Ik-Bum Kang. 2012. “S-wave Velocity Structure Beneath the KS31 Seismic Station in Wonju, Korea Using the Joint Inversion of Receiver Functions and Surface-wave Dispersion Curves and the H-κ Stacking Method”. *Geophysics and Geophysical Exploration*, 15(1): 8-15.

To estimate the S-wave velocity structure beneath the KS31 broad-band station in Wonju, Korea, we used H-κ stacking and joint inversion of receiver functions and surface-wave dispersion curves derived from 297 teleseismic events (Mw > 5.5) recorded during the period between 2002 and 2009. We thereby determined that the average depth to a nearly flat Moho is 32.4 ± 0.5 km within tens of kilometer radius of the seismic station. For the crust at this location, we estimate an average shear-wave velocity of

3.69 km/s and a ratio of P- to S-wave velocities, V_P/V_S, of 1.72 ± 0.04, as is typical for continental crust. A negative phase in the receiver functions at 1 s indicates the presence of a shearwave low velocity layer in a depth interval of 10 to 18 km in the upper crust beneath the KS31 station.

2-9 **Kang, Jung-Ho**, Min-Hee Son, **Soon Do Hur**, and 4 others. 2012. "Deposition of organochlorine pesticides into the surface snow of East Antarctica". *Science of the Total Environment,* 433: 290-295.
doi: 10.1016/j.scitotenv.2012.06.037

Organochlorine pesticides (OCPs) were measured in surface snow collected on a ~1400 km inland traverse beginning from the coastal regions of East Antarctica during the Japanese Antarctic Research Expedition (JARE) of 2007/2008. Of the 22 OCPs, α-hexachlorocyclohexane (HCH), γ-HCH, and hexachlorobenzene (HCB) were frequently detected in the snow with concentration ranges of 17.5–83.2, 33–137, and ND–182 pg L^{-1}, respectively. The most abundant pesticide was γ-HCH, with a mean concentration of 69.9 pg L^{-1}, followed by α-HCH, with an average concentration of 44.5 pg L^{-1}. The spatial variability of α-HCH and γ-HCH was narrow, and the concentrations of α-HCH and γ-HCH increased slightlywith increasing altitude along the traverse route. Dome Fuji, the highest altitude sampling point, had the highest γ-HCH concentrations in the snow. Backward air trajectory analysis showed that the air masses at the sampling sites came mainly from the Indian and Atlantic Oceans and over the Antarctic continent, indicating that the OCPs were subjected to long-range atmospheric transport and were deposited in the surface snow. Our data suggest that the snow of Antarctica contains low levels of OCPs.

2-10 Kim, Jin Cheul, Yong Il Lee, **Hyoun Soo Lim**, and SeongBok Yi. 2012. "Geochemistry of Quaternary sediments of the Jeongokri archaeological site, Korea: implications for provenance and palaeoenvironments during the Late Pleistocene". *Journal of Quaternary Science,* 27(3): 260-268.
doi: 10.1002/jqs.1540

The geochemical characteristics of an approximately 6-m-long sediment core collected from the Jeongokri archaeological site (Hantan River, Korea) were examined to determine the provenance of the sediments and to reconstruct the palaeoenvironment of the study area during the Late Pleistocene (200–127 ka). The core sediments were subdivided into two parts based on grain size: an upper (0–.380cm depth) and lower part (>380cm depth). The lower part was deposited primarily by fluvial processes during an interglacial period [marine isotope stage (MIS) 7]with warm and humid conditions. Conversely, the upper part was mainly deposited by aeolian processes during a cold and dry glacial period (MIS 6). Geochemical characteristics, represented by major, trace and rare earth element (REE) compositions, and textures of the Jeongokri core sediments show distinct differences between the upper and lower parts. The mineralogy and major, trace and REE compositions indicate that the influence of felsic source rocks (e.g. granite) was dominant in the lower sediments, which were derived from the Hantan River. In contrast, increased quartz content and the very fine and homogeneous grain size in the upper sediments indicate an aeolian origin. REE ratios and distribution patterns, and geochemical signatures indicate that these sediments were derived predominantly from Chinese loess deposits and partially from local sediments from the Korean Peninsula; the possible source area of the upper sediments is the northern part of the Yellow Sea basin. The Yellow Sea basin, having mixed geochemical signatures between Chinese loess and Korean-derived sediments, was exposed because of low sea levels during MIS 6. The exposed Yellow Sea basin was located in the path of winter-monsoon winds, which may have carried a great deal of airborne sediments from the basin to the Jeongokri area.

2-11 Kim, Kyu Han, Seungyeol Lee, Keisuke Nagao, Hirochika Sumino, Kyounghee Yang, and **Jong Ik Lee**. 2012. "He-Ar-H-O isotopic signatures in Au-Ag bearing ore fluids of the Sunshin epithermal gold-silver ore deposits, South Korea". *Chemical Geology,* 320-321: 128-139. doi: 10.1016/j.chemgeo.2012.05.027

Helium ($^{3}He/^{4}He$), argon ($^{40}Ar/^{36}Ar$) and oxygen ($^{18}O/^{16}O$) isotopic ratios in fluid inclusions trapped in quartz and pyrite from the Sunshin epithermal gold-silver ore deposits in South Korea were analyzed to investigate the magmatic contribution to ore forming fluids. Mantle helium with high $^{3}He/^{4}He$ ratios (up to $^{3}He/^{4}He \sim 9R_A$, where $R_A=1.4\times10^{-6}$ for air) were identified from fluid inclusions in auriferous quartz veins, which are characterized as low sulfidation (adularia-sericite) type. The ratios provide direct evidence of links between low sulfidation ore fluids in epithermal gold deposits and magma from a mantle source. Interestingly, the oxygen and hydrogen isotopic compositions of the ore fluids ($\delta^{18}O=-1.9$ to -6.6‰, $\delta D=-82$ to-100‰), calculated from ore quartz, indicate that meteoric waters were predominant during precipitation of the Au\Ag ore. Microthermometric measurements for fluid inclusions indicate relatively low temperatures (≤ 300℃) for the formation of the low sulfidation epithermal ore deposits.

2-12 **Kim, Sookwan** and **Jong Kuk Hong**. 2012. "Swell Noise Attenuation Using a Cascade of F-X Filter and Median Filter". *Geophysics and Geophysical Exploration,* 15(4): 199-208. doi: 10.7582/GGE.2012.15.4.199

High-amplitude swell noises (HASN) are very difficult to eliminate from the marine seismic data. In this paper, we applied F-X filter and median filter in order to suppress HASN. Test data have been acquired on the northern offshore of the South Shetland Islands in December, 2010. Parts of data have been contaminated by HASN caused by bad weather during the cruise. We applied F-X filter and median filter to test data with HASN. After F-X filtering, most of noncoherent noises and small-amplitude swell noises are eliminated effectively but HASN are still remained significantly. With median filter, HASN was suppressed better than F-X filter, however some of non-coherent noises are still remains. We applied a cascade of two filters and results show HASN and non-coherent noises are suppressed effectively. After the cascade of two filtering, it is possible to define reflection layers clearly on the velocity spectrum and to produce better stacked section with a good signal-to-noise ratio.

2-13 Lawver, L., **J. Lee**, **Y. Kim**, and F. Davey. 2012. "Flat-topped mounds in western Ross Sea: Carbonate mounds or subglacial volcanic features?". *Geosphere,* 8(3): 645-653. doi: 10.1130/GES00766.1

Detailed multibeam bathymetry data in the western Ross Sea, Antarctica, delineate a field of unusual flat-topped seafloor mounds located ~50 km west of Franklin Island and an arcuate zone of pockmarks to the northwest and west of Franklin Island. Sixteen mounds occur in an area about 30 km square at a depth of ~500 m, within the Terror Rift, the active extensional part of the Victoria Land Basin. The mounds tend to be circular in the east and linear in the west, with their steepest slope to the southeast, and shallowest slope to the northwest, consistent with erosion by northwest ice-sheet movement. The largest mound is ~4 km across and 100 m high. Five similar features were delineated to the south and east of Franklin Island at depths of 400–650 m. Seismic, gravity, and magnetic data indicate that the mounds are largely low-density , nonmagnetic bodies overlying a largely nondisrupted sedimentary section, but some mounds have an associated small (~50 nT), short-wavelength, normal or reversed magnetic anomaly, indicating a magnetic core to the mounds. Their proximity to inferred subsurface gas hydrates suggests they may be carbonate banks, but they also occur close to volcanic centers including Franklin Island. Our preferred interpretation is that they are of volcanic origin, erupted during a geomagnetic reversal and under a grounded ice sheet forming hyaloclastite edifices, previously unknown under the Ross Sea. The pockmarks range from 200 m to 500 m in diameter.

2-14 **Lee, Choon-Ki**, **Ki-Weon Seo**, and 3 others. 2012. “Ice velocity mapping of Ross Ice Shelf, Antarctica by matching surface undulations measured by ICESat laser altimetry”. *Remote Sensing of Environment,* 124: 251-258. doi: 10.1016/j.rse.2012.05.017

We present a novel method for estimating the surface horizontal velocity on ice shelves using laser altimetry data from the Ice Cloud and land Elevation Satellite (ICESat; 2003–2009). The method matches undulations measured at crossover points between successive campaigns. Elevation measurements are first relocated into a time-varying (moving) coordinate system using an initial velocity (e.g., from VELMAP), and then crossover height differences are minimized with an adjustment vector. Errors in geolocation of the ICESat tracks result in some error in the adjustment vectors, but these are small relative to the velocity adjustment for fast-moving ice shelves. We use the algorithm to estimate changes in the ice velocity of Ross Ice Shelf between an earlier mapping (from VELMAP) and the ICESat period. The new velocity field is compared with velocities from in situ measurements and satellite radar interferometry. The slowdown of 98 ± 34 m yr^{-1} (~23%) is observed in the ice shelf downstream of Whillans Ice Stream, and the deceleration rate is 3.1 ± 1.1 m yr^{-2} during last three decades. The method can be expanded to the simultaneous mapping of ice horizontal velocity, ice thickness change, and surface deformation for Antarctic ice shelves as well as a more accurate mapping using future ICESat-2 measurements.

2-15 **Lee, Choon-Ki**, Shin-Chan Han, Dieter Bilitza, and **Ki-Weon Seo**. 2012. “Global characteristics of the correlation and time lag between solar and ionospheric parameters in the 27-day period”. *Journal of Atmospheric and Solar-Terrestrial Physics,* 77: 219-224. doi: 10.1016/j.jastp.2012.01.010

The 27-day variations of topside ionosphere are investigated using the in situ electron density measurements from the CHAMP planar Langmuir probe and GRACE K-band ranging system. As the two satellite systems orbit at the altitudes of ~370 km and ~480 km, respectively, the satellite data sets are greatly valuable for examining the electron density variations in the vicinity of F2-peak. In a 27-day period, the electron density measurements from the satellites are in good agreements with the solar flux, except during the solar minimum period. The time delays are mostly 1–2 day and represent the hemispherical asymmetry. The globally-estimated spatial patterns of the correlation between solar flux and in situ satellite measurements show poor correlations in the (magnetic) equatorial region, which are not found from the ground measurements of vertically-integrated electron content. We suggest that the most plausible cause for the poor correlation is the vertical movement of ionization due to atmospheric dynamic process that is not controlled by the solar extreme ultraviolet radiation.

2-16 Lee, Dong-Chan, Jino Park, **Jusun Woo**, and 11 others. 2012. "Revised stratigraphy of the Xiazhen Formation (Upper Ordovician) at Zhuzhai, South China, based on palaeontological and lithological data". *Alcheringa,* 36: 1–20.
doi: 10.1080/03115518.2012.658724

Three exposures of the Upper Ordovician Xiazhen Formation at Zhuzhai, Yushan, Jiangxi Province, China are re-measured and described in detail. Comparison of palaeontological and lithological data from the exposures (designated sub-sections ZU1, ZU2 and ZU3) reveals that the sub-sections overlap stratigraphically. Nearly identical assemblages of trilobites and brachiopods occur in mudstones of ZU1 and ZU3, whereas a different assemblage occurs in those of ZU2. Identical coral species occur in the overlapped intervals of ZU1 and ZU2, and ZU1 and ZU3, respectively. In addition, a distinctive identical lithological succession consisting of brachiopod-bearing nodular limestone at the base to coral floatstone at the top is evident in the overlapped interval of ZU1 and ZU2; prism-cracked algal laminites are found in the same interval; and bioclastic limestone beds, which represent bioherms consisting mainly of corals and stromatoporoids, occur in both ZU1 and ZU3. A thrust fault system appears to be responsible for the repetition in the subsections, and the faulting was probably due to the major post-Ordovician structural movements exerted on the Zhe-Gan Platform of the Jiangnan Region of the South China Block.

2-17 Lee, Hyo Min, **Jong Ik Lee**, **Mi Jung Lee**, and 2 others. 2012. "The A-type Pirrit Hills Granite, West Antarctica: an example of magmatism associated with the Mesozoic break-up of the Gondwana supercontinent". *Geosciences Journal,* 16(4): 421-433.
doi: 10.1007/s12303-012-0041-4

The Mesozoic geology of West Antarctica is largely related with the break-up of the Gondwana supercontinent and offers a good example for understanding magmatism associated with the continental break-up process. West Antarctica can be divided into five crustal blocks with relatively thin crust. The blocks are separated by deep rift zones and have moved during the Mesozoic break-up of Gondwana. The Pirrit Hills granite occurs as an isolated pluton in the Ellsworth-Whitmore Mountains block, which is the center of five blocks in the present configuration. The granite consists of quartz, perthitic alkali feldspar, and plagioclase with minor amounts of interstitial biotite and muscovite. The granite is a highly homogeneous, strongly fractionated, and mildly peraluminous granite and belongs to A-type granites with A2-type characteristics, suggesting its generation in an anorogenic environment. The strong enrichment of HREE and significant negative Eu anomalies suggest that the granitic magma was produced by a small degree of partial melting of a garnet granulitic source in the unusually hot lower crust. A weighted mean $^{206}Pb/^{238}U$ age of zircons is 164.5 ± 2.3 Ma (MSWD = 1.3), which is 8 to 9 Mys younger than a former Rb-Sr whole rock age (173 ± 3 Ma), and corresponds to the first rifting stage of the break-up of Gondwana (at 165 Ma). We suggest this age to be the emplacement age of the Pirrit Hills granite. The A-type Pirrit Hills granite was emplaced in the Middle Jurassic accompanying crustal thinning due to the break-up of Gondwana.

2-18 **Lee, Jeonghoon**. 2012. "Development of Mathematical Model for Both Solute Transport in Snow and Isotopic Evolution of Snowmelt". *Journal of Soil and Groundwater Environment,* 17(5): 31-39.
doi: 10.7857/JSGE.2012.17.5.031

Chemical and isotopic variations of snowmelt provide important clues for understanding snowmelt processes and the timing and contribution of snowmelt to catchment or watershed in spring. The newly developed model includes a hydraulic exchange between mobile and immobile water (ω), and isotopic exchanges between both mobile water and ice (f_1) and immobile water and ice (f_2). Since the new model is based on the mobile-immobile water conceptualization, which is widely used for describing chemical tracer transport in snow, it allows simultaneous calculations of chemical as well as isotopic variations in snowpack discharge. We compare the model results with a study of solute transport and isotopic evolution of snowmelt in snow, using artificial rain-on-snow experiments with conservative anion (Br^-). These observations are used to test the newly developed model and to better understand physical processes in a seasonal snowpack where our model simulates the chemical and isotopic variations.

2-19 **Lee, Jeonghoon**. 2012. "Validations of a Numerical Model of Solute Transport in a Snowpack". *Economic and Environmental Geology,* 45(5): 525-533.

Snowmelt from seasonal snow covers can be significant in many environments of northern and alpine areas. Water flow and chemical transport resulting from snowmelt have been studied for an understanding of contributions to watersheds or catchments. A Mobile-Immobile water Model (MIM) was developed to describe the movement of ionic tracers through a snowpack by Lee *et al.* (2008a) and Lee *et al.* (2008b). To validate the model used in the studies, mass balance calculations of the model were conducted and comparisons were made between model results and analytical solutions in this work. Mass balance was calculated based on the fact that change in total mass within a snowpack with time is equal to sum of any change in the flux of water or ionic tracers into and out of the snowpack. Calculations of both water and ionic mass show almost perfect agreement between changes of two water and solute mass fluxes. Comparisons between model results and analytical solutions including wave velocity and effective saturation show almost perfect agreement.

2-20 Lee, Jung-Eun, Benjamin R. Lintner, J. David Neelin, Xianan Jiang, Pierre Gentine, C. Kevin Boyce, Joshua B. Fisher, J. Taylor Perron, Terence L. Kubar, **Jeonghoon Lee**, and John Worden. 2012. "Reduction of tropical land region precipitation variability via transpiration". *Geophysical Research Letters,* 39: L19704(1-6).
doi: 10.1029/2012GL053417

Tropical rainforests are known to exhibit low intraseasonal precipitation variability compared with oceanic areas with similar mean precipitation in observations and models. In the present study, the potential role of transpiration for this difference in precipitation variability is investigated using the National Center for Atmospheric Research (NCAR) atmospheric general circulation model. Comparing model results with and without transpiration shows that in the absence of transpiration, mean precipitation decreases as may be expected. However the incidence of both higher daily total column water and more intense precipitation increases without transpiration; consequently the variability of precipitation increases substantially. These results can be understood in terms of the complex interplay of local nearsurface and remote moist dynamical processes with both local positive (boundary-layer drying) and large-scale negative (increased large-scale convergence) feedbacks when transpiration is disabled in the model. It is also shown that surface turbulent fluxes over tropical rainforests are highly correlated with incoming solar energy but only weakly correlated with wind speed, possibly decoupling land precipitation from large-scale disturbances like the Madden-Julian Oscillation.

2-21 Lee, Seung-Gu, Hyomin Lee, Yoshihiro Asahara, **Mi-Jeong Lee**, **MiKyeong Choo**, and SeungRyeol Lee. 2012. “Ln-resin and HIBA Method for La-Ce and Sm-Nd Isotope Measurement”. *Journal of the Petrological Society of Korea,* 21(4): 431-439.

A column chemistry is the most useful tools for isolating the elements of interest in isotope geochemistry. Here we introduce the chemical experimental procedure for Sm, Nd, La and Ce separation such as Teflon powder or Ln-resin method using HDEHP of KIGAM, KBSI, KOPRI and α-HIBA(α-Hydroxy Isobutyric acid) method of Nagoya University, Japan. This technical report will provide an useful information in selecting the experiment method for rare earth element isotope system study such as Sm-Nd and La-Ce isotope system.

2-22 **Lee, Won Sang**, **Yongcheol Park**, **Sukyoung Yun**, **Ki-Weon Seo**, Tae-Gyu Yee, **Hanjin Choe**, **Ho Il Yoon**, and **Namyi Chae**. 2012. “Installation of Very Broadband Seismic Stations to Observe Seismic and Cryogenic Signals, Antarctica”. *Geophysics and Geophysical Exploration,* 15(3): 144-149. doi: 10.7582/GGE.2012.15.3.144

Korea Polar Research Institute (KOPRI) has successfully installed two autonomous very broadband threecomponent seismic stations at the King George Island (KGI), Antarctica, during the 24th KOPRI Antarctic Summer Expedition (2010 ~ 2011). The seismic observation system is originally designed by the Incorporated Research Institutions for Seismology Program for Array Seismic Studies of the Continental Lithosphere Instrument Center, which is fully compatible with the Polar Earth Observing Network seismic system. The installation is to achieve the following major goals: 1. Monitoring local earthquakes and icequakes in and around the KGI, 2. Validating the robustness of seismic system operation under harsh environment. For further intensive studies, we plan to move and install them adding a couple more stations at ice shelf system, e.g., Larsen Ice Shelf System, Antarctica, in 2013 to figure out ice dynamics and physical interaction between lithosphere and cryosphere. In this article, we evaluate seismic station performance and characteristics by examining ambient noise, and provide operational system information such as frequency response and State-Of-Health information.

2-23 Minami, Hirotsugu, Kazuya Tatsumi, Akihiro Hachikubo, Satoshi Yamashita, Hirotoshi Sakagami, Nobuo Takahashi, Hitoshi Shoji, **Young Keun Jin**, and 3 others. 2012. “Possible variation in methane flux caused by gas hydrate formation on the northeastern continental slope off Sakhalin Island, Russia”. *Geo-Marine Letters,* 32(5-6): 525-534. doi: 10.1007/s00367-012-0287-x

The Sakhalin Slope Gas Hydrate Project (SSGH) is an international collaborative effort by scientists from Japan, Korea, and Russia to investigate natural gas hydrates (GHs) that have accumulated on the continental slope off Sakhalin Island, Okhotsk Sea. From 2009 to 2011, field operations of the SSGH-09, -10, and -11 projects were conducted. GH-bearing and -free sediment cores were retrieved using steel hydro- and gravity corers. The concentrations of sulfate ions in sediment pore waters were measured to investigate sulfate concentration–depth profiles. Seventeen cores showed linear depth profiles of sulfate concentrations. In contrast, eight cores and two cores showend concave-up and -down profiles plausibly explained by sudden increase and decrease in methane flux from below, respectively, presumably caused by the formation of gas hydrate adjacent to the core sampling sites.

2-24 **Park, Tae-Yoon** and Duck K. Choi. 2012. “MIDDLE FURONGIAN (LATE CAMBRIAN) SHUMARDIIDS FROM THE SESONG FORMATION, TAEBAEK GROUP, KOREA”. *Journal of Paleontology,* 86(1): 51-59.

The trilobite family Shumardiidae is characterized by small size, lack of eyes, yoked librigenae, and a small number of thoracic segments. Here we report the successive occurrence of three middle Furongian shumardiid species from the Sesong Formation of Korea: *Elaphraella*? *taebaeksanensis* n. sp., *Elaphraella microforma*, and *Elaphraella nodus*. They appear to represent the oldest shumardiid morphology known so far. This genus lacks the anterolateral swellings on the glabella and has a conical glabella. Its yoked librigenae also encompass a comparatively wide genal field. *Elaphraella*? *taebaeksanensis* has a highly inflexed facial suture which may reflect the presence of small palpebral lobes. Taken together, the plesiomorphic morphology of the Shumardiidae can be summarized as having a conical glabella, small palpebral lobes, highly arched anterior cephalic margin, a wide librigenal field, and no anterolateral swellings on the glabella.

2-25 **Park, Tae-Yoon** and Duck K. Choi. 2012. “Recent achievements on the ontogenetic studiees of the trilobites from the Taebaek Group: contributinos to the phylogeny of trilobites”. *Journal of Paleontological Society of Korea,* 28(1-2): 1-9.

Despite the long history of research, trilobite classification has remained unstable, mainly due to the lack of understanding on the phylogeny of the Cambrian trilobites. The trilobite research in Korea was initiated by Kobayashi in the early twentieth century. During the nineties, the trilobite biostratigraphy of the Yeongwol Group were actively examined, and that of the Taebaek Group also has recently been studied as well. Notably, the discovery of silicified trilobite fauna from the Taebaek Group enables the trilobite research in the phylogenetic aspect. Recent ontogenetic studies on the three trilobite species, *Tsinania canens* (Walcott, 1905), *Asioptychaspis subglobosa* (Sun, 1924), and *Haniwa quadrata* Kobayashi, 1933 from the *Asioptychaspis Zone of the Furongian (late Cambrian) Hwajeol Formation*, suggested that the two synapomorphies of the Order Asaphida, the ventral median suture and the “asaphoid” protaspid morphology, evolved multiple times in the trilobite evolutionary history. Accordingly, some of the superfamilies included previously in the Order Asaphida were excluded from the order, and accordingly the concept of the Order Asaphida has become in need of emendation. The silicified trilobite faunas from the Cambro–Ordovician of the Taebaek Group, which are yet to be studied, are expected to provide more significant contributions to the trilobite classification in the future.

2-26 **Park, Tae-Yoon**, and 3 others. 2012. "OCCURRENCE OF THE ISOPOD *ARCHAEONISCUS COREAENSIS* NEW SPECIES FROM THE LOWER CRETACEOUS JINJU FORMATION, KOREA". *Journal of Paleontology,* 86(4): 626-640.
doi: 10.5061/dryad.898c4

The fossil isopod crustacean genus *Archaeoniscus* has been known to occur in England, France and Germany during the Upper Jurassic, and in Mexico and Egypt during the Lower Cretaceous. The morphology of this genus is unique in having dorsoventrally compressed body, the cephalon set deeply into the first pereionite, pleon as wide as pereion, and a broad semicircular pleotelson. These features have resulted in placing the classification of the genus in the monotypic family Archaeoniscidae. However, due to the lack of detailed morphological data, suprafamilial classification of this genus has remained unclear, as well as its ecology and lifestyle. Here we report *Archaeoniscus coreaensis* n. sp. from the Jinju Formation, Gyeongsang Basin, Korea. The occurrence of *Archaeoniscus* in the East Asia implies that the genus may have had a worldwide distribution. The Gyeongsang Basin was a Cretaceous backarc basin, which consists of exclusively non-marine sedimentary sequences. The occurrence of this genus, therefore, indicates that *Archaeoniscus* successfully adapted to a freshwater ecosystem as well. Detailed anatomy including antennulae, antennae, pereiopods, and uropods was observed from well-preserved multiple specimens, which allows better understanding of the morphology of *Archaeoniscus*. The axial structure in the posterior part of the body, which was previously interpreted as a unique brood pouch characterizing the family, turned out to be a remnant of the hindgut. Females of all isopods and most of the members of the superorder Peracarida have a thoracic ventral brood pouch, modified from the thoracic coxal endites. Based on the morphology of the largely unmodified ambulatory pereiopods of *A. coreaensis*, the possibility of *Archaeoniscus* being ectoparasitic is discounted. Instead, the flattened body and the form of limbs of *A. coreaensis* would have been suitable for a benthic lifestyle.

2-27 **Park, Tae-Yoon**, Jang Won Sohn, and Duck K. Choi. 2012. "Middle Furongian (late Cambrian) polymerid trilobites from the upper part of the Sesong Formation, Taebaeksan Basin, Korea". *Geosciences Journal,* 16(4): 381-398.
doi: 10.1007/s12303-012-0037-0

The upper part of the Sesong Formation of the Taebaek Group, Taebaeksan Basin, Korea, is known to contain the *Kaolishania* Zone which can be equated to the *Kaolishania* Zone of North China. Silicified trilobite sclerites were recovered from six horizons of the upper part of the Sesong Formation at the Sagundari section, which include a total of thirteen polymerid species: i.e., *Shirakiella elongata* Kobayashi, 1935, *Shirakiella* sp. 1, *Taishania*? sp. 1, *Acanthometopus* sp. 1, *Pagodia* sp. cf. *P. spina* Qian, 1994, *Kaolishania granulosa* Kobayashi, 1933, *Gumunsoia triangularis* gen. et sp. nov., *Gumunsoia* sp. 1, kaolishaniid genus and species indeterminate 1, *Elaphraella*? *taebaeksanensis* Park and Choi, 2012, *Elaphraella microforma* Lu and Qian, 1983, *Elaphraella nodus* (Qian, 1994), and *Lingyuanaspis* sp. The occurrence of *Kaolishania* suggests that the studied interval may be part of the *Kaolishania* Zone. However, *Kaolishania* occurs only from the lowermost horizon, and the full stratigraphic range of *Kaolishania* is unknown at present. Accordingly, the studied interval is provisionally called the *Kaolishania* fauna. The uppermost interval of this *Kaolishania* fauna produces *Acanthometopus* sp. 1, and thus can be correlated with the

Acanthometopus Zone in Northeast China, which is underlain by the *Kaolishania* Zone.

2-28 **Park, Yongcheol**, Kwang-Hee Kim, **Joohan Lee**, **Hyun Jae Yoo**, and Milton P. Plasencia L.. 2012. "*P*-wave velocity structure beneath the northern Antarctic Peninsula: evidence of a steeply subducting slab and a deep-rooted low-velocity anomaly beneath the central Bransfield Basin". *Geophysical Journal International,* 191(3): 915-926.
doi: 10.1111/j.1365-246X.2012.05684.x

Upper-mantle structure between 100 and 300 km depth below the northern Antarctic Peninsula is imaged by modelling *P*-wave traveltime residuals from teleseismic events recorded on the King Sejong Station (KSJ), the Argentinean/Italian stations (JUBA and ESPZ), an IRIS/GSN Station (PMSA) and the Seismic Experiment in Patagonia and Antarctica (SEPA) broadband stations. For measuring traveltime residuals, we applied a multichannel cross-correlation method and inverted for upper-mantle structure using VanDecar's method. The new 3-D velocity model reveals a subducted slab with a $\sim 70^{\circ}$ dip angle at 100–300 km depth and a strong low-velocity anomaly confined below the SE flank of the central Bransfield Basin. The low velocity is attributed to a thermal anomaly in the mantle that could be as large as 350–560 K and which is associated with high heat flow and volcanism in the central Bransfield Basin. The low-velocity zone imaged below the SE flank of the central Bransfield Basin does not extend under the northern Bransfield Basin, suggesting that the rifting process in that area likely involves different geodynamic processes.

2-29 Rauf, Naseem, S.S. Tahir, **Jung-Ho Kang**, and Yoon-Seok Chang. 2012. "Equilibrium, thermodynamics and kinetics studies for the removal of alpha and beta endosulfan by adsorption onto bentonite clay". *Chemical Engineering Journal,* 192: 369-376.
doi: 10.1016/j.cej.2012.03.047

Batch adsorption experiments were carried out for the sorption of alpha and beta endosulfan onto bentonite clay. The effect of various experimental parameters such as contact time, adsorbent dosage, initial endosulfan concentration, pH and temperature was investigated. The equilibrium endosulfan concentrations were measured with GC/ECD. The equilibrium data were fitted to Langmuir, Freundlich, Dubinin–Radushkevich (D–R) and Temkin isotherm models and the isotherm constants were calculated for alpha and beta endosulfan. Five error functions namely ERRSQ, HYBRID, MPSD, ARE and EABS were applied to the isothermal equilibrium data in order to know the best fit isotherm model for the system. Kinetic studies were also undertaken in terms of pseudo-first-order, pseudo-second-order and intra-particle diffusion rates for alpha and beta endosulfan onto bentonite. The values of the thermodynamic parameters, i.e. enthalpy change ($\triangle H^{o}$), entropy change ($\triangle S^{o}$) and free energy change ($\triangle G^{o}$) were computed from the Van't Hoff plot of ln K_D vs $1/T$.

2-30 **Seo, Ki-Weon**, Duane E. Waliser, Baijun Tian, **Baek-Min Kim**, and 4 others. 2012. "Evidence of the Recent Decade Change in Global Fresh Water Discharge and Evapotranspiration Revealed by Reanalysis and Satellite Observations". *Asia-Pacific Journal of Atmospheric Sciences,* 48(2): 153-158.
doi: 10.1007/s13143-012-0015-5

Variations of global evapotranspiration (*ET*) and fresh water discharge from land to oceans (*D*) are important components of global climate change, but have not been well monitored. In this study, we present an estimate of twenty years (1989 to 2008) variations of global *D* and *ET* derived from satellite remote-sensed measurements and recent reanalysis products, ERA-Interim and CFSR, by using a novel application of the water balance equations separately over land and over oceans. Time series of annual mean global *D* and *ET* from both satellite observations and reanalyses show clear positive and negative trends, respectively, as a result of modest increase of oceanic evaporation (*Eo*). The inter-annual variations of *D* are similar to the in-situ-based observations, and the negative trend of *ET* supports the previous result that relative humidity has decreased while temperature has increased on land. The results suggest considerable sensitivity of the terrestrial hydrological cycles (e.g. *D* and *ET*) to small changes in precipitation and oceanic evaporation.

2-31 Sobanska, Sophie, **HeeJin Hwang**, and 6 others. 2012. “Investigation of the Chemical Mixing State of Individual Asian Dust Particles by the Combined Use of Electron Probe X-ray Microanalysis and Raman Microspectrometry”. *Analytical Chemistry,* 84(7): 3145-3154. doi: 10.1021/ac2029584

In this work, quantitative electron probe X-ray microanalysis (EPMA) and Raman microspectrometry (RMS) were applied in combination for the first time to characterize the complex internal structure and physicochemical properties of the same ensemble of Asian dust particles. The analytical methodology to obtain the chemical composition, mixing state, and spatial distribution of chemical species within single particles through the combined use of the two techniques is described. Asian dust aerosol particles collected in Incheon, Korea, during a moderate dust storm event were examined to assess the applicability of the methodology to resolve internal mixtures within single particles. Among 92 individual analyzed particles, EPMA and RMS identified 53% of the particles to be internally mixed with two or more chemical species. Information on the spatial distribution of chemical compounds within internally mixed individual particles can be useful for deciphering the particle aging mechanisms and sources. This study demonstrates that the characterization of individual particles, including chemical speciation and mixing state analysis, can be performed more in detail using EPMA and RMS in combination than with the two single-particle techniques alone.

2-32 **Soyol-Erdene**, **Tseren-Ochir** and Youngsook Huh. 2012. “Dissolved platinum in major rivers of East Asia: Implications for the oceanic budget”. *Geochemistry Geophysics Geosystems,* 13(6): Q06009(1-13). doi: 10.1029/2012GC004102

Dissolved platinum concentrations of eleven large pristine river systems in East Asia (~200 samples) were determined to better constrain the oceanic platinum budget. Most samples had concentrations less than 1.4 pM; relatively high concentrations up to 5.8 pM were measured in only approximately 6% of the samples. The median Pt concentrations of the individual river systems had only a small range, from 0.18 pM (Duman) to 0.63 pM (Huang He), and the difference in Pt yield mainly resulted from the difference in runoff. The rivers draining the eastern Tibetan Plateau – the Salween, Mekong, Chang Jiang (Yangtze), Hong (Red), and Huang He (Yellow) – had higher Pt yield than the rivers of the Russian Far East – the Amur, Lena, Yana, Indigirka, and Kolyma. If the discharge-weighted mean Pt concentration of our samples (0.36 pM) is extrapolated globally, the estimated riverine flux of dissolved Pt to the ocean is 13 x 10^3 mol y^{-1}. Based on this riverine flux, the estimated oceanic residence time of Pt is 24 ± 10 kyrs.

A 50% release and 50% uptake of Pt in estuaries would modify this to 16 kyrs and 45 kyrs, respectively.

2-33 Yang, Junmo, **Choon-Ki Lee**, and 3 others. 2012. “1-D crustal resistivity structure revealed by sea effect corrected magnetotelluric (MT) data obtained at Jeju Island, Korea”. *Journal of Applied Geophysics,* 76: 92-101.
doi: 10.1016/j.jappgeo.2011.10.011

Jeju Island, a volcanic island in South Korea, has been one of the main targets of geophysical and/or geological studies because of its tectonic importance associated with the volcanism and tectonic link to the southern Korean Peninsula. In this study, we reinterpret deep structures of Jeju Island based on the 1-D inversion results for the sea effect corrected MT data. Among 108MT sites, we select 11MT sites, which are uniformly spread out across the island and have good quality data for frequencies ranging from 10^3 to 10^{-3} Hz to examine the 1-D deep structures. The sea effect correction makes remarkable changes in the observed MT data at frequencies below about 1 Hz, playing an important role in revealing the deep structure. The 1-D resistivitymodels obtained from sea effect corrected MT data are greatly similar to one another, commonly showing the discontinuity at a depth of 18 km on average. This discontinuity can be interpreted as the transition zone separating resistive upper crust and conductive lower crust. This interpretation is consistent with the geophysical interpretations made for the southern part of the Peninsula which seems to be tectonically linked to Jeju Island. Reversely, this agreement can be the evidence supporting that Jeju Island is the extension of the Korean Peninsula. Considering the tectonic environment and formation process of Jeju Island, it is noted that the low resistivity of the continental lower crust (CLC) beneath the island can be explained by the interconnected saline fluids which are associated with metamorphic and/or magmatic activity forming the island. All the results convince us that the newly built 1-D model for Jeju Island matches other geophysical and geological evidences.

2-34 Yun, Sang Woong, **Hyoun Soo Lim**, Youngyun Park, Hyun-Mi Choi, Jin-Yong Lee, and **Ho Il Yoon**. 2012. “Analysis of fracture system and meltwater flow in glaciers around the King Sejong Station, West Antarctica”. *Journal of the Geological Society of Korea,* 48(2): 201-208.

PART 3

Ocean Environment Sciences

3-1 Choi, Keun-Hyung, **Eun Jin Yang**, and 4 others. 2012. “The influence of coastal waters on distributions of heterotrophic protists in the northern East China Sea, and the impact of protist grazing on phytoplankton”. *Journal of Plankton Research,* 34(10): 886-904.
doi: 10.1093/plankt/fbs046

Spatial and temporal variations in the abundance and biomass of heterotrophic protists and of their grazing impact were investigated during five cruises between July 2006 and February 2009 in the continental shelf waters of the northern East China Sea (ECS). Strongly patchy distributions were observed on all cruises, generally with a higher biomass in the western areas affected by the Changjiang River discharge. An opposite pattern was observed in February when the Kuroshio onshore transport is greatest, with a greater biomass in the eastern area. Small heterotrophic dinoflagellates (< 20 μm) were most abundant numerically, whereas ciliates contributed the most to the biomass, accounting for 28–58% of the total heterotrophic protist biomass. Small heterotrophic dinoflagellates were more strongly correlated with phytoplankton biomass than were other types of protists. The total protist biomass was often most strongly related to amounts of particulate organic carbon of non-phytoplankton origin, suggesting that their abundance distribution often depended on prey other than phytoplankton, such as heterotrophic bacteria. Heterotrophic protists consumed 30.1–91.5% of Chl a production (mean 68.2%), with grazing rates increasing with the phytoplankton biomass. The results suggest that heterotrophic protists were the major consumers of primary production, and that their grazing is one of the most important losses affecting the phytoplankton biomass in the northern ECS.

3-2 Dolan, John R., Richard W. Pierce, **Eun Jin Yang**, and Sun Young Kim. 2012. “Southern Ocean Biogeography of Tintinnid Ciliates of the Marine Plankton”. *Journal of Eukaryotic Microbiology,* 59(6): 511-519.
doi: 10.1111/j.1550-7408.2012.00646.x

Ciliate microzooplankton are important grazers in most pelagic ecosystems and among them, tintinnids, with their largely species-specific loricas, allow relatively easy assessment of questions of diversity and distributions. Herein, we present the results of a survey of species records of tintinnids from the Southern Ocean (locations below 40°S) reported in 56 publications yielding 2,047 species records (synonyms included) from 402 locations. The 192 species reported can be parsed into two main groups: 32 endemic Southern Ocean species, known only from 40°S and further south, and a second group of 181 widespread species, forms with extensive geographic ranges extending into the Southern Ocean. Widespread species reported from the Southern Ocean can be further divided into a group of 81 species, each recorded multiple times in the Southern Ocean waters and 70 apparent “stray” species which have only been found but once. The endemic and widespread species of the Southern Ocean show both distinct distributional patterns and morphological differences. The assemblage of Southern Ocean endemics is found mostly within the Antarctic zone delimited by the average location of the Polar Front and contains a relatively large portion of wide-mouthed forms. We give suggestions for future study.

3-3 **Ha, Ho Kyung** and Kyeong Park. 2012. “High-resolution comparison of sediment dynamics under different forcing conditions in the bottom boundary layer of a shallow, micro-tidal estuary”. *Journal of Geophysical Research,* 117: C06020(1-14).
doi: 10.1029/2012JC007878

Data for high-resolution profiles of current velocity and suspended sediment concentration (SSC) were collected in bottom boundary layer (BBL) of Mobile Bay, Alabama. The data were used to study the vertical and temporal variability in SSC under various forcing conditions of tide, wind and freshwater discharge. During the winter stormy season, the background SSC was low (0.015–0.03 $g\ell^{-1}$). An episodic storm-induced erosion/resuspension was responsible for the short-lasting high SSC in BBL. During the spring flooding period, the background SSC was relatively high (0.04–0.07 $g\ell^{-1}$) likely due to the large amount of suspended sediment from the fluvial input and bed softening, and the contribution of wind forcing to sediment resuspension was somewhat enhanced by the destratification in BBL. When the freshwater discharge was extremely high (>5000 $m^3\ s^{-1}$), the entire water column in shallow areas of the Bay was influenced by freshwater input. Therefore, the thermohaline anomaly’s contribution to the stratification considerably weakened, while the SSC’s contribution strengthened. When the freshwater discharge was relatively low (<5000 $m^3 s^{-1}$), a critical wind stress for sediment erosion (0.08–0.1 Pa) was observed to abruptly increase the SSC. Despite a micro-tidal regime, Mobile Bay exhibited the cyclic erosion and deposition pattern induced by the tidal acceleration and deceleration.

3-4 Kim, Dongseon, **Eun Jin Yang**, Kyung Hee Kim, Chang-Woong Shin, **Jisoo Park**, and 2 others. 2012. "Impact of an anticyclonic eddy on the summer nutrient and chlorophyll a distributions in the Ulleung Basin, East Sea (Japan Sea)". *ICES Journal of Marine Science,* 69(1): 23-29.
doi: 10.1093/icesjms/fsr178

The impact of the anticyclonic Ulleung Warm Eddy (UWE) on the vertical distributions of nutrient and chlorophyll *a* (Chl *a*) concentrations in the Ulleung Basin (UB) was investigated during the contrasting summers of 2005 and 2007. The physical structure of the water column was characterized by an intrathermocline eddy (ITE) in 2005, whereas the UWE remained distant from the sampling transect in 2007. Water column structures appeared to be highly stratified, and nutrients in the surface waters were totally depleted at all stations. In 2005, an exceptionally high concentration of Chl *a* (5.5 mg m^{-3}) was measured below the surface mixed layer in the eddy core (station D3), and values of ~2.5 mg m^{-3} were observed at the eddy edge (stations D2 and D4). Formation of an ITE efficiently mixed surface and deep-ocean waters, the latter supplying sufficient nutrients to generate an extremely high concentration of Chl *a* at the base of the subsurface layer. Overall, the results indicated that the anticyclonic UWE plays a key ecological role in supporting substantial phytoplankton biomass in the nutrient-depleted surface waters in summer and maintaining high benthic mineralization in the deep-sea sediments of the UB.

3-5 **Kim, So-Young**, and 2 others. 2012. "Dinoflagellate cyst assemblages from the northern shelf sediments of the East China Sea: An indicator of marine productivity". *Marine Micropaleontology,* 96-97: 75-83.
doi: 10.1016/j.marmicro.2012.09.003

The dinoflagellate cyst assemblages from the northern shelf of the East China Sea were examined to assess their potential use as indicators of marine productivity in shelf environments. A characteristic disparity in the species compositions of dinoflagellate cysts between coastal sediments and outer-shelf sediments was observed. Coastal areas affected by fluvial freshwater input adjacent to the Changjiang River mouth were dominated by protoperidinioid species, whereas open sea shelf areas were dominated by gonyaulacoid species. The rarity of protoperidinioid cysts in the shelf sediment is primarily attributable to the deficit of silicate in the waters overlying the northern East China Sea shelf, associated with low supplies of suspended particulate matter from the adjacent continent. This would limit the growth of the protoperidinioid species, which feed on diatoms. In contrast, a constant supply of nitrogen generated by microbial nitrogen fixation appeared to have played an important role in supporting the production of gonyaulacoid species in this shelf region. Thus it was determined that dinoflagellate cyst assemblages in marine sediments are closely linked to significant changes in nutrient composition, leading to a selective advantage for the growth of favored taxa. This result suggests that gonyaulacoid dinoflagellate cysts are a potentially useful proxy indicator for low nutrient concentration levels, especially of silicate, in the shelf environment.

3-6 Kim, Young-Ok, Kyoungsoon Shin, Pung-Guk Jang, Hyun-Woo Choi, Jae-Hoon Noh, **Eun-Jin Yang**, and 2 others. 2012. "Tintinnid Species as Biological Indicators for Monitoring Intrusion of the Warm Oceanic Waters into Korean Coastal Waters". *Ocean Science Journal,* 47(3): 161-172.
doi: 10.1007/s12601-012-0016-4

This study examined seasonal and annual occurrences of warm oceanic tintinnid species in southern Korea coastal waters. The indicative species of tintinnids was monitored using three approaches: monitoring from cruises traveling from the warm pool in the western North Pacific to the Korea Strait; biweekly or monthly monitoring in the Korea Strait; and daily monitoring in the nearshore water. Annual pulses of warm oceanic indicator species were regularly observed in the Korea Strait. In September 2008 recorded a maximum species number of warm water indicators, a representative species for warm oceanic waters, *Climacocylis scalaroides* was simultaneously detected in the nearshore water as well as the Korea Strait. The result indicates that the greater warm water extension into Korean coastal areas was in September 2008. Sharp declines in species diversity were observed in the transitional area between neritic and Kuroshio zone in East China Sea (ECS). *Epiplocyloides reticulata*, reported previously as a Kuroshio indicator, was considered an ECS indicator species, as it was undetected in the western North Pacific central zone but was found abundantly in the ECS. Tintinnid species can be used as biological indicators to detect the inflow of warm oceanic waters into Korean coastal waters.

3-7 Kim, Yun-Jung, **Hyun-Cheol Kim**, and 5 others. 2012. "Verification of CDOM Algorithms Based on Ocean Color Remote Sensing Data in the East Sea". *Korean Journal of Remote Sensing,* 28(4): 421-434.
doi: 10.7780/kjrs.2012.28.4.6

Colored Dissolved Organic Matter (CDOM) is one of the important components of optical properties of seawater to determine ecosystem dynamics in a given marine area. The optical characteristics of CDOM may depend on the various ecosystem and environmental variables in the sea and those variables may vary region to region. Therefore, the retrieval algorithm for determining light absorption coefficient of CDOM (a_{CDOM}) using satellite remote sensing reflectance (R_{rs}) developed from other region may not be directly applicable to the other region, and it must be validated using an *in-situ* ground-truth observation. We have tested 6 known CDOM algorithms (three Semi-analytical and three Empirical CDOM algorithms) developed from other regions of the world ocean with laboratory determined in-situ values for the East Sea using field data collected during seven oceanographic cruises in the period of 2009~2011. Our field measurements extended from the coastal waters to the open oceanic type CASE-1 Waters. Our study showed that Quasi-Analytical Algorithm (QAA_v5) derived $a_{CDOM}(412)$ appears to match in-situ $a_{CDOM}(412)$ values statistically. Semi-analytical algorithms appeared to underestimate and empirical ones overestimated aCDOM in the East Sea. $a_{CDOM}(412)$ value was found to be relatively high in the relatively high satellite derived-chlorophyll-a area. $a_{CDOM}(412)$ value appears to be influenced by the amount of chlorophyll-a in seawater. The outcome of this work may be referenced to develop aCDOM algorithm for the new Korean Geostationary Ocean Color Imager (GOCI).

3-8 Lee, Chang-Rae, Keun-Hyung Choi, Hyung-Ku Kang, **Eun Jin Yang**, and 2 others. 2012. "Biomass and trophic structure of the plankton community in subtropical and temperate waters of the northwestern Pacific Ocean". *Journal of Oceanography,* 68: 473-482. doi: 10.1007/s10872-012-0111-2

This study examined the biomass structure of autotrophic and heterotrophic plankton along a trophic gradient in the northwestern Pacific Ocean in an attempt to understand planktonic food web structure. Autotrophic biomass exceeded that of heterotrophic organisms in all sampling regions, but with lesser contribution to total planktonic biomass at stations of higher phytoplankton biomass, including the northern East China Sea, compared to the regions of lower phytoplankton biomass. The proportion of the biomass of heterotrophic bacteria, nanoflagellates (HNF), and dinoflagellates (HDF) relative to that of phytoplankton was all inversely related to phytoplankton biomass, but positive relationships were observed for both ciliates and mesozooplankton. Mesozooplankton biomass inclined greater than phytoplankton along the gradient of phytoplankton biomass, with biomass rise being most closely associated with ciliate and HDF biomass and, to a lesser degree, with large phytoplankton (>3 µm). Both bacteria and picophytoplankton were significantly and positively related to the biomass ratio of mesozooplankton to the sum of HDF and ciliates (i.e., proxy of mesozooplankton predation on protozoans), but no positive relationship was apparent either for HNF or for large phytoplankton. Such relationships may result from predation relief on lower food webs associated with mesozooplankton feeding on protistan plankton.

3-9 **Lee, Doo B.**, and 3 others. 2012. "Copepod feeding in a coastal area of active tidal mixing: diel and monthly variations of grazing impacts on phytoplankton biomass". *Marine Ecology,* 33: 88-105. doi: 10.1111/j.1439-0485.2011.00453.x

This study examined monthly feeding rates and grazing impact on phytoplankton biomass, as well as diel feeding rhythms of four key copepod species in a tidally well mixed estuary (Asan Bay, Korean Peninsula). Monthly ingestion rates estimated based on gut pigment analysis were closely associated with their peak densities, but not with phytoplankton biomass, implying high ingestion may be related to reproductive output for population growth. The three smaller copepods, *Acartia hongi*, *Acartia pacifica* and *Paracalanus parvus*, showed feeding preference for smaller phytoplankton (<20 µm) with higher clearance rates, whereas the larger *Calanus sinicus* preferred larger phytoplankton. *Acartia pacifica* and *P. parvus* showed distinct increased nocturnal feeding rates as measured with gut fluorescence, whereas *A. hongi* showed no significant day–night differences. Copepod diel feeding patterns were not associated with food quantity, and endogenous physiological rhythm might be hypothesized as responsible for the observed diel feeding patterns. Grazing impact on phytoplankton biomass by the four copepods in the estuary was on average 8% (range 0.2–29.8%) of the phytoplankton standing stock, similar to values reported in other coastal waters. Very high copepod abundances but low daily carbon ration (<20% for all copepods) provided by feeding on phytoplankton indicate that copepods also grazed on other non-phytoplankton foods in Asan Bay.

3-10 Lee, Sang H., Dean A. Stockwell, **Hyoung-Min Joo**, and 3 others. 2012. "Phytoplankton production from melting ponds on Arctic sea ice". *Journal of Geophysical Research,* 117: C04030(1-11). doi: 10.1029/2011JC007717

Recently, the areal extent of melt ponds within sea ice has rapidly increased during the Arctic Ocean summer. However, the biological impacts of melt ponds on the Arctic marine ecosystem have rarely been studied. Carbon and nitrogen uptake rates of phytoplankton were measured at 26 different melt ponds in 2005 and 2008, using a ^{13}C-^{15}N dual stable isotope tracer technique. Generally, the open ponds had relatively higher nutrients than closed ponds, but the nutrient concentrations in the open ponds were within a range similar to those in surrounding surface seawaters. Chlorophyll *a* (Chl *a*) concentrations in melt ponds ranged from 0.1 to 2.9 mg Chl *a* m^{-3} with a mean of 0.6 mg Chl *a* m^{-3} (SD = 0.8 mg Chl *a* m^{-3}) in the Canada Basin in 2005, whereas the range of the Chl *a* concentrations was from 0.1 to 0.3 mg Chl *a* m^{-3} with a mean of 0.2 mg Chl α m^{-3} (SD = 0.1 mg Chl *a* m^{-3}) in the central Arctic Ocean in 2008. The average annual carbon production in sea ice melt ponds was 0.67 g C m^{-3} (SD = 1.03 g C m^{-3}) in the Arctic Ocean. Based on this study, recent annual carbon production of all melt ponds was roughly estimated to be approximately 2.6 Tg C, which is less than 1% of the total production in the Arctic Ocean.

3-11 Lee, Sang Heon, Bo Kyung Kim, Mi Sun Yun, HuiTae Joo, **Eun Jin Yang**, Young Nam Kim, **Hyoung Chul Shin**, and **SangHoon Lee**. 2012. “Spatial distribution of phytoplankton productivity in the Amundsen Sea, Antarctica”. *Polar Biology,* 35(11): 1721-1733. doi: 10.1007/s00300-012-1220-5

To date, no direct measurements of primary production were taken in the Amundsen Sea, which is one of the highest primary productivity regions in the Antarctic. Phytoplankton carbon and nitrogen uptake experiments were conducted at 16 selected stations using a ^{13}C–^{15}N dual isotope tracer technique. We found no statistically significant depletions of major inorganic nutrients (nitrate + nitrite, ammonium, and silicate) although the concentrations of these nutrients were markedly reduced in the surface layer of the polynya stations where large celled phytoplankton (>20μm) predominated (ca. 64 %). The average chl-*a* concentration was significantly higher at polynya stations than at non-polynya stations (p<0.01). Average daily carbon and nitrogen uptake rates by phytoplankton at polynya stations were 2.2 g C m^{-2} day^{-1} (SD = ±1.4 g C m^{-2} day^{-1}) and 0.9 g N m^{-2} day^{-1} (SD = ±0.2 g N m^{-2} day^{-1}), respectively, about 5–10 times higher than those at non-polynya stations. These ranges are as high as those in the Ross Sea, which has the highest productivity among polynyas in the Antarctic Ocean. The unique productivity patterns in the Amundsen Sea are likely due to differences in iron limitation, phytoplankton productivity, the timing of phytoplankton growing season, or a combination of these factors.

3-12 Park, Jeong Soo, **In-Young Ahn**, and Eun Ju Lee. 2012. “Influence of soil properties on the distribution of *Deschampsia antarctica* on King George Island, Maritime Antarctica”. *Polar Biology,* 35(11): 1703-1711. doi: 10.1007/s00300-012-1213-4

The extremely cold and infertile Antarctic is one of the harshest terrestrial ecosystems for the growth of vegetation, except for the grass species *Deschampsia antarctica*. We examined the main soil variables that determine the distribution of *D. antarctica* in King George Island by using Bayesian analysis of variance and regression methods. This study compared the density of *D. antarctica* between 2 sites; the density remained relatively stable at site 1, whereas it severely decreased in site 2 over a period of 3 years. Although site 2 showed better soil conditions for the growth of *D. antarctica* such as organic matter content, available phosphorus, NO_3-N, and extractable cations, its poor drainage and low soil pH may affected the survival of *D. antarctica* by altering nutrition availability and inhibiting root respiration. Poisson analysis of covariance showed that the early melting of snow was also an important factor in the distribution of *D. antarctica*. The results also showed that seabirds and mammals might have greatly influenced the distribution of the grass species in King George Island by transferring nutrients from the sea onto land; thus, changing the chemical characteristics of the soil.

3-13 Shaha, Dinesh Chandra, Yang-Ki Cho, **Tae-Wan Kim**, and 2 others. 2012. "Spatio-Temporal Variation of Flushing Time in the Sumjin River Estuary". *Terrestrial, Atmospheric and Oceanic Sciences,* 23(1): 119-130.
doi: 10.3319/TAO.2011.08.22.01(Hy)

Flushing is a very complicated process in estuarine environments. In order to examine the effects of tidal amplitude, river discharge, and stratification on the spatially varying flushing time of the Sumjin River Estuary (SRE), 24 longitudinal salinity transects were obtained during spring and neap tides from August 2004 to April 2007. The widely accepted freshwater fraction method has been used to calculate the flushing time for multiple estuarine segments using a spatially varying freshwater fraction. The effects of tidal amplitude, river discharge, and stratification on estuarine flushing were identified reasonably well by the spatially varying time scale. The flushing time appears to be close to the semidiurnal (M_2) tidal period during spring tide, but it is twice as long during a neap tide near the mouth. The flushing time increases in the central regions with a decrease in the tidal amplitudes and reduces in the inner-most regions owing to the strong influence of gravitational circulation. A linear function negatively relates estuarine flushing to the tidal amplitudes near the mouth of the estuary, whereas a power-law function relates estuarine flushing to the freshwater inflow near the head. In addition, strong stratification induced by freshwater discharge and small tidal amplitude exerts dominant control to reduce the estuarine flushing in the central and upper regions of the estuary during a neap tide.

3-14 Wåhlin, A. K., R. D. Muench, L. Arneborg, G. Björk, **H. K. Ha**, **S. H. Lee**, and H. Alsén. 2012. "Some Implications of Ekman Layer Dynamics for Cross-Shelf Exchange in the Amundsen Sea". *Journal of Physical Oceanography,* 42(1): 1461-1474.
doi: 10.1175/JPO-D-11-041.1

The exchange of warm, salty seawater across the continental shelves off West Antarctica leads to subsurface glacial melting at the interface between the ocean and the West Antarctic Ice Sheet. One mechanism that contributes to the cross-shelf transport is Ekman transport induced by along-slope currents over the slope and shelf break. An investigation of this process is applied to the Amundsen Sea shelfbreak region, using recently acquired and historical field data to guide the analyses. Along-slope currents were observed at transects across the eastern and western reaches of the Amundsen slope. Currents in the east flowed eastward, and currents farther west flowed westward. Under the eastward-flowing currents, hydrographie isolines sloped upward paralleling the seabed. In this layer, declining buoyancy forces rather than friction were bringing the velocity to zero at the seabed. The basin water in the eastern part of the shelf was dominated by water originating from 800-1000-m depth off shelf, suggesting that transport of such water across the shelf frequently occurs. The authors show that arrested Ekman layers mechanism can supply deep water to the shelf break in the eastern section, where it has access to the shelf. Because no unmodified off-shelf water was found on the shelf in the western part, bottom layer Ekman transport does not appear a likely mechanism for delivery of warm deep water to the western shelf area. Warming of the warm bottom water was most pronounced on the western shelf, where the deep-water temperature increased by 0.6℃ during the past decade.

3-15 Yamaguchi, Hisashi, **Hyun-Cheol Kim**, and 5 others. 2012. “Seasonal and summer interannual variations of SeaWiFS chlorophyll a in the Yellow Sea and East China Sea”. *Progress in Oceanography,* 105: 22-29.
doi: 10.1016/j.pocean.2012.04.004

Seasonal variability in satellite chlorophyll a concentrations (SCHL) in the Yellow Sea and the East China Sea (YECS) was investigated using 10-year averages of monthly data collected between September 1997 and October 2006. Interannual variations were also assessed to help clarify the influence of Changjiang River discharge (CRD) during summer. The YECS was represented by 12 areas each with different seasonal variability in SCHL. SCHL were overestimated during winter due to re-suspension of sediment near the Changjiang Bank and near coastal areas. Increases of SCHL were observed over large areas of the YECS during spring, as would be expected with the occurrence of spring blooms. The spatial distribution of the summer maximum of SCHL shifted from the Changjiang River mouth to just east of Jeju Island from July to September. An eastward shift of the high SCHL water coincided with the movement of the Changjiang diluted water (CDW), taking approximately 2 months to move from Changjiang River mouth to Jeju Island. Summer SCHL between 1998 and 2006 in this region were positively correlated with CRD with a time lag of 0–2 months, suggesting that the interannual variation of SCHL was controlled by the interannual variation of CRD. SCHL during summer in the Yellow Sea gradually increased over the 10 years, indicating possible eutrophication.

3-16 **Yang, Eun Jin**, Jung-Ho Hyun, Dongseon Kim, **Jisoo Park**, **Sung-Ho Kang**, **Hyoung Chul Shin**, and **SangHoon Lee**. 2012. “Mesoscale distribution of protozooplankton communities and their herbivory in the western Scotia Sea of the Southern Ocean during the austral spring”. *Journal of Experimental Marine Biology and Ecology,* 428: 5-15.
doi: 10.1016/j.jembe.2012.05.018

The distribution and structure of protozooplankton communities and the impact of their grazing on phytoplankton during spring were studied as part of the 15th Korean Antarctic Research Program in the western Scotia Sea. Water mass identities were determined based on physicochemical properties, with four regions identified: north of the Polar Front (NPF), Polar Front (PF), South of the Polar Front (SPF), and the South Antarctic Circumpolar Current region (SACCr). Physicochemical characteristics of the water column significantly influenced the distribution and structure of phytoplankton and protozooplankton communities. The NPF was characterized by relatively warmer water, low nutrient, low chlorophyll *a* (chl*a*), and pico-sized phytoplankton predominance (i.e., cyanobacteria and eukaryotic picoflagellates). Nano-sized phytoplankton such as *Phaeocystis antarctica* and *Cryptomonas* sp. dominated in the SACCr with its colder water, higher nutrient, and higher chl*a* concentrations. Despite the relatively slightly high chl*a* concentration in the PF, microsized phytoplankton, especially diatoms, were abundant. Large changes in protozooplankton biomass and community were observed between water masses. Heterotrophic nanoflagellates including choanoflagellates and nanociliates declined in abundance from the NPF to SACCr, whereas heterotrophic dinoflagellates (HDF) and microciliates increased in abundance from the NPF to SACCr. Ciliates declined in importance from the NPF to SACCr, accounting for over 50% of the total protozooplankton biomass in the NPF. In contrast, HDF comprised over 50% of the total in the SPF, PF, and SACCr. The depth-integrated protozooplankton biomass ranged from 443.2 to 934.0 mg C m^{-2}, and was highest in the PF and lowest in the NPF. These relationships suggest that the spatial variation in the community and biomass of protozooplankton appears to be primarily governed by the community and size structure of phytoplankton. Protozooplankton consumed an average of 76.9% of daily phytoplankton production. Therefore, protozooplankton were the major consumers of the diverse phytoplankton community, and protozooplankton grazing is one of the most important loss processes affecting phytoplankton biomass and composition during spring in the western Scotia Sea.

PART 4

Life Sciences

4-1 Ahn, Joon-Woo, Kwon Hwangbo, **Soo Young Lee**, **Han-Gu Choi**, and 3 others. 2012. “A new Arctic Chlorella species for biodiesel production”. *Bioresource Technology,* 125(4): 340–343.
doi: 10.1016/j.biortech.2012.09.026

Microalgae are a potential resource for biodiesel production. A green alga, *Chlorella* sp., was isolated from Arctic sea ice, which was named ArM0029B. These algae displayed faster growth at a wide temperature range of 4–32 ℃ compared to *Chlorella vulgaris*. ArM0029B also accumulated high levels of total fatty acids under nitrogen starvation conditions, reaching 39% of dry cell weight, with the proportion of oleic acid (18:1) and linoleic acid (18:2) reaching 54% of total fatty acids. Taken together, these results indicate that the newly identified *Chlorella* species, ArM0029B, is a promising candidate for biodiesel production.

4-2 Ahn, Mija, Ravichandran N. Murugan, **Eunjung Kim**, **Jun Hyuck Lee**, Chaejoon Cheong, Shin Won Kang, Hee Jung Park, Song Yub Shin, **Hak Jun Kim**, and Jeong Kyu Bang. 2012. “Studies on the Effect of Number of Sugar Moiety in the Antifreeze Activity of Homodimeric AFGPs”. *The Bulletin of the Korean Chemical Society,* 33(7): 2411-2414.
doi: 10.5012/bkcs.2012.33.7.2411

Antifreeze glycoproteins (AFGPs) are found in the plasma of deep sea polar fish such as the Antarctic nototheioids and the northern cods. The AFGPs consists of repeating tripeptides unite, Alanyl -Alanyl-Threonyl (Ala-Ala-Thr)$_{n=4-50}$ unites, connected with the disaccharide β-D- galactosyl-(1→3)-α-D-*N* -acetylgalactosamine through a glycosidic bond at the second hydroxyl group of the threonine residue. Eight distinct AFGP subtypes exist. Among them, AFGP1 is the largest weight (33.7 kDa) and AFGP 8 is the lowest molecular weight (2.6 kDa). AFGPs are able to depress the freezing temperature of the blood serum in fish enough to keep them from freezing in their sub- zero environment while the melting temperature remains unchanged. Despite AFGPs have been consider as a potent cryopreservation, obstacle to develop AFGPs as medicinal and industrial application is mainly due to the problem of understanding how AFGPs inhibit ice crystal growth. To investigate the effect of number of hydroxyl group on antifreeze activity, we designed and synthesized the dimeric AFGP.

4-3 Ahn, Mija, Ravichandran N. Murugan, Song Yub Shin, **Eunjung Kim**, **Jun Hyuck Lee**, **Hak Jun Kim**, and Jeong Kyu Bang. 2012. “Synthesis of Cyclic Antifreeze Glycopeptide and Glycopeptoids and Their Ice Recrystallization

Inhibition Activity”. *The Bulletin of the Korean Chemical Society,* 33(11): 3565-3570.
doi: 10.5012/bkcs.2012.33.11.3565

Until now, few groups reported the antifreeze activity of cyclic glycopeptides; however, the tedious synthetic procedure is not amenable to study the intensive structure activity relationship. A series of *N*-linked cyclic glycopeptoids and glycopeptide have been prepared to evaluate antifreeze activity as a function of peptide backbone cyclization and methyl stereochemical effect on the rigid Thr position. This study has combined the cyclization protocol with solid phase peptide synthesis and obtained significant quantities of homogeneous cyclic glycopeptide and glycopeptoids. Analysis of antifreeze activity revealed that our cyclic peptide demonstrated RI activity while cyclic glycopeptoids showed no RI activity. These results suggest that the subtle changes in conformation and Thr orientation dramatically influence RI activity of *N*-linked glycopeptoids.

4-4 Ahn, Mija, Ravichandran N. Murugan, Song Yub Shin, **Hak Jun Kim**, and Jeong Kyu Bang. 2012. “Peptoid-based Positional Scanning Derivatives: Revealing the Optimum Residue Required for Ice Recrystallization Inhibition Activity for Every Position in the AFGPs”. *The Bulletin of the Korean Chemical Society,* 33(12): 3931-3932.
doi: 10.5012/bkcs.2012.33.12.3931

4-5 Byeon, Hye-Eun, Bong-Kyun Park, **Joung Han Yim**, **Hong Kum Lee**, and 3 others. 2012. “Stereocalpin A inhibits the expression of adhesion molecules in activated vascular smooth muscle cells”. *International Immunopharmacology,* 12(2): 315-325.
doi: 10.1016/j.intimp.2011.11.020

Up-regulation of cell adhesionmolecules on vascular smoothmuscle cells (VSMCs) and leukocyte recruitment to the vascularwall contribute to vascular inflammation and atherosclerosis. Stereocalpin A, a chemical compound of the Antarctic lichen *Ramalina terebarata*, displays tumoricidal activity against several different tumor cell types. However, other biological activities of stereocalpin A and its molecular mechanisms remain unknown. In this study, our work is directed toward studying the in vitro effects of stereocalpin A on the ability to suppress the expression of adhesion molecules induced by TNF-α in vascular smooth muscle cells. Pretreatment of VSMCs for 2 h with stereocalpin A at nontoxic concentrations of 0.1–10 ㎍/ml inhibited TNF-α-induced adhesion of THP-1 monocytic cells and expression of vascular cell adhesion molecule-1 (VCAM-1) and intercellular adhesion molecule-1 (ICAM-1). Stereocalpin A reduced TNF-α-induced production of intracellular reactive oxygen species (ROS) and phosphorylation of p38, ERK, JNK and Akt. Stereocalpin A also inhibited NK-κB activation induced by TNF-α. Moreover, stereocalpin A inhibited TNF-α-induced IκB kinase activation, subsequent degradation of IκBα, and nuclear translocation of NF-κB. Hence, we describe a new anti-inflammatory activity and mechanism of stereocalpin A, owing to the negative regulation of TNF-α-induced adhesion molecule and MCP-1 expression, monocyte adhesion and ROS production in vascular smooth muscle cells. These results suggest that stereocalpin A has the potential to exert a protective effect by modulating inflammation within the atherosclerotic lesion.

4-6 Byeon, Hye-Eun, Sung Hee Um, **Joung Han Yim**, **Hong Kum Lee**, and Suhkneung Pyo. 2012. “Ohioensin F suppresses TNF-α-induced adhesion molecule expression by inactivation of the MAPK, Akt and NF-κB pathways in vascular smooth muscle cells”. *Life Sciences,* 90(11): 396-406.

doi: 10.1016/j.lfs.2011.12.017

Aims: The expression of cell adhesion molecules on vascular smooth muscle cells is central to leukocyte recruitment and progression of atherosclerotic disease. Ohioensin F, a chemical compound of the Antarctic moss *Polyerichastrum alpinum*, exhibited inhibitory activity against protein tyrosine phosphatase 1B and antioxidant activity. However, published scientific information regarding other biological activities and pharmacological function of ohioensin F is scarce. In the present study, we aimed to examine the in vitro effects of ohioensin F on the ability to suppress TNF-α-induced adhesion molecule expression in vascular smooth muscle cells (VSMCs). *Main methods*: The inhibitory effect of ohioensin F on TNF-α-induced upregulation in expression of adhesion molecules was investigated by enzyme-linked immunosorbent assay, cell adhesion assay, RT-PCR, western blot analysis, immunofluorescence, and transfection and reporter assay, respectively. *Key findings*: Pretreatment of VSMCs with ohioensin F at nontoxic concentrations of 0.1–10 μg/ml dosedependently inhibited TNF-α-induced expression of vascular cell adhesion molecule-1 (VCAM-1) and intercellular adhesion molecule-1 (ICAM-1). In addition, ohioensin F suppressed adhesion of THP-1 monocytes to TNF-α-stimulated VSMCs. Ohioensin F reduced TNF-α-induced production of intracellular reactive oxygen species (ROS) and phosphorylation of p38, ERK, JNK and Akt. Finally, ohioensin F inhibited TNF-α-induced CAM mRNA expression and NK-κB translocation. *Significance*: These results suggest a new mechanism of ohioensin F's anti-inflammatory action, owing to the negative regulation of TNF-α-induced adhesion molecule expression, monocyte adhesion and ROS production in vascular smooth muscle cells. Our finding also supports ohioensin F as a potential pharmacological, anti-inflammatory molecule that has a protective effect on the atherosclerotic lesion.

4-7 Cui, Yinglan, **Joung Han Yim**, and 3 others. 2012. “New diterpene furanoids from the Antarctic lichen *Huea* sp.”. *Bioorganic & Medicinal Chemistry Letters,* 22: 7393–7396. doi: 10.1016/j.bmcl.2012.10.063

In the course of ongoing research on protein tyrosine phosphatase 1B (PTP1B) inhibitory compounds from Antarctic lichens, four new diterpene furanoids, hueafuranoids A–D (1–4) have been isolated from the MeOH extract of Antarctic lichen Huea sp. by various chromatographic methods. The structures of these compounds were elucidated by analysis of NMR and MS data, and comparing their spectral data with those in the literature. Compound 1 showed inhibitory activity against therapeutically targeted protein, PTP1B with an IC_{50} value of 13.9 μM. The kinetic analysis of PTP1B inhibition by hueafuranoid A (1) suggested that the diterpene furanoids encountered in this study inhibited PTP1B activity in a non-competitive manner.

4-8 **Do, Hackwon**, **Jun Hyuck Lee**, **Sung Gu Lee**, and **Hak Jun Kim**. 2012. “Crystallization and preliminary X-ray crystallographic analysis of an ice-binding protein (FfIBP) from *Flavobacterium frigoris* PS1”. *Acta Crystallographica Section F,* 68(7): 806-809. doi: 10.1107/S1744309112020465

Ice growth in a cold environment is fatal for polar organisms, not only because of the physical destruction of inner cell organelles but also because of the resulting chemical damage owing to processes such as osmotic shock. The properties of ice-binding proteins (IBPs), which include antifreeze proteins

(AFPs), have been characterized and IBPs exhibit the ability to inhibit ice growth by binding to specific ice planes and lowering the freezing point. An ice-binding protein (FfIBP) from the Gram-negative bacterium *Flavobacterium frigoris* PS1, which was isolated from the Antarctic, has recently been overexpressed. Interestingly, the thermal hysteresis activity of FfIBP was approximately 2.5 K at 50 μM, which is ten times higher than that of the moderately active IBP from Arctic yeast (LeIBP). Although FfIBP closely resembles LeIBP in its amino-acid sequence, the antifreeze activity of FfIBP appears to be much greater than that of LeIBP. In an effort to understand the reason for this difference, an attempt was made to solve the crystal structure of FfIBP. Here, the crystallization and X-ray diffraction data of FfIBP are reported. FfIBP was crystallized using the hanging-drop vapour-diffusion method with 0.1 M sodium acetate pH 4.4 and 3 *M* sodium chloride as precipitant. A complete diffraction data set was collected to a resolution of 2.9 Å. The crystal belonged to space group $P4_122$, with unit-cell parameters $a = b = 69.4$, $c = 178.2$ Å. The asymmetric unit contained one monomer.

4-9 Ha, Sun-Yong, **Young-Nam Kim**, Mi-Ok Park, **Sung-Ho Kang**, **Hyun-choel Kim**, and Kyung-Hoon Shin. 2012. "Production of mycosporine-like amino acids of *in situ* phytoplankton community in Kongsfjorden, Svalbard, Arctic". *Journal of Photochemistry and Photobiology B: Biology,* 114: 1–14. doi: 10.1016/j.jphotobiol.2012.03.011

The spatial distribution of UV-absorbing compounds (mycosporine-like amino acids, MAAs), was investigated by comparing the phytoplankton community structures in the inner and outer waters of the Kongsfjorden inlet, which is located in arctic Svalbard. *Thalassiosira* sp. and *Phaeocystis* sp. were dominant in the outer waters of the Kongfjorden inlet, demonstrating high chlorophyll *a* (chl *a*) concentrations and low MAA concentrations in the outer bay waters. However, Kongsfjorden Bay was dominated by *Phaeocystis* sp. and demonstrated high MAA concentrations despite low chl *a* concentrations. The carbon fixation rate at a station located inside Kongsfjorden Bay (T05) was significantly photo-inhibited by UV radiation, demonstrating higher production rates of MAA and chl a than at a station (B09) in outer bloom waters. Additionally, the turnover rates of individual MAAs were faster inside the Kongsfjorden Bay than in the outside waters. As a result, the natural phytoplankton community demonstrated different UV adaptation mechanisms according to the phytoplankton species, in this case, *Thalassiosira* sp. vs. *Phaeocystis* sp. It is possible to understand real-time changes for newly photosynthesized MAAs as UV-absorbing compounds in the natural phytoplankton community. This takes place via determination of in situ MAA production rates using ^{13}C tracer and High Performance Liquid Chromatography (HPLC) combined with an isotope ratio mass spectrometer (irMS).

4-10 Han, Jiwon, Jaejoon Jung, Seunghun Hyun, **Hyun Park**, and Woojun Park. 2012. "Effects of Nutritional Input and Diesel Contamination on Soil Enzyme Activities and Microbial Communities in Antarctic Soils". *Journal of Microbiology,* 50(6): 916-924. doi: 10.1007/s12275-012-2636-x

Pollution of Antarctic soils may be attributable to increased nutritional input and diesel contamination via anthropogenic activities. To investigate the effect of these environmental changes on the Antarctic terrestrial ecosystem, soil enzyme activities and microbial communities in 3 types of Antarctic soils were evaluated. The activities of alkaline phosphomonoesterase and dehydrogenase were dramatically increased, whereas the activities of β-glucosidase, urease, arylsulfatase, and fluorescein diacetate hydrolysis were negligible. Alkaline phosphomonoesterase and dehydrogenase activities in the 3 types of soils increased 3- to 10-fold in response to nutritional input, but did not increase in the presence of diesel contamination. Consistent with the enzymatic activity data, increased copy numbers of the *phoA* gene, encoding an alkaline phosphomonoesterase, and the 16S rRNA gene were verified using quantitative real-time polymerase chain reaction. Interestingly, dehydrogenase activity and 16S rRNA gene copy number increased slightly after 30 days, even under diesel contamination, probably because of adaptation of the bacterial population. Intact Antarctic soils showed a predominance of Actinobacteria phylum (mostly *Pseudonorcarida* species) and other phyla such as *Proteobacteria*, *Chloroflexi*, *Planctomycetes*, *Firmicutes*, and *Verrucomicrobia* were present in successively lower proportions. Nutrient addition might act as a selective pressure on the bacterial community, resulting in the prevalence of *Actinobacteria* phylum (mostly *Arthrobacter* species). Soils contaminated by diesel showed a predominance of *Proteobacteria* phylum (mostly *Phyllobacterium* species), and other phyla such as *Actinobacteria*, *Bacteroidetes*, *Planctomycetes*, and *Gemmatimonadetes* were present in successively lower proportions. Our data reveal that nutritional input has a dramatic impact on bacterial communities in Antarctic soils and that diesel contamination is likely toxic to enzymes in this population.

4-11 Hemmes, Hans, Rossana Henriques, In-Cheol Jang, Sanghee Kim, and Nam-Hai Chua. 2012. "Circadian Clock Regulates Dynamic Chromatin Modifications Associated with *Arabidopsis CCA1/LHY* and *TOC1* Transcriptional Rhythms". *Plant & Cell Physiology,* 53(12): 2016–2029.
doi: 10.1093/pcp/pcs148

Circadian clocks enable organisms to adapt to a 24 h diurnal cycle and anticipate rhythmic changes in the environment. The *Arabidopsis* central oscillator contains three genes encoding core clock components. CIRCADIAN CLOCK ASSOCIATED 1 (CCA1)/LATE ELONGATED HYPOCOTYL (LHY) and TIMING OF CAB EXPRESSION 1 (TOC1) reciprocally repress genes encoding each other and are critical for the generation of circadian rhythms controlling many clock outputs. A precise regulation of transcriptional events is, therefore, essential for proper circadian function. Here, we investigated histone 3 (H3) tail modifications of *CCA1*, *LHY* and *TOC1* under various conditions. We found specific association of only H3K4Me3 and H3K9/14Ac with the translational start site of these three genes. These H3 marks were enriched at circadian time points of their increased transcription at different photoperiods and under free-running conditions, suggesting circadian regulation of H3 modifications. Analysis of clock-compromised CCA1-overexpressing lines provided evidence that light/dark photoperiods signal the establishment of these chromatin changes which are gated by the clock.

4-12 **Hwang, Chung Yeon**, **Hye Min Kim**, and **Yoo Kyung Lee**. 2012. "Reclassification of *Nocardioides basaltis* Kim et al. 2009 as a later synonym of *Nocardioides salarius* Kim et al. 2008, and emendation of the species description". *Antonie van Leeuwenhoek,* 102(4): 695-701.
doi: 10.1007/s10482-012-9768-1

The taxonomic relationship between *Nocardioides salarius* CL-Z59^T and *Nocardioides basaltis* J112^T was established. The 16S rRNA gene sequences of the type strains showed 99.6 % similarity. The △Tm for genomic DNA–DNA hybridization of *N. salarius* CL-Z59^T and *N. basaltis* J112^T was 0.6–1.6 ℃, indicating that both strains belong to a single species. Phenotypic and chemotaxonomic characteristics showed no pronounced differences between the two species. Based on the results of the polyphasic approach, it is proposed that *N. basaltis* J112^T is a later heterotypic synonym of *N. salarius* CL-Z59^T. An emended description of the species *N. salarius* is given.

4-13 Im, Jong Hee, **Hyoungseok Lee**, 3 others. 2012. "Soybean MAPK, GMK1 Is Dually Regulated by Phosphatidic Acid and Hydrogen Peroxide and Translocated to Nucleus during Salt Stress". *Molecules and Cells,* 34(3): 271-278. doi: 10.1007/s10059-012-0092-4

Mitogen-activated protein kinase (MAPK) is activated by various biotic and abiotic stresses. Salt stress induces two well-characterized MAPK activating signaling molecules, phosphatidic acid (PA) *via* phospholipase D and phospholipase C, and reactive oxygen species (ROS) *via* nicotinamide adenine dinucleotide phosphate (NADPH)-oxidase. In our previous study, the activity of soybean MAPK, GMK1 was strongly induced within 5 min of 300 mM NaCl treatment and this early activity was regulated by PA. In this study, we focused on the regulation of GMK1 at the later stage of the salt stress, because its activity was strongly persistent for up to 30 min. H_2O_2 activated GMK1 even in the presence of PA generation inhibitors, but GMK1 activity was greatly decreased in the presence of diphenyleneiodonium, an inhibitor of NADPH-oxidase after 5 min of the treatment. On the contrary, the n-butanol and neomycin reduced GMK1 activity within 5 min of the treatment. Thus, GMK1 activity may be sustained by H_2O_2 10 min after the treatment. Further, GMK1 was translocated into the nucleus 60 min after NaCl treatment. In the relationship between GMK1 and ROS generation, ROS generation was reduced by SB202190, a MAPK inhibitor, but was increasedin protoplast overexpressing TESD-GMKK1. However, these effects were occurred at prolonged time of NaCl treatment. These data suggest that GMK1 indirectly regulates ROS generation. Taken together, we propose that soybean GMK1 is dually regulated by PA and H_2O_2 at a time dependant manner and translocated to the nucleus by the salt stress signal.

4-14 Im, Jong Hee, **Hyoungseok Lee**, and 5 others. 2012. "A Salt Stress-activated Mitogen-activated Protein Kinase in Soybean Is Regulated by Phosphatidic Acid in Early Stages of the Stress Response". *Journal of Plant Biology,* 55(4): 303-309. doi: 10.1007/s12374-011-0036-8

Salt stress inhibits plant growth and development and plants activate kinase-dependent survival pathways in response to salt stress. However, the role of soybean mitogenactivated protein kinases (MAPKs) in salt stress response has yet to be characterized. In this study, we found that salt stress activates *Glycine max* MAP kinase 1 (GMK1), a soybean MAPK. The activity of GMK1 induced with increasing salt concentrations, up to 300 mM NaCl, after 5 min of the treatment and was regulated by post-translational modification. We found that mastoparan, a heteromeric G-protein activator, also activated GMK1, and that *n*-butanol, a phospholipase D inhibitor, and neomycin, a phospholipase C inhibitor, inhibited its activity. Moreover, GMK1 activity was reduced by suramin, a heteromeric G-protein inhibitor, and by two inhibitors of phosphatidic acid (PA) generation after 5 min of 300 mM NaCl treatment. Endogenous PA levels were highest 5 min after induction of salt stress, and exogenous PA directly activated GMK1. From these data, we propose that salt stress signaling is transduced from heteromeric G-protein to GMK1 via phospholipases in the early stages of the response to salt stress in soybean.

4-15 Jeon, Jeong-Min, Bo-Kwang Kim, **Jun Hyuck Lee**, **Hak Jun Kim**, and 3 others. 2012. "Two type I crustacean hyperglycemic hormone (CHH) genes in Morotoge shrimp (*Pandalopsis japonica*): Cloning and expression of eyestalk and pericardial organ isoforms produced by alternative splicing and a novel type I CHH with predicted structure shared with type II CHH peptides". *Comparative Biochemistry and Physiology, Part B,* 162(4): 88-89.
doi: 10.1016/j.cbpb.2012.04.003

Crustacean hyperglycemic hormone (CHH) peptide family members play critical roles in growth and reproduction in decapods. Three cDNAs encoding CHH family members (Pj-CHH1ES, Pj-CHH1PO, and Pj-CHH2) were isolated by a combination of bioinformatic analysis and conventional cloning strategies. Pj-CHH1ES and Pj-CHH1PO were products of the same gene that were generated by alternative mRNA splicing, whereas Pj-CHH2 was the product of a second gene. The Pj-CHH1 and Pj-CHH2 genes had four exons and three introns, suggesting the two genes arose from gene duplication. The three cDNAs were classified in the type I CHH subfamily, as the deduced amino acid sequences had a CHH precursor-related peptide sequence positioned between the N-terminal signal sequence and C-terminal mature peptide sequence. The Pj-CHH1ES isoform was expressed at a higher level in the eyestalk X-organ/sinus gland (XO/SG) complex and at a lower level in the gill. The Pj-CHH1PO isoform was expressed at higher levels in the XO/SG complex, brain, abdominal ganglion, and thoracic ganglion and at a lower level in the epidermis. Pj-CHH2 was expressed at a higher level in the thoracic ganglion and at a lower level in the gill. Real-time polymerase chain reaction was used to quantify the effects of eyestalk ablation on the mRNA levels of the three Pj-CHHs in the brain, thoracic ganglion, and gill. Eyestalk ablation reduced expression of Pj-CHH1ES in the brain and Pj-CHH1PO and Pj-CHH2 in the thoracic ganglion. Sequence alignment of the Pj-CHHs with CHHs from other species indicated that Pj-CHH2 had an additional alanine at position #9 of the mature peptide. Molecular modeling showed that the Pj-CHH2 mature peptide had a short alpha helix (α1) in the N-terminal region, which is characteristic of type II CHHs. This suggests that Pj-CHH2 differs in function from other type I CHHs.

4-16 Jung, Jae-Ho, **Sanghee Kim**, and 7 others. 2012. "Development of Single-Nucleotide Polymorphism-Based Phylum-Specific PCR Amplification Technique: Application to the Community Analysis Using Ciliates as a Reference Organism". *Molecules and Cells,* 34: 383-391.
doi: 10.1007/s10059-012-0169-0

Despite recent advance in mass sequencing technologies such as pyrosequencing, assessment of culture-independent microbial eukaryote community structures using universal primers remains very difficult due to the tremendous richness and complexity of organisms in these communities. Use of a specific PCR marker targeting a particular group would provide enhanced sensitivity and more in-depth evaluation of microbial eukaryote communities compared to what can be achieved with universal primers. We discovered that many phylum- or groupspecific single-nucleotide polymorphisms (SNPs) exist in small subunit ribosomal RNA (SSU rRNA) genes from diverse eukaryote groups. By applying this discovery to a known simple allele-discriminating (SAP) PCR method, we developed a technique that enables the identification of organisms belonging to a specific higher taxonomic group (or phylum) among diverse types of eukaryotes. We performed an assay using two complementary methods, pyrosequencing and clone library screening. In doing this, specificities for the group (ciliates) targeted in this study in bulked environmental samples were 94.6% for the clone library and 99.2% for pyrosequencing, respectively. In particular, our novel technique showed high selectivity for rare species, a feature that may be more important than the ability to identify quantitatively predominant species in community structure analyses. Additionally, our data revealed that a target-specific library (or ciliate-specific one for the present study) can better explain the ecological features of a sampling locality than a universal library.

4-17 Jung, Keong-Tsul, **Han-Woo Kim**, and 4 others. 2012. "Identification of the First Archaeal Arylsulfatase from *Pyrococcus furiosus* and Its Application to Desulfatation of Agar". *Biotechnology and Bioprocess Engineering,* 17(6): 1140-1146.
doi: 10.1007/s12257-012-0228-6

A gene encoding a putative arylsulfatase from the hyperthermophilic archaeon *Pyrococcus furiosus* was identified, cloned, and expressed as a fusion protein with a Sce VMA intein and chitin binding domain (CBD) residue. The gene (PF1345) from *P. furiosus* encoding a 35 kDa protein showed some similarity (17 ~ 19%) with other arylsulfatases from the bacteria. The recombinant fusion arylsulfatase was overexpressed in *E. coli* and partially purified. Its molecular mass was estimated to be 90 kDa by SDS-PAGE. The optimal temperature and pH for arylsulfatase activity were found to be 45℃ and 9.5, respectively. Various divalent cations (Ca^{2+}, Mg^{2+}, Co^{2+}, Cu^{2+}, Zn^{2+}, and Mn^{2+}) slightly activated the arylsulfatase activity in a narrow range of concentrations (below 0.5 mM), whereas Zn^{2+} concentrations above 2.0 mM significantly inhibited the activity. After the reaction of agar with recombinant fusion arylsulfatase for 12 h at 50℃, 75% of the sulfate in the agar was removed, and the DNA migration was greatly enhanced. Therefore, the arylsulfatase in this study could be applicable for the production of electrophoretic grade agarose by removing sulfate groups in agar.

4-18 **Jung, Woongsic**, **Sung Gu Lee**, Se Won Kang, Yong Seok Lee, **Jun Hyuck Lee**, **Sung-Ho Kang**, Eon Seon Jin, and **Hak Jun Kim**. 2012. "Analysis of expressed sequence tags from the Antarctic psychrophilic green algae, *Pyramimonas gelidicola". Journal of Microbiology and Biotechnology,* 22(7): 902-906.
doi: 10.4014/jmb.1201.01002

Expressed sequence tags (ESTs) from the Antarctic green algae *Pyramimonas gelidicola* were analyzed to obtain molecular information on cold acclimation of psychrophilic microorganisms. Total 2,112 EST clones were sequenced, generating 222 contigs and 219 singletons, and 200 contigs and 391 singletons from control (4℃) and cold-shock conditions (-2℃), respectively. The complete EST sequences were deposited to the DDBJ EST database (http://www.ddbj.nig.ac.jp/index-e.html) and the nucleotide sequences reported in this study are available in the DDBJ/EMBL/GenBank. These EST databases of Antarctic green algae can be used in a wide range of studies on psychrophilic genes expressed by polar microorganisms.

4-19 Kang, Ilnam, Kiyoung Lee, Seung-Jo Yang, Ahyoung Choi, Dongmin Kang, **Yoo Kyoung Lee**, and Jang-Cheon Cho. 2012. "Genome Sequence of "*Candidatus Aquiluna*" sp. Strain IMCC13023, a Marine Member of the

Actinobacteria Isolated from an Arctic Fjord". *Journal of Bacteriology,* 194(13): 3550-3551. doi: 10.1128/JB.00586-12

We report the genome sequence of actinobacterial strain IMCC13023, isolated from arctic fjord seawater. Phylogenetic analysis of 16S rRNA gene showed that the strain is related to "*Candidatus* Aquiluna rubra". The genome information suggests that strain IMCC13023 is a photoheterotroph carrying actinorhodopsin, with the smallest genome ever reported for a free-living member of the *Actinobacteria*.

4-20 Kang, SeokHa, JiYeon Kim, JunHee Lee, **SangHee Kim**, and 2 others. 2012. "The complete mitochondrial genome of an ectoparasitic monopisthocotylean fluke *Benedenia hoshinai* (Monogenea: Platyhelminthes)". *Mitochondrial DNA,* 23(3): 176-178. doi: 10.3109/19401736.2012.668900

An exponential growth of mitochondrial genome information has brought significant progress in understanding the organismal phylogeny and mitochondrial genome evolution for many metazoans including platyhelminth groups. In this study, we determined the complete mitochondrial genome sequence for *Benedenia hoshinai*, an ectoparasitic monogenean species, and compared it with its congener *Benedenia seriolae*. The complete mitochondrial genome is 13,554 bp in length and contains 12 protein-coding genes (lacking the *atp8* gene), 2 rRNA genes, and 22 tRNA genes, all encoded in the same direction as found in all other platyhelminth species sequenced to date. The gene arrangement of *B. hoshinai* mtDNA is almost identical to *B. seriolae*, differing only by the translocation of trnT between *cox1* and *rrnL*. It is unclear whether the shared position of *trnT* between *B. hoshinai* and *Gyrodactylus* represents evidence for their phylogenetic affinity; testing this hypothesis requires further mitogenomic evidence.

4-21 Kim, Bo-Mi, Jae-Sung Rhee, Jung Soo Seo, **Il-Chan Kim**, **Young-Mi Lee**, and Jae-Seong Lee. 2012. "8-OxoguanineDNA glycosylase 1 (*OGG1*) from the copepod *Tigriopus japonicus*: Molecular characterization and its expression in response to UV-B and heavy metals". *Comparative Biochemistry and Physiology, Part C,* 155: 290-299. doi: 10.1016/j.cbpc.2011.09.010

8-OxoguanineDNA glycosylase 1 (EC 3.2.2.23) is encoded by *OGG1* gene and plays a key role in removing 8-oxo-7,8-dihydroguanine (8-oxoG) base in DNA lesion by reactive oxygen species (ROS). To identify and characterize *OGG1* gene (*TJ-OGG1*) in the copepod *Tigriopus japonicus*, the full-length cDNA sequence, genomic structure, and promoter region was analyzed. In addition, to investigate transcriptional change of *TJ-OGG1* mRNA under oxidative stress conditions, *T. japonicus* were exposed to environmental oxidative inducers, H_2O_2, UV-B, and heavy metals (Cd, Cu, and Zn), respectively. The full-length cDNA of *TJ-OGG1* gene was 1708 bp in length, encoding 343 amino acid residues. The deduced amino acid sequences of *TJ-OGG1* showed a 56% similarity with human. Two conserved motifs (HhH and PVD loop) and two conserved residues (lysine and aspartic acid) in active sites were also observed. *TJ-OGG1* genome structure contained six exons and five introns and putative transcription factor binding sites such as Nrf-2, p53, ERE-half sites, and XRE were detected on the promoter region. *TJ-OGG1* mRNA level was increased at approximately three-fold ($P<0.05$) at 1 mMand approximately 4-fold ($P<0.01$) at 10mMof H_2O_2, respectively. UV-B enhanced the expression of *TJ-OGG1* mRNA at 15 kJ/m^2 ($P<0.05$) and more ($P<0.001$). In a time-course experiment, *TJ-OGG1* gene was highly transcribed within 12 h after exposure of 10 kJ/m^2 ($P<0.01$) and 20 kJ/m^2 ($P<0.001$). The expression of *TJ-OGG1* mRNA after exposure to Cu and Cd for 96 hwas significantly up-regulated at 0.1 μg/L and then remarkably reduced in a dose-dependent manner. Their transcript levels did not change at low dose (0.1 and 1 μg/L) but were dose-dependently down-regulated at high dose (10 and 100 μg/L). These findings suggest that H_2O_2, UV-B, and heavy metals induce oxidative stress and generate oxidatively damaged DNA. Consequently, the enhanced *TJ-OGG1* gene expressionwould be associatedwith active involvement of *TJ-OGG1* gene in DNA repair process as a cellular protectionmechanism. This is the first report on the cloning and characterization of *OGG1* gene in aquatic animals. This study is helpful for a better understanding of themolecular mechanisms of cellular protection against various environmental oxidative stress inducers such as UV-B and heavy metals in aquatic invertebrates.

4-22 Kim, Hee Gon, Gui Hwan Han, **Dockyu Kim**, and 2 others. 2012. "Comparative analysis of two types of methanol dehydrogenase from *Methylophaga aminisulfidivorans* MP^T grown on methanol". *Journal of Basic Microbiology,* 52(2): 141-149.
doi: 10.1002/jobm.201000479

Two types of methanol dehydrogenase (MDH) were obtained from a novel marine methylotrophic bacterium, *Methylophaga aminisulfidivorans* MP^T, grown on methanol. Type I MDH consisted of two identical dimers of α (65.98 kDa) and β (7.58 kDa) subunits organized to form the $\alpha_2\beta_2$ tetramer. Type II MDH contained an additional MxaJ protein (27.86 kDa) and had more specific activity than type I MDH. The K_m values of type I and II MDH for methanol under cytochrome c_L reduction assay system were estimated to be 50.3 and 13.0 μM, respectively, and the isoelectric points of type I and II MDH were determined to be 5.4 and 5.8, respectively. The average molar ratios of α : β, α :MxaJ, and β :MxaJ in type II MDH were approximately 1:0.99, 1:0.41 and 1:0.42, respectively. Based on these results, the original conformation of the MDH of *M. aminisulfidivorans* MP^T is most likely the $\alpha_2\beta_2$-MxaJ complex. During purification, the lysozyme and freeze-thawing cell disruption method significantly increased the amount of type II MDH in the soluble fraction compared with strong physical disruption methods such as sonication and French Press.

4-23 Kim, Jung A, **Soon Gyu Hong**, and 3 others. 2012. "A new reducing polyketide synthase gene from the lichen-forming fungus *Cladonia metacorallifera". Mycologia,* 104(2): 362-370.
doi: 10.3852/11-001

Lichens produce unique polyketide secondary metabolites including depsides, depsidones, dibenzofurans and depsones. The biosynthesis of these compounds is governed by polyketide synthase (PKS), but the mechanism via which they are produced has remained unclear until now. We reported the 6-methylsalicylic acid synthase (6-MSAS) type of PKS gene, which is a member of the fungalreducing PKSs. A cultured mycobiont of *Cladonia metacorallifera* was employed in the isolation and characterization of a polyketide synthase gene (*CmPKS1*). The complete sequence information for *CmPKS1* was acquired via the screening of a Fosmid genomic library with a 456 bp fragment corresponding to part of the acyl transferase (AT) domain as a probe. CmPKS1 contains ß-ketoacyl synthase (KS), AT, dehydratase (DH), ketoreductase (KR) and phosphopantetheine attachment site (PP) domains.: The domain organization of CmPKS1 (KSAT-DH-KR-PP) is a typical 6-MSAS-type PKS, and the results of phylogenetic analysis showed that *CmPKS1* grouped with other fungal-reducing PKSs. Quantitative real time PCR analyses showed that CmPKS1 was expressed preferentially in the early growth stage of the axenically cultured mycobiont. Furthermore *CmPKS1* expression was found to be dependent on the carbon sources and concentrations in the medium.

4-24 Kim, Meehyein, **Joung Han Yim**, So-Yeon Kim, Hae Soo Kim, Woo Ghil Lee, **Sung Jin Kim**, **Pil-Sung Kang**, and Chong-Kyo Lee. 2012. *"In vitro* inhibition of influenza A virus infection by marine microalga-derived sulfated polysaccharide p-KG03". *Antiviral Research,* 93: 253-259.
doi: 10.1016/j.antiviral.2011.12.006

The sulfated polysaccharide, p-KG03, purified from the marine microalga, *Gyrodinium impudium*, is a unique compound comprising homogenous galactose units conjugated to uronic acid and sulfated groups. Although previous studies showed that p-KG03 suppresses tumor cell growth and infection by encephalomyocarditis virus, its effect against enveloped virus infection and the biological mechanism of action have not been elucidated. In this report, the inhibitory activity of p-KG03 against influenza virus was examined and compared with that of other sulfated polysaccharides (fucoidan and pentosan polysulfate) and antiviral agents (oseltamivir phosphate, oseltamivir carboxylate, amantadine, and ribavirin). The results of a cytopathic effect reduction assay using MDCK cells demonstrated that p-KG03 exhibited the 50% effective concentration (EC_{50}) values of 0.19–0.48 µg/ml against influenza type A virus infection (selectivity index >200) but not all influenza type B viruses. Mechanism studies showed that inhibition of influenza virus replication was maximized when p-KG03 was added during or within 6 h after viral infection, suggesting that mainly the viral adsorption and internalization steps are targeted by this compound. The results of influenza virus binding assay to p-KG03 and fluorescence microscopy indicate that the antiviral activity of p-KG03 is directly associated with its interaction with viral particles. The sulfated polysaccharide p-KG03 is a potent and specific influenza A viral entry inhibitor and may be a candidate for antiviral drug development.

4-25 Kim, Mi-Kyeong, **Hyun Park**, and Tae-Jin Oh. 2012. "Antioxidant Activities of Bacterial Culture Extracts Isolated from Arctic Lichens". *Korean Journal of Microbiology and Biotechnoloy,* 40(4): 333–338.
doi: 10.4014/kjmb.1207.07027

Lichens are a symbiosis between fungi, algae and cyanobacteria. Our group recently studied the antioxidant properties of some bacterial species isolated from Arctic lichens and we confirmed that they possess high antioxidant activities. In this paper, we investigated the antioxidant capacity of 5 microorganisms newly isolated from 4 Arctic lichen species, *Cladonia* sp., *Sterocaulon* sp., *Umbilicaria* sp. and *Cetraria* sp., using various solvent extractions. We carried out 1,1-diphenyl-2-picryl-hydrazyl (DPPH) and 2,2'-azino-bis(3-ethyl benzothiazoline-6-sulphonic acid) (ABTS) free radical scavenging activity test and ferric reducing antioxidant power (FRAP) assay. Also total phenolic and flavonoid content assays were performed. Among the bacterial culture extracts of the tested lichen-microorganisms, ethyl acetate extracts of *Burkholderia sordidicola* S5-B(T) had not only a high antioxidant activity (72.9%) when compared with the ascorbic acid used as the control (51.3%) in the DPPH assay, but also a high amount of phenolic content as well as flavonoid content. As a result, these lichen-microorganisms may be potentially useful sources of natural antioxidants.

4-26 Kim, Mi-Kyeong, **Hyun Park**, and Tae-Jin Oh. 2012. "Antibacterial Properties Associated with Microorganisms Isolated from Arctic Lichens". *Korean Journal of Microbiology and Biotechnoloy,* 40(4): 380-388.
doi: 10.4014/kjmb.1207.07028

A total of 5 different polar microorganisms were isolated from Arctic lichens and their bioactive compounds were extracted from cell culture using different solvents including acetone, water, chloroform, diethylether, ethanol, ethyl acetate, methanol, and petroleum ether. The antibacterial properties of the extracts were evaluated by disk diffusion tests and minimal inhibitory concentration tests against 6 bacterial pathogens; *Staphylococcus aureus*, *Bacillus subtilis*, *Micrococcus luteus*, *Enterobacter cloacae*, *Pseudomonas aeruginosa* and *Escherichia coli*. Among the extraction samples, ethyl acetate extracts of *Burkholderia sordidicola* S5-B^{T} (KOPRI 26644) showed the highest activity (inhibition zone, 7-10 mm; MIC value, 57.5-1000 μg/ml) against targeted bacteria. Among the various solvents used for extraction, chloroform extract exhibited the weakest, but still obvious, activity.

4-27 **Kim, Ok-Sun Kim**, Namyi Chae, Hyun Soo Lim, **Ahnna Cho**, **Jeong Hoon Kim**, **Soon Gyu Hong**, and Jeongsu Oh. 2012. "Bacterial Diversity in Ornithogenic Soils Compared to Mineral Soils on King George Island, Antarctica". *Journal of Microbiology,* 50(6): 1081–1085.
doi: 10.1007/s12275-012-2655-7

In the Narębski Point area of King George Island of Antarctica, ornithogenic soils form on land under Chinstrap and Gentoo Penguin rookeries. The purpose of this study was to compare the bacterial community compositions in the gradient of contamination by penguin feces; mineral soil with no contamination, and soils with medium or high contamination. The discrimination between mineral soils and ornithogenic soils by characterization of physicochemical properties and bacterial communities was notable. Physicochemical analyses of soil properties showed enrichment of carbon and nitrogen in ornithogenic soils. *Firmicutes* were present abundantly in active ornithogenic soils, Bacteroidetes and *Proteobacteria* in a formerly active one, and several diverse phyla such as *Proteobacteria*, *Actinobacteria*, and *Acidobacteria* in mineral soils. Some predominant species belonging to the *Firmicutes* and *Gammaproteobacteria* may play an important role for the mineralization of nutrients in ornithogenic soils. Results of this study indicate that dominant species may play an important role in mineralization of nutrients in these ecosystems.

4-28 **Kim, Ok-Sun**, and 11 others. 2012. "Introducing EzTaxon-e: A Prokarotic 16S rRNA Gene Sequence Database with Phylotypes that Represent Uncultured Species". *International Journal of Systematic and Evolutionary Microbiology,* 62(3): 716-721.
doi: 10.1099/ijs.0.038075-0

Despite recent advances in commercially optimized identification systems, bacterial identification remains a challenging task in many routine microbiological laboratories, especially in situations where taxonomically novel isolates are involved. The 16S rRNA gene has been used extensively for this task when coupled with a well-curated database, such as EzTaxon, containing sequences of type strains of prokaryotic species with validly published names. Although the EzTaxon database has been widely used for routine identification of prokaryotic isolates, sequences from uncultured prokaryotes have not been considered. Here, the next generation database, named EzTaxon-e, is formally introduced. This new database covers not only species within the formal nomenclatural system but also phylotypes that may represent species in nature. In addition to an identification function based on Basic Local Alignment Search Tool (BLAST) searches and pairwise global sequence alignments, a new objective method of assessing the degree of completeness in sequencing is proposed. All sequences that are held in the EzTaxon-e database have been subjected to phylogenetic analysis and this has resulted in a complete hierarchical classification system. It is concluded that the EzTaxon-e database provides a useful taxonomic backbone for the identification of cultured and uncultured prokaryotes and offers a valuable means of communication among microbiologists who routinely encounter taxonomically novel isolates. The database and its analytical functions can be found at http://eztaxon-e.ezbiocloud.net/.

4-29 **Kim, SangHee**, JiYeon Kim, **Han-Gu Choi**, and 2 others. 2012. “Complete mitochondrial genome of the northern mauxia shrimp *Acetes chinensis* (Decapoda, Dendrobranchiata, Sergestoidae)”. *Mitochondrial DNA,* 23(1): 28-30.
doi: 10.3109/19401736.2011.643878

Here, we report the first complete mitochondrial genome sequence of northern mauxia shrimp *Acetes chinensis* (Decapoda, Dendrobranchiata, Sergestoidae). The genome sequence was 15,740 bp in size, and the gene content, gene order and transcriptional polarity were almost identical to the pancrustacean ground pattern, with the one exception that an extra ${}_{trn}S_1^{AGC}$ was adjacent to the original ${}_{trn}S_1^{AGA}$. The two tandemly duplicated ${}_{trn}S_1$ showed a high sequence similarity (82.3%), with almost identical secondary structure lacking a DHU arm. Comparison of codon usage suggests that both of the ${}_{trn}S_1$ genes were functional.

4-30 **Kim, SangHee**, Mi-Hyun Park, Jae-Ho Jung, Dong-Ha Ahn, Tahera Sultana, SeJoo Kim, Joong-Ki Park, **Han-Gu Choi**, and Gi-Sik Min . 2012. “The mitochondrial genomes of *Cambaroides similis* and *Procambarus clarkii* (Decapoda: Astacidea: Cambaridae): the phylogenetic implications for Reptantia”. *Zoologica Scripta,* 41(3): 281-292.
doi: 10.1111/j.1463-6409.2012.00534.x

We determined the complete mitochondrial (mt) genome sequences of two northern hemisphere freshwater crayfish species, *Cambaroides similis* and *Procambarus clarkii* (Decapoda: Astacidea: Cambaridae). These species have an identical gene order with typical metazoan mt genome compositions. However, their gene arrangement was very distinctive compared with the pan-crustacean ground pattern because of the presence of a long inverted block, which included 19 coding genes and a control region (CR). Because the CR was inverted, their nucleotide frequencies showed a reversed strand-specific bias compared with the other decapods. Based on a comparative analysis of mt genome arrangements between southern and northern hemisphere crayfish and their putative close marine relative (*Homarus americanus*, a true clawed lobster), we postulated that the ancestor of freshwater crayfish had a typical pan-crustacean mtDNA gene order, similar to its marine relatives. Based on this assumption, we traced the most parsimonious gene rearrangement scenario of the northern hemisphere crayfish. In a phylogenetic study on the infraordinal relationships in reptan decapods, the lineage Lineata [Thalassinidea (Brachyura, Anomura)] was well supported, while the infraorder positions of Achelata and Astacidea remained unidentified.

4-31 Kim, Su Jin, **Seung Chul Shin**, **Soon Gyu Hong**, **Yung Mi Lee**, **Hyoungseok Lee**, **Jungeun Lee**, In-Geol Choi, and **Hyun Park**. 2012. “Genome

Sequence of *Janthinobacterium* sp. Strain PAMC 25724, Isolated from Alpine Glacier Cryoconite". *Journal of Bacteriology,* 194(8): 2096.
doi: 10.1128/JB.00096-12

The draft genome of *Janthinobacterium* sp. PAMC 25724, which is a violacein-producing psychrotolant bacterium, was determined. The strain was isolated from glacier cryoconite of Alps mountain permafrost region. The sequence will allow identification and characterization of the genetic determination of its cold adaptive properties.

4-32 Kim, Su Jin, **Seung Chul Shin**, **Soon Gyu Hong**, **Yung Mi Lee**, In-Geol Choi, and **Hyun Park**. 2012. "Genome Sequence of a Novel Member of the Genus *Psychrobacter* Isolated from Antarctic Soil". *Journal of Bacteriology,* 194(9): 2403.
doi: 10.1128/JB.00234-12

Psychrobacter spp. have shown characteristics indicating remarkable capabilities at subzero temperatures that identify them as potential model organisms for the study of low-temperature adaptations. Here we present the draft genome sequence of *Psychrobacter* sp. PAMC 21119, which was isolated from permafrost soil of Antarctica; this information could provide insight into adaptation and evolution strategies under extreme environmental conditions.

4-33 Kim, Wonduck, Yu Ri Park, Seonghun Im, **Dockyu Kim**, and Si Wouk Kim. 2012. "Expression and bioconversion of recombinant *m*- and *p*-hydroxybenzoate hydroxylases from a novel moderate halophile, *Chromohalobacter* sp.". *Biotechnology Letters,* 34(9): 1687-1692.
doi: 10.1007/s10529-012-0950-3

p-Hydroxybenzoate hydroxylase (pobA) and *m*-hydroxybenzoate hydroxylase (mobA) genes, from the moderate halophile *Chromohalobacter* sp. HS-2, were expressed and characterized. Solubilities of over expressed recombinant MobA and PobA were enhanced by the induction of the heat-shock proteins DnaJ and DnaK. Each MobA and PobA maintained stable activity under highNaCl concentrations. V_{max} and K_m values for MobA with *m*-hydroxybenzoate were 70 μmol min^{-1} mg^{-1} protein and 81 μM, respectively. Similarly, those of PobA with *p*-hydroxybenzoate as substrate were 5 μmol min^{-1} mg^{-1} protein and 129 μM, respectively. The *Escherichia coli* expression system, including induction of heat shock proteins, was used to convert hydroxybenzoates into protocatechuate (3,4-dihydroxybenzoate) and revealed that resting cells harboringmobAconverted 15 mM *m*-hydroxybenzoate to 15 mM protocatechuate while those harboring pobA converted 50 mM *p*-hydroxybenzoate to 35 mM protocatechuate at 30℃, respectively.

4-34 **Koh, Hye Yeon**, **Sung Gu Lee**, **Jun Hyuck Lee**, Shawn Doyle, Brent C. Christner, and **Hak Jun Kim**. 2012. "Draft Genome Sequence of *Paenisporosarcina* sp. Strain TG-14, a Psychrophilic Bacterium Isolated from Sediment-Laden Stratified Basal Ice from Taylor Glacier, McMurdo Dry Valleys, Antarctica". *Journal of Bacteriology,* 194(23): 6656-6657.
doi: 10.1128/JB.01795-12

The psychrophilic bacterium, *Paenisporosarcina* sp. TG-14 was isolated from sediment-laden stratified basal ice from Taylor Glacier, McMurdo Dry Valleys, Antarctica. Here we report the draft genome sequence of this strain, which could provide useful information on cold-adaptation mechanism in extremely variable environments.

4-35 Kwon, Yerim, Si-in Yu, **Hyoungseok Lee**, **Joung Han Yim**, and 2 others. 2012. *"Arabidopsis* Serine Decarboxylase Mutants Implicate the Roles of Ethanolamine in Plant Growth and Development". *International Journal of Molecular Sciences,* 13(3): 3176-3188.
doi: 10.3390/ijms13033176

Ethanolamine is important for synthesis of choline, phosphatidylethanolamine (PE) and phosphatidylcholine (PC) in plants. The latter two phospholipids are the major phospholipids in eukaryotic membranes. In plants, ethanolamine is mainly synthesized directly from serine by serine decarboxylase. Serine decarboxylase is unique to plants and was previously shown to have highly specific activity to L-serine. While serine decarboxylase was biochemically characterized, its functions and importance in plants were not biologically elucidated due to the lack of serine decarboxylase mutants. Here we characterized an *Arabidopsis* mutant defective in serine decarboxylase, named *atsdc-1* (*Arabidopsis thaliana serine decarboxylase-1*). The *atsdc-1* mutants showed necrotic lesions in leaves, multiple inflorescences, sterility in flower, and early flowering in short day conditions. These defects were rescued by ethanolamine application to *atsdc-1*, suggesting the roles of ethanolamine as well as serine decarboxylase in plant development. In addition, molecular analysis of serine decarboxylase suggests that *Arabidopsis* serine decarboxylase is cytosol-localized and expressed in all tissue.

4-36 **Lee, Hyoungseok**, **Seung Chul Shin**, **Jungeun Lee**, Su Jin Kim, Bum-Keun Kim, **Soon Gyu Hong**, **Eun Hye Kim**, and **Hyun Park**. 2012. "Genome Sequence of *Sphingomonas* sp. Strain PAMC 26621, an Arctic-Lichen-Associated Bacterium Isolated from a *Cetraria* sp.". *Journal of Bacteriology,* 194(11): 3030.
doi: 10.1128/JB.00395-12

The lichen-associated bacterial strain *Sphingomonas* sp. PAMC 26621 was isolated from an Arctic lichen *Cetraria* sp. on Svalbard Islands. Here we report the draft genome sequence of this strain, which could provide novel insights into the molecular principles of lichen-microbe interactions.

4-37 **Lee, Jun Hyuck**, Ae Kyung Park, **Hackwon Do**, **Kyoung Sun Park**, Sang Hyun Moh, Young Min Chi, and **Hak Jun Kim**. 2012. "Structural Basis for Antifreeze Activity of Ice-binding Protein from Arctic Yeast". *Journal of Biological Chemistry,* 287(14): 11460-11468.
doi: 10.1074/jbc.M111.331835

Arctic yeast *Leucosporidium* sp. produces a glycosylated icebinding protein (LeIBP) with a molecular mass of 25 kDa, which can lower the freezing point below the melting point once it binds to ice. LeIBP is a member of a large class of ice-binding proteins, the structures of which are unknown. Here, we report the crystal structures of non-glycosylated LeIBP and glycosylated LeIBP at 1.57- and 2.43-Å resolution, respectively. Structural analysis of the LeIBPs revealed a dimeric right-handed β-helix fold, which is composed of three parts: a large coiled structural domain, a long helix region (residues 96–115 form a long α-helix that packs along one face of the β-helix), and a C-terminal hydrophobic loop region (^{243}PFVPAPEVV^{251}). Unexpectedly, the C-terminal hydrophobic loop region has an extended conformation pointing away from the body of the coiled structural domain and forms intertwined dimer interactions. In addition, structural analysis of glycosylated LeIBP with sugar moieties attached to Asn^{185} provides a basis for interpreting previous biochemical analyses as well as the increased stability and secretion of glycosylated LeIBP. We also determined that the aligned Thr/Ser/Ala residues are critical for ice binding within the B face of LeIBP using sitedirected mutagenesis. Although LeIBP has a common β-helical fold similar to that of canonical hyperactive antifreeze proteins, the ice-binding site is more complex and does not have a simple ice-binding motif. In conclusion, we could identify the ice-binding site of LeIBP and discuss differences in the ice-binding modes compared with other known antifreeze proteins and ice-binding proteins.

4-38 **Lee, Jun Hyuck**, and 4 others. 2012. "The metavinculin tail domain directs constitutive interactions with raver1 and vinculin RNA". *Journal of Molecular Biology,* 422(5): 697-704. doi: 10.1016/j.jmb.2012.06.015

Vinculin is a key regulator of the actin cytoskeleton attachment to the cell membrane at cellular adhesion sites, which is crucial for processes such as cell motility and migration, development, survival, and wound healing. Vinculin loss results in embryonic lethality, cardiovascular diseases, and cancer. Its tail domain, Vt, is crucial for vinculin activation and focal adhesion turnover and binds to the actin cytoskeleton and acidic phospholipids upon which it unfurls. The RNA binding protein raver1 regulates the assembly of focal adhesions transcriptionally by binding to vinculin. The muscle-specific splice form, metavinculin, is characterized by a 68-residue insert in the tail domain (MVt) and correlates with hereditary idiopathic dilated cardiomyopathy. Here, we report that metavinculin can bind to raver1 in its inactive state. Our crystal structure explains this permissivity, where an extended coil unique to MVt is unfurled in the MVtΔ954:raver1 complex structure. Our binding assays show that raver1 forms a ternary complex with MVt and *vinculin* mRNA. These findings suggest that the metavinculin:raver1:RNA complex is constitutively recruited to adhesion complexes.

4-39 **Lee, Jun Hyuck**, **Hye Yeon Koh**, **Sung Gu Lee**, Shawn Doyle, Brent C. Christner, and **Hak Jun Kim**. 2012. "Draft Genome Sequence of *Paenisporosarcina* sp. Strain TG-20, a Psychrophilic Bacterium Isolated from the Basal Ice of Taylor Glacier". *Journal of Bacteriology,* 194(23): 6636. doi: 10.1128/JB.01472-12

We report the draft genome sequence of *Paenisporosarcina* sp. strain TG-20, which is 4.12 Mb in size and consists of 4,071 protein-coding genes and 76 RNA genes. The genome sequence of *Paenisporosarcina* sp. TG-20 may provide useful information about molecular adaptations that enhance survival in icy subsurface environments.

4-40 **Lee, Jungeun**, **Seung Chul Shin**, Su Jin Kim, Bum-Keun Kim, **Soon Gyu Hong**, **Eun Hye Kim**, **Hyun Park**, and **Hyoungseok Lee**. 2012. "Draft Genome Sequence of a *Sphingomonas* sp., an Endosymbiotic Bacterium Isolated from an Arctic Lichen *Umbilicaria* sp.". *Journal of Bacteriology,* 194(11): 3010. doi: 10.1128/JB.00360-12

Sphingomonas sp. strain PAMC 26617 has been isolated from Arctic lichen *Umbilicaria* sp. on Svalbard Islands. Here we present the draft genome sequence of this strain which represents a valuable resource for understanding symbiotic mechanism between endosymbiotic bacteria and lichens surviving in extreme environments.

4-41 Lee, Kyoo, Dong Uk Han, Jin Oh Hyun, Young Sim Hwang, **Yoo Kyung Lee**, and Eun Ju Lee. 2012. "List of Korean Names for the Vascular Plants in Spitsbergen Island, in the Arctic Region". *Ocean and Polar Research,* 34(1): 101-110. doi: 10.4217/OPR.2012.34.1.101

In this study, we attempted to provide Korean names to the arctic vascular plants observed around the Dasan Korean Arctic Station and Longyearbyen in Spitsbergen Island, in the Arctic region. To obtain recognizable results, plants were named according to the following naming rules. (1) When Korean names already existed, those names were used. (2) When there was no Korean name for a plant species, a scientific name for the plant was translated into a Korean name. (3) If the meaning of the scientific name was unclear, an English common name was translated into Korean name. (4) If the scientific names had meaning to the Arctic inhabitation, the Korean names included the word 'Buk-geuk'. (5) If the distribution of the plant was limited to the Arctic area or the original species lived in the polar region, the Korean name included the word 'Buk-geuk'. (6) If the plant had no Korean generic name, a particular suffix '~a-jae-bi' was added to the closely related genus name of the plant species, or a new Korean genus name was used by translating a common English name. (7) If the same generic name had two or more Korean names, a generic name that better reflected the characteristics of the plant was selected. In this paper, we reported Korean names for 46 plants species belonging to 15 families and 28 genera. Eight plants had an existing Korean name and the other species were given new Korean names based on the criteria outlined above. We also made new Korean generic names for three genera, *Braya*, *Micranthes* and *Cassiope*.

4-42 **Lee, Sung Gu**, **Hye Yeon Koh**, **Jun Hyuck Lee**, **Sung-Ho Kang**, and **Hak Jun Kim**. 2012. "Cryopreservative effects of the recombinant ice-binding protein from the Arctic yeast *Leucosporidium* sp. on red blood cells". *Applied Biochemistry and Biotechnology,* 167: 824-834.
doi: 10.1007/s12010-012-9739-z

Antifreeze proteins (AFPs) have important functions in many freeze-tolerant organisms. The proteins non-colligatively lower the freezing point and functionally inhibit ice recrystallization in frozen solutions. In our previous studies, we found that the Arctic yeast *Leucosporidium* sp. produces an AFP (LeIBP), and that the protein could be successfully produced in *Pichia* expression system. The present study showed that recombinant LeIBP possesses the ability to reduce the damage induced to red blood cells (RBCs) by freeze thawing. In addition to 40 % glycerol, both 0.4 and 0.8 mg/ml LeIBPs significantly reduced freeze–thaw-induced hemolysis at either rapid- (45 ℃) or slow-warming (22 ℃) temperatures. Post-thaw cell counts of the cryopreserved RBCs were dramatically enhanced, in particular, in 0.8 mg/ml LeIBP. Interestingly, the cryopreserved cells in the presence of LeIBP showed preserved cell size distribution. These results indicate that the ability of LeIBP to inhibit ice recrystallization helps the RBCs avoid critically damaging electrolyte concentrations, which are known as solution effects. Considering all these data, LeIBP can be thought of as a key component in improving RBC cryopreservation efficiency.

4-43 **Lee, Sung Gu**, **Hye Yeon Koh**, **Jun Hyuck Lee**, **Sung-Ho Kang**, and **Hak Jun Kim**. 2012. "Draft Genome Sequence of *Moritella dasanensis* Strain ArB 0140, a Psychrophilic Bacterium Isolated from the Arctic Ocean". *Journal of Bacteriology,* 194(19): 5452-5453.
doi: 10.1128/JB.01203-12

The psychrophilic bacterium *Moritella dasanensis* strain ArB 0140 was isolated near a glacier in Kongsfjorden, Svalbard Archipelago, Norway. Here we report a 4.89-Mb draft genome sequence of *Moritella dasanensis* ArB 0140, which could provide comprehensive information on a psychrophilic mechanism in extreme environments.

4-44 **Lee, Yung Mi**, **GoHeung Kim**, **You-Jung Jung**, Cheng-Dae Choe, **Joung Han Yim**, **Hong Kum Lee**, and **Soon Gyu Hong**. 2012. "Polar and Alpine Mic robial Collection (PAMC): a culture collection dedicated to polar and alpine microorganisms". *Polar Biology,* 35: 1433-1438.
doi: 10.1007/s00300-012-1182-7

Microorganisms in polar areas may have important ecological roles in biogeochemical cycles and the food chain. They are adapted to polar environments by means of special physiological adaptation mechanisms that include cold-adapted enzymes and cryoprotectants such as exopolysaccharides. Culture collections for polar microorganisms can provide research resources for ecological and physiological studies. The Polar and Alpine Microbial Collection (PAMC) is a specialized culture collection for maintenance and distribution of polar and alpine microorganisms. A database system was developed to share important data fields with DarwinCore2 and Ocean Biogeographic Information System database schemas. Approximately 1,500 out of 5,500 strains maintained in PAMC have been identified and belonged primarily to the phyla *Actinobacteria*, *Bacteroidetes*, *Firmicutes*, and *Proteobacteria*. Many of the microbial strains can grow at low temperature and produce proteases, lipases, and/or exopolysaccharides. PAMC provides search tools based on keywords such as taxonomy, geographical origin, habitat, and physiological characteristics. Biological materials and information provided by PAMC will be important resources for ecological and physiological studies on polar and alpine microorganisms.

4-45 Oh, Chang Jae, Ho Bang Kim, Jitae Kim, Won Jin Kim, **Hyoungseok Lee**, and Chung Sun An. 2012. "Organization of nif gene cluster in *Frankia* sp. EuIK1 strain, a symbiont of *Elaeagnus umbellata". Archives of Microbiology,* 194(1): 29-34.
doi: 10.1007/s00203-011-0732-7

The nucleotide sequence of a 20.5-kb genomic region harboring *nif* genes was determined and analyzed. The fragment was obtained from *Frankia* sp. EuIK1 strain, an indigenous symbiont of *Elaeagnus umbellata*. A total of 20 ORFs including 12 *nif* genes were identified and subjected to comparative analysis with the genome sequences of 3 *Frankia* strains representing diverse host plant specificities. The nucleotide and deduced amino acid sequences showed highest levels of identity with orthologous genes from an *Elaeagnus*-infecting strain. The gene organization patterns around the *nif* gene clusters were well conserved among all 4 *Frankia* strains. However, characteristic features appeared in the location of the *nif*V gene for each *Frankia* strain, depending on the type of host plant. Sequence analysis was performed to determine the transcription units and suggested that there could be an independent operon starting from the *nif*W gene in the EuIK strain. Considering the organization patterns and their total extensions on the genome, we propose that the *nif* gene clusters remained stable despite genetic variations occurring in the *Frankia* genomes.

4-46 **Park, Chae Haeng**, GaJin Jeong, and **Soon Gyu Hong**. 2012. "Possible multiple introductions of *Cladonia borealis* to King George Island". *Antarctic Science,* 24(4): 359-366.
doi: 10.1017/S0954102012000223

Many lichens have extensive distributional ranges covering several climatic zones and are able to colonize extreme habitats, including high alpine and polar regions. *Cladonia borealis*, one of the dominant lichen species on King George Island, is a cosmopolitan species inhabiting polar, subpolar, and alpine areas. It is usually found on soil, humus, and mosses, and is morphologically highly diverse. To understand the phylogeographic history of *C. borealis* on King George Island, we compared specimens from there with specimens from Norway and Chile. We conducted phylogenetic and haplotype network analyses of the partial SSU, ITS1-5.8S-ITS2, and partial LSU rDNA sequences including intron sequences in LSU rRNA genes. Nuclear rDNA locus of *C. borealis* from King George Island was separated into two monophyletic lineages. It is suggested that they originated in multiple independent introduction events after long-distance dispersal from other continents.

4-47 Park, Eunji, Dae-Sik Hwang, Jae-Seong Lee, Jun-Im Song, **Tae-Kun Seo**, and Yong-Jin Won. 2012. "Estimation of divergence times in cnidarian evolution based on mitochondrial protein-coding genes and the fossil record". *Molecular Phylogenetics and Evolution,* 62: 329-345.
doi: 10.1016/j.ympev.2011.10.008

The phylum Cnidaria is comprised of remarkably diverse and ecologically significant taxa, such as the reef-forming corals, and occupies a basal position in metazoan evolution. The origin of this phylum and the most recent common ancestors (MRCAs) of its modern classes remain mostly unknown, although scattered fossil evidence provides some insights on this topic. Here, we investigate the molecular divergence times of the major taxonomic groups of Cnidaria (27 Hexacorallia, 16 Octocorallia, and 5 Medusozoa) on the basis of mitochondrial DNA sequences of 13 protein-coding genes. For this analysis, the complete mitochondrial genomes of seven octocoral and two scyphozoan species were newly sequenced and combined with all available mitogenomic data from GenBank. Five reliable fossil dates were used to calibrate the Bayesian estimates of divergence times. The molecular evidence suggests that cnidarians originated 741 million years ago (Ma) (95% credible region of 686–819), and the major taxa diversified prior to the Cambrian (543 Ma). The Octocorallia and Scleractinia may have originated from radiations of survivors of the Permian–Triassic mass extinction, which matches their fossil record well.

4-48 **Park, Ha Ju**, **Seung Chul Shin**, and **Dockyu Kim**. 2012. "Draft Genome Sequence of Arctic Marine Bacterium *Pseudoalteromonas issachenkonii* PAMC 22718". *Journal of Bacteriology,* 194(15): 4140.
doi: 10.1128/JB.00744-12

The psychrotolerant *Pseudoalteromonas issachenkonii* PAMC 22718 was isolated for its higher chitinase and protease activities from cold seawater in the Kara Sea, Arctic. Here, we present the draft genome sequence of PAMC 22718 to provide further information for the ecological function of the genus *Pseudoalteromonas* in a cold marine environment.

4-49 **Park, Heeyong**, **Sung Gu Lee**, **Tai Kyoung Kim**, **Se Jong Han**, and **Joung Han Yim**. 2012. "Selection of Extraction Solvent and Temperature Effect on Stability of the Algicidal Agent Prodigiosin". *Biotechnology and Bioprocess Engineering,* 17(6): 1232-1237.
doi: 10.1007/s12257-012-0210-3

An organic solvent for extracting prodigiosin from culture broth was selected and a test to determine the long-term stability of prodigiosin was performed to develop prodigiosin as a biological control agent against *Chattonella antiqua*, a harmful alga that can cause red tides. Prodigiosin was extracted using nine solvents, and the extracts were analyzed by liquid chromatography-mass spectroscopy. Acetone was selected as the best organic solvent because of its high extraction efficiency and less processing time. Stability tests for prodigiosin were performed at various temperatures, and algicidal activity against *C. antiqua* was also tested. Ultimately, > 98% stability was sustained after 30 days at 4℃, whereas < 30% stability was maintained after 30 days at 37℃. Although prodigiosin was kept for 30 days in an optimum organic solvent, its stability was safely maintained and algicidal activity was sustained at 4℃. These results indicate that acetone is a very useful extraction and storage solvent for prodigiosin.

4-50 Park, Heeyong, **Tai Kyoung Kim**, **Se Jong Han**, and **Joung Han Yim.** 2012. “Enhancement of the Stability and Solubility of Prodigiosin Using β-Cyclodextrin in Seawater”. *Korean Society for Biotechnology and Bioengineering Journal,* 27(2): 109-113.

This research was to examine the effects of various cyclodextrins on the solubility and stability of prodigiosin in seawater. Among them, β-cyclodextrin was found to have the best efficiency and formation of the inclusion complex was saturated when prodigiosin and β-cyclodextrin were mixed in a ratio of 1 : 8 and shaken at 25℃ and pH 8.0 for 6 h. The maximum algicidal activity against *Chattonella antiqua* using the inclusion complex stored at 4℃ for 5 weeks of culture was obtained, 52.28 ± 3.41%, which was about 5.0 fold higher than that of control. Our results suggest that inclusion complexes of prodigiosin and β-cyclodextrin could serve as effective algicidal agents.

4-51 **Park, Kyoung Sun**, **Hackwon Do**, **Jun Hyuck Lee**, Seung Il Park, **Eun jung Kim**, Soon-Jong Kim, **Sung-Ho Kang**, and Hak Jun Kim. 2012. “Characterization of the ice-binding protein from Arctic yeast *Leucosporidium* sp. AY30”. *Cryobiology,* 64(3): 286-296. doi: 10.1016/j.cryobiol.2012.02.0

Previously, we reported the ice-binding protein (LeIBP) from the Arctic yeast *Leucosporidium* sp. AY30. In this study we provide physicochemical characterization of this IBP, which belongs to a class of IBPs that exhibited no significant similarity in primary structure to other known antifreeze proteins (AFPs). We compared native, glycosylated and non-glycosylated recombinant LeIBPs. Interestingly, size-exclusion chromatography and analytical ultracentrifugation revealed that LeIBP self-associates with a reversible dimer with K_d values in the range $3.45–7.24\times10^{-6}$ M. Circular dichroism (CD) spectra showed that LeIBP, glycosylated or non-glycosylated, is predominantly composed of β-strand secondary structural elements (54.6%), similar to other β-helical antifreeze proteins (AFPs). In thermal hysteresis (TH) activity measurements, native LeIBP was twice more active (0.87 ℃ at 15 mg/mL) than that of the recombinant IBPs (0.43–0.42 ℃ at 10.8 mg/mL). This discrepancy is probably due to uncharacterized enhancing factors carried over during ice affinity purification, because glycosylated and non-glycosylated recombinant proteins displayed similarly low activity. Ice recrystallization inhibition (RI) activities of the native and recombinant LeIBPs were comparable. Measurements of CD, TH activity, and RI showed that glycosylation does not cause structural changes and is not required for function. An ice-etching experiment using green fluorescent protein-tagged IBP revealed that LeIBP binds, just as hyperactive AFPs, to both basal and pyramidal prism planes of the ice crystal. Taken together, our results indicate that LeIBP, structurally similar to hyperactive AFPs, is moderately active and that a reversible dimer has no effect on its activity.

4-52 Park, Yon Mi, **Jeong-Hoon Kim**, Se Hun Gu, Sook Young Lee, Min-Goo Lee, Yoon Kyoo Kang, **Sung-Ho Kang**, **Hak Jun Kim**, and Jin-Won Song. 2012. “Full genome analysis of a novel adenovirus from the South Polar skua (*Catharacta maccormicki*) in Antarctica”. *Virology,* 422: 144-150. doi: 10.1016/j.virol.2011.10.008

Adenoviruses have been identified in humans and a wide range of vertebrate animals, but not previously from the polar region. Here, we report the entire 26,340-bp genome of a novel adenovirus, detected by PCR, in tissues of six of nine South Polar skuas (*Catharacta maccormicki*), collected in Lake King Sejong, King George Island, Antarctica, from 2007 to 2009. The DNA polymerase, penton base, hexon and fiber genes of the South Polar skua adenovirus (SPSAdV) exhibited 68.3%, 75.4%, 74.9% and 48.0% nucleotide sequence similarity with their counterparts in turkey hemorrhagic enteritis virus. Phylogenetic analysis based on the entire genome revealed that SPSAdV belonged to the genus *Siadenovirus*, family *Adenoviridae*. This is the first evidence of a novel adenovirus, SPSAdV, from a large polar seabird (family Stercorariidae) in Antarctica.

4-53 **Park, Yu Kyung**, **Jung Eun Kim**, **Hyoungseok Lee**, **Ji Hyun Kim**, **Ha Ju Park**, **Dockyu Kim**, **Mira Park**, **Joung Han Yim**, and **Il-Chan Kim.** 2012. “Characterization of a Chitinase Gene and Screening of Cold Active Chitinase from Polar Microorganisms”. *Korean Journal of Microbiology,* 48(4): 293-297. doi: 10.7845/kjm.2012.030

Of the 169 strains of microorganisms stored in Polar and Alpine Microbial Collection of Korea Polar Research Institute, 27 strains were selected for their chitinase activity on ZoBell plates supplemented with 0.4% colloidal chitin. Among them, PAMC 21693 strain have shown the highest chitinolytic enzyme activity toward pNP-(GlcNAc)$_1$ at low temperature and the highest growth rate at 4℃. We cloned a full-length chitinase gene of 2,857 bp which contains an open reading frame of 2,169 bp encoding 872-amino acid polypeptide. Recombinant chitinase protein was expressed in *E. coli* and its molecular weight was confirmed 96 kDa. In this paper, we suggest the potential use of cold-active chitinase from polar microorganisms in the field of biotechnology.

4-54 **Paudel, Babita**, **Hari Datta Bhattarai**, and **Joung Han Yim.** 2012. *“In vitro* antioxidant activity of the Antarctic lichen *Caloplaca regalis* and its GC/MS based phytochemical analysis”. *Journal of Biomolecule Reconstruction,* 9(1): 15-23.

Antioxidant agents, which inhibit the destructive actions of free radicals or reactive oxygen species (ROS), are widely used as food additives as well as in medicines and cosmetics. Antioxidant agents derived from natural sources are believed to be safer than synthetic compounds. In order to identify a new potential source of natural antioxidant compounds, we evaluated various antiradical and antioxidant activities of an ethanolwater extract of *Caloplaca regalis* (Vain.) Zahlbr. (Teloschistaceae), a lichen collected from the Antarctica. The experimental data indicated that even the crude extract of *C. regalis* exhibited a significant potential to inhibit free radical production. The GC/MS analysis showed that *C. regalis* extract contained various derivatives of benzoic acids, furanone, anthraquinone and several fatty acids. In addition, the total phenolic content in the lichen extract was found to be more than 8% by weight. We conclude that *C. regalis* does indeed produce antioxidant active compounds, which would have much strong activities if tested in a purified form. Thus, further research should be conducted to purify and characterize the compounds responsible for the antioxidant activity of *C. regalis* extract, as these compounds may be an alternative source of medically relevant antioxidant.

4-55 **Paudel, Babita**, **Hari Datta Bhattarai**, Durga Prasad Pandey, Jae Seoun Hur, **Soon Gyu Hong**, **Il-Chan Kim**, and **Joung Han Yim**. 2012. "Antioxidant, Antibacterial activity and Brine shrimp toxicity test of some Mountainous Lichens from Nepal". *Biological Research,* 45(4): 387-391.

A total of twenty four lichen species belonging to six families were collected from mountainous region of Nepal. The methanol extracts of each species were tested for antimicrobial and antioxidant activities in vitro. It was found that extracts of twenty one lichen species were active against *B. subtilis* and seven species were active against *S. aureus*. Similarly, in DPPH assay, three species *Peltigera* sp., *Cladonia* sp., and *Canoparmelia* sp. showed comparable activity with commercial standard, BHA. In ABTS+ assay, extracts of *Parmoterma* sp., *Ramalina* sp., *Peltigera* sp. and *Cladonia* sp. showed stronger activity than ascorbic acid. The observed data after comparison with previously published reports indicated that the high altitude lichens contain stronger antioxidant and antibacterial constituents. Similarly, the methanol extracts of *Heterodermia* sp. and *Ramalina* sp. showed comparable toxicity eff ect with commercial standard berberine chloride indicating a potent source of anticancer drugs.

4-56 Raymond, James A. and **Hak Jun Kim**. 2012. "Possible role of horizontal gene transfer in the colonization of sea ice by algae". *PLoS ONE,* 7(5): e35968.
doi: 10.1371/journal.pone.0035968

Diatoms and other algae not only survive, but thrive in sea ice. Among sea ice diatoms, all species examined so far produce ice-binding proteins (IBPs), whereas no such proteins are found in non-ice-associated diatoms, which strongly suggests that IBPs are essential for survival in ice. The restricted occurrence also raises the question of how the IBP genes were acquired. Proteins with similar sequences and ice-binding activities are produced by ice-associated bacteria, and so it has previously been speculated that the genes were acquired by horizontal transfer (HGT) from bacteria. Here we report several new IBP sequences from three types of ice algae, which together with previously determined sequences reveal a phylogeny that is completely incongruent with algal phylogeny, and that can be most easily explained by HGT. HGT is also supported by the finding that the closest matches to the algal IBP genes are all bacterial genes and that the algal IBP genes lack introns. We also describe a highly freeze-tolerant bacterium from the bottom layer of Antarctic sea ice that produces an IBP with 47% amino acid identity to a diatom IBP from the same layer, demonstrating at least an opportunity for gene transfer. Together, these results suggest that the success of diatoms and other algae in sea ice can be at least partly attributed to their acquisition of prokaryotic IBP genes.

4-57 Rhee, Jae-Sung, Bo-Mi Kim, Chang-Bum Jeong, Toshihiro Horiguchi, Young-Mi Lee, **Il-Chan Kim**, and Jae-Seong Lee. 2012. "Immune gene mining by pyrosequencing in the rockshell, *Thais clavigera*". *Fish & Shellfish Immunology*, 32: 700-710.
doi: 10.1016/j.fsi.2012.01.017

The rockshell, *Thais clavigera* (Gastropoda: Muricidae) has been shown to be a useful species as a potential indicator for diverse pollution in the marine environment. However, their genetic information is still not widely available. Here, we performed an extensive transcriptome analysis of *T. clavigera* using the pyrosequencing method, and selected innate immune-related genes. Among the unigenes obtained in this species, we annotated a number of immune system-related genes (e.g. adhesive protein, antimicrobial protein, apoptosis- and cell cycle-related protein, cellular defense effector, immune regulator, pattern recognition protein, protease, protease inhibitor, reduction/oxidation-related protein, signal transduction-related protein and stress protein), which are potentially useful for immunity research in this species. To confirm the usefulness of potential immune-biomarker genes, we checked the transcript level of specific immune genes in both different tissues and LPS-exposed rockshells within the *T. clavigera* transcript database. This study would be helpful to extend our knowledge on the immune system of rockshell in comparative aspects. Also it would be useful to develop the rockshell as a potential test organism for monitoring of marine environment quality.

4-58 Rhee, Jae-Sung, Bo-Mi Kim, Jung Soo Seo, **Il-Chan Kim**, and 2 others. 2012. “Cloning of growth hormone, somatolactin, and their receptor mRNAs, their expression in organs, during development, and on salinity stress in the hermaphroditic fish, *Kryptolebias marmoratus”. Comparative Biochemistry and Physiology, Part A,* 161: 436-442. doi: 10.1016/j.cbpa.2012.01.004

Salinity is an important parameter that affects survival and metabolism in fish. In fish, pituitary growth hormone (GH) regulates physiological functions including adaptation to different salinity as well as somatic growth. GH is stimulated by growth hormone-releasing hormone (GHRH) and exerts its function via binding to growth hormone receptor (GHR). As *Kryptolebias marmoratus* is a euryhaline fish, this species would be a useful model species for studying the adaptation to osmotic stress conditions. Here, we cloned *GH, -GHR*, somatolactin (*SL*), and somatolactin receptor (*SLR*) genes, and analyzed their expression patterns in different tissues and during early developmental stages by using real-time RT-PCR. We also further examined expression of them after acclimation to different salinity. Tissue distribution studies revealed that Km-GH and -SL mRNAs were remarkably expressed in brain and pituitary, whereas Km-GHR and -SLR mRNAs were predominantly expressed in liver, followed by gonad, muscle, pituitary, and brain. During embryonic developmental stages, the expression of their mRNA was increased at stage 3 (9 dpf). The *Km-GH* and *-SL* mRNA transcripts were constantly elevated until stage 5 (5 h post hatch), whereas *Km-GHR* and *-SLR* mRNA levels decreased at this stage. After we transferred *K. marmoratus* from control (12 psu) to hyper-osmotic condition (hyperseawater, HSW; 33 psu), *Km-GH*, *-SL,* and *GHR* mRNA levels were enhanced. In hypo-osmotic conditions like freshwater (FW), *Km-GH* and *-SL* expressions were modulated 24 h after exposure, and Km-SLR transcripts were significantly upregulated. This finding suggests that Km-GH and -SL may be involved in the osmoregulatory mechanism under hyper-osmotic as well as hypo-osmotic stress. This is the first report on transcriptional modulation and relationship of GH, GHR, SL, and SLR during early development and after salinity stress. This study will be helpful to a better understanding on molecular mechanisms of adaptation response to salt stress in euryhaline fish.

4-59 Rhee, Jae-Sung, Jang-Seu Ki, Dae-Sik Hwang, **Hyun Park**, **In-Young Ahn**, and Jae-Seong Lee. 2012. “Complete mitochondrial genome of the Arctic green sea urchin *Strongylocentrotus*

droebachiensis (Strongylocentrotidae, Echinoidea)". *Mitochondrial DNA,* 23(5): 369–370.
doi: 10.3109/19401736.2012.696629

The complete mitochondrial genome was obtained from the assembled genome data sequenced by next-generation sequencing technology from the Arctic green sea urchin *Strongylocentrotus droebachiensis*. The mitochondrial genome sequence was 15,710 bp in size, and the gene order and contents were identical with previously reported sea urchin mitochondrial genomes. Of 13 protein-coding genes (PCG$_S$), 1 gene (*Cytb*) had an incomplete stop codon. The base composition of the mitogenome of Arctic *S. droebachiensis* showed high A þ T (58.36%) and anti-G bias (14.86%) on the third position of PCGs.

4-60 Ryu, Jong-Seong and **Joung-Han Yim**. 2012. "Effects of *In Vitro* Antioxidant and *In Vivo* Anti-aging Improvement of Finished Cosmetic Products Containing Ramalin". *Korean Society for Aesthetics and Cosmetology,* 10(2): 345-352.

Although the studies of ingredient with antioxidant effect have been performing, *in vitro* and *in vivo* study of product containing antioxidant was not sufficient relatively. Potential antioxidants are very unstable due to auto-oxidation despite of their stabilized form exposed to air or sunlight. Especially, cosmetics were made through the process of high temperature, homogenization and mixture of a lot of ingredients. So, we cannot assure whether antioxidants keep the anti-oxidative efficacy on the finished product without any confirming test. In this study, we investigated antioxidant effect through DPPH and ORAC method and human volunteer test of three types of products with Actosome Ramalin as a stabilized form of Ramalin reported potent antioxidant previously. IC$_{50}$ value of finished products, Essence, Ample and Cream, was 6.7%, 41.62% and 3.2% respectively. ORAC value showed 1034.52μM TE/g, 953.41μM TE/g and 1023.49μM TE/g. In *in vivo* human test of Essence, skin hydration, texture, brightness and lifting were statistically improved after 3 weeks and 6 weeks compared to before using product. In the case of Ample, skin elasticity of R5 parameter on the side of eye was statistically improved after 2 weeks and 4 weeks compared to before using product. Cream statistically improved skin texture and skin tone after 2 weeks and 4 weeks. Any problem in the skin was not revealed in human volunteer test. From these results, we suggest that we can claim the skin anti-oxidative effect of product in the demonstration of anti-oxidative effect of finished product. And products formulated only antioxidant as active ingredient were improved and alleviated phenomena of facial skin aging in human volunteer test. Therefore, anti-oxidative efficacy demonstration of products containing anti-oxidant will be more practical and realistic approach to measure anti-oxidative level than raw material test.

4-61 Salma, Umme, Md. Hasan Uddowla, Meesun Kim, Jong Min Kim, Bo Kwang Kim, Hae-Ja Baek, **Hyun Park**, and 2 others. 2012. "Five hepatopancreatic and one epidermal chitinases from a pandalid shrimp (*Pandalopsis japonica*): Cloning and effects of eyestalk ablation on gene expression". *Comparative Biochemistry and Physiology, Part B,* 161: 197-207.
doi: 10.1016/j.cbpb.2011.11.005

Six cDNAs encoding chitinase proteins in *Pandalopsis japonica* were isolated by using polymerase chain reaction (PCR) cloning methods and bioinformatic analysis of expressed sequence tags (ESTs). The cDNAs, designated Pj-Cht1, 2, 3A, 3B, 3C, and 4, encoded proteins ranging from 388 to 607 amino acid residues in length (43.61–67.62 kDa) and displayed a common structural organization: an N-terminal catalytic domain, a Thr/Pro-rich linker region, and either 0 (Pj-Cht2, 3A), 1 (Pj-Cht1, 3B, and 3C), or 2 (Pj-Cht4) C-terminal chitinbinding domain(s) (CBD). Pj-Cht1 and 2 lacked the 5′ end of the open reading frame (ORF); the other Pj-Chts contained the complete ORF. All known decapod crustacean chitinases were segregated into at least four groups based on phylogenetic analysis and domain organization. Group 1 chitinases, represented by Pj-Cht1, were most closely related to insect group I chitinases and may function in the digestion of the peritrophic membrane. Group 2 chitinases including Pj-Cht2 show different domain organizations and pI value from other chitinases and appear to function in degradation of the old exoskeleton during the premolt period. Group 3 chitinases, represented by Pj-Cht3A, 3B, and 3C, may function in digestion of chitin-containing food and defense against pathogens. Group 4 chitinases, represented by Pj-Cht4, have two CBDs and their functions are unknown. Five Pj-Chts (Pj-Cht1, 3A, 3B, 3C, and 4) are expressed in the hepatopancreas and intestine, whereas Pj-Cht2 is expressed in epidermis and SG/XO complex suggesting crustacean chitinases can be classified into two groups (hepatopancreatic and epidermal) based on the expression profile. Eyestalk ablation (ESA) down-regulated the hepatopancreatic chitinase expression (Pj-Cht1, 3A, and 3C); Pj-Cht3B expression was not significantly affected by ESA. By contrast, mRNA levels of Pj-Cht2 were significantly upregulated in 7 days post-ESA. Pj-Cht4 mRNA levels were too low for measurement with quantitative polymerase chain reaction. ESA had no significant effect on chitinase expression in the intestine. These data indicate that Pj-Cht1, 3A, 3B, 3C, and 4 are hepatopancreatic chitinases that may function in the digestion of ingested chitin and the modification of peritrophic membrane in the intestine. By contrast, epidermal chitinase, Pj-Cht2 may play a role in chitin metabolism during molt cycle as shown in other crustacean group 2 chitinases.

4-62 **Shin, Seung Chul**, **Do Hwan Ahn**, **Jong Kyu Lee**, Su Jin Kim, **Soon Gyu Hong**, **Eun Hye Kim**, and **Hyun Park**. 2012. “Genome Sequence of *Sphingomonas* sp. Strain PAMC 26605, Isolated from Arctic Lichen (*Ochrolechia* sp.)”. *Journal of Bacteriology,* 194(6): 1607.
doi: 10.1128/JB.00004-12

The endosymbiotic bacteria *Sphingomonas* sp. PAMC 26605, was isolated from Arctic lichen (*Ochrolechia* sp.) on Svalbard Islands. Here we report the draft genome sequence of this strain, which could provide further insights into symbiotic mechanism of lichen on extreme environments.

4-63 **Shin, Seung Chul**, **Jin Cho**, **Jong Kyu Lee**, **Do Hwan Ahn**, **HyoungSeok Lee**, and **Hyun Park**. 2012. “Complete mitochondrial genome of the Antarctic amphipod *Gondogeneia antarctica* (Crustacea, amphipod)”. *Mitochondrial DNA,* 23(1): 25-27.
doi: 10.3109/19401736.2011.643877

The complete sequence of the mitochondrial genome of the Antarctic amphipod *Gondogeneia antarctica* was determined to be 18,424 bp in length, and to contain 13 protein-coding genes (PCG$_S$), 22 tRNA genes, and large (*rrnL*) and small (*rrnS*) rRNA genes. Its total A＋T content is 70.1%. The *G. antarctica* mitogenome is the largest known among those of crustaceans, due to the existence of two relatively large intergenic non-coding sequences. The PCG arrangement of *G. antarctica* is identical to that of the ancestral pancrustacean ground pattern, although the tRNA arrangement differs somewhat. The complete mitogenome sequences of 68 species of pancrustacea have been added to the NCBI database, only 4 of which represent complete mitogenome sequences from amphipods. This is the first report of a mitogenome sequence of an Antarctic amphipod, and provides insights into the evolution of crustacean mitochondrial genomes, particularly in amphipods.

4-64 **Shin, Seung Chul**, Su Jin Kim, **Do Hwan Ahn**, **Jong Kyu Lee**, and **Hyun Park**. 2012. "Draft Genome Sequence of *Sphingomonas echinoides* ATCC 14820". *Journal of Bacteriology,* 194(7): 1843.
doi: 10.1128/JB.00046-12

Sphingomoas is a Gram-negative, yellow-pigmented, chemoheterotrophic, strictly aerobic bacterium. The bacterium is known to be metabolically versatile and can utilize a wide range of natural compounds as well as some types of environmental contaminants such as creosote, polychlorinated biphenyls, etc. Here, we report the draft genome sequence of *Sphingomonas echinoides* ATCC 14820, which will provide additional information to enhance our understanding of metabolic versatility of *Sphingomonas*.

4-65 **Shin, Seung Chul**, Su Jin Kim, **Do Hwan Ahn**, **Jong Kyu Lee**, **Hyoungseok Lee**, **Jungeun Lee**, **Soon Gyu Hong**, **Yung Mi Lee**, and **Hyun Park**. 2012. "Genome Sequence of a *Salinibacterium* sp. Isolated from Antarctic Soil". *Journal of Bacteriology,* 194(9): 2404.
doi: 10.1128/JB.00235-12

The draft genome of *Salinibacterium* sp. PAMC 21357, isolated from permafrost soil of Antarctica, was determined. Here we present a 3.1-Mb draft genome sequence of *Salinibacterium* sp. that could provide further insight into the genetic determination of its cold-adaptive properties.

4-66 **Shin, Seung Chul**, Su Jin Kim, **Jong Kyu Lee**, **Do Hwan Ahn**, **Min Gyu Kim**, **Hyoungseok Lee**, **Jungeun Lee**, Bum-Keun Kim, and **Hyun Park**. 2012. "Transcriptomics and Comparative Analysis of Three Antarctic Notothenioid Fishes". *PLoS ONE,* 7(8): e43762.
doi: 10.1371/journal.pone.0043762

For the past 10 to 13 million years, Antarctic notothenioid fish have undergone extraordinary periods of evolution and have adapted to a cold and highly oxygenated Antarctic marine environment. While these species are considered an attractive model with which to study physiology and evolutionary adaptation, they are poorly characterized at the molecular level, and sequence information is lacking. The transcriptomes of the Antarctic fishes *Notothenia coriiceps*, *Chaenocephalus aceratus*, and *Pleuragramma antarcticum* were obtained by 454 FLX Titanium sequencing of a normalized cDNA library. More than 1,900,000 reads were assembled in a total of 71,539 contigs. Overall, 40% of the contigs were annotated based on similarity to known protein or nucleotide sequences, and more than 50% of the predicted transcripts were validated as full-length or putative full-length cDNAs. These three Antarctic fishes shared 663 genes expressed in the brain and 1,557 genes expressed in the liver. In addition, these cold-adapted fish expressed more Ub-conjugated proteins compared to temperate fish; Ub-conjugated proteins are involved in maintaining proteins in their native state in the cold and thermally stable Antarctic environments. Our transcriptome analysis of Antarctic notothenioid fish provides an archive for future studies in molecular mechanisms of fundamental genetic questions, and can be used in evolution studies comparing other fish.

4-67 **Shin, Seung Chul**, Su Jin Kim, **Soon Gyu Hong**, **Do Hwan Ahn**, **Yung Mi Lee**, **Hyoungseok Lee**, **Jungeun Lee**, and **Hyun Park**.2012. "Genome Sequence of *Pseudomonas* sp. Strain PAMC 25886, Isolated from Alpine Glacial Cryoconite". *Journal of Bacteriology,* 194(7): 1844.
doi: 10.1128/JB.00057-12

Pseudomonas spp. have shown characteristics of efficiently metabolizing environmental pollutants and also producing exopolysaccharides known as biofilms. Here we present the draft genome sequence of *Pseudomonas* sp. strain PAMC 25886, which was isolated from glacier cryoconite in the Alps mountain permafrost region and which may provide further insight into biodegradative and/or biofilm-producing mechanisms in a cold environment.

4-68 Song, Jun-Im, Sung-Jin Hwang, **Hye-Won Moon**, and **In-Young Ahn**. 2012. "Taxonomic Study of Suborder Calcaxonia (Alcyonacea: Octocorallia: Anthozoa) from King Sejong Station, Antarctic". *Animal Systematics, Evolution and Diversity,* 28(2): 84-96.
doi: 10.5635/ASED.2012.28.2.084

Some gorgonians in the families, Primnoidae and Isididae within the suborder Calcaxonia were collected from subtidal zones between depths of 10 and 45 m in the coastal regions of King Sejong Station (62°13′S, 058°47′W), Korea Polar Research Institute of Korea Ocean Research and Development Institute (KORDI) by SCUBA diving from 2009 to 2011. Three species in the Primnoidae, *Arntzia gracilis* (Molander, 1929), *Thouarella* (*Thouarella*) *antarctica* (Valenciennes, 1846) and *Onogorgia nodosa* (Molander, 1929), and also one species in the family Isididae, *Tenuisis microspiculata* (Molander, 1929) are newly recorded to octocorallian fauna in Marian Cove and Potter Cove of King George Island. These four species have been described in detail.

4-69 Yoo, Miyoun, **Dockyu Kim**, and 4 others. 2012. "Draft Genome Sequence and Comparative Analysis of the Superb Aromatic-Hydrocarbon Degrader *Rhodococcus* sp. Strain DK17". *Journal of Bacteriology,* 194(16): 4440.
doi: 10.1128/JB.00844-12

Rhodococcus sp. strain DK17 is capable of utilizing various derivatives of benzene and bicyclics containing both aromatic and alicyclic moieties as sole carbon and energy sources. Here, we present the 9,107,362-bp draft genome sequence of DK17 and its genomic analysis in comparison with other members of the genus *Rhodococcus*.

4-70 Zhang, Jun, Jin-Wei Zheng, Byung Cheol Cho, **Chung Yeon Hwang**, and 3 others. 2012. "*Sphingobacterium wenxiniae* sp. nov., a cypermethrin-degrading species from activated sludge". *International Journal of Systematic and Evolutionary Microbiology,* 62(3): 683-687.
doi: 10.1099/ijs.0.033118-0

A Gram-negative, non-motile, non-spore-forming, non-flagellated rod capable of degrading cypermethrin, designated LQY-18^{T}, was isolated from activated sludge of a wastewater treatment plant in China. Strain LQY-18^{T} grew at 8–40℃ (optimum 30℃), at pH 5.0–10.0 (optimum pH 7.0) and with 0–5% (w/v) NaCl (optimum 1%). The predominant menaquinone was MK-7 (97%) and the major fatty acids were summed feature 3 (comprising $C_{16:1}\omega6c$ and/or $C_{16:1}\omega7c$), iso-$C_{15:0}$ and iso-$C_{17:0}$ 3-OH. The DNA G+C content was 40.3 mol%. Phylogenetic analysis revealed that the isolate belonged to the genus *Sphingobacterium* of the phylum *Bacteroidetes* and showed low 16S rRNA gene sequence similarity with recognized members of the genus *Sphingobacterium*. The closest neighbour was *Sphingobacterium mizutaii* ATCC 33299^T (92.9% 16S rRNA gene sequence similarity). On the basis of phenotypic, genetic and phylogenetic data, strain LQY-18^T (=ACCC 05410^T = CCTCC AB 2010005^T = KCTC 23009^T) should be classified as a representative of a novel species of the genus *Sphingobacterium*, for which the name *Sphingobacterium wenxiniae* sp. nov. is proposed.


KOPRI
극지연구소


KOPRI
극지연구소


KOPRI
극지연구소

ISSN 2289-0734

KOPRI ABSTRACTS Volume 4 (2010-2012)

Published on May, 2014
Published by Korea Polar Research Institute

Contact information
- **Editor** On, Nara onnara@kopri.re.kr
- **Editorial committee** Kang, Cheon Yun cykang@kopri.re.kr
  Park, Hyunyi hypark@kopri.re.kr
- **Editorial office** KOPRI Library
  26 Songdomirae-ro, Yeonsu-gu, Incheon,
  406-840, South Korea
  Tel +82-32-770-8484 **Fax** +82-32-770-8488
  E-mail hypark@kopri.re.kr

Cover Photo Chung, Hosung
Design & Printing Designintro Co.